

POLITECNICO DI TORINO

Corso di Laurea Magistrale in Ingegneria Civile

Tesi di Laurea Magistrale

Improvement of Ferrocement Durability by Nanomaterials for Preservation of Pier Luigi Nervi's Structural Heritage



Relatori

Prof. Rosario Ceravolo
Prof. Mario A. Chiorino

Candidato

Arturo D'Alessandro

firma dei relatori

.....
.....

firma del candidato

.....

Exchange University Supervisors

[Northwestern University – Evanston, IL USA]
Prof. David Corr
Prof. Surendra P. Shah

A.A. 2017-2018

DEDICATION

This thesis is dedicated to my family, for their love and support throughout my life. Their good examples have taught me to work hard for the things that I aspire to achieve.

ACKNOWLEDGMENTS

I would like to express my very great appreciation to my advisors at Northwestern University, Professor David Corr and Professor Surendra P. Shah, for their guidance and support in my journey through this research. I have learned much more than I ever expected, not just about the specifics of the project, but the overall process of research and academics.

I am particularly grateful for the assistance given by my Italian advisors Professor Mario A. Chiorino and Professor Rosario Ceravolo, who always gave me useful suggestions and orientation, and worked actively to provide me with the great opportunity to undergo a research exchange abroad.

My grateful thanks are also extended to all of those with whom I had the pleasure to work during this project: Dr. Yuan Gao, Raul Marrero, and others.

Lastly, I would like to acknowledge the other faculty of the Civil and Environmental Engineering Department, who made my experience at Northwestern University a truly positive one.

ABSTRACT

Ferrocement is a construction material which provided to have superior qualities of crack control, impact resistance, and toughness, largely due to the geometrical properties, i.e., uniform dispersion and high specific surface of reinforcement within the material. However, while extensive literature exists on the deterioration mechanisms and maintenance of reinforced concrete structures, little attention has been given to the durability of ferrocement. Given the lack of knowledge of maintenance and repair strategies on ferrocement structures, along with the paucity of literature on deterioration mechanisms taking place in this material, further studies are necessary to define guidelines for diagnosis, structural assessment (including the new need of seismic assessment), structural rehabilitation and remedial actions for durability of ferrocement spatial structural architectures.

In this study, the adoption of newly developed nanomaterials, such as ethyl silicate, to improve durability of ferrocement is investigated. Such nanomaterials are expected to penetrate the cementitious matrix without changing the appearance of the surface. Once penetrated, pozzolanic behavior is displayed forming calcium silicate hydrate and consequently increase durability and mechanical performance. Particular attention was given to the carbonation-induced corrosion of reinforcement, which should be considered as a major concern in ferrocement due to the initially small diameter of the mesh wires (even a small cross section loss of the wire is of great importance) and the incredibly thin mortar cover (the time required for the carbonation to reach the depth of the steel can be very short). Laboratory tests revealed that ethyl silicate can be effective in reducing the ingress of aqueous substances through the pore structure of the cementitious matrix, although other protective agents (i.e., sodium silicate “waterglass” sealer, and Isobutyl-triethoxy-silane sealer) exhibited better performances with respect to water absorption. The single most conspicuous observation to emerge from the data comparison was that ethyl silicate featured much better performance with respect to carbonation resistance than with respect to water absorption, while the other protective agents were almost ineffective in preventing the penetration of carbonation into the cement mortar matrix.

Moreover, the present thesis sheds new light on the sensitive issue of maintenance, repair and conservation of ferrocement architectural heritage. In fact, special focus has

been given to the work of the Italian engineer-architect Pier Luigi Nervi, who employed ferrocement in many of his landmarks, combining this extremely versatile material with his prefabrication technique, namely structural prefabrication.

Among Nervi's works, Turin Exhibition Center represents the first large scale ferrocement construction ever completed. The corrugated vault and the related ribbed apse of the main Hall B, and the refined texture of the vault of the adjacent Hall C represent an international icon of the twentieth century. Unfortunately, the Nervi's structural masterpiece now exists in a state of semi-neglect and decay; however, a restoration and redevelopment project was drawn up by the Town of Turin and by Politecnico di Torino. Moreover, Politecnico di Torino, in conjunction with PLN Pier Luigi Nervi Project Association, is preparing a submission for a "Keeping it Modern" grant of the Getty Foundation.

Keywords: Ferrocement, Durability, Carbonation Resistance, Pier Luigi Nervi,
Nanomaterials, Heritage Structures

TABLE OF CONTENTS

| | |
|--|------|
| ACKNOWLEDGMENTS | iii |
| ABSTRACT..... | iv |
| LIST OF TABLES..... | xi |
| LIST OF FIGURES | xiii |
| 1. INTRODUCTION | 1 |
| 1.1 Concrete as the Most Widely Used Construction Material | 1 |
| 1.2 Ferrocement as a Member of the Cement-Based Composites Family..... | 3 |
| 1.3 Reinforced Concrete and Ferrocement Heritages | 4 |
| 1.4 Durability of Cement-Based Composites | 6 |
| 2. CEMENTS AND CEMENT PASTE | 9 |
| 2.1 Components of Modern Concrete | 9 |
| 2.1.1 Hydraulic Cements | 11 |
| 2.2 Hydration of Portland Cement..... | 13 |
| 2.2.1 Hydration of the Aluminates..... | 15 |
| 2.2.2 Hydration of the Silicates | 16 |
| 2.3 Morphology of the Main Hydration Products..... | 18 |
| 2.3.1 Calcium Silicate Hydrate (C-S-H)..... | 20 |
| 2.3.2 Calcium Hydroxide (CH)..... | 22 |
| 2.3.3 Calcium Sulfoaluminates Hydrates | 22 |
| 2.3.4 Capillary Porosity | 23 |
| 2.3.5 Unhydrated Clinker Grains..... | 23 |
| 2.3.6 Other Phases | 23 |
| 2.4 Microstructure of the Hydrated Cement Paste..... | 23 |
| 2.4.1 Hydrated Cement Particles | 26 |
| 2.4.2 Outer Hydration Product..... | 26 |
| 2.4.3 Large Pores | 26 |
| 2.5 Microstructure of Concrete | 26 |
| 2.6 The Pore Structure of Cement Paste | 28 |

| | | |
|-------|---|----|
| 2.6.1 | Classification of Pore Sizes | 29 |
| 2.6.2 | Factors Influencing Pore Structure | 31 |
| 3. | TRANSPORT PROCESSES IN CEMENT-BASED MATERIALS | 33 |
| 3.1 | Water in the Hydrated Cement Paste | 34 |
| 3.1.1 | Capillary Water | 35 |
| 3.1.2 | Adsorbed Water | 36 |
| 3.1.3 | Interlayer Water | 36 |
| 3.1.4 | Chemically Combined Water..... | 36 |
| 3.2 | Diffusion | 37 |
| 3.3 | Capillary Suction | 39 |
| 3.3.1 | Capillary Water Absorption Coefficient..... | 41 |
| 3.4 | Permeation | 42 |
| 3.5 | Migration..... | 44 |
| 3.6 | Mechanisms and Significant Parameters for Transport Processes | 46 |
| 3.7 | Presence of More Than One Transport Mechanism | 48 |
| 4. | DURABILITY OF REINFORCED CEMENT-BASED STRUCTURES | 50 |
| 4.1 | Factors Affecting Durability | 51 |
| 4.1.1 | Aggressiveness of the Environment | 51 |
| 4.1.2 | Concrete Quality | 52 |
| 4.1.3 | Cracking..... | 52 |
| 4.1.4 | Thickness of the Cover | 53 |
| 4.2 | Deterioration Mechanisms of Cement-Based Materials | 53 |
| 4.2.1 | Physical Deterioration Mechanisms | 55 |
| 4.2.2 | Chemical deterioration mechanisms | 56 |
| 4.3 | General Aspect on Corrosion..... | 57 |
| 4.3.1 | Initiation Phase in Carbonation-Induced Corrosion | 58 |
| 4.3.2 | Factors Influencing the Carbonation rate..... | 59 |
| 4.3.3 | Propagation Phase: Corrosion Process After Depassivation | 61 |
| 4.3.4 | Testing for Corrosion..... | 64 |
| 4.4 | Effect of Cracks on Corrosion | 65 |

| | | |
|-------|---|-----|
| 4.4.1 | Effect of Crack Widths | 66 |
| 4.4.2 | Effect of Crack Frequency | 67 |
| 4.4.3 | Effect of Crack Depth | 67 |
| 5. | PRINCIPLES FOR MAINTENANCE AND REPAIR OF HERITAGE STRUCTURES..... | 68 |
| 5.1 | Project Phases of the Concrete Repair and Protection Process..... | 69 |
| 5.2 | Anamnesis and Diagnosis: Inspection, Condition Assessment, and Identification of the causes of Damage and Decay..... | 73 |
| 5.2.1 | Visual Inspection | 74 |
| 5.2.2 | Detailed Survey..... | 75 |
| 5.2.3 | Diagnosis: Identification of the Causes of Damage and Decay..... | 76 |
| 5.3 | Therapy: Methods for Maintenance and Repair | 77 |
| 6. | INTRODUCTION TO FERROCEMENT..... | 80 |
| 6.1 | History of Ferrocement | 80 |
| 6.2 | Definition of Ferrocement..... | 83 |
| 7. | PIER LUIGI NERVI..... | 85 |
| 7.1 | The Nervi System | 85 |
| 7.2 | Nervi's Ferro-Cementitious Felt | 87 |
| 7.3 | Turin Exhibition Center | 91 |
| 7.3.1 | Hall B for Turin Exhibition Center..... | 92 |
| 7.3.2 | Hall C for Turin Exhibition Center..... | 96 |
| 7.3.3 | Visual Inspection and Durability Assessment of Hall B | 98 |
| 8. | CONSTITUENTS OF FERROCEMENT, COMPOSITION, AND REINFORCING PARAMETERS..... | 101 |
| 8.1 | Mortar Matrix..... | 103 |
| 8.2 | Skeletal Steel..... | 105 |
| 8.3 | Mesh Reinforcement..... | 107 |
| 8.4 | Similarities and Differences Between Ferrocement and Reinforced Concrete | 110 |
| 8.5 | Geometrical Properties of Reinforcement | 112 |
| 8.5.1 | Cover..... | 112 |

| | | |
|--------|---|-----|
| 8.5.2 | Volume Fraction of Reinforcement | 112 |
| 8.5.3 | Specific Surface of Reinforcement | 114 |
| 8.6 | Mechanical Properties of Ferrocement | 115 |
| 8.6.1 | Tensile behavior | 116 |
| 8.6.2 | First Crack | 117 |
| 9. | DURABILITY OF FERROCEMENT | 120 |
| 9.1 | Deterioration Associated with the Mortar Matrix | 120 |
| 9.2 | Deterioration Associated with Reinforcement | 121 |
| 9.3 | Considerations on Durability of Ferrocement | 121 |
| 9.3.1 | Cracking Behavior | 122 |
| 9.3.2 | Corrosion | 122 |
| 9.3.3 | Alkali-Silica Reaction | 123 |
| 9.4 | Techniques to Improve Durability of Ferrocement | 124 |
| 10. | EXPERIMENTAL STUDY ON IMPROVEMENT OF FERROCEMENT DURABILITY BY NANOMATERIALS | 126 |
| 10.1 | Introduction | 126 |
| 10.1.1 | Classification of Surface Treatments | 127 |
| 10.1.2 | Inorganic Surface Treatments | 128 |
| 10.1.3 | Hydrophobic impregnation | 130 |
| 10.1.4 | Ethyl Silicate for Surface Treatment of Cement-Based Materials | 134 |
| 10.2 | Materials Used in This Study | 137 |
| 10.2.1 | Cement and Mortar Mixtures | 137 |
| 10.2.2 | Sample Preparation and Curing | 139 |
| 10.2.3 | Mortar Samples | 140 |
| 10.2.4 | Ferrocement Samples | 140 |
| 10.2.5 | Surface Treatments | 143 |
| 10.2.6 | Climatic Chamber | 144 |
| 10.3 | Test Methods | 146 |
| 10.3.1 | Flexure Test on Mortar and Ferrocement | 146 |
| 10.3.2 | ESEM-EDS Analysis | 148 |

| | |
|--|-----|
| 10.3.3 Carbonation Depth..... | 151 |
| 10.3.4 Water absorption..... | 153 |
| 10.4 Results..... | 154 |
| 10.4.1 Flexure Test on Mortar and Ferrocement | 154 |
| 10.4.2 ESEM-EDS Analysis..... | 164 |
| 10.4.3 Carbonation Depth..... | 174 |
| 10.4.4 Water Absorption Test..... | 176 |
| 10.5 Discussion..... | 180 |
| 10.5.1 Flexure Test on Mortar and Ferrocement | 180 |
| 10.5.2 ESEM-EDS Analysis..... | 181 |
| 10.5.3 Water Absorption on TEOS-Treated Samples MOR-S1 | 182 |
| 10.5.4 Carbonation Depth..... | 183 |
| 10.5.5 Water Absorption on Samples MOR-S2 and FERRO-S | 184 |
| 11. SUMMARY AND CONCLUSIONS | 187 |
| BIBLIOGRAPHY | 190 |

LIST OF TABLES

| | |
|---|-----|
| Table 2.1: Typical concrete mix design..... | 10 |
| Table 2.2: Commonly used abbreviations for oxides and clinker compounds..... | 11 |
| Table 2.3: Classification of pore sizes according to the general classification by IUPAC and concrete science technology | 29 |
| Table 3.1: Typical values for the parameter S | 41 |
| Table 3.2: Typical values for the coefficient of permeability (Bertolini, Elsener, Pedferri, Redaelli, & Polder, 2004) | 43 |
| Table 3.3: Reduction in permeability of a 0.7 w/c cement paste with the progress of hydration (Powers, Copeland, Hayes, & Mann, 1954)..... | 44 |
| Table 3.4: Values of mobility of various ions at infinite dilution at 25°C (in $10^{-4}\text{m}^2 \text{V}^{-1} \text{s}^{-1}$) (Bertolini, Elsener, Pedferri, Redaelli, & Polder, 2004)..... | 45 |
| Table 3.5: Properties of concrete relevant with regard to different durability requirements (Bertolini, Elsener, Pedferri, Redaelli, & Polder, 2004)..... | 47 |
| Table 4.1: Frequent mistakes taking place during construction phases (Coppola & Buoso, 2015)..... | 54 |
| Table 4.2: Typical values of corrosion rate (Bertolini, Elsener, Pedferri, Redaelli, & Polder, 2004) | 63 |
| Table 4.3: Proposed relationship between corrosion rate and remaining service life (Clear, 1985)..... | 63 |
| Table 4.4: Main tests for assessing the condition of deteriorated concrete | 65 |
| Table 8.1: Summary of ranges of composition, reinforcing parameters, and mechanical properties in ferrocement (Naaman, 2000)..... | 103 |
| Table 8.2: Grading requirements for sand, provided by ASTM C 33 | 104 |
| Table 8.3: Common types and sizes of steel meshes used in ferrocement (ACI Committee 549, 1993) | 109 |
| Table 8.4: Common types and sizes of steel meshes used in ferrocement (ACI Committee 549, 1993) | 110 |
| Table 8.5: Recommended design values of the global efficiency factor of mesh reinforcement η_0 for uniaxial tension or bending (ACI Committee 549, 1993)..... | 113 |

| | |
|---|-----|
| Table 8.6: Mechanical properties of ferrocement reinforced with conventional steel meshes and cement mortar matrices (Naaman, 2000)..... | 115 |
| Table 10.1: Physiochemical properties of cement..... | 138 |
| Table 10.2: Particle size distribution of sand | 138 |
| Table 10.3: List of the samples utilized in the study | 140 |
| Table 10.4: Details of the ferrocement samples | 141 |
| Table 10.5: Application techniques | 144 |
| Table 10.6: Mean values for mortar specimens MOR-FL..... | 154 |
| Table 10.7: Comparison of strengths and deflections of ferrocement specimens FERRO-FL | 155 |
| Table 10.8: Mean values for ferrocement specimens FERRO-FL | 155 |
| Table 10.9: Details of crack width for different pre-cracked specimens FERRO-S ... | 158 |
| Table 10.10: Samples FERRO-S grouped for surface treatments, prior to water absorption test..... | 163 |
| Table 10.11: Samples FERRO-CARB, increase of carbonation resistance compared to non-treated samples | 176 |
| Table 10.12: Samples MOR-S1, decrease in permeability compared to non-treated samples | 177 |
| Table 10.13: Samples MOR-S2, decrease in permeability compared to non-treated samples | 178 |
| Table 10.14: Samples FERRO-S, decrease in permeability compared to non-treated samples | 179 |

LIST OF FIGURES

| | |
|---|----|
| Figure 1.1: Family of the structural cement-based composites, viewed as two-components composites or their hybrid combinations (Naaman, 2000) | 3 |
| Figure 1.2: Centennial Hall in Wrocław, erected in 1911-1913 by Max Berg as a multi-purpose recreational building; it became a key reference in the later development of reinforced concrete structures..... | 4 |
| Figure 1.3: The Sydney Opera House (designed by Jørn Utzon and inaugurated in 1973) comprises three groups of interlocking vaulted shells which are set upon a vast platform and are surrounded by terrace areas that function as pedestrian concourses..... | 4 |
| Figure 1.4: Turin Exhibition Center, Hall B..... | 6 |
| Figure 2.1: Flow diagram of the dry process for Portland cement manufacture (Mehta & Monteiro, 2006)..... | 12 |
| Figure 2.2: Schematic of the rate of hydration or heat evolution as a function of time | 15 |
| Figure 2.3: Schematic representation of the main chemical reactions during the hydration of Portland cement. The rectangular areas indicate the relative proportions (Bertolini, 2006) | 15 |
| Figure 2.4: Model for C-S-H (Neville, Properties of concrete, 1995) | 17 |
| Figure 2.5: (a) Typical rates of formation of hydration products in an ordinary Portland cement paste (Soroka, 1979); (b) Influence of formation of hydration products on setting time, porosity, permeability, and strength of cement paste (Mehta & Monteiro, 2006)..... | 18 |
| Figure 2.6: SEM images showing the hexagonal crystal habit of calcium hydroxide, needle-like habit of ettringite and the sheet-like habit of C-S-H. In the upper image (a) crystal growth into a void, where space restrictions are minimal, allowing development of euhedral forms..... | 19 |
| Figure 2.7: The fibrous C-S-H crystals under SEM (Kurdowski & Wieslaw, 2014) ... | 20 |
| Figure 2.8: Rate of hydration vs. time, showing when the low-density and high-density morphologies form | 21 |
| Figure 2.9: Development of the microstructure of a Portland cement during hydration (Bertolini, 2006) | 24 |
| Figure 2.10: Microstructure of a hydrated cement paste (Mehta & Monteiro, 2006) ... | 25 |
| Figure 2.11: Backscattered SEM image of a mature cement paste showing the main micro-structural feature | 25 |

| | |
|--|----|
| Figure 2.12: Polished section from a concrete specimen (Mehta & Monteiro, 2006) .. | 27 |
| Figure 2.13: Dimensional range of solids and pores in hydrated cement paste (Mehta & Monteiro, 2006)..... | 30 |
| Figure 2.14: Pore size distribution in hydrated cement pastes (Mehta & Monteiro, 2006)..... | 30 |
| Figure 3.1: Principal factors involved in the transport processes in concrete (Bertolini, Elsener, Pedferri, Redaelli, & Polder, 2004) | 34 |
| Figure 3.2: Representation of water present in capillary pores in concrete in equilibrium with a non-saturated atmosphere (CEB, 1992)..... | 36 |
| Figure 3.3: Schematic representation of water content in the pores of concrete as a function of the relative humidity of the environment, in conditions of equilibrium (CEB, 1992)..... | 37 |
| Figure 3.4: Schematic representation of the diffusion process (Bertolini, 2006)..... | 37 |
| Figure 3.5: Behavior of a hydrophilic material and of a Hydrophobic one (Bertolini, 2006)..... | 39 |
| Figure 3.6: Flow due to the Hydraulic head (Bertolini, 2006) | 43 |
| Figure 3.7: Example of combination of transport mechanisms (CEB, 1992) | 49 |
| Figure 4.1: Causes of deterioration of reinforced concrete structures (Bertolini, Elsener, Pedferri, Redaelli, & Polder, 2004) | 54 |
| Figure 4.2: Physical causes of concrete deterioration (Mehta & Gerwick, 1982) | 55 |
| Figure 4.3: Types of chemical reactions responsible for concrete deterioration (Mehta & Gerwick, 1982)..... | 57 |
| Figure 4.4: Influence of relative humidity on the rates of carbonation and corrosion (Bertolini, Elsener, Pedferri, Redaelli, & Polder, 2004)..... | 60 |
| Figure 4.5: The anodic, cathodic, oxidation and hydration reactions of corroding steel in concrete..... | 62 |
| Figure 4.6: Schematic representation of the corrosion rate in the carbonated concrete as a function of the resistivity of concrete (Alonso, Andrade, & Gonzales, 1988) | 64 |
| Figure 5.1: General flow of conservation process procedures for new and existing structures (Fib, 2010)..... | 73 |
| Figure 5.2: Example of integrated methodology of inspection for assessing corrosion in reinforcement (Bertolini, Elsener, Pedferri, Redaelli, & Polder, 2004) | 75 |

| | |
|--|-----|
| Figure 5.3: Principles of repair to stop corrosion of reinforcement (RILEM Technical Committee 124-SRC, 1994) | 79 |
| Figure 6.1: Lambot's patent on "fer-ciment" | 81 |
| Figure 6.2: Original 1848 Lambot's boat preserved in Brignoles Museum..... | 81 |
| Figure 7.1: Italian patent n. 377969, "Structural prefabrication technique", 1939 | 86 |
| Figure 7.2: Aircraft Hangar, Orbetello. Pier Luigin Nervi & Bartoli, 1939-1941 | 87 |
| Figure 7.3: Italian patent n. 406296, "ferro-cementitious felt", 1943 | 88 |
| Figure 7.4: Italian patent n. 429331, 2 nd supplement to patent n. 406296, 1944..... | 89 |
| Figure 7.5: Shed in Via della Magliana, namely Magliana Warehouse (1945) | 90 |
| Figure 7.6: Shed in Via della Magliana, detail of a V-shaped module | 91 |
| Figure 7.7: Cross section of Hall B | 92 |
| Figure 7.8: Italian patent n. 445781, Ferrocement wave, 1948 | 93 |
| Figure 7.9: Hall B, cross section through a waved vault element | 94 |
| Figure 7.10: Hall B, reinforcement of spurs (Nervi, 1957) | 95 |
| Figure 7.11: Hall B, Ferrocement elements "Tavellone" connected by site-cast reinforced concrete | 96 |
| Figure 7.12: Hall B, the half-dome during construction | 96 |
| Figure 7.13: Map of Hall C | 97 |
| Figure 7.14: Assembling the vault, 1950..... | 98 |
| Figure 7.15: Wave ashlar, assessment of the carbonation depth (P.Q.R.S. s.r.l., Laboratorio Prove Materiali) | 99 |
| Figure 8.1: Typical sections of ferrocement (Naaman, 2000)..... | 102 |
| Figure 8.2: Armature system (ACI Committee 549, 1993)..... | 106 |
| Figure 8.3: Assumed longitudinal and transverse directions of reinforcement (ACI Committee 549, 1993) | 107 |
| Figure 8.4: Typical steel meshes used in ferrocement applications | 108 |
| Figure 8.5: Rectangular mesh..... | 114 |

| | |
|---|-----|
| Figure 8.6: Schematic load-elongation curve of reinforced concrete in tension (Naaman, 2000) | 116 |
| Figure 8.7: Schematic load-elongation curve of ferrocement in tension (Naaman, 2000) | 117 |
| Figure 8.8: Influence of specific surface of reinforcement on stress at first cracking (Naaman, 2000) | 118 |
| Figure 8.9: Typical quantitative influence of specific surface of reinforcement on properties of ferrocement (Naaman, 2000)..... | 118 |
| Figure 10.1: SEM images of nano-SiO ₂ /ethyl silicate-treated mortar: (a) control, (b) nano-SiO ₂ , (c) TEOS (Hou, Cheng, Qian, & Shah, 2014) | 130 |
| Figure 10.2: Illustration of the difference between a hydrophilic and a hydrophobic material by the means of a contact angle: on top capillary pores and underneath a water droplet (Johansson, 2005)..... | 131 |
| Figure 10.3: Molecular structure of silane and of siloxane (Salander, 2010) | 131 |
| Figure 10.4: Reactions between silane/siloxane and cementitious substrate (Woo, Zhu, Chow, Leung, & Kim, 2008)..... | 133 |
| Figure 10.5: Hydrolysis reaction scheme for ethyl silicate (Et = C ₂ H ₅), with silanol and ethanol formation (Sandrolini, Franzoni, & Pigino, 2012)..... | 134 |
| Figure 10.6: Simplified condensation reaction scheme in presence of -OH groups in the stone (Sandrolini, Franzoni, & Pigino, 2012)..... | 135 |
| Figure 10.7: Pore partially filled with calcium silicate gel, due to the reaction between penetrated ethyl silicate and Portlandite (Pigino, Leemann, Franzoni, & Lura, 2012) | 136 |
| Figure 10.8: Superficial XRD patterns of TEOS-treated cement pastes at 10 h and 7 days old (Hou, Cheng, Qian, & Shah, 2014)..... | 137 |
| Figure 10.9: Flow Table and Flow Mold | 139 |
| Figure 10.10: Reinforcement for samples FERRO-CARB | 141 |
| Figure 10.11: Cross section of samples, dimensions in mm | 142 |
| Figure 10.12: Mold and steel mesh reinforcement used for both specimens FERRO-FL and FERRO-S (left); FERRO-FL samples after curing (right) | 142 |
| Figure 10.13: Ultrasonic cleaner Branson 5510 | 143 |
| Figure 10.14: Surface treatment of mortar sample by dipping it into the treatment agent | 144 |

| | |
|---|-----|
| Figure 10.15: Climatic chamber for curing of surface treatments (dimensions in mm) | 145 |
| Figure 10.16: Experimental setup..... | 147 |
| Figure 10.17: Schematic representation of the experimental setup..... | 147 |
| Figure 10.18: Hitachi S-3400N-II SEM | 149 |
| Figure 10.19: Sample MOR-ESEM cut to expose the cross section (dimensions in mm) | 150 |
| Figure 10.20: Buehler EcoMet 250 Polisher | 150 |
| Figure 10.21: Samples MOR-ESEM after polishing..... | 150 |
| Figure 10.22: sample FERRO-CARB during the accelerated carbonation test | 152 |
| Figure 10.23: Accelerated carbonation test chamber (dimensions in mm)..... | 152 |
| Figure 10.24: Samples MOR-S1/MOR-S2 and FERRO-S during the water absorption test..... | 153 |
| Figure 10.25: Load-C.M.O.D. curves for 28 days old mortar specimens MOR-FL ... | 154 |
| Figure 10.26: Bending response of ferrocement specimens FERRO-FL..... | 156 |
| Figure 10.27: Bending response of ferrocement specimens FERRO-S | 157 |
| Figure 10.28: Surface of pre-cracked specimens observed by means of optical microscopy | 162 |
| Figure 10.29: Sample MOR-ESEM, area under examination (dimensions in mm).... | 164 |
| Figure 10.30: ESEM images of MOR-ESEM, Control..... | 165 |
| Figure 10.31: ESEM images of MOR-ESEM, TEOS | 166 |
| Figure 10.32: ESEM images of MOR-ESEM, SS..... | 167 |
| Figure 10.33: ESEM images of MOR-ESEM, ISOB | 168 |
| Figure 10.34: ESEM image (top) and X-ray spectra (bottom) for areas A and B of sample MOR-ESEM Control | 169 |
| Figure 10.35: ESEM image (top) and X-ray spectra (bottom) for areas A and B of sample MOR-ESEM, TEOS-treated..... | 170 |
| Figure 10.36: ESEM image (top) and X-ray spectra (bottom) for areas A and B of sample MOR-ESEM, SS-treated | 171 |

| | |
|---|-----|
| Figure 10.37: ESEM image (top) and X-ray spectra (bottom) for areas A and B of sample MOR-ESEM, ISOB-treated | 172 |
| Figure 10.38: Comparison between X-ray spectra obtained from the outer (top) and inner (bottom) layer of each sample | 173 |
| Figure 10.39: Ca/Si ratios obtained from the quantitative analysis associated with the obtained spectra | 174 |
| Figure 10.40: Penetration depth of untreated and treated ferrocement samples FERRO-CARB | 175 |
| Figure 10.41: Water absorption test on treated and untreated mortar samples MOR-S1 | 177 |
| Figure 10.42: Water absorption test on treated and untreated mortar samples MOR-S2 | 178 |
| Figure 10.43: Water absorption test on treated and untreated ferrocement samples FERRO-S..... | 179 |
| Figure 10.44: Typical load-deflection response of ferrocement illustrating various stages of behavior (Naaman, 2000) | 181 |

CHAPTER 1

INTRODUCTION

1.1 Concrete as the Most Widely Used Construction Material

In an article published by the Scientific American in April 1964, S. Brunauer and L.E. Copeland, two eminent scientists in the field of cement and concrete wrote (Mehta & Monteiro, 2006):

The most widely used construction material is concrete, commonly made by mixing Portland cement with sand, crushed rock, and water. Last year in the U.S. 63 million tons of Portland cement were converted into 500 million tons of concrete, five times the consumption by weight of steel. In many countries the ratio of concrete consumption to steel consumption exceeds ten to one. The total world consumption of concrete last year is estimated at three billion tons, or one ton for every living human being. Man consumes no material except water in such tremendous quantities.

Today, the rate at which concrete is used is much higher than it was 40 years ago. It is estimated that the present consumption of concrete in the world is of the order of 11 billion metric tons every year.

Considering that concrete is not as strong as steel begs the question: why is concrete the most widely used engineering material? Prof. Povindar K. Mehta (Mehta & Monteiro, 2006) identified three main reasons. First, concrete possesses excellent resistance to water, which makes it the ideal material for building structures to control, store, and transport water. The second reason is the possibility to form structural concrete element into a variety of shapes and sizes. The third reason is that concrete is usually the cheapest and most readily available material on the job.

Different considerations can be done to further understand the use of concrete over steel as the construction material of choice:

- *Maintenance.* Concrete structures require less maintenance than steel structures. The reason for this is that – in a proper designed structure – concrete does not corrode, needs no surface treatment, and its strength increases with time. On the other hand, steel structures can undergo heavy corrosion, require protection and surface treatments.
- *Fire resistance.* In most cases, concrete does not require any additional fire-protection because of its built-in resistance to fire. It is also worth pointing out that concrete forms a basic method of fire protection for steel structures. After the great fire of Chicago, all steel structures were coated with a basic form of concrete to provide fire protection. Therefore, the fire resistance is perhaps the area in which the advantages of concrete are most evident.
- *Resistance to cyclic loading.* The fatigue strength of steel structures is greatly influenced by local stress fields in welded joints, corrosion pitting and sudden changes in geometry. On the other hand, the fatigue strength of concrete is generally not a problem because in most codes of practice the allowable concrete stresses are limited to about 50 percent of the ultimate strength.

In previous centuries, most of the historical heritage structures were built with masonry and wood. However, the advent of reinforced concrete at the late 19th and early 20th centuries led to the massive construction of reinforced concrete structures such as buildings, bridges, etc., that replaced the previous masonry and timber structures. The advantages in reinforced concrete in the 20th century captured the imagination of architects and engineers, resulting in some spectacular structures that are now being recognized for their cultural significance and considered to be heritage structure by international organizations, such as UNESCO.

1.2 Ferrocement as a Member of the Cement-Based Composites Family

Reinforced concrete belongs to a much broader family, that is, the *cement-based composites family* (Figure 1.1). Cement-based composites are generally simplified as two-component materials: the cement-based matrix (e.g., mortar, concrete) and the reinforcement. The family includes conventional reinforced concrete, prestressed concrete, partially prestressed concrete, fiber reinforced concrete and several of their combination. This thesis place emphasis on *ferrocement*, which is an important member of the structural concrete family.

Ferrocement can be considered a rather peculiar material, because even though it truly represents the first invention of reinforced concrete, it can also be considered as an evolution of the latter. In fact, ferrocement was almost forgotten for 100 years after its invention, due to the rapid development of reinforced concrete. Only the early 40's Pier Luigi Nervi, a noted Italian engineer-architect, revived the original concept of ferrocement as a construction material for boats and terrestrial structures.

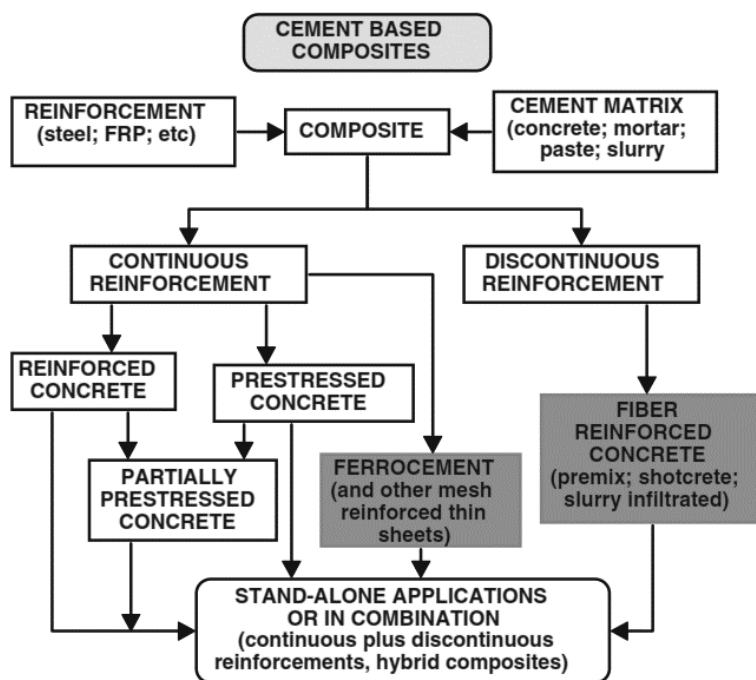


Figure 1.1: Family of the structural cement-based composites, viewed as two-components composites or their hybrid combinations (Naaman, 2000)

1.3 Reinforced Concrete and Ferrocement Heritages

Heritage structures are those which were designed and constructed by architects and designers around the world at the end of the 19th century and at the beginning of the 20th century. Organizations such as UNESCO classify these structures as heritages due to their architectural or social relevance.



Figure 1.2: Centennial Hall in Wrocław, erected in 1911-1913 by Max Berg as a multi-purpose recreational building; it became a key reference in the later development of reinforced concrete structures



Figure 1.3: The Sydney Opera House (designed by Jørn Utzon and inaugurated in 1973) comprises three groups of interlocking vaulted shells which are set upon a vast platform and are surrounded by terrace areas that function as pedestrian concourses

Over the past decades, there has been a growing awareness in the world of the importance of preserving our heritage. Preservation professionals and scholars became concerned that buildings and sites of our modern heritage were reaching an age of increased endangerment without advocates for their preservation. As a matter of fact, there is very little information about the repair and strengthening of reinforced concrete heritage structures, however there are lots of techniques for repair and strengthening of newly built reinforced concrete structures. These techniques are consequently used on reinforced concrete heritage structures as well. Though, considering that reinforced concrete is a relatively new construction material, it is reasonable to argue that most of the problems of the modern reinforced concrete structures also exist in the historic ones. Thus, one may be persuaded that testing, repair, and strengthening methods of modern concrete could be successfully used for reinforced concrete heritage structures. However, due to strict requirements related to the preservation of the original materials and texture, conventional repair techniques such as replacement of carbonated concrete are not applicable to structures that belong to the cultural heritage (Bertolini, Carsana, Gastaldi, Lollini, & Redaelli, 2011). Given the constant need of finding a compromise between the restoration of structural safety and the preservation of the original materials and surface, the conservation of reinforced concrete structures of the cultural heritage is a challenge.

Amongst all the heritage structures scattered all around the world, special attention in this thesis will be given to the grand legacy of the works built by the Italian engineer Pier Luigi Nervi, whose heritage is today at risk. One of the Nervi's most iconic works is Turin Exhibition Center (Figure 1.4), for which the Italian engineer-architect perfected his construction technique, combining the use of ferrocement and prefabrication. Turin Exhibition Center is nowadays recognized by DOCOMOMO ("Documentation and Conservation of Buildings, Sites and Neighbourhoods of the Modern Movement") as a protected historical and cultural monument.



Figure 1.4: Turin Exhibition Center, Hall B

1.4 Durability of Cement-Based Composites

Just like every other construction material, reinforced concrete may suffer durability issues if preventive measures are not adopted during the design and construction phases. Experience has shown that deterioration mechanisms and aggressive environments can severely undermine the durability of reinforced concrete structures. Needless to say, there is important concern about historic and heritage structures, given both their age and the lack of knowledge under which they were built.

At the beginning, designers of concrete structures have been mostly interested in the strength characteristics of the material. In fact, concrete was initially regarded as having an inherently high durability: it was a common belief that reinforced concrete structures are intrinsically durable and substantially immune to decay even if left in a particularly aggressive environment. However, as the passage of time shows, this material that once believed to be eternal shows durability problems due to deterioration/distress of the structure on the long term.

Whereas properly constructed, placed, and cured concrete can be durable under most natural and industrial environments, cases of premature deterioration of concrete structures do occur and they provide valuable lessons for control of factors responsible for the lack of durability. Due to the lack of knowledge, unexpected maintenance and repairs arose very early in the specified service life of structures. This caused enormous financial burdens to clients. The US Department of Defense funded a major research

project entitled *Concrete durability – a multibillion dollar opportunity* (National Research Council Committee on Concrete, 1988). The goal was to determine whether the concrete durability issues were a technical or an institutional problem. It concluded that:

Most of the knowledge exists which, if properly applied, would produce durable concrete. The lack of proper application may be attributed to a lack of knowledge by practitioners and the system's failure to make durability the responsibility of the organization which can most directly provide it — the contractor.

Therefore, a major role is played by the failure to recognize the magnitude and financial costs of potential durability problems. During the last decades, starting from the 80's, the perspective has drastically changed. It is now evident that designers of concrete structures must become durability-conscious. It was clear that the cost of adequate prevention carried out during the stages of design and execution are minimal compared to the savings they make possible during the service life and even more so, compared to the costs of rehabilitation that might be required at later dates. For example, the origin of corrosion can often be traced to simple errors that could have been avoided without any appreciable increase in cost.

More recent experiences have shown that prevention of concrete deterioration begins in the design phase, when a structure is conceived, along with structural calculations, choice of proper materials and design of details. To ensure proper durability, particular attention must also be given to the preparation, casting, compaction, and curing of concrete. Prevention will eventually continue throughout the entire service life of the structure, with programmed inspections, monitoring and maintenance.

As for deterioration and durability issues, many of the masterpieces that are nowadays considered to be heritage are no exception. Due to the deterioration/distress of these reinforced concrete heritage structures, their repair and maintenance is becoming imperative to prolong their service life. In order to provide an economic and effective remedy to building defects, it is essential to identify properly the cause to address the problem. *Building pathology* is the scientific study of the nature of building failure and its causes, processes, development and consequences.

The low cost of steel-reinforced concrete and the ready availability of raw materials with which it is formed make it the most widely used structural material available. Many

reinforced concrete structures have given excellent service with minimal maintenance. However, as the structure has aged it has become apparent that some environments were more severe than originally thought, and some construction and design problems have led to lower service lives and higher maintenance costs than originally envisaged. Because of the typical urban or rural exposure conditions of these buildings, carbonation-induced corrosion of reinforcement is often the main deterioration mechanism, leading to spalling, cracking, rust stains and loss of reinforcement cross-sectional area. Furthermore, chloride-induced corrosion of reinforcement may also concern buildings exposed to de-icing salts or marine environments.

In recent decades, corrosion has created a multi-billion-dollar infrastructure deficit (Poursae, 2016). One of the latest estimates from the USA (Transportation Research Board, 1991) is that the cost of damage due to deicing salts alone is between \$325 and \$1000 million per year to bridges and car parks. In the UK the Department of Transport estimates a total repair cost of £616.5 million due to corrosion damage to motorway bridges (Wallbank, 1983). Similar statistics are available in Europe.

Given the evident societal and economical importance of the impact of corrosion when developing advanced structures and the fact that some aspects of ferrocement (that will be explained later) lead to be concerned about corrosion, it is important that this critical deterioration mechanism receives much more attention in this thesis.

CHAPTER 2

CEMENTS AND CEMENT PASTE

The protection that concrete provides to the embedded steel and, more in general, its ability to withstand various types of degradation, depend on its microstructure and composition. This chapter illustrates the properties of the cement and the microstructure of cement-based materials.

Knowledge of the very heterogeneous and complex microstructure of cement-based materials, as well as the properties of the individual components of the cement-matrix and their relationships to each other, is useful for exercising control on the durability properties of the material. Nevertheless, it is important to point out that a durable material is only one of the ingredients that lead to a durable structure.

2.1 Components of Modern Concrete

The following definitions are adapted from ASTM C 125 (ASTM, 2016) and ACI Committee 116 (ACI Committee 116, 2000):

- *Concrete* is a composite material that consists essentially of a binding medium within which are embedded particles or fragments of aggregate. In hydraulic-cement concrete, the binder is formed from a mixture of hydraulic cement and water.
 - *Aggregate* is the granular material, such as sand, gravel, crushed stone, crushed blast-furnace slag, or construction and demolition waste that is used with a cementing medium to produce either concrete or mortar. The term coarse aggregate refers to the aggregate particles larger than 4.75 mm (No. 4 sieve), and the term fine aggregate refers to the aggregate particles smaller than 4.75 mm but larger than 75 μm (No. 200 sieve).
 - *Gravel* is the coarse aggregate resulting from natural disintegration by weathering of rock.

- *Sand* is the fine aggregate resulting from either natural weathering or crushing of stone.
- *Crushed stone* is the product resulting from industrial crushing of rocks, boulders, or large cobblestones.
- *Iron blast-furnace slag*, a by-product of the iron industry, is the material obtained by crushing blast-furnace slag that solidified by slow cooling under atmospheric conditions.
- *Aggregates from construction and demolition waste* are to the product obtained from recycling of concrete, brick, or stone rubble.
- *Mortar* is a mixture of sand, cement, and water. It is similar to concrete but without coarse aggregates.
- *Cement* is a finely pulverized, dry material that by itself is not a binder but develops the binding property as a result of hydration reactions between cement minerals and water.

Cement is rather pricy compared to aggregate, since it is manufactured using an energy-intensive process while the latter undergoes only a small amount of processing. Fortunately, there is a lot more aggregate than cement in concrete. The process used to define the weight and volume of the various components that must be combined to make one cubic meter of concrete is called *mix design*. Table 2.1 shows a typical mix design for concrete; one may notice that cement makes up only about 15% by weight.

Table 2.1: Typical concrete mix design

| | Dosage, kg/m³ | Percent by weight | Percent by volume |
|------------------|---------------------------------|--------------------------|--------------------------|
| Water | 325 | 195 | 19.5 |
| Cement | 591 | 355 | 11.3 |
| Coarse aggregate | 1863 | 1104 | 42.0 |
| Fine aggregate | 1231 | 721 | 27.2 |
| Total | 4010 | 2375 | 100 |

2.1.1 Hydraulic Cements

Cements that not only harden by reacting with water but also form a water-resistant product are called *hydraulic cements*. On the other hand, the cements derived from the calcination of gypsum or calcium carbonates are *nonhydraulic* because their products of hydration are not resistant to water.

Although Portland cement consists essentially of various compounds of calcium, the results of routine chemical analysis are reported in terms of oxides of the elements presents. In addition to that, it is customary to express the individual oxides and clinker compounds by using the abbreviations showed in Table 2.2.

According to EN 197-1 (CEN - European Committee for standardization, 2000), Portland cement is a hydraulic binder, i.e. a finely ground inorganic material which, when mixed with water, forms a paste which sets and hardens by means of hydration reactions and processes and which, after hardening, retains its strength and stability even under water.

Table 2.2: Commonly used abbreviations for oxides and clinker compounds

| Oxide | Abbreviation | Compound | Abbreviation |
|-------------------------|------------------|---|--------------------------------------|
| CaO | C | $3\text{CaO}\cdot\text{SiO}_2$ | C_3S |
| SiO_2 | S | $2\text{CaO}\cdot\text{SiO}_2$ | C_2S |
| Al_2O_3 | A | $3\text{CaO}\cdot\text{Al}_2\text{O}_3$ | C_3A |
| Fe_2O_3 | F | $4\text{CaO}\cdot\text{Al}_2\text{O}_3\cdot\text{Fe}_2\text{O}_3$ | C_4AF |
| MgO | M | $4\text{CaO}\cdot 3\text{Al}_2\text{O}_3\cdot\text{SO}_3$ | $\text{C}_4\text{A}_3\bar{\text{S}}$ |
| SO_3 | $\bar{\text{S}}$ | $3\text{CaO}\cdot 2\text{SiO}_2\cdot 3\text{H}_2\text{O}$ | $\text{C}_3\text{S}_2\text{H}_3$ |
| H_2O | H | $\text{CaSO}_4\cdot 2\text{H}_2\text{O}$ | $\text{C}\bar{\text{S}}\text{H}_2$ |

Cement conforming to EN 197-1, namely CEM cement, when appropriately batched and mixed with aggregate and water, be capable of producing concrete or mortar which retains its workability for a sufficient time and shall after defined periods attain specified strength levels and also possess long-term volume stability.

Portland cement represents the basis for most of cement-based materials used nowadays, and it is obtained by mixing clinker and a small amount of gypsum. The dry process for Portland cement manufacture is shown in Figure 2.1; Portland cement clinker is produced through the intergrinding and high temperature calcining of calcareous and siliceous raw materials (Moss, 1998) containing elements, usually expressed as oxides, CaO, SiO₂, Al₂O₃, Fe₂O₃ and small quantities of other materials. Since calcium silicates are the primary constituents of Portland cement, the raw must provide calcium and silica in suitable form and proportions. To reach the sintering temperature of about 1,450 °C (2,640 °F), a rotary kiln is used.

This system transforms the raw mix into clinkers, which are gray, glass-hard, spherically shaped nodules that range from 0.32 to 5.1 centimeters (cm) in diameter. The final operation in the Portland cement manufacturing process consists of pulverizing the clinker to an average particle between 10 and 15 μm. The operation is carried out in ball mills. Approximately 5 percent gypsum is usually mixed with clinker to control the early setting and hardening behavior of the cement.

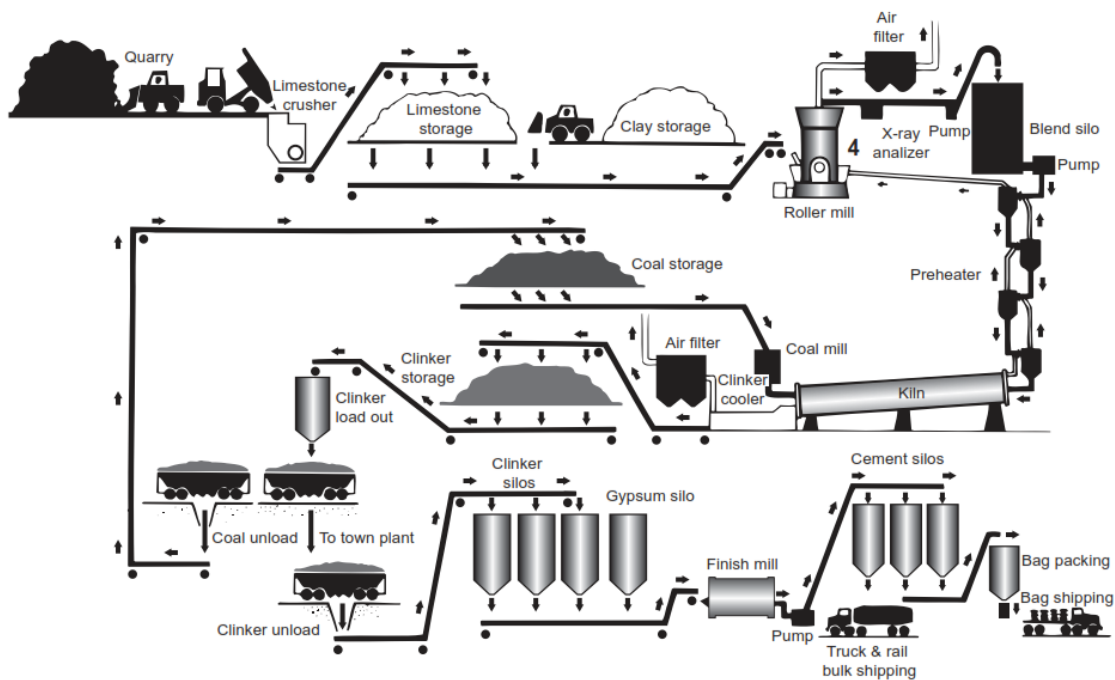


Figure 2.1: Flow diagram of the dry process for Portland cement manufacture (Mehta & Monteiro, 2006)

The chemical composition of the principal clinker compounds corresponds to:

- $3\text{CaO}\cdot\text{SiO}_2$ (or C_3S in cement notation): *tricalcium silicate*
- $2\text{CaO}\cdot\text{SiO}_2$ (or C_2S in cement notation): *dicalcium silicate*
- $3\text{CaO}\cdot\text{Al}_2\text{O}_3$ (or C_3A in cement notation): *tricalcium aluminate*
- $4\text{CaO}\cdot\text{Al}_2\text{O}_3\cdot\text{Fe}_2\text{O}_3$ (C_4AF): *ferrite*

These are known as the main crystalline phases of anhydrous Portland cement. In ordinary Portland cement their respective amounts usually range between 45 and 60, 15 and 30, 6 and 12, 6 and 8 percent (Mehta & Monteiro, 2006).

According to EN 197-1 (CEN - European Committee for standardization, 2000) Portland cement clinker shall consist of at least two-thirds by mass of calcium silicates (C_3S and C_2S), the remainder consisting of aluminum and iron containing clinker phases and other compounds.

In addition to the crystalline phases, other oxides are present in Portland cement clinker, particularly magnesium, titanium, manganese, potassium, and sodium oxides. Among these, Sodium oxide and Potassium oxide play an important role in the pore solution alkalinity, which is crucial for steel reinforcement protection against corrosion.

It is beyond the scope of this thesis to discuss in detail of the highly complex crystal structures of cement compounds. However, these crystal structures account for differences in the reactivity between the cement compounds.

2.2 Hydration of Portland Cement

Anhydrous Portland cement is a gray powder composed of angular particles typically in the size range from 1 to 50 μm , which cannot bind aggregates. In fact, it must be mixed with water to exhibit his binding properties. The chemical reactions between cement and water are commonly referred to as the hydration process, which leads to products that possess setting and hardening characteristics.

A schematic representation of the rate of hydration of Portland cement is showed in Figure 2.2; however, the mechanism is much more complicated than it first appears. Two hydration mechanisms have been proposed. The first mechanism is called *through-solution hydration*. It yields to a complete reorganization of the constituents of the original compounds and can be divided into the following stages:

- *Dissolution* of anhydrous compounds into their ionic constituents. The cement dissolves, releasing ions into the mix water. The mix water is thus no longer pure H₂O but an aqueous solution containing a variety of ionic species, called the pore solution. The concentrations of ionic species in the pore solution increase rapidly as soon as the cement and water are combined.
- Formation of hydrates forming a supersaturated solution. Eventually the concentrations increase to the point that the pore solution is supersaturated, meaning that it is energetically favorable for some of the ions to combine into new solid phases rather than remain dissolved.
- *Precipitation* of hydrates due to their low solubility. The new precipitated solid phases are called hydration products and are different from the starting cement minerals.

Thus, cement hydration is a continuous process by which the cement minerals are replaced by new hydration products, with the pore solution acting as a necessary transition zone between the two solid states.

The second hydration mechanism is called *solid-state hydration*. In this case the hydration reactions take place directly at the surface of the anhydrous cement compounds without the compounds going into solution. It appears that the through-solution mechanism is dominant in the early stages of cement hydration. Eventually, when the ionic mobility in the solution becomes restricted, the hydration of residual anhydrous cement compounds seems to occur by solid-state reactions.

During the hydration process, all the compounds react simultaneously with water. However, they do not hydrate at the same rate. In fact, the aluminates (C₃A) hydrate at a much faster rate than the silicates (C₃S, C₂S).

The loss of consistency (*stiffening*) and the solidification (*setting*) of a hydraulic cement paste are mainly determined by the aluminates hydration. On the other hand, the silicates play a dominant role in the strength development (*hardening*).

A schematic representation of the main chemical reactions involved in the hydration of Portland cement is shown in Figure 2.3. For a better understanding of the processes, it is best to discuss the hydration reactions of silicates and aluminates separately.

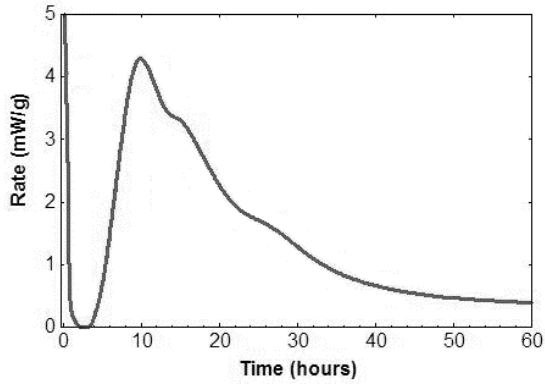


Figure 2.2: Schematic of the rate of hydration or heat evolution as a function of time

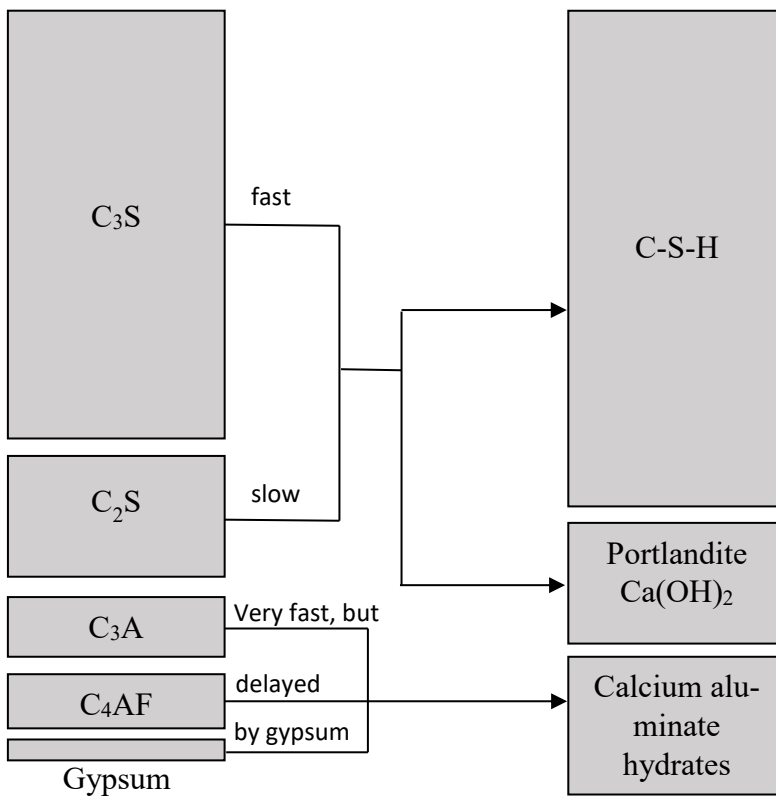


Figure 2.3: Schematic representation of the main chemical reactions during the hydration of Portland cement. The rectangular areas indicate the relative proportions (Bertolini, 2006)

2.2.1 Hydration of the Aluminates

The reaction of C_3A with water is immediate, with the formation of crystalline hydrates (such as C_3AH_6) and a large amount of heat is produced. The reaction sequence is:



where the first reaction is very rapid, and the second reaction occurs more slowly. The final reaction product (C_3AH_6) is called *hydrogarnet*. The initial reaction is so rapid that it must be slowed in order for the Portland cement to be used for construction applications, which require that a proper workability at early ages. Therefore, for practical purposes, approximately 5 percent gypsum ($C\bar{S}H_2$) is usually mixed with clinker. In presence of gypsum, the hydration of C_3A is delayed.

When the ferrite phase (C_4AF) reacts with water in presence of sulfate, the products formed are structurally similar to those formed from the hydration of C_3A , even though the reactivity of C_4AF is somewhat slower than C_3A . The hydration process described below is applicable to both the C_3A phase and the ferrite phase in Portland cement; although, for sake of simplicity, only C_3A is discussed next.

Gypsum is highly soluble, rapidly releasing calcium (Ca^{2+}) and sulfate ions (SO_4^-) into the pore solution. These ions immediately react with aluminate ions ($[AlO_4]^-$) to form mineral ettringite ($3CaO \cdot Al_2O_3 \cdot 3CaSO_4 \cdot 32H_2O$, abbreviated $C_3A\bar{S}_3H_{32}$) which covers the surface of the anhydrous cement compounds. If the gypsum in the cement reacts completely before the C_3A , then the concentration of sulfate ions in the pore solution decreases drastically and the ettringite becomes unstable and converts to a different solid phase known as monosulfate hydrate ($3CaO \cdot Al_2O_3 \cdot CaSO_4 \cdot 12H_2O$, abbreviated $C_3A\bar{S}H_{12}$), which has less sulfate. Most cements do not contain enough gypsum to react with all the C_3A , and as a result the early-forming ettringite converts to monosulfate hydrate after a period of several hours, allowing the C_3A to undergo renewed rapid hydration, with the formation of crystalline hydrates.

2.2.2 Hydration of the Silicates

The hydration of C_3S and C_2S in Portland cement produces a family of calcium silicate hydrates which are structurally similar but very widely in calcium/silica ratios and the content of chemically combined water. However, since the composition differences among the calcium silicate hydrates have a little effect on their physical characteristics, and the chemical composition of the calcium silicate hydrates in hydrating Portland cement pastes varies with the w/c, temperature, and age of hydration, it has become usual to refer to these hydrates simply as C-S-H (Figure 2.4). This notation does not imply a fixed chemical composition. The stoichiometric reactions can be expressed as



where CH is calcium hydroxide $Ca(OH)_2$, which has the mineral name Portlandite.

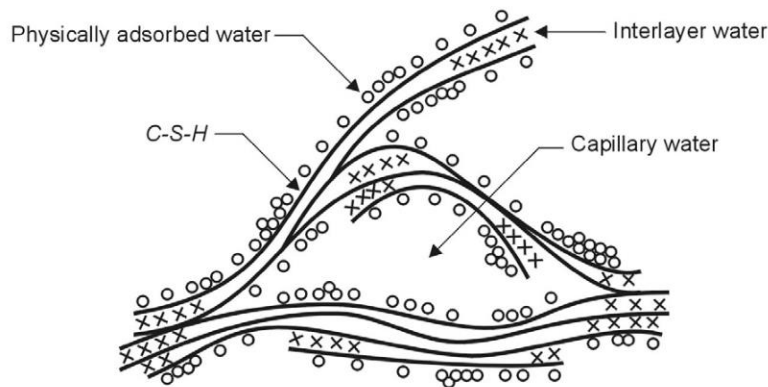


Figure 2.4: Model for C-S-H (Neville, Properties of concrete, 1995)

Therefore, from an engineering point of view both C_3S and C_2S yield to the same hydration products but stoichiometric calculations show that C_3S hydration would produce 61 percent $C_3S_2H_3$ and 39 percent calcium hydroxide, whereas the C_2S hydration would produce 82 percent $C_3S_2H_3$ and 18 percent calcium hydroxide. C-S-H is poorly crystalline and forms a porous solid which exhibits features of a rigid gel. The properties and microstructure of C-S-H will be discussed later. The stoichiometric equations of C_3S and C_2S hydration do not tell anything about the reaction rates. It appears that C_3S hydrates at a much faster rate than C_2S .

Since each component in hydraulic cement features a different hydration rate (Figure 2.5), different properties develop in different time periods.

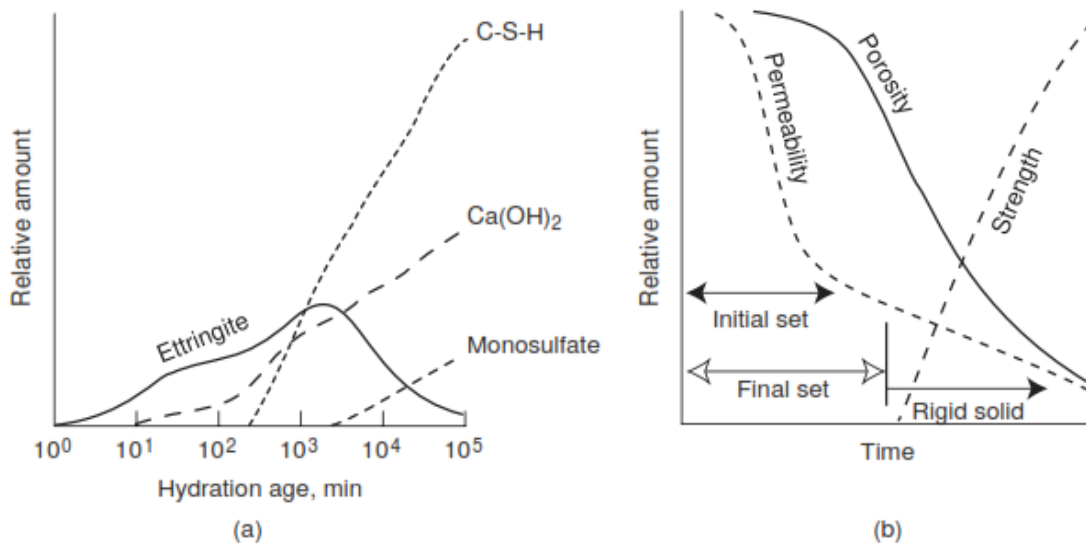


Figure 2.5: (a) Typical rates of formation of hydration products in an ordinary Portland cement paste (Soroka, 1979); (b) Influence of formation of hydration products on setting time, porosity, permeability, and strength of cement paste (Mehta & Monteiro, 2006)

2.3 Morphology of the Main Hydration Products

The morphology of a solid phase can be defined as its shape, form, or structure at the microscopic scale, that is, the scale of nanometers and microns. The morphology of a solid phase inside cement paste and concrete has a greater impact on its macroscopic properties than its chemical composition. One of the major reasons that the science of cement and concrete is so complex is that the morphology of hydration products is both complex and highly variable. It will depend on many factors, including the crystal structure, the mechanism of formation, the temperature, and the space available for a phase to form.

The term *hydrated cement paste* as used here refers to a material formed as the result of chemical reactions between Portland cement compounds and water. When Portland cement is dispersed in water, the liquid phase gets rapidly saturated with various ionic species. Within a few minutes, needle-shaped crystals of ettringite first make their appearance (Figure 2.6a). A few hours later, cement particles begin to dissolve, large prismatic crystals of calcium hydroxide (CH) and very small fibrous crystals of calcium silicate hydrates (C-S-H) begin to fill the space previously occupied by water (Figure 2.6b and Figure 2.6). After a few days ettringite becomes unstable and will eventually

decompose to form monosulfate hydrate, which has a hexagonal-plate morphology. Hexagonal-plate morphology is also the characteristic of hydration products of the aluminates.

The standard approach for studying a complex material such as cement and concrete involves breaking it down into individual phases or steps.

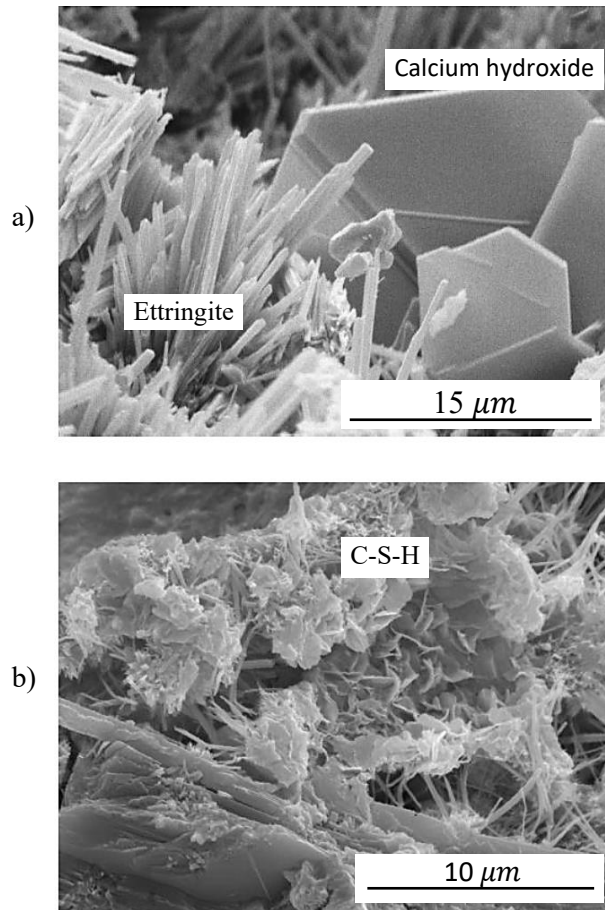


Figure 2.6: SEM images showing the hexagonal crystal habit of calcium hydroxide, needle-like habit of ettringite and the sheet-like habit of C-S-H. In the upper image (a) crystal growth into a void, where space restrictions are minimal, allowing development of euhedral forms.

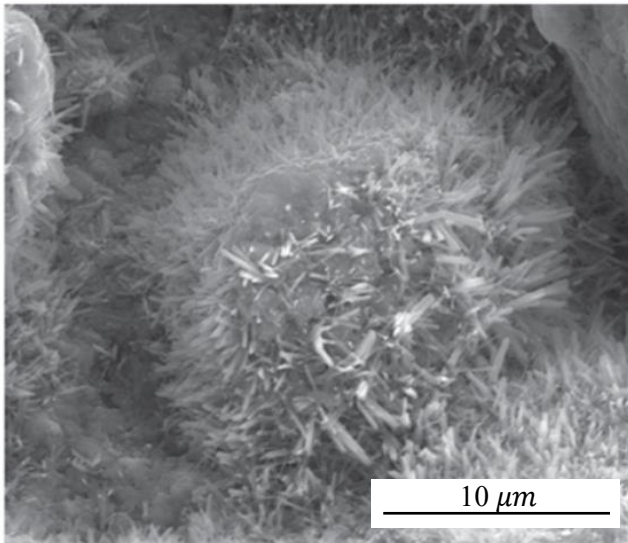


Figure 2.7: The fibrous C-S-H crystals under SEM (Kurdowski & Wieslaw, 2014)

2.3.1 *Calcium Silicate Hydrate (C-S-H)*

C-S-H is not a well-defined compound, the calcium/silicate ratio varies between 1.5 and 2.0 and the structural water content varies even more. C-S-H can have either a poorly crystalline fiber morphology or a reticular network morphology. In older literature, the material is often referred to as C-S-H gel. Even though the exact structure of C-S-H is unknown, several models have been proposed. For instance, according to Powers-Brunauer model (Powers, 1958; Brunauer, 1962), the material has a layer structure with a very high surface area. Depending on the measurement technique, surface area on the order of 100 to 700 m²/g have been proposed for C-S-H, and the strength of the material is attributed mainly to van der Waal's forces between the fibrous particles constituting the material.

C-S-H is not only the most abundant reaction product, occupying up to 50 to 60 percent of the paste volume, but it is also responsible for most of the engineering properties of cement paste. This is because C-S-H forms a continuous layer that binds together the original cement particles into a cohesive whole which is almost entirely responsible in the development of the overall strength. The ability of C-S-H to act as a binding phase arises from its nanometer-level structure.

C-S-H grows outward from the cement particles; thus, it does not take the form of a monolithic solid phase but instead develops an internal system characterized by the presence of *gel pores*. Although the liquid water in the gel pores is not part of the solid

C-S-H phase in a chemical sense, it is physically isolated and thus cannot undergo further chemical reaction with the cement minerals. C-S-H, including its internal gel pores, occupies significantly more volume than the original C_3S and C_2S mineral that it replaces. This causes the layers of C-S-H to expand outward and interconnect into a continuous phase, causing the cement paste to first set and then harden into a strong solid. The increase in the volume of solid phases causes the capillary pore system to decrease in volume and, if the w/c is reasonably low, to become discontinuous. This greatly decreases the permeability of the cement paste, meaning that it is more difficult for liquid water and dissolved ions to move through the pore system.

When a hydrated cement paste is viewed in a microscope two apparently different types or morphologies of C-S-H can be seen. One of these is less dense (more porous) and appears to occupy space that was originally water-filled, while the other appears denser and is found primarily in areas originally occupied by the cement particles. Figure 2.8 indicates that the less dense morphology, which can be called *low-density C-S-H*, forms rapidly during the early hydration period surrounding setting; while the denser morphology, which can be called *high-density C-S-H*, fills in more slowly over days and weeks. Since the most important characteristic of C-S-H is its tendency to grow outward into the porosity, the low-density C-S-H is much more important than the high-density C-S-H.

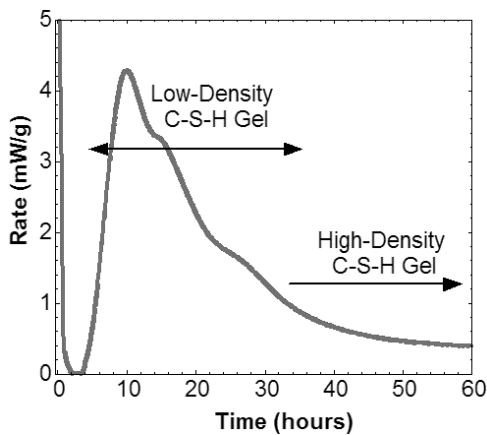


Figure 2.8: Rate of hydration vs. time, showing when the low-density and high-density morphologies form

2.3.2 *Calcium Hydroxide (CH)*

Abbreviated as CH, it constitutes 20 to 25 percent of the volume of solids in the hydrated paste. It is also known by its mineral name *Portlandite*. CH forms as crystals with a wide range of shapes and sizes, depending primarily on the amount of room available for growth. Crystals that initially form in the capillary pores tend to form irregular hexagonal plate-shaped crystals several microns across, large enough to be seen in an optical microscope.

A significant proportion of the CH forms as an intimate mixture with C-S-H, particularly the low-density C-S-H. Since their growth is hindered by the surrounding solid, these crystals tend to be much smaller, with many under 1 μm in diameter. There is some evidence of nanometer-scale CH in cement pastes as well.

CH contributes slightly to the strength and impermeability of the paste, because it reduces the total pore volume by converting some of the liquid water into solid form. However, CH is much less important than C-S-H with respect to strength development. From the durability point of view, CH contributes to the alkalinity of the cement paste pore solution, which is important to delay carbonation. Moreover, it must be noticed that CH is a weak link in cement and concrete, since it is the most soluble of the hydration products. If the paste is exposed to fresh water, the CH will leach out (dissolve), increasing the porosity and thus making the paste more vulnerable to further leaching and chemical attack.

Blended cement pastes have little or no CH, as the CH that forms from cement hydration is consumed along with the mineral admixtures to form additional C-S-H. This has beneficial effects on the strength and permeability, but detrimental effects on carbonation resistance can be observed.

2.3.3 *Calcium Sulfoaluminates Hydrates*

Calcium sulfoaluminates hydrates are the hydration products that form from C_3A and C_4AF minerals; they occupy 15 to 20 percent of the solid volume in the hydrated paste and, therefore, play a minor role in the properties related to the microstructure. It has already been said that needle-shaped prismatic crystals of ettringite form during the early stages of hydration. This ettringite eventually transforms to monosulfate hydrate,

which forms hexagonal-plate crystals. The presence of monosulfate hydrate in Portland cement concrete makes the concrete vulnerable to sulfate attack.

2.3.4 *Capillary Porosity*

The most important phase not discussed above is the capillary porosity, which can occupy anywhere from a few percent to 20 percent or more of the paste volume, depending on the degree of hydration and the initial w/c. The morphology of the pore system of cement paste is discussed in detail later. Under most conditions, the pore system of concrete will be at least partially filled with the aqueous pore solution. This important phase acts as a link between the solid hydration products and the outside environment.

2.3.5 *Unhydrated Clinker Grains*

Most cement pastes will contain some unreacted cement, in the form of cores of the largest original particles. These do not contribute to the engineering properties, but neither do they detract from them, except for the potential loss of hydration product. High strength concrete is made by using such low w/c values that a significant fraction of the cement must remain unhydrated due to a lack of space for hydration products to form.

2.3.6 *Other Phases*

Other solid phases that may be found in normal cement pastes include hydrogarnet, which is a calcium aluminate phase with a cubic structure, brucite ($\text{Mg}(\text{OH})_2$), which has the same structure and morphology as CH, and syngenite (KCS_2H), which is found only in very high-alkali pastes. None of these have any engineering importance, although their presence or absence can provide important information about the original cement composition to a cement scientist or petrographer.

2.4 **Microstructure of the Hydrated Cement Paste**

Microstructure is the type, amount, size, shape and distribution of phases present in a solid constitute. On the other hand, the term *macrostructure* is generally used for the gross microstructure visible to the human eye (the limit of which is approximately 200

μm). Therefore, microstructure is the subtle structure of a material that is resolved with the help of a microscope. Moreover, it is essential to note that the cement paste microstructure changes and develops with time (Figure 2.8).

As can be seen in Figure 2.10, the structure of a hydrated cement paste does not look homogeneous if observed at a relatively low-magnification ($200\times$). In fact, while some areas are dense, the others are highly porous. In the porous area, it is possible to resolve the individual hydrated phases by using higher magnifications. For example, CH crystals, long and slender needles of ettringite, and aggregation of small fibrous crystals of C-S-H can be seen at $2000\times$ and $5000\times$ magnifications.

The hydration products in cement paste do not exist in isolation, but are entangled with one another at the scale of microns and even nanometers. Thus, to describe the microstructure of cement past is important to focus on the overall distribution of solid phases and porosity, rather than the structure of the individual solid phases.

A basic but useful description of cement paste microstructure is comprised of just three "phases", as showed in Figure 2.11. The various phases are neither uniformly distributed nor are they uniform in size and morphology.

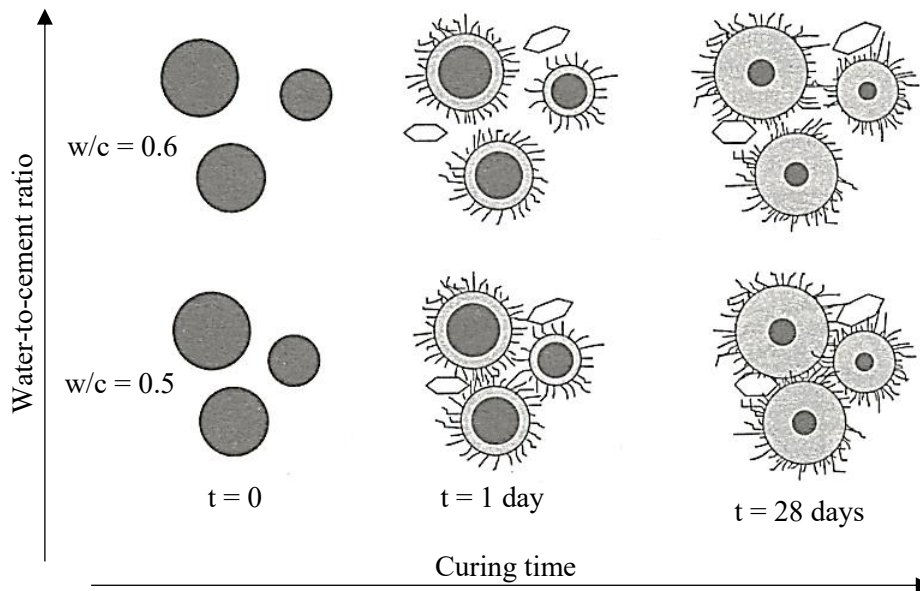


Figure 2.9: Development of the microstructure of a Portland cement during hydration (Bertolini, 2006)

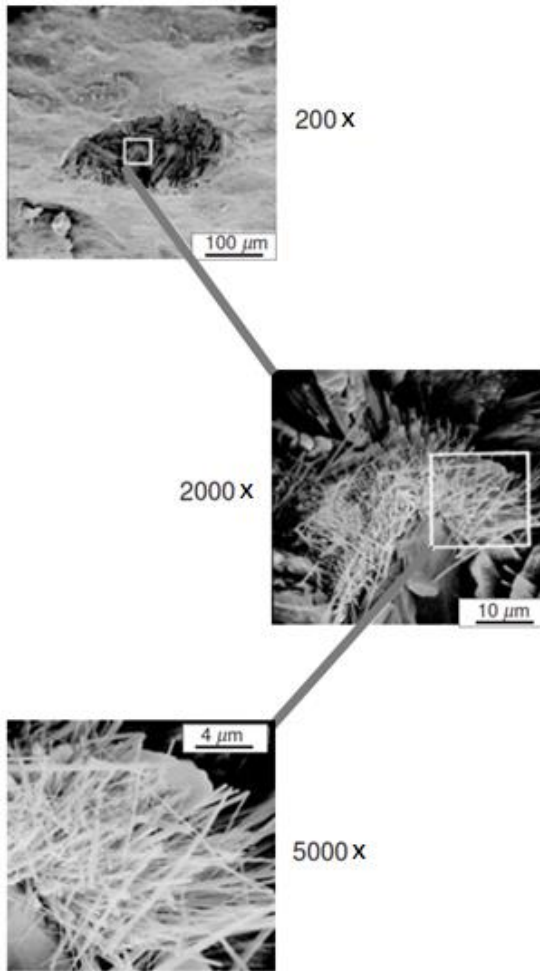


Figure 2.10: Microstructure of a hydrated cement paste (Mehta & Monteiro, 2006)

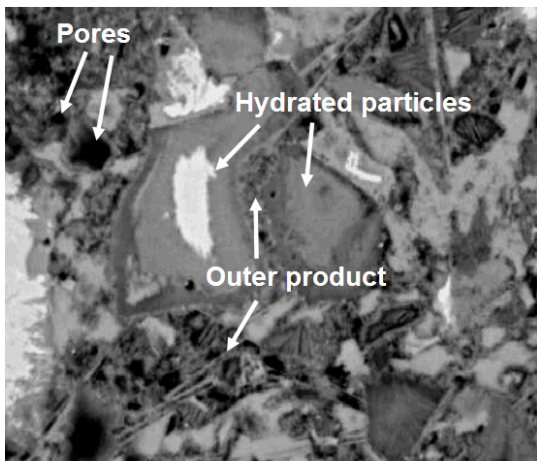


Figure 2.11: Backscattered SEM image of a mature cement paste showing the main microstructural feature

2.4.1 *Hydrated Cement Particles*

They consist of high-density C-S-H, and in some cases an inner core of unhydrated cement. These behave as individual solid particles within a continuous matrix analogous to the aggregate particles in concrete.

2.4.2 *Outer Hydration Product*

This is the continuous phase that grows within the capillary pore space and binds the cement together. It plays a role similar to cement paste in concrete. It consists of solid C-S-H, gel pores, calcium hydroxide, and calcium sulfoaluminate phases. The most important individual phase is the low-density C-S-H (and its gel pores), because its high surface area gives this phase its strength.

2.4.3 *Large Pores*

These consist of true capillary pores, entrapped air voids, and the entrained air system. These features appear as discrete black voids in a microscope. The large pore system can be continuous or discontinuous, depending on the degree of hydration and starting w/c, but this cannot be determined from microscopy.

If several specimens of concrete are examined at various time intervals, it can be seen that the volume of capillary voids in the hydrated cement paste decrease with decreasing of the w/c.

2.5 **Microstructure of Concrete**

Concrete has a highly heterogeneous structure. It is very difficult to constitute realistic models of its microstructure from which the behavior of the material can be reliably predicted. From the examination of a cross section of concrete (Figure 2.12) at the macroscopic scale, two phases can be easily distinguished:

- Aggregate particles;
- Binding medium, composed of an incoherent mass of the hydrated cement paste.

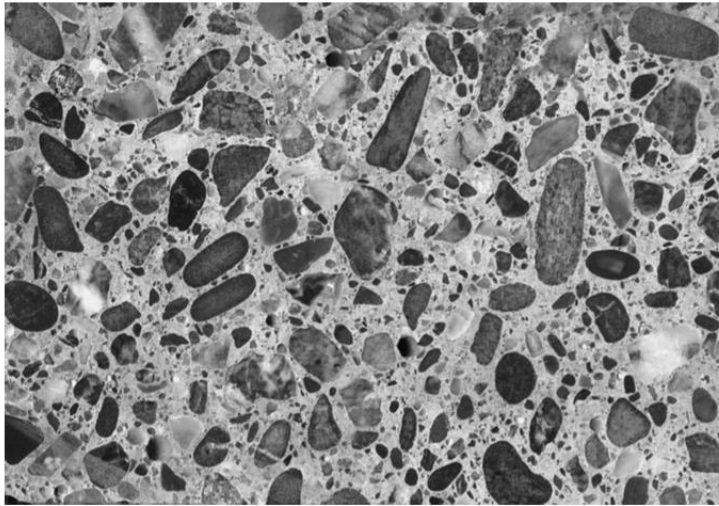


Figure 2.12: Polished section from a concrete specimen (Mehta & Monteiro, 2006)

At a macroscopic level, concrete may be considered as a two-phase material. If the microscopic level is then analyzed the complexities of the concrete microstructure become evident. For instance, in some areas the hydrated cement paste mass appears to be as dense as the aggregates, while in others it is highly porous.

For a well-hydrated cement paste, the inhomogeneous distribution of solids and voids can perhaps be ignored when modelling the behavior of the material. However, microstructural studies have shown that this cannot be done for the hydrated cement paste present in concrete. This is because the microstructure of hydrated cement paste in the vicinity of large aggregate particles is usually very different from that of bulk paste or mortar in the system. The so called *interfacial transition zone* (ITZ) can be identified, which represents a small region (typically 10 to 50 μm thick) next to the particles of coarse aggregates and is generally weaker than both the aggregate and the bulk hydrated cement paste.

Another unique feature of the concrete microstructure is the fact that each phase can be further divided into different phases. For instance, each aggregate particle may contain several minerals in addition to microcracks and voids. Both the bulk hydrated cement paste and the ITZ contain a heterogeneous distribution of different types and amount of solid phases.

And finally, unlike other engineering materials, the microstructure of concrete is not an intrinsic characteristic of the material because the hydrate cement paste and the ITZ are subjected to change with time, environmental humidity and temperature.

2.6 The Pore Structure of Cement Paste

All the engineering properties of cement and concrete are related to the porosity, and characterization of the pore system is often a better predictor of performance than characterization of the solid phases. Characterizing the porosity of hydrated cement paste is difficult. In fact, due to the large range of pore sizes (from a few nanometers to tens of micrometers) no single technique can adequately characterize all the important components of the pore system.

There are three general parameters of interest in the pore system, that is, *total porosity*, *pore size distribution*, and *specific surface area*. The specific surface area is the area of the interface between cement paste and the pore system per unit amount of material. It arises almost entirely from the low-density C-S-H, which is the most important phase in cement paste.

Experimental techniques for characterizing the pore system can be divided into two categories: those that involve the intrusion of a fluid into the pore system (pyknometry, mercury intrusion, gas sorption), and those that use particles or fields to probe the material (small-angle scattering, NMR). The latter has a significant advantage, that is, the specimen does not need to be dried. However, these techniques require highly specialized equipment and the data are more difficult to interpret.

Measurement of the specific surface area is by far the most commonly performed analysis of cement paste pore systems. This attests the utility of having a single parameter such as surface area to describe the overall fineness of the microstructure on a nanometer scale and to correlate closely to important properties such as durability. Values reported for surface area in the literature vary over two orders of magnitude, depending on the considered technique and the interpretation of the results. This variability is related to different factors, the most important of which is the difficulties with data analysis. For example, obtaining quantitative surface area values from scattering and NMR techniques is difficult due to the many models and assumptions needed to convert the raw data. The specific surface area varies with the age of the paste, the w/c, the cement composition, and other processing variables, which determine the amount of finely divided hydration product in the material.

2.6.1 Classification of Pore Sizes

The typical sizes of both the solid phases and the voids in hydrated cement paste are illustrated in Figure 2.13, whereas typical pore size distribution plots of several hydrated cement paste specimens tested by the mercury intrusion technique are shown in Figure 2.14.

It is important to note that it is not the total porosity but the pore size distribution that actually controls the strength, permeability, and volume changes in a hardened cement paste. Pore size distributions are affected by water-to-cement ratio, and the age (degree) of cement hydration.

Two possible classifications of pore sizes are listed in Table 2.3. The durability of a cement-based material is largely influenced by its permeability, which is in turn influenced by the pore structure of the cement paste. Even though mechanical strength is essentially influenced by the whole porosity, it has been shown (Molhotra & Carino, 1991) that only the pores with a radius of more than 50 nm contribute to the water permeability. These pores are commonly called *macropores* (Aligizaki, 2006).

Table 2.3: Classification of pore sizes according to the general classification by IUPAC and concrete science technology

| According to IUPAC (Chefdeville, 1953) | | According to Mehta (Mehta & Monteiro, 2006) | |
|--|-----------|---|-------------|
| Name | Diameter | Pore type | Size range |
| Micropores | < 2nm | Inter-particle space between C-S-H sheets | 1 ÷ 3 nm |
| Mesopores | 2 ÷ 50 nm | Capillary pores (low w/c) | 10 ÷ 50 nm |
| Macropores | > 50 nm | Capillary pores (high w/c) | 3 ÷ 5 μm |
| | | Entrained air voids | 50 μ ÷ 1 mm |

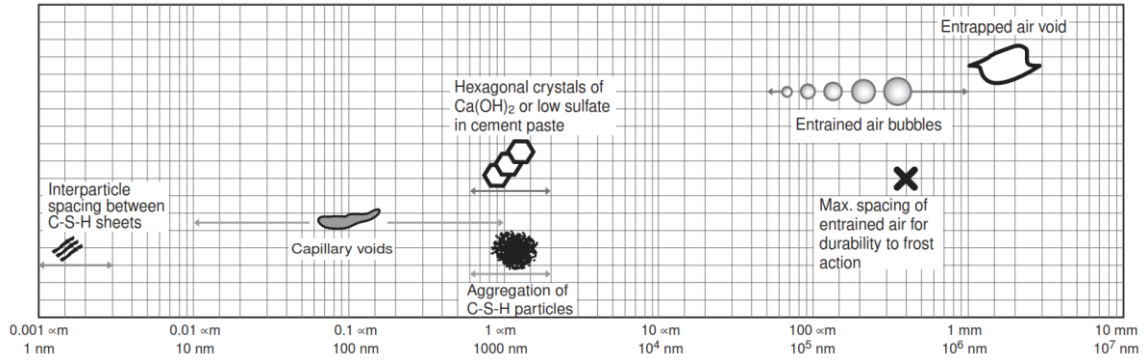


Figure 2.13: Dimensional range of solids and pores in hydrated cement paste (Mehta & Monteiro, 2006)

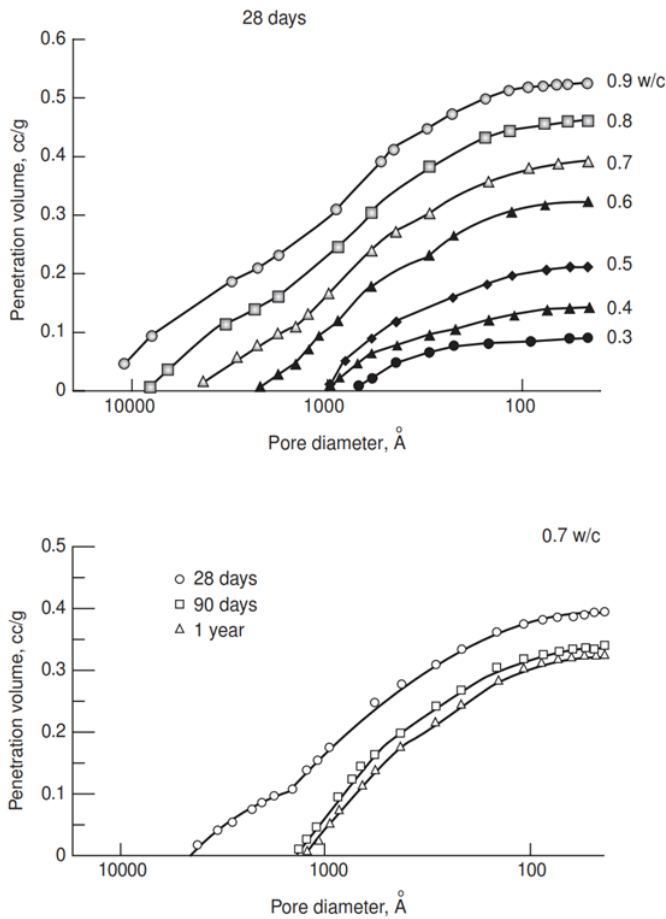


Figure 2.14: Pore size distribution in hydrated cement pastes (Mehta & Monteiro, 2006)

The main types of pores in hydrated cement paste are:

- *Interlayer space in C-S-H.* Powers assumed the width of the interlayer space within the C-S-H structure to be 18 Å (Powers, 1958) ($1 \text{ \AA} = 10^{-10} \text{ m}$) and that it

accounts for 28 percent porosity in solid C-S-H. However, relatively recent work by Feldman and Sereda suggested that these spaces vary from 5 to 25 Å (Feldman & Sereda, 1968). This interlayer space is too small to have a deleterious effect on the strength and the permeability of hydrated cement paste.

- *Capillary voids.* Capillary pores represent the space not filled by solid components of the hydrated cement paste. Therefore, the volume and size of the capillary voids depend on the distance between unhydrated cement particles in the freshly mixed cement paste and the degree of hydration (Kurtz & Long, 1943). In well hydrated and low w/c ratio pastes, the capillary voids may range from 10 to 50 nm, whereas in high w/c ratio pastes at early ages of hydration the capillary voids may be as large as 3 to 5 µm (Chefdeville, 1953).
- *Air Voids.* Air voids in concrete are due to either entrapped air during casting or intentionally entrained by using air-entraining agent. The entrapped air may be as large as 3 mm and the entrained air may range from 50 to 200 µm. Therefore, both the entrapped air voids and entrained air void are much bigger than the capillary voids and have a significant role in the permeability of concrete.

2.6.2 *Factors Influencing Pore Structure*

The main factors influencing the pore structure of the hydrated cement paste include the w/c ratio, degree of hydration, use of supplementary cementitious materials, the presence of chemical admixtures and curing conditions. In general, the higher the w/c ratio for a given degree of hydration, the higher will be the volume of larger pores in the hydrated cement paste (Klieger & Lamond, 1994). Additionally, the type of cement used, and its age may also influence the pore structure.

The use of supplementary cementitious materials, such as pulverized-fuel ash (also known as fly ash), microsilica (also known as silica fume) and metakaolin, is extremely useful in refining the pore structure of concrete. This refining effect is obtained mainly by producing secondary C-S-H.

The pore structure of hydrated cement paste is also greatly influenced by the presence of different chemical admixtures. This is mainly due to the change in the degree of hydration of cement. For example, at a constant w/c ratio, the addition of superplasticizer

is variously reported to refine the pore structure (Mor & Mehta, 1984; Khatib & Mangat, 2002).

Proper curing of concrete is widely recognized as a necessity for assuring adequate performances in terms of both mechanical strength and durability. To achieve proper curing conditions, it is necessary to minimize evaporation of the mix water, but it is equally recognized as important to provide a source of external or internal curing water to replace that consumed by chemical shrinkage during the hydration, which would lead to the creation of coarse capillary pores. For a w/c ratio greater than approximately 0.42, there is sufficient water in the mix such that complete hydration of the cement can be achieved theoretically without supplying additional water to the cement paste. Even if complete hydration was achievable, the lack of additional curing water could still result in the creation of relatively large pores within the final microstructure. In this case, the addition of curing water would assure that all pores remain water-filled and eligible as locations for the precipitation and growth of hydration products throughout the curing process.

CHAPTER 3

TRANSPORT PROCESSES IN CEMENT-BASED MATERIALS

Since any cement-based material has a porous structure, it can be penetrated, through its pores, by gasses (e.g., nitrogen, oxygen, and carbon dioxide present in the atmosphere), ions, and liquid substances (e.g., water, in which various ions are dissolved). The property of a cement-based material to allow the ingress of gasses and liquid substances is called *permeability*. This property is not only important for water-retaining structures but is a decisive factor in the durability of the structure. The mechanisms of transport and the main parameters that define them are discussed in this chapter.

Figure 3.1 provides a schematic of mechanisms involving transport of gasses, ions, and liquid substances through the porous material. transport of these substances may occur by *capillary-suction-driven flow* (absorption), *concentration-driven flow* (diffusion), *pressure-driven flow* (permeation) or *electrical transport* (migration). Generally, the overall potential for the ingress of the substances into concrete by these four modes is referred to as its permeability.

- *Absorption* is the process by which the cementitious material takes in a fluid due to capillary suction in pores to fill the space within the material. (Concrete Society, 1988; Rose, 1965)
- *Diffusion* is the random motion of free molecules or ions in a saturated pore system under the influence of a concentration gradient (Concrete Society, 1988; Feldman & Sereda, 1968). The diffusion can be in either gaseous or ionic form. A typical example of gaseous diffusion is the diffusion of carbon dioxide into the cementitious material, whereas a typical example for ionic diffusion is chloride diffusion (Nanukuttan, 2007).
- *Permeation* is the process by which a fluid passes into and through the body of the cement-based material under a pressure difference (Concrete Society, 1988;

Feldman & Sereda, 1968; Mercer, 1945). A typical example of permeation is what occurs in deep-water marine structures or the bases of retaining structures.

- *Migration* involves the transport of ions in solution under an electrical field.

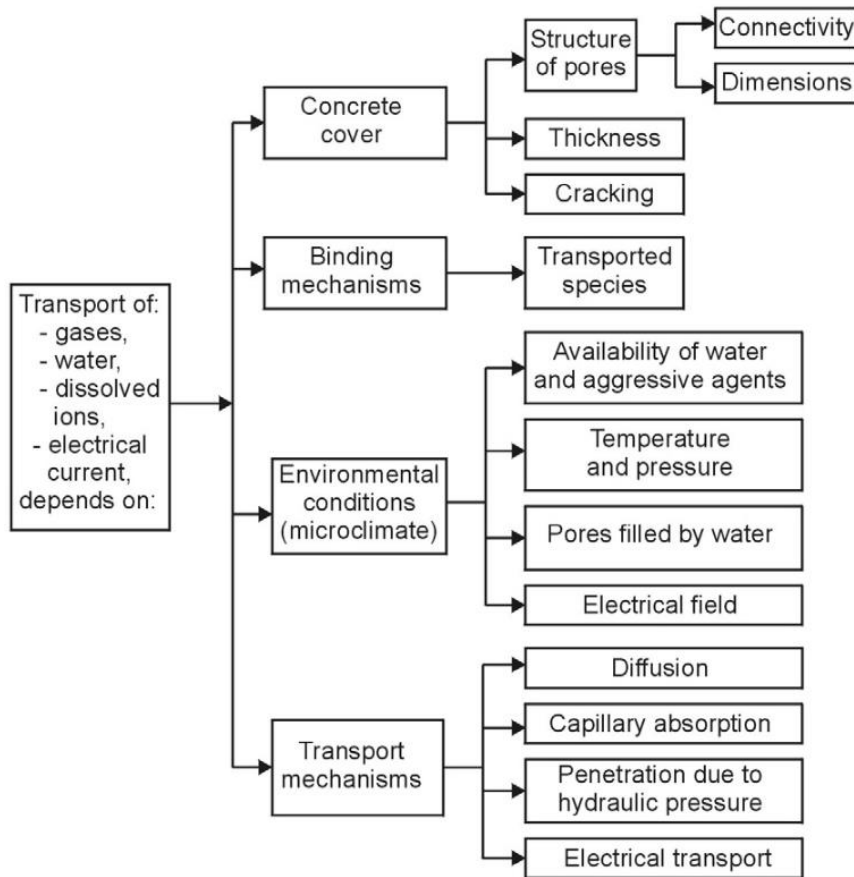


Figure 3.1: Principal factors involved in the transport processes in concrete (Bertolini, Elsener, Pedeferri, Redaelli, & Polder, 2004)

3.1 Water in the Hydrated Cement Paste

The actual amount of water in the pores of the hydrated cement paste, namely moisture content, depends on the humidity of surrounding environment. In addition, it is a quite concentrated aqueous solution, since several ions produced by the hydration of cement are dissolved in the pore liquid.

Water may be present in the hydrated cement paste in many forms that may be classified according to the degree of difficulty with which it can be removed (Mehta & Monteiro, 2006).

3.1.1 *Capillary Water*

The water contained in capillary pores accounts for the greatest part of water in concrete and is the most important part with regard to diffusion mechanisms.

The aqueous solution contained in pore larger than 50 nm in diameter (macropores) can be considered free of bonding forces with the solid surface. Therefore, as the relative humidity of the environment decreases below 100%, this water will evaporate without causing any significant shrinkage in the cement paste. The transport properties of this solution seem to be analogous to those of a bulk solution, that is, the mobility of various ions and thus the electrical conductivity, can be considered analogous to those of an electrolytic solution having the same composition.

The aqueous solution contained in pore smaller than 50 nm in diameter is influenced by chemical and physical interactions with the solid surface. As a result, it will evaporate at lower values of the relative humidity as the diameter of the pores decreases. In this case, evaporation can produce significant shrinkage of the cement paste. In addition, the mobility of ions is affected by chemical and physical interactions between the liquid and the solid and is therefore lower than that of a solution of the same composition.

Figure 3.2 represents the capillary pores as spherical cavities connected by narrow capillary cylinders whose dimensions are considered to be statistically distributed. For a concrete that is exposed to the atmosphere of a certain relative humidity, pores whose diameters are below a given value are filled with water, while those with diameters above this value are filled with air. The presence of pores that are both filled with water and interconnected with each other has a remarkable influence on the kinetics of transport properties. On the one hand, the presence of these pores blocks processes that take place easily in the gaseous phase (e.g., O₂ and CO₂ diffusion); on the other hand, it facilitates processes that occur in aqueous solution (e.g., diffusion of chlorides, or ions in general)

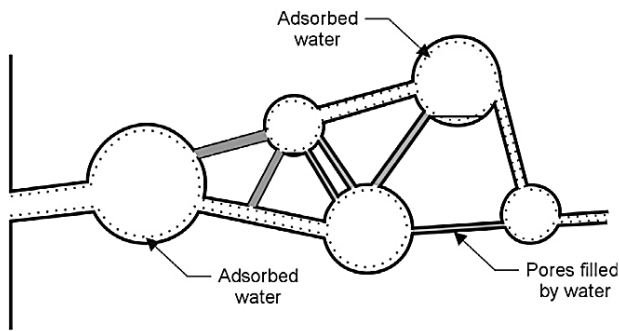


Figure 3.2: Representation of water present in capillary pores in concrete in equilibrium with a non-saturated atmosphere (CEB, 1992)

3.1.2 Adsorbed Water

Even if water has completely evaporated from the capillary pores, some water still remains adsorbed to the inner surface in the form of a very thin layer. This water can be removed if the external humidity falls below 30% and it contributes little to transport phenomena. However, its removal causes shrinkage of the cement paste and influences creep behavior.

3.1.3 Interlayer Water

The water retained between the C–S–H layers evaporates if the external humidity falls below 11%. This water does not contribute to transport phenomena, since gel pores are too small to allow transport processes at any appreciable rate. However, just like adsorbed water, its removal influences shrinkage and creep.

3.1.4 Chemically Combined Water

Chemically combined water is an integral part of C–S–H or other hydration products. This water can only be released when the hydrates decompose on heating, which happens at temperatures higher than 1000 °C. It does not contribute to any transport phenomena.

If a concrete exposed to the atmosphere under equilibrium conditions and in the absence of wetting is considered, the water content can be related to the relative humidity of the environment, as depicted in Figure 3.3.

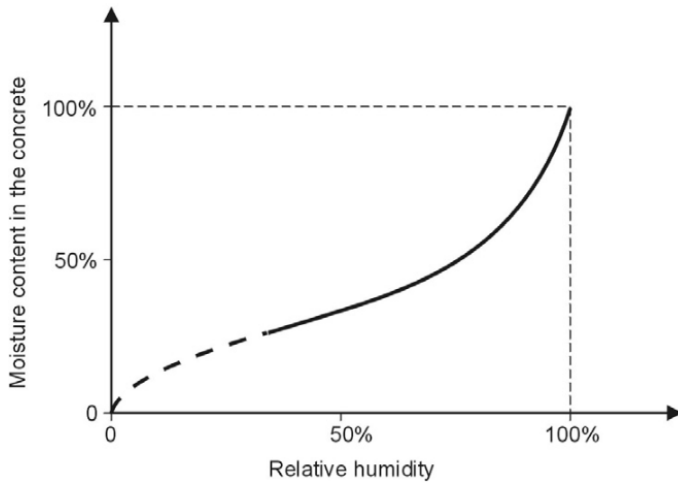


Figure 3.3: Schematic representation of water content in the pores of concrete as a function of the relative humidity of the environment, in conditions of equilibrium (CEB, 1992)

3.2 Diffusion

Diffusion of aggressive species, such as gases (e.g., O₂ and CO₂) and ions (e.g., Cl⁻ and SO₄²⁻), happens by the effect of a concentration gradient (Figure 3.4). Gases diffuse much more rapidly through open pores than through water-saturated ones, while ions diffuse only when dissolved in pore water; moreover, the diffusion is more effective in saturated than in partially saturated pores.

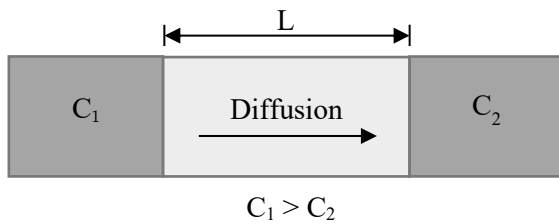


Figure 3.4: Schematic representation of the diffusion process (Bertolini, 2006)

The unidirectional and constant mass transfer by diffusion is known as *stationary diffusion*. The Phenomenon is described by *Fick's first law*:

$$F = -D \frac{dC}{dx} \quad (3-1)$$

where: F is the flux (kg/m² s) and C is the concentration of the diffusing species (kg/m³) present at distance x from the surface. D is the diffusion coefficient (m²/s), which depends

on the diffusing species, on the characteristics of the concrete (every aspect influencing the pore structure) and on the environmental conditions. This coefficient can change as a function of position and time, following variations in the pore structure (i.e., due to hydration of the cement paste), or in the external humidity (thus the degree of saturation of pores) or the temperature.

Diffusion rarely reaches stationary conditions in concrete structures. Therefore, *nonstationary diffusion* takes place, the flux depends on time t , and the phenomenon is governed by *Fick's second law*:

$$\frac{\partial C}{\partial t} = D \frac{\partial^2 C}{\partial x^2} \quad (3-2)$$

Eq. (3-2) is usually integrated under the following assumptions:

- the concentration of the diffusing ions which is measured on the surface of the concrete is constant in time and is equal to C_s ($C = C_s$ for $x = 0$ and for any t);
- the concentration of the diffusing ions inside concrete is initially null ($C = 0$ for $x > 0$ and $t = 0$);
- the coefficient of diffusion D is constant through time;
- concrete is homogeneous, so that D does not vary through the thickness of concrete.

Thus, the solution obtained is:

$$C(x, t) = C_s \left[1 - \operatorname{erf} \left(\frac{x}{2\sqrt{Dt}} \right) \right] \quad (3-3)$$

where $\operatorname{erf}(z)$ is the error function whose values have been tabulated:

$$\operatorname{erf}(z) = \frac{2}{\sqrt{\pi}} \int_0^z e^{-t^2} dt \quad (3-4)$$

Eq. (3-3) is often utilized to describe mathematically the experimental profiles of chloride concentration found in nonsteady-state laboratory tests or from structures exposed in the field.

Species that diffuse into concrete can bind to a certain degree with components of the cement matrix. For instance, chlorides bind with aluminate phases or are absorbed on

C-S-H, whereas carbon dioxide reacts with alkaline components, particularly calcium hydroxide. The gradual consumption of these compounds modifies the conditions of diffusion, which can no longer simply be described by Fick's second law but require a corrective term. Since it is difficult to estimate the corrective term, often the effects of chemical reactions in concrete are disregarded (this is particularly true for chloride penetration).

It has been shown (Yu, Sergi, & Page, 1993) that binding can be neglected in the first approach, thus the diffusion coefficient is termed *apparent* (D_{app}). Therefore, Eq. (3-3) is only used as a mathematical tool to analyze experimental chloride profiles, and D_{app} is used instead of D .

3.3 Capillary Suction

When water comes into contact with a porous material, it is absorbed due to the underpressure in the pores. This phenomenon is called capillary suction and it depends on the surface tension, viscosity, density of the liquid, angle of contact between the liquid and the pore walls, and the radius of the pore.

The contact angle is small due to the presence of molecular attraction between the liquid and the substrate (i.e., between water and cement paste). Therefore, a drop will spread on a flat surface and the meniscus of a capillary pore will rise above the level of the surrounding liquid and be concave toward the dry side (Figure 3.5). This aspect can be changed by means of hydrophobic treatment.

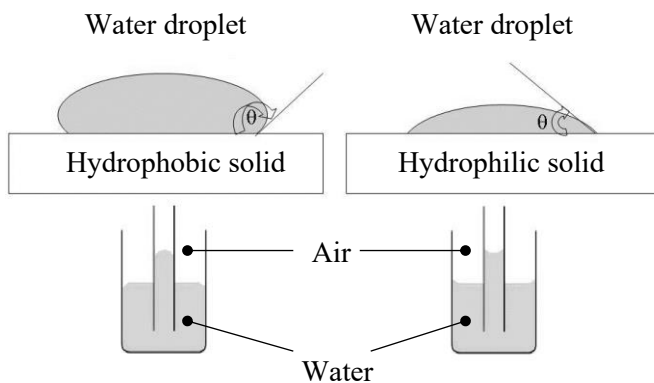


Figure 3.5: Behavior of a hydrophilic material and of a Hydrophobic one (Bertolini, 2006)

Capillary action is stronger as the pore dimensions decrease. On the other hand, the smaller the pores become, the slower the transport will be due to increasing friction. Regarding the usual range of pore dimensions in concrete, a more porous concrete absorbs more water and faster than a denser concrete.

A sorptivity test is usually carried out to measure capillary suction in concrete. In this test, the bottom face of a previously dried sample is placed in contact with water at atmospheric pressure. Capillary absorption (i , g/m² for mass or m³/m² for volume) is the mass (or volume) of liquid absorbed per unit of surface. The following equation describes the development of i as a function of time:

$$i = S t^a \quad (3-5)$$

Laboratory tests are used to empirically derive the parameter S , which is termed *capillary water absorption coefficient*. For very porous materials a square root law is generally used ($a = 0.5$), while in concrete with a low w/c ratio experimental results showed a better fitting if the square root law is changed with exponent lower than 0.5 (Elsener, Flückiger, & Böhni, 2000).

S is expressed in g/(m²s^{0.5}) (if mass change is determined) or m/s^{0.5} (if absorbed volume is determined) and is adopted as a representative parameter of the characteristics of concrete with regard to capillary absorption. Typical values for the parameter S are listed in Table 3.1.

The parameter S depends on various factors; the main one is the degree of drying to which the samples have been previously subjected. For example, oven desiccation at 105 °C modify the water content in hydration products and cause microcracks that favor capillary absorption. If the drying temperature is decreased, the procedure will require much longer time. In EN 13057 a procedure for capillary absorption tests on repair materials is suggested, involving oven drying at 40 °C (EN 13057, 2002). This method of drying is probably the best compromise between quickly establishing low-moisture condition and avoiding damage to the microstructure.

A procedure for testing water absorption of concrete is given by BS 1881 part 122 (British Standards Institution, 1983). It involves placing specimens (cubes, cores) for 72 hours in a drying oven in which the temperature is controlled at 105 °C. After cooling down for 24 hours in the air, specimens are weighed and then immersed for 30 minutes

in a tank containing water with a temperature of 20 °C. Finally, the specimens are weighed after removing all free water from the surface. The water absorption is calculated as the increase in mass resulting from immersion as a percentage of the mass of the dry specimen. As an additional result, the wet density is calculated. It is worth noting that the high temperature used during this test to dry the specimens may damage their microstructure and thereby render the result nonrepresentative for concrete under field conditions.

Table 3.1: Typical values for the parameter S

| Type of concrete | w/c | Compressive strength, MPa | Typical values of S , $\text{g}/(\text{m}^2\text{s}^{0.5})$ |
|------------------|------|---------------------------|---|
| Normal-strength | 0.50 | 43 | 1.5 |
| High-strength | 0.3 | 90 | 0.7 |

3.3.1 Capillary Water Absorption Coefficient

The coefficient S is one of the most important features of a building material, because it governs the liquid moisture movement into it and expresses the rate of absorption of water due to capillary forces.

There are many European and international standards and recommendations by which researchers estimate the capillary water absorption coefficient of building materials. European standard EN 1015-18 (EN 1015-18, 2002) refers to hardened mortars, EN 13057 (EN 13057, 2002) describes the measurement of the capillary water absorption of hardened concrete, EN 480-5 (EN 480-5, 2005), describes the determination of the water capillary absorption coefficient of concrete, mortars and grouts.

The experimental setup for a water absorption experiment as described in the EN standards and recommendations is quite common (Hall, 1989). After drying each sample at 60 °C to constant mass in a hot-air oven, its dry mass is measured. Each sample is cooled to room temperature and is putted on a tray of distilled water. The position of the waterfront is gradually approaching the opposite side of the sample and the water intake is governed by capillary and viscous forces. The quantity of the absorbed water is

measured at standard time intervals by weighing the specimen. Each weighing should be completed as quickly as possible (typically within 30 seconds).

According to EN 1015-18 (EN 1015-18, 2002), the capillary water absorption coefficient is the gradient of the straight line obtained by plotting the cumulative mass of water absorbed per unit area against the square root of time (t) obtained from this first stage according to the following equation:

$$S = \frac{\Delta m}{A \sqrt{t}} \quad (3-6)$$

where A (m^2) is the surface area of the cross section of the specimen (the surface in contact with water) and Δm (g) is the mass of the absorbed water.

Many researchers have investigated the capillary water absorption coefficient as a part of their research works. However, they have been using different standards every time (Karagiannis, Karoglou, Bakolas, & Moropoulou, 2016). While the experimental procedure estimating the capillary water absorption coefficient of building materials remains unquestionable, the comparison of S values is difficult since a building material is often observed to present different S values depending on the estimation method.

3.4 Permeation

When a liquid (assumed incompressible and entirely viscous) penetrated concrete that is previously saturated by a liquid due to a pressure difference, the flow through the pores is defined by Darcy's law (Figure 3.6):

$$\frac{dq}{dt} = \frac{K \Delta P A}{L \mu} \quad (3-7)$$

where: dq/dt is the flow (m^3/s), μ is the viscosity of the fluid ($\text{N s}/\text{m}^2$), K is the intrinsic permeability of concrete (m^2), ΔP is the pressure head applied (Pa), A is the surface of the cross section (m^2), and L is the thickness (m) of the specimen.

Permeation tests are usually carried out with water. One side of a concrete sample is placed in contact with water (with pressure up to 10 bar) and either the depth of penetration by water in a given time, the time necessary for water to penetrate the entire thickness of the sample, or the flow through the sample are measured.

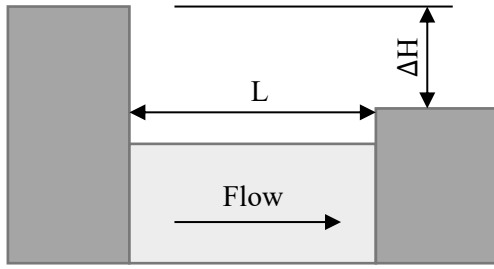


Figure 3.6: Flow due to the Hydraulic head (Bertolini, 2006)

If the penetration involves the entire thickness of the sample, so that it is possible to measure the flow, Eq. (3-7) can be written as:

$$\frac{dq}{dt} = \frac{k \Delta H A}{L} \quad (3-8)$$

where: dq/dt is the flow (m^3/s), ΔH (m) represents the height of the column of water pressure differential across the sample ($\Delta P = \Delta H \cdot \delta \cdot g$, with δ is the water density and g is the acceleration of gravity). In this case the coefficient of permeability $k = K \delta g / \mu$ is measured in m/s and depends on the density and on the viscosity of the liquid (for water $K \cong 10^{-7}k$). Typical values for k are listed in Table 3.2.

In hardened cement paste, at any point in time during the hydration process, the size and continuity of the pores would control the coefficient of permeability. The mixing water (w/c ratio) is indirectly responsible for the permeability of hydrated cement paste because its content determines, first, the total space and, subsequently, the unfilled space after the water has been consumed by either hydration process and evaporation. Therefore, it is clear that k decreases as the w/c ratio decreases and as hydration proceeds.

Table 3.2: Typical values for the coefficient of permeability (Bertolini, Elsener, Pedferri, Redaelli, & Polder, 2004)

| w/c (-) | Typical values of k (when the liquid is water), m/s |
|---------|---|
| 0.75 | 10^{-10} |
| 0.45 | $10^{-12} - 10^{-11}$ |

With the progress of hydration, as the capillary porosity decreases, so does the coefficient of permeability (Table 3.3). However, there is no direct proportionality between the two. For instance, when the capillary porosity decreases from 40 to 30 percent, the

coefficient of permeability drops by a much greater amount. However, a further decrease in the porosity from 30 to 20 percent brings only a small drop in permeability. This happens because at the beginning, as the cement hydration process progresses, even a small decrease in the total capillary porosity is associated with considerable segmentation of large pores and a great reduction of the size and number of channels of flow in the cement paste.

Table 3.3: Reduction in permeability of a 0.7 w/c cement paste with the progress of hydration (Powers, Copeland, Hayes, & Mann, 1954)

| Age days | Coefficient of permeability, $\text{m/s} \times 10^{-9}$ |
|----------|--|
| Fresh | 20,000,000 |
| 5 | 4,000 |
| 6 | 1,000 |
| 8 | 400 |
| 13 | 50 |
| 24 | 10 |
| Ultimate | 6 |

If a gas is considered to be penetrating concrete, the gas permeability coefficient is determined by measuring the flow of gas under pressure through a sample. In this case the fluid is compressible, and the flow can be expressed by the following equation:

$$\frac{dq}{dt} = \frac{k_{gas} A (P_1^2 - P_2^2)}{L \mu 2 P_2} \quad (3-9)$$

where: dq/dt is the flow, P_1 is the upstream pressure, and P_2 the downstream pressure.

3.5 Migration

The migration mechanism involves the transport of ions in solution under an electric field. Ion movement is influenced by the strength of the electric field, the charge and the hydrated size of the ion. A comparison of different ions is possible based on their *mobility* (u) (Table 3.4).

Table 3.4: Values of mobility of various ions at infinite dilution at 25°C (in $10^{-4}\text{m}^2 \text{V}^{-1} \text{s}^{-1}$) (Bertolini, Elsener, Pedefferri, Redaelli, & Polder, 2004)

| Ion | H ⁺ | Na ⁺ | K ⁺ | Ca ²⁺ | OH ⁻ | Cl ⁻ | 1/2 SO ₄ ²⁻ | 1/2 CO ₃ ²⁻ |
|-------|----------------|-----------------|----------------|------------------|-----------------|-----------------|-----------------------------------|-----------------------------------|
| u_i | 349 | 50.1 | 73.9 | 59.5 | 198 | 75.2 | 79.8 | 69.5 |

The ion mobility describes the ion movement under an electric field. Positive ions (Na⁺, K⁺, Ca²⁺) migrate in direction of the current while negative ones (OH⁻, So₄²⁻, Cl⁻) migrate in the opposite direction. Moore (1972) showed that the mobility of the ion "i" (u_i) is directly related to the diffusion coefficient D_i , which describes the movement under a concentration gradient (Moore, 1972; Ackermann, Jugelt, Möbius, Suschke, & Werner, 1974):

$$D_i = \frac{RTu_i}{|z_i|F} \quad (3-10)$$

where: R is the gas constant (J/[Kmol]), T the temperature (K), F the Faraday's constant (96'490 C/mol) and z_i is the valence of ion i .

The contribution of a certain ion to the total current flowing I_{tot} is called the transference number or transport number t_i :

$$t_i = \frac{I_i}{I_{tot}} = \frac{c_i u_i |z_i|}{\sum c_j u_j |z_j|} \quad (3-11)$$

The transport number increases with the concentration c_i and the mobility u_i .

Electrical current flow by ion migration in concrete is important for electrochemical rehabilitation techniques such as chloride removal, but also for corrosion process (ion migration of concrete can be considered a measure of its resistance to chloride penetration using migration tests).

The principles that apply to aqueous solutions are also valid for concrete because the transport of electrical current is due to ion movement in the water filled pore system. However, unlike in aqueous solutions, the ions are not able to move by the shortest route, but they must find their way along the tortuous capillary pores. Therefore, their actual travel distance is much longer than the geometrical one. In addition to that, ions can be transported only in water-filled and interconnected pores. As a consequence of these

aspects, velocity of migration (and diffusion) of ions in concrete is governed by the pore volume and the pore geometry and distribution. For this reason, ion migration (and diffusion) even in water-saturated cement-based materials is 2 to 3 orders of magnitude lower than aqueous solutions (Elsener, 1990). The drastic influence of the pore volume can be modeled using the *percolation theory* (Elsener, Flückiger, & Böhni, 2000; Bürchler, Elsener, & Böhni, 1996).

Resistivity of concrete is an important parameter related to the ion transport process. It is used to describe for example, the degree of water saturation, the resistance to chloride penetration or the corrosion rate. The resistivity of concrete is strictly related to (Polder R. , 1996):

- the w/c ratio, which increases when the concrete is drying out;
- the presence of chloride ions which increase the conductivity of pore solution;
- whether the concrete is carbonated or not, since carbonation increases the resistivity of the pore solution.

Moreover, temperature changes have important effects on concrete resistivity, since higher temperature causes higher ion mobility in the pore solution, hence increasing the resistivity (Bertolini, Elsener, Pedferri, Redaelli, & Polder, 2004).

The easiest laboratory method to assess the resistivity of concrete is pressing steel plates to two parallel faces of a sample (using a wet cloth to ensure good electrical contact).

3.6 Mechanisms and Significant Parameters for Transport Processes

Theoretically, these parameters can be used in the design of concrete structures to calculate the evolution in time of any type of degradation as a function of concrete properties and environmental conditions.

Table 3.5 shows the parameters that are relevant to different situations. Each transport process that lead to concrete degradation can be defined by a parameter:

- *S*: capillary absorption;

- K : permeation;
- D : diffusion;
- ρ : electrical resistivity.

Theoretically, these parameters can be used in the design of concrete structures to calculate the evolution in time of any type of degradation as a function of concrete properties and environmental conditions.

Table 3.5: Properties of concrete relevant with regard to different durability requirements (Bertolini, Elsener, Pedefferri, Redaelli, & Polder, 2004)

| Function requirements | S | K | | D | | ρ | Primary influencing factors |
|--|-----|-----|-----|-----|-----|--------|---|
| | | H2O | Gas | Ion | Gas | | |
| Protection of rebar | | | | | | | |
| Chloride ingress | | | | ✓ | | ✓ | Type of cement |
| Carbonation | | | ✓ | | ✓ | | Moisture content |
| Reduction in corrosion rate | ✓ | | | ✓ | ✓ | ✓ | Moisture content affects S , K , D , and ρ |
| Resistance to concrete degradation (sulfate attack, ASR, etc.) | | | | | | | |
| Low pressure | ✓ | | | ✓ | | | For ASR and sulfates chemical effects dominate |
| High pressure | | ✓ | | ✓ | | | |
| Containment of fluids | | | | | | | |
| Low pressure | ✓ | | | | | | Time, moisture content |
| High pressure | | ✓ | ✓ | | | | |

The kinetics of the different transport processes are correlated among themselves because they depend on the porous structure of concrete. However, these correlations are not of a general nature, but vary in relation to the composition or other properties of concrete. For example, if the type of cement is fixed, correlations between the water permeability (k) and the diffusion coefficient of chlorides (D) can be established. But if different kinds of cement are considered (that is, changing from Portland cement to blended cement) the relationships are no longer valid. Another example may be represented by the

correlations between water permeability (k) and capillary absorption (S), which lose their validity if the surface of the concrete is subjected to a hydrophobic treatment (hydrophobic treatment will considerably reduce S but not k).

As a result, it is necessary to determine the specific property of concrete concerned. Analogous considerations can be made for correlations between properties of concrete and its compressive strength, which are valid in some cases but cannot be generalized. Nevertheless, such correlations may be useful for the design of new structures.

In fact, unlike compressive strength, transport properties are not a simple function of the volume of the capillary pores, but also depend on the dimensions, distribution, form, tortuosity, and continuity of these pores and thus may vary even if the pore volume remains constant.

3.7 Presence of More Than One Transport Mechanism

The transport of aggressive species through concrete takes place by a combination of mechanisms, as seen in Figure 3.7. For example, a structure can be subjected to wetting-drying cycles. In this case, water will penetrate the concrete by capillary absorption or permeation. Eventually, the evaporation of the penetrated water, which always occurs much more slowly than absorption, will facilitate the ingress of oxygen and deposits the salt that were absorbed with the water. A succession of wet and dry conditions leads to cyclic changes in humidity, which will therefore favor both the penetration of water soluble species (e.g., chlorides) and the transport of gases (e.g., oxygen). Thus, it will favor the corrosion process.

It has been showed (McCarter, Emerson, & Ezirim, 1995; Chrisp, McCarter, Starrs, Basheer, & Blewett, 2002) that the response of concrete under variations of the external humidity is a complex function of the length of wet and dry cycles, the concrete composition and the hydration of the cement.

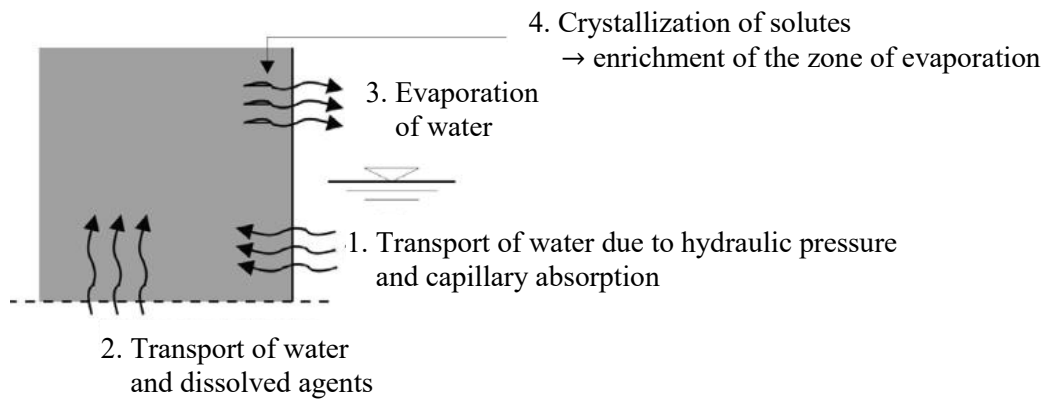


Figure 3.7: Example of combination of transport mechanisms (CEB, 1992)

CHAPTER 4

DURABILITY OF REINFORCED CEMENT-BASED STRUCTURES

Durability of hydraulic-cement concrete is determined by its ability to resist weathering action, chemical attack, abrasion, or any other process of deterioration (American Concrete Institute, 2008). Durable concrete will keep its original form, quality and serviceability when exposed to its environment.

Prevention of deterioration begins in the design phase; engineering structures are designed to perform over a stated period of time, namely *design service life*, during which their functions (such as structural safety) must remain intact. Structures often exhibit unexpected defects in one or more functions during the design service life. One of the main reasons for these defects is the lack of prompt knowledge about the performance of structures and materials, which is reflected in the standards where guidance to determine the service life of products is generally very limited (Bijen, 2003). Another important factor to be considered is that a long service life is far beyond the horizon of designers and builders. In fact, many deterioration mechanisms manifest themselves only after 10÷15 years, while designers and builders are generally not liable for more than ten years after completion of the structure. With respect to the construction process, several durability problems are due to low-quality job execution. A typical example is the custom of adding water on site to increase the mixture workability, which inevitably causes a dramatic fall in resistance.

Design for durability should include the structure's maintenance program during service life, that is, parts of the structure will have to be replaced or repaired to maintain performance at an acceptable level during the design service life. If monitoring and maintenance of the structure are taken into account in the design stage, the initial requirements for durability could be relaxed (Bertolini, Elsener, Pedferri, Redaelli, & Polder, 2004). In reality, maintenance is often not part of the design and a maintenance program at a later date is only begun as defects become obvious.

The main factors affecting durability of reinforced cement-based structures will be discussed in this chapter, and an overview of both physical and chemical deterioration mechanisms will be given. On top of that, carbonation-induced corrosion and the parameters that define it will be discussed. Chloride-induced corrosion will not be considered as it falls outside the scope of this thesis. For more details, the reader is referred to the classic literature on degradation of concrete (ACI Committee 201, 2016; Bertolini, Elsener, Pedferri, Redaelli, & Polder, 2004; Mehta & Monteiro, 2006; Soutsos, 2010; Dodge Woodson, 2009).

4.1 Factors Affecting Durability

4.1.1 *Aggressiveness of the Environment*

Certain conditions or environments exist that will lead to concrete deterioration. Furthermore, the effects of an aggressive environment can be enhanced by design and construction mistakes. Environmental aggressiveness is a function of numerous factors that are not always independent of each other. Although relative humidity and temperature are important variables of the external environment surrounding the structure, local microclimatic conditions are established by the structure itself. The following outline summarizes the environmental aggressiveness under the most frequent exposure conditions (Bertolini, Elsener, Pedferri, Redaelli, & Polder, 2004): 1) the environment is not aggressive if the concrete is sufficiently dried, because every degradation mechanism requires a fairly high relative humidity to exhibit significant effects; 2) the environment is not aggressive with regard to corrosion if the structure is in conditions of total and permanent saturation with water, because under these conditions oxygen cannot effectively reach the surface of the reinforcement; 3) in the absence of chlorides, for $RH > 70\%$ that remains constant or shows only modest changes that do not lead to condensation, the environment is moderately aggressive in temperate climates and aggressive in tropical or equatorial climates; 4) for $RH > 70\%$ with widespread and frequent variations, or if condensation takes place on the surface or wetting-drying cycles occur, the environment is aggressive in temperate climates and very aggressive in hot climates; 5) conditions in which the concrete surface is subjected to wetting-drying cycles are generally the most severe with regard to reinforcement corrosion since they incentivize penetration of both

water and gasses (such as carbon dioxide and oxygen); 6) conditions of exposure to marine atmosphere, even if not in direct contact with seawater, are aggressive; and 7) exposure conditions in the splash zone of marine structures or on viaducts where deicing salts are used are extremely aggressive.

4.1.2 *Concrete Quality*

The ability of a structure to resist aggressive agents is strongly related to the properties of cementitious matrix which are generally taken together in the term “quality of concrete”. Moreover, the reinforcement concrete cover provides the natural protection against corrosion. Thus, the achievement of a low-porosity cementitious matrix is one of the main concerns if a durable structure is desired. According to (Neville, 1995), important concrete quality items are water-to-cement ratio (w/c), cement content, cement type, mixing, placing, compaction, curing, cracking (both on the macroscopic and microscopic scale), and other aspects such as admixtures and air content.

4.1.3 *Cracking*

Cement-based materials easily crack in tension, flexure and shear, as well as due to various environmental factors such as thermal cracking, shrinkage cracking, and freeze-thaw. Cracking often represents the first display of the ongoing degradation process; thus, when conducting an inspection, the presence of cracks is the first important aspect to investigate.

It should be noted that cracks in concrete structures may have many different origins and characteristics. Whatever the cause is, cracking of concrete often fosters the ingress of aggressive substances and therefore accelerates the deterioration mechanisms. Surface crack width is considered to be the most important parameter that effects the corrosion of steel in concrete. The crack depths, cracking frequency and healing of cracks also influence the corrosion of steel in concrete.

Generally, if the crack width is modest (e.g., it is below 0.3÷0.5 mm), chemical processes in the cement paste and formation of corrosion products may seal the crack near the reinforcement and even allow the protective oxide film to form again. For carbonation-induced corrosion, repassivation can take place when the migration of alkalinity from

the surrounding cementitious matrix brings the pH of the pore solution in contact with the corrosion products to values above 11.5.

4.1.4 Thickness of the Cover

An increase in the thickness of the concrete cover increases the barrier to the various aggressive species moving towards the reinforcement layer. Since the rate of corrosion decreases with time (as shown in Eq. (4-1)) a slight increase in concrete cover will result in a considerable increase in corrosion initiation time.

As the environmental aggressiveness increases, it is theoretically possible to maintain a constant level of durability by increasing the thickness of the concrete cover. However, very high cover (above 70 to 90 mm) may have less favorable barrier properties than expected, since it may lead to the formation of multiple cracks due to drying shrinkage.

4.2 Deterioration Mechanisms of Cement-Based Materials

An overview of the processes involved in the degradation of cement-based materials is shown in Figure 4.1. In practice, these processes frequently occur simultaneously, giving rise to synergic action. Some other alterations occur before the structure has been completed, that is, within the first hours to months after casting (such as cracking due to plastic settlement, plastic or drying shrinkage, creep, thermal shrinkage). However, these are not considered among the phenomena of deterioration; instead, they are related to mistakes during design and/or construction phases. Obviously, such alterations should be prevented since they can undermine the whole durability of the structure.

The various factors influencing durability and the particular mechanism of deterioration should be considered in the context of the environmental conditions to which the concrete will be subjected. Moreover, material's features (reinforcing material, cement, aggregates, etc.) should receive proper consideration to accurately describe deterioration mechanisms. In fact, erroneous choice of raw materials, mistakes made during the production of the cementitious conglomerate, and erroneous construction and curing techniques can cause deterioration mechanisms to take place within few hours after casting.

Examples of frequent mistakes happening during construction phases are shown in Table 4.1.

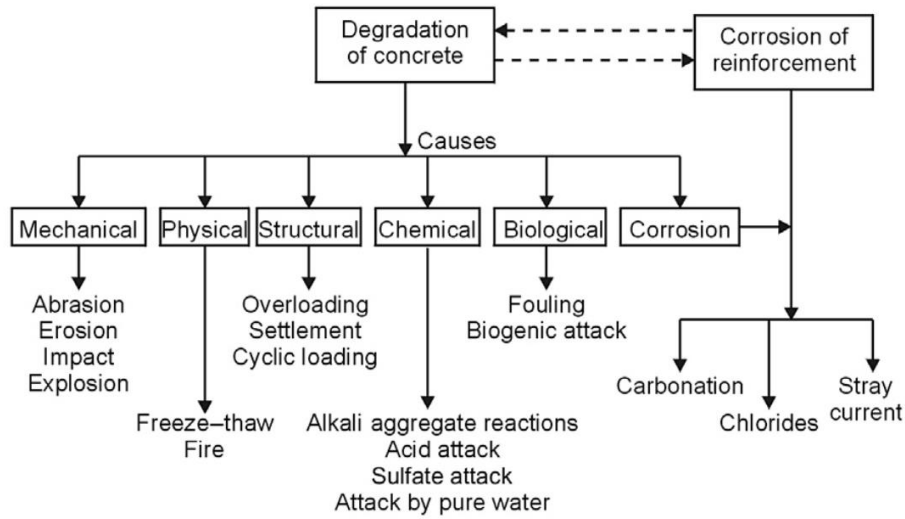


Figure 4.1: Causes of deterioration of reinforced concrete structures (Bertolini, Elsener, Pedferri, Redaelli, & Polder, 2004)

Table 4.1: Frequent mistakes taking place during construction phases (Coppola & Buoso, 2015)

| Phase | Frequent mistakes |
|---|--|
| Concrete production | <ul style="list-style-type: none"> • Erroneous choice of raw materials; • poor humidity control of aggregates, leading to large variation in w/c. |
| Concrete processing at the worksite | <ul style="list-style-type: none"> • Water addition; • poor preparation and removal of the formworks; • insufficient or erroneous curing. |
| Mix design and reinforced concrete design | <ul style="list-style-type: none"> • Use of non-durable concrete; • thin concrete cover; • erroneous reinforcement disposition; • inadequate design of the construction details, especially the ones related to the water control and re-impregnation. |

4.2.1 Physical Deterioration Mechanisms

Physical degradation of concrete is primarily controlled by its strength. For a typical structure, the amount of water required to make the cement fully hydrated is approximately 30% of the total mass of cement (w/c of 0,3). To ensure the proper workability, i.e. to have a less stiff fresh concrete mix, a bigger w/c is used along with admixtures such as superplasticizers. This excess water will not be chemically combined with cement to form calcium silicate hydrate (C-S-H), therefore it causes the formation of voids. A more porous cement paste leads to a weaker concrete in terms of mechanical strength.

Mehta and Gerwick (Mehta & Gerwick, 1982) grouped the physical causes of concrete deterioration into two categories (Figure 4.2):

- surface wear: loss of mass due to abrasion, erosion, and cavitation;
- cracking due to normal temperature and humidity gradients, crystallization of salts in pores, structural loading, and exposure to temperature extremes such as freezing or fire.

A comprehensive report on the causes, mechanisms and control of cracking in concrete was published by ACI Committee 224 (ACI Committee 224, 2001).

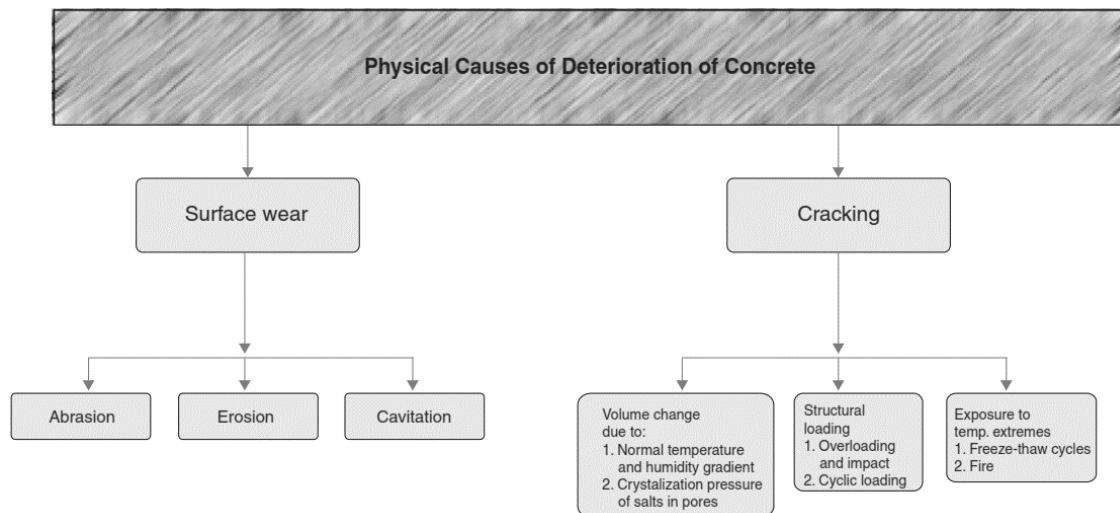


Figure 4.2: Physical causes of concrete deterioration (Mehta & Gerwick, 1982)

4.2.2 *Chemical deterioration mechanisms*

Concrete can suffer chemical damage from contaminants added during manufacturing or by the action of external aggressive agents, or by a combination of both. Chemical attacks always manifest themselves into detrimental physical effects, such as increase in the porosity and permeability decrease in the strength, and cracking and spalling.

Mehta and Gerwick (Mehta & Gerwick, 1982) grouped the chemical causes of concrete deterioration into three categories (Figure 4.3):

- hydrolysis of the cement paste components by soft water;
- cation-exchange reactions between aggressive fluids and the cement paste;
- reactions leading to formation of expansive products, such as sulfate attack, alkali-aggregate reaction, and corrosion of reinforcing steel in concrete.

In practice, several chemical and physical deterioration processes act at the same time and have a synergic effect.

The deterioration mechanisms caused by chemical reactions generally involve chemical interactions between the aggressive agents in the environment and the constituents of the cement paste. However, there are a few exceptions to this:

- alkali-aggregate reactions, which occur between the alkalies present in the cement paste and certain reactive materials in the concrete;
- delayed formation of crystalline CaO and MgO, when present in excessive amounts in Portland cement;
- delayed ettringite formation.

In a well-hydrated Portland cement paste, the solid phase exists in a state of stable equilibrium with a high-pH pore solution. The pH value ranges from 12.5 to 13.5 and is influenced by the concentration of Na^+ , K^+ , and OH^- ions. As a result, at least theoretically, any environment with less than 12.5 pH may be considered aggressive because a reduction of the alkalinity of the pore fluid would lead to destabilization of the cementitious products of hydration. Thus, most industrial and natural waters will theoretically be aggressive to Portland cement paste. However, when the permeability of concrete is low, and the pH of the aggressive fluid is above 6, the rate of chemical attack is too slow to be

taken seriously. Free CO₂ in soft water and stagnant water, sulfate (SO₄²⁻) and chloride (Cl⁻) ions in groundwater and seawater are responsible for lowering the pH below 6.

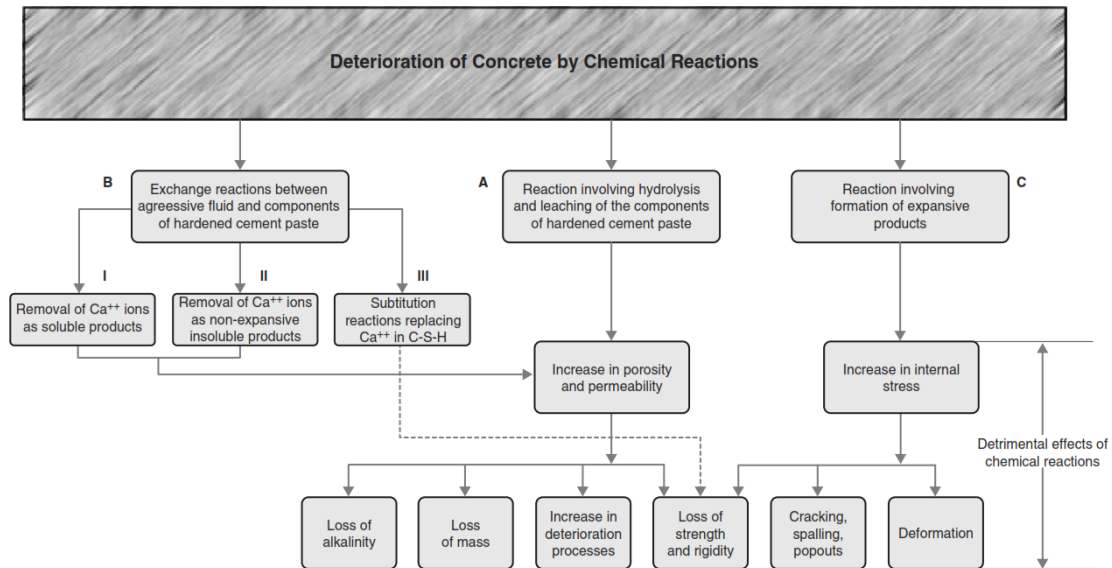


Figure 4.3: Types of chemical reactions responsible for concrete deterioration (Mehta & Gerwick, 1982)

4.3 General Aspect on Corrosion

During hydration of cement, the presence of sodium and potassium hydroxide translates into the production of a highly alkaline pore solution with pH values between 13 and 13.8. If an ordinary reinforcing steel bar is embedded in alkaline cement paste or concrete, a protective oxide film (named *passive film*) is formed spontaneously (Pourbaix, 1973; Arup, 1983) with a few nanometers in thickness (< 10 nm), thus decreasing the dissolution rate of steel to negligible levels (Zakroczymski, Fan, & Szklarska-Smialowska, 1985; Montemor, Simoes, & Ferreira, 1998; Carnot, Frateur, Marcus, & Tribollet, 2002). However, this protection may be destroyed by carbonation of concrete or by the presence of chloride ions; as a result, the reinforcing steel is depassivated (Pedferri & Bertolini, 2000).

With respect to the corrosion mechanism, the service life of reinforced concrete structures can be divided into two distinct phases:

- *Initiation phase:* the reinforcement is passive but certain reactions take place inside the pore solution leading to loss of passivity. More specifically, carbonation

or chloride penetration in the concrete cover are by far the most common phenomena.

- *Propagation phase*: it begins when the steel is depassivated, hence corrosion initiates.

4.3.1 *Initiation Phase in Carbonation-Induced Corrosion*

When concrete is exposed to air, the alkaline constituents of concrete react with water and carbon dioxide in the air. These alkaline constituents are present in both the pore liquid and the solid hydration products, for example Ca(OH)_2 or C-S-H.

More precisely, Gaseous CO_2 enters the pores in the concrete and dissolves in the pore water to form carbonic acid (H_2CO_3), which then reacts with dissolved calcium hydroxide to form insoluble calcium carbonate as summarized by Eq. (4-1). Finally, calcium carbonate precipitates out of solution and lines the pores (Soutsos, 2010). The phenomenon is called carbonation, it is generalized and relatively homogeneous (unlike chloride-induced corrosion).



There is no significant deleterious effect of the carbonation process on the concrete itself; however, carbonation reduces the pH value of the surface layer of concrete to less than 8.3, which is a sufficient value to make the passive layer on the steel reinforcement unstable (Allen & Forrester, 1983). The duration of the initiation phase depends on a wide range of factors: cover depth, penetration rate of the aggressive agents (which is influenced by the fineness of the pore structure and by the microclimatic conditions, i.e., wetting-drying cycles), and concentration necessary to depassivate the steel. The propagation phase ends when a limiting state is reached beyond which consequences of corrosion cannot be further tolerated. This obviously depends on the kind and nature of the considered reinforced concrete structure.

The depth of carbonation increases with time, but with an ever-decreasing rate. In fact, a very common equation used to describe the penetration with time of carbonation is represented by:

$$d = K \cdot t^{1/n} \quad (4-2)$$

where d is the depth of carbonation (mm), t is the time (years), and K is called carbonation coefficient ($\text{mm}/\text{year}^{1/n}$). Indicatively: $2 < K < 6$ for concrete of low porosity, $6 < K < 9$ for concrete of medium porosity, and $K > 9$ for highly porous concrete (Bertolini, Elsener, Pedferri, Redaelli, & Polder, 2004). Often, n is chosen with a value of 2; however, in dense and/or wet concrete, the reduction of the carbonation rate with time is stronger, so that $n > 2$.

Some other empirical models have been proposed to take into direct account the effect of several parameters that influence the carbonation rate. These models require as input some experimental constants whose evaluation is practically difficult (Tuutti, 1982; Bakker, 1994; Parrott, 1994).

The ever-decreasing nature of the carbonation rate is due to three factors: 1) the gas has to penetrate further into the concrete; 2) concrete continues to hydrate and becomes more impermeable as it ages; and 3) carbonation itself decreases permeability because CaCO_3 precipitates in the existing pores and water is produced which may result in increased hydration (see Eq. (4-1)) (Hansson, Poursae, & Jaffer, 2017).

Carbonation depth is defined as the average distance from the surface of concrete or mortar where carbon dioxide has reduced the alkalinity of the hydrated cement. The depth of carbonation can be determined by different techniques. The most common technique consists in applying pH-sensitive liquid indicators such as phenolphthalein to freshly fractured surface of concrete. Upon application of phenolphthalein, non-carbonated areas turn red or purple while carbonated areas remain colorless.

4.3.2 *Factors Influencing the Carbonation rate*

The rate of carbonation depends on both environmental factors (humidity, temperature, concentration of carbon dioxide) and factors related to the concrete (mainly its alkalinity and permeability).

Carbonation rate is significantly influenced by the moisture content of the cement-based material. Rates of carbonation are highest in the range 50 to 75 percent relative humidity (Figure 4.4). Below about RH 45% the water in the pores is not in a state that

encourages dissolution of calcium hydroxide or carbon dioxide and this reduces the reaction rate (Richardson, 2002; Bertolini, Elsener, Pedferri, Redaelli, & Polder, 2004). On the other hand, above RH 75% the influence of water filling the pores becomes significant, therefore the resulting carbonation rate is slower.

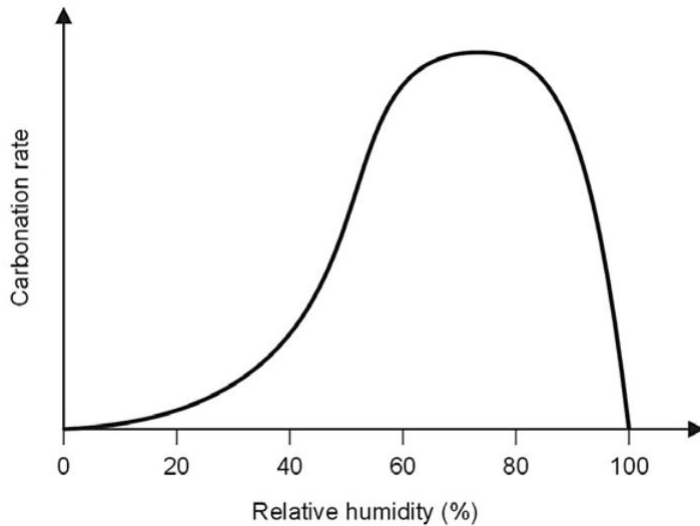


Figure 4.4: Influence of relative humidity on the rates of carbonation and corrosion (Bertolini, Elsener, Pedferri, Redaelli, & Polder, 2004)

In addition to the mere relative humidity in the pore structure, the microclimate plays an essential role in carbonation. In fact, carbonation rate may be lower if the structure is subjected to periodic wetting (Wierig, 1994; Parrott, Carbonation, Moisture and Empty Pores, 1992): since wetting of concrete is fastest than drying, more frequent although shorter periods of wetting are more effective in reducing the penetration of carbonation.

The concentration of CO₂ in the atmosphere may vary from 0.03% in rural environments to more than 0.1% in urban environments. All other conditions being equal, an increase in temperature and/or CO₂ concentration will raise the rate of carbonation.

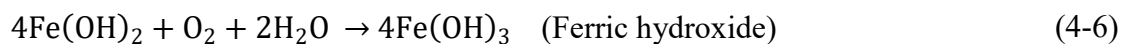
The concrete composition deeply influences the carbonation process. This is mainly due to two reasons: 1) a decrease in w/c ratio and a proper curing decrease the capillary porosity, thus slowing down the penetration of CO₂; and 2) the capacity of concrete to fix CO₂ is proportional to the alkalinity in its cement paste. For example, a blended cement has a lower Ca(OH)₂ content that may increase the carbonation rate

4.3.3 Propagation Phase: Corrosion Process After Depassivation

Regardless of the source of the depassivation of steel (either carbonation or chlorides), once it has occurred, active corrosion of steel bars begins and develops with the same mechanism. Corrosion of steel in concrete is an electrochemical process which will occur only if water and oxygen are present on the surface of the reinforcement.

Corrosion is an electrochemical reaction which consists of anodic and cathodic half-cell reactions. For steel embedded in concrete:

- *anodic process*: Iron dissolves, initially producing soluble ferrous ions (Fe^{2+}) and electrons (e^-) (Eq. (4-3));
- *cathodic process*: the electrons react with water and oxygen, to form hydroxide ions (Eq. (4-4));
- ferrous ions react with hydroxide ions, then water and oxygen, to ultimately form rust (Eq. (4-5) to (4-7)).



If active dissolution and the corresponding cathodic half-cell reaction take place at adjacent parts of the same metal piece the phenomenon is called *microcell corrosion* (Figure 4.5).

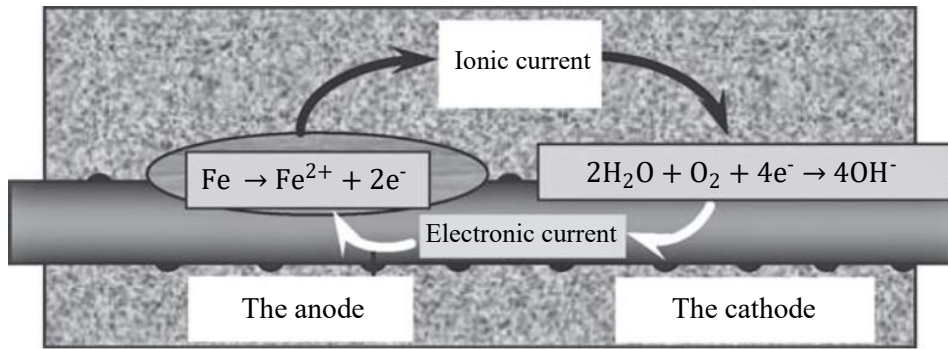


Figure 4.5: The anodic, cathodic, oxidation and hydration reactions of corroding steel in concrete

Not only corrosion results in loss of cross section of the reinforcement, but since $\text{Fe}_2\text{O}_3 \cdot \text{H}_2\text{O}$ is an expansive oxide corrosion often manifests itself through cracking of concrete cover much earlier than structural consequences occur.

The propagation stage defines the period during which the *corrosion rate* and the cumulative amount of corrosion products gradually increase until an unacceptable level of damage has occurred (Andrade & Alonso, *Corrosion Rate Monitoring in the Laboratory and on Site*, 1996). The duration of the propagation stage depends on the definition of "acceptable corrosion damage", which directly depends on the corrosion rate. The corrosion rate is usually expressed as the penetration rate and is measured in $\mu\text{m}/\text{year}$ or in electrochemical units (e.g. mA/m^2). In the case of steel, 1 mA/m^2 corresponds to a loss of mass equal to approximately 9 $\text{g}/\text{m}^2/\text{year}$ and a penetration rate of about 1.17 $\mu\text{m}/\text{year}$. Typical values of corrosion rate are listed in Table 4.2. For typical conditions of atmospheric exposure, maximum values of corrosion rate are between 5 and 50 $\mu\text{m}/\text{year}$, while average values are one order of magnitude lower.

A relationship between corrosion rate and service life in terms of probability of corrosion damage was proposed by Clear (1985) and is listed in Table 4.3.

As depicted in Figure 4.6, corrosion rate is governed by the resistivity of concrete (as described in Section 3.5), which, in turn, is mainly influenced by the moisture content and the microstructure of the concrete.

Table 4.2: Typical values of corrosion rate (Bertolini, Elsener, Pedferri, Redaelli, & Polder, 2004)

| Corrosion Rate, $\mu\text{m}/\text{year}$ | Severity of Damage |
|---|---------------------------|
| < 2 | Negligible |
| 2 ÷ 5 | Low |
| 5 ÷ 10 | Moderate |
| 10 ÷ 50 | Intermediate |
| 50 ÷ 100 | High |
| > 100 | Very high |

Table 4.3: Proposed relationship between corrosion rate and remaining service life (Clear, 1985)

| Corrosion Rate, $\mu\text{m}/\text{year}$ | Severity of Damage |
|---|--|
| < 2.3 | No corrosion damage expected |
| 2.3 ÷ 12 | Corrosion damage possible in 10-15 years |
| 12 ÷ 120 | Corrosion damage expected in 2-10 years |
| > 120 | Corrosion damage expected in 2 years or less |

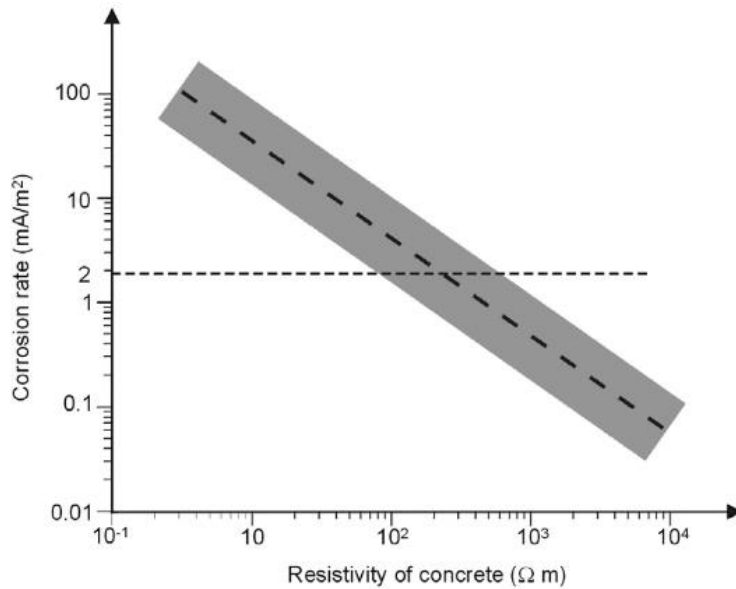


Figure 4.6: Schematic representation of the corrosion rate in the carbonated concrete as a function of the resistivity of concrete (Alonso, Andrade, & Gonzales, 1988)

What is interesting is the fact that, at least in high-quality concrete, the rate of corrosion is negligible for relative humidities below 80%. Therefore, it can be assumed that corrosion propagates only while concrete is wet, that is $RH > 80\%$. Moreover, it has been observed that the corrosion rate tends to decrease with time because the corrosion products can somehow reduce the corrosion rate (Alonso & Andrade, 1994). In conclusion, to achieve a high corrosion rate, either one of the following two conditions must be verified: 1) high humidity; 2) the duration and frequency of periods of condensation of water on the concrete surface cause variations in the moisture content at the depth of reinforcement.

4.3.4 Testing for Corrosion

There is a wide range of tests available for assessing the condition of deteriorated concrete. Prior to perform any systematic survey, a detailed visual inspection should be conducted and cracks, spalled and delaminated concrete, and exposed rebars will be noted. The most common tests for assessing presence and gravity of corrosion are listed in Table 4.4. For more details, guidance on testing and surveying the reader is referred to the classic literature and standards (see Table 4.4).

Table 4.4: Main tests for assessing the condition of deteriorated concrete

| Test | Purpose | Literature |
|--|---|---|
| Half-cell or reference electrode potential survey | Assessing the corrosion state of rebars | (ASTM, 2009; Concrete Society, 2004; Elsener, Müller, Suter, & Böhni, 1990) |
| Polarization resistance or linear polarization (LPR) | Measuring corrosion rate | (Broomfield, 2006; Concrete Society, 2004; Andrade, et al., 2004; Polder, Peelen, Bertolini, & Guerrieri, 2002) |
| Four-probe resistivity meter or Wenner probe | Measuring concrete resistivity | (Broomfield, 2006; Concrete Society, 2004; Millard, Harrison, & Edwards, 1989; Polder, et al., 2000) |

4.4 Effect of Cracks on Corrosion

Cracks can be divided into two categories: 1) cracks on concrete surface that are perpendicular to the reinforcing steel are known as *transverse cracks*; and 2) cracks parallel to longitudinal reinforcing steel are known as *longitudinal cracks*. Transverse cracks are the most common and studied in reinforced concrete, while longitudinal cracks form after the corrosion of steel and are considered more dangerous than the former.

Cracks hinder the durability of reinforced concrete structures by creating preferential paths for the penetration of corrosion-inducing species. The effect of cracks varies not only with their width but also with effective depth, frequency, orientation (relative to the steel reinforcement) and self-healing characteristics (Arya & Darko, 1996; Arya & Wood, 1995; Bentur, Diamond, & Berke, 1997; Neville, 2002). All these factors should be included in transport properties and service life prediction models; however, since the influence of cracks is often neglected, these models may provide an incomplete description of the behavior of a structure (Otieno, Alexander, & Beushausen, 2010). Otieno et al. identified two reasons why the influence of cracking is often omitted from service life predictions: 1) insufficient knowledge on the effect of cracks; and 2) the introduction of cracks into the model greatly complicates the analysis.

Two schools of thought exist with regard to the influence of cracks on corrosion. On the one hand, it is believed that cracks accelerate both corrosion initiation and propagation, but these are dependent on the concrete quality and cover depth (Pettersson & Jorgensen, 1996; Scott & Alexander, 2007; Suzuki, Ohno, Praparntanatorn, & Tamura, 1990). On the other hand, some researchers state that there is no direct relationship between crack width and corrosion rate (Arya & Wood, 1995; Beeby, 1983; Bentur, Diamond, & Berke, 1997), that is, cracks may accelerate corrosion initiation but not its propagation.

4.4.1 Effect of Crack Widths

Regarding corrosion, a vast number of experiments shows that there is no precise correlation between the crack width and the risk of corrosion, as long as the crack width remains below 0.3÷0.5 mm. However, cracks may reduce the corrosion initiation time, since they provide a preferential path for the penetration of carbonation and chlorides. Despite numerous experiments have been conducted (Otieno, Alexander, & Beushausen, 2010; Mohammed, Otsuki, & Hamada, 2001; Sistonen, Kari, Tukiainen, & Huovinen, 2007; Quero, Garcia, & Bremner, 2010; Sahmaran & Yaman, 2008; Montes, Bremner, & Lister, 2004), it is difficult to establish a direct relationship on the effect of widths of transverse cracks on the corrosion of steel in cracked concrete (Shaikh, 2018). This is because different researchers used different crack widths, water-cement ratios, concrete types, corrosion periods, as well as different methods of corrosion evaluation. However, for smaller crack widths (up to 0.3 mm) the corrosion of steel seems to be increasing with an increase in crack width (Shaikh, 2018).

While extensive studies on the effect of cracking on chloride penetration and chloride induced corrosion of steel in cracked concrete have been conducted, little attention has been given to carbonation induced corrosion of steel in cracked concrete. Using cracked ring-shaped mortar specimens, Al-Ahmad et al. found that the crack opening significantly affect the ability of carbon dioxide to diffuse along the crack walls (Al-Ahmad, Toumi, Verdier, & Francois, 2009). On the other hand, Dang et al. reported that the carbon dioxide reached the interface between the steel and the mortar and caused corrosion regardless of the crack width (Dang, Francois, & Hostis, 2013).

4.4.2 *Effect of Crack Frequency*

Crack frequency is defined as the number of cracks per specific length. Arya and Darko showed that the corrosion of steel increases with increase in frequency of transverse cracks (Arya & Darko, 1996). In that study, the transverse cracks had the same width of 2.4 mm. Opposite results have been reported by Schiebl and Raupach, who showed that the increase in crack frequency decreased the corrosion rate (Schiebl & Raupach, 1997). A possible explanation for this phenomenon is that by reducing the crack spacing through increasing the number of cracks, the size of the cathode areas between the cracks are decreased, which reduced the corrosion rate.

4.4.3 *Effect of Crack Depth*

Studies about crack depth affecting the chloride penetration and subsequent steel corrosion are rarely available. Moreover, the different concrete cover lead to different shapes of crack. In fact, the thicker the concrete cover the higher the possibility of forming *V-Shape* cracks than *Parallel-Wall* cracks, which tend to form more often in the case of thin concrete cover (Shaikh, 2018). Regarding corrosion, it can be argued that *Parallel-Wall* cracks are more detrimental than *V-Shape* cracks, since the width of a *V-Shape* crack decreases towards the reinforcing steel (Scott & Alexander, 2007).

CHAPTER 5

PRINCIPLES FOR MAINTENANCE AND REPAIR OF HERITAGE STRUCTURES

Reinforced concrete structures damaged by deterioration mechanisms, such as steel corrosion, need maintenance or repair interventions aimed at restoring the safety and serviceability to the required performance level and, in the meantime, providing a reasonable residual service life to the structure (RILEM Technical Committee 124-SRC, 1994). The knowledge of the present state of conservation of a structure and the evaluation of its likely evolution in the future are a crucial task in order to properly plan a restoration work. A correct design of restoration measures is made after a careful evaluation of the present state of conservation of the structure and the evaluation of its likely evolution in the future. Additionally, three general objectives must be considered during maintenance works on engineering structures (Coppola & Buoso, 2015): 1) to restore the structural safety; 2) to restore the serviceability; 3) to improve or restore the esthetic. Furthermore, three specific objectives must be pursued: 1) to eliminate the causes responsible for the structural distress, the loss of serviceability, and/or the esthetic problems; 2) to eliminate the structural instabilities and stop the degradation mechanisms to take place; 3) to protect the structure during the residual service life.

Based on this approach, it is clear that a proper evaluation of the deterioration mechanisms taking place in the structure, along with a distress survey, are necessary to accurately design maintenance or repair interventions.

In this chapter, the principles to be followed during a maintenance or repair intervention on a structure, with particular regard to reinforced concrete heritages, are discussed. Since most of the heritage structures suffer damage due to corrosion, restoration of reinforced concrete structures damaged by corrosion deserves more attention.

5.1 Project Phases of the Concrete Repair and Protection Process

Architectural heritages present many challenges in diagnosis and restoration which limit the application of modern legal codes and building standards. These structures are characterized by a complex history and, if compared to more recent works, they were built with different construction techniques and materials. For this reason, a multidisciplinary team should work together from the beginning, that is, from the initial survey of the site and the preparation of the investigation program (International Council on Monuments and Sites, 2003).

Since codes prepared for the design of modern structures are often inappropriate for historic structures, it is necessary to follow the guidelines and principles that are incorporated in charters and documents formulated at national and international level. In this context, mechanical and engineering sciences play a crucial role and the recognition of their importance gradually increased over the last decades (D'Ayala & Forsyth, 2007). A description of the gradual evolution of principles and guidelines incorporated in charters and documents can be found in the literature (Benvenuto, 1981; Chiorino M. , 2016).

In the first decades of the second half of 20th century, one of the most relevant event concerning restoration of heritage structures is represented by the 2nd International Congress of Restoration (Venice, 1965), which resulted in the establishment of ICOMOS International Council on Monuments and Sites and the drafting of the International Charter for the Conservation and Restoration of Monuments and Sites. ICOMOS defines essential recommendations for those involved in structural conservation and restoration of architectural heritage (International Council on Monuments and Sites, 2003). This organization pointed out that the peculiarity of heritage structures requires a multidisciplinary approach in which the studies and analysis are organized in steps that are similar to those used in medicine:

- *anamnesis*, corresponding to condition survey;
- *diagnosis*, corresponding to identification of the causes of damage and decay. Diagnosis “is based on historical information and qualitative and quantitative approaches”, and that “the quantitative approach requires material and structural tests, monitoring and structural analysis”;

- *therapy*, corresponding to the diagnosis, that is, the choice of the remedial measures;
- *controls*, corresponding to the control of the efficiency of the interventions.

A combination of approaches must be used to put these steps into practice; thus, to establish rules and codes for conservation and restoration of architectural heritages is a delicate matter. The rehabilitation process should address both the structural elements and the heritage value.

Design and repair options are outlined in the European Standard EN 1504 “Products and Systems for the repair and protection of concrete structures – definitions, requirements, quality control and evaluation of conformity”, which defines the procedures and characteristics of products used to repair, maintain and protect concrete structures.

According to EN 1504-9, design of a maintenance or repair intervention can be divided in the following steps:

- 1) *Information about the structure*. A study is carried out at the beginning of a project to collect information about the structure and understand its existing conditions. This may include:
 - general condition and history;
 - documentation (e.g., calculations, drawings and specifications, etc.);
 - repair and maintenance schedule.
- 2) *Inspection and condition assessment*. A survey of the visible and not readily visible defects of the structure is made to address the root causes of the damage. This will be used to assess the ability of the structure to perform its function.
- 3) *Management strategy*. Based on the assessment of the survey, the owner has a number of options to be selected while deciding the relevant actions to meet the future requirements of the structure. For example, the following repair options can be defined:
 - do nothing or downgrade the capacity;
 - prevent or reduce further damage without repair;
 - repair all or part of the structure;
 - reconstruction of all or part of the structure;
 - demolition.

- 4) *Design of repair work.* The design philosophy for repair should take into consideration the following points:
 - type, causes and extend of defects;
 - future service conditions;
 - future maintenance program.
- 5) *Repair work;*
- 6) *Acceptance of repair work.* Complete records of all the materials used in the work should be provided for future reference at the end of each project. Moreover, these should contain information on the anticipated new life expectancy, the inspection period, remedial work required in case of further deterioration.

Moreover, American Concrete Institute (ACI) provides a series of guidelines for the design of maintenance and repair interventions:

- ACI 201.1R-08: Guide for Conducting a Visual Inspection of Concrete in Service (ACI Committee 201, 2008);
- ACI 201.2R-16: Guide to Durable Concrete (ACI Committee 201, 2016);
- ACI 228.2R-13: Report on Nondestructive Test Methods for Evaluation of Concrete in Structures (ACI Committee 228, 2013);
- ACI 562-16: Code for Assessment, Repair, and Rehabilitation of Existing Concrete Structures (ACI Committee 562, 2016);
- ACI 546R-14: Guide to Concrete Repairs (ACI Committee 546, 2014);
- ACI 546.3R-14: Guide to Materials Selection for Concrete Repair (ACI Committee 546, 2014).

It is worth noting that when repair and strengthening are applied to heritage structures there are limitations in use (Berkowski & Dmochowski., 2014).

Brocklebank (Brocklebank, 2005) discussed the draft European Standard DD ENV 1504-9 “Products and systems for the protection and repair of concrete structures. Definitions, requirements, quality control and evaluation of conformity. General principles for use of products and systems”. The author pointed out that conservation philosophy was not considered in the preparation of the standard. Furthermore, several reinforced concrete repair methods are discussed by Brocklebank, including the application of anti-

carbonation coatings, patch repair, electrochemical methods, impressed current cathodic protection, and realkalization.

The recent Model Code of the International Federation for Structural Concrete (*fib*) proposes the following activities to be followed during a *conservation process* (Fib, 2010) (Figure 5.1):

- *condition survey*. It allows to gather information on the current condition of the structure;
- *condition assessment*. It implies assessing available information to obtain an indication of current performance and to make a prognosis of future performance, including the identification of deterioration mechanisms and prediction of damage;
- *condition evaluation and decision-making activities*. It involves the evaluation of potential conservation options, the selection of an appropriate intervention and the implications that such intervention will have on the structure;
- *execution of preventive or remedial works*;
- *through-life condition surveys and/or monitoring*

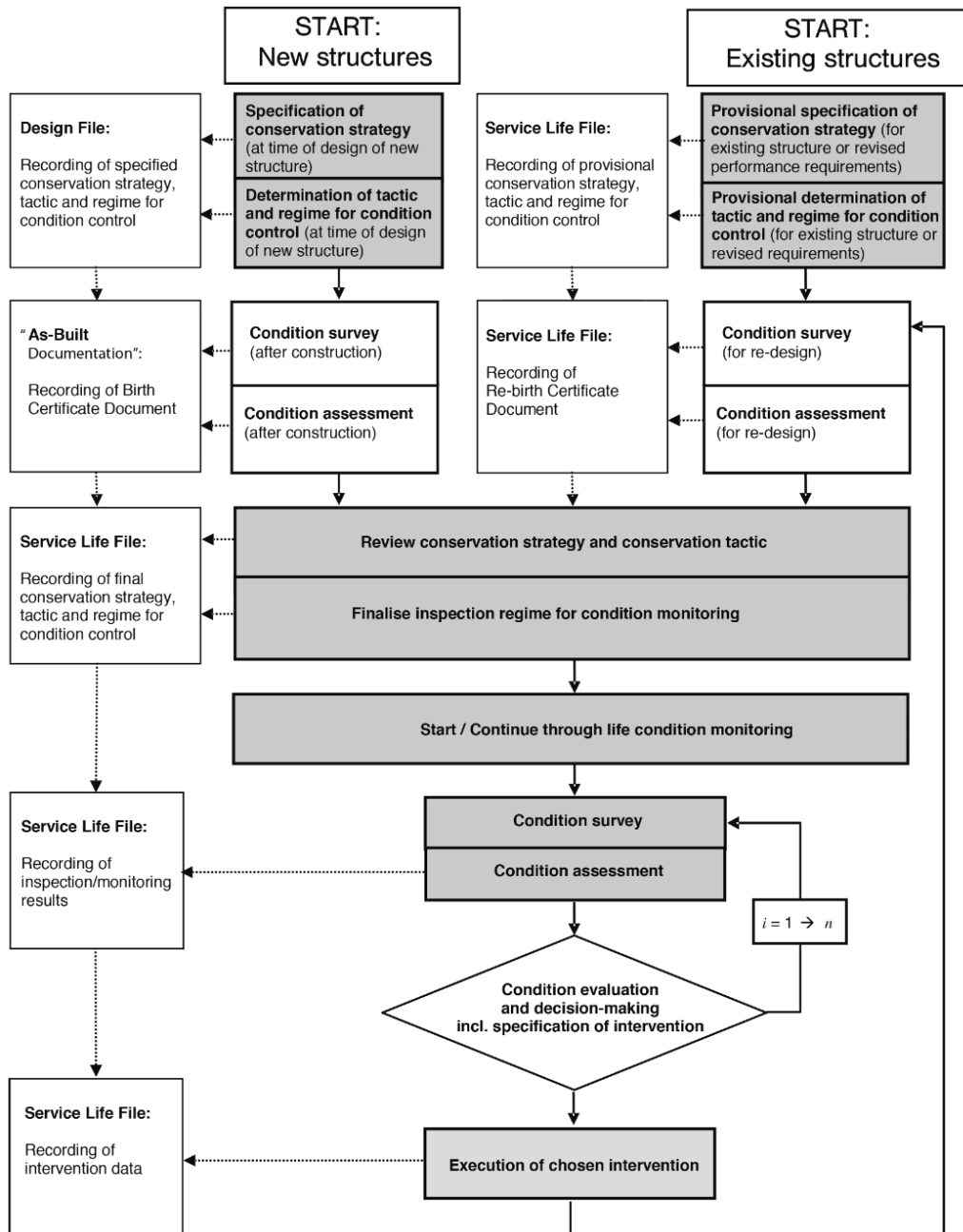


Figure 5.1: General flow of conservation process procedures for new and existing structures (Fib, 2010)

5.2 Anamnesis and Diagnosis: Inspection, Condition Assessment, and Identification of the causes of Damage and Decay

To find the optimum repair solution a thorough condition assessment of the structure must be performed. Considering structures of the cultural heritage, the conservation of the structure, the materials and the surface is of primary importance. The design of a

restoration work should start with an accurate investigation of the structure, aimed both at collecting information on the materials, since properties of concrete used in the past may be quite different from those of more recent concretes, and on the corrosion of embedded steel. Therefore, any planning for structural conservation requires both qualitative data, based on the direct observation of material decay and structural damage, and quantitative data based on specific tests and mathematical models of the kind used in modern engineering.

Proper evaluation of concrete requires several steps. A full evaluation normally consists of two steps: a *preliminary survey* (mainly based on a visual inspection) should identify the nature of the problem and give the basis for planning the *detailed survey*, where several investigation techniques are adopted. Visual inspections (preliminary surveys) often reveal a need for further evaluation and testing (detailed survey).

5.2.1 *Visual Inspection*

Visual inspection is the first step in any investigation because it gives a first indication of the extent of damage. When the visual inspection is concluded, the standard procedure is to create a map of potential defects that are encountered; all the defects visible on the concrete surface are registered, with particular regard to the presence of cracks, spalling, wet areas, signs of water run off or rust staining. Furthermore, the types of defects that are sought in surface mapping may include pop-outs, honeycombing, exudation, unusual discoloration, erosion, cavitation, joint condition, corrosion of reinforcement materials.

Cracks negatively influence the durability of the structure, in that they provide pathways for aggressive substances; moreover, cracks can reflect a lack of durability since they can be symptomatic of deterioration mechanisms occurring in the structure.

When a visual inspection is carried out, each type of cracking should be recognized, and appropriate action should be taken. Cracking can be an important sign that corrosion is occurring, although it should be pointed out that chloride-induced localized corrosion might originate visible cracks only in a very advanced state.

Regarding corrosion, an important nondestructive test that is often combined with visual inspection is the measurement of the concrete cover. Magnetic covermeters can be

used to obtain a cover mapping survey, which is useful to explain why certain areas of the structure are corroding and to identify areas of future corrosion risk.

If a visual inspection is conducted, a surface mapping is important when establishing the history of a concrete surface

5.2.2 Detailed Survey

Every piece of information obtained during the previous steps leads to the formulation of a document, namely *anamnesis form*, which describes the current condition of the structure. The primary aim of the anamnesis form is to help the engineer in identifying the main causes of damage.

However, historical information and visual inspection may not be enough to ascertain the causes of damage; therefore, after the visual inspection, further surveys may be necessary especially to assess the corrosion state of reinforcement (Figure 5.2), assess the characteristics of the material and evaluate the presence of cracks and defects that are not visible from the surface.

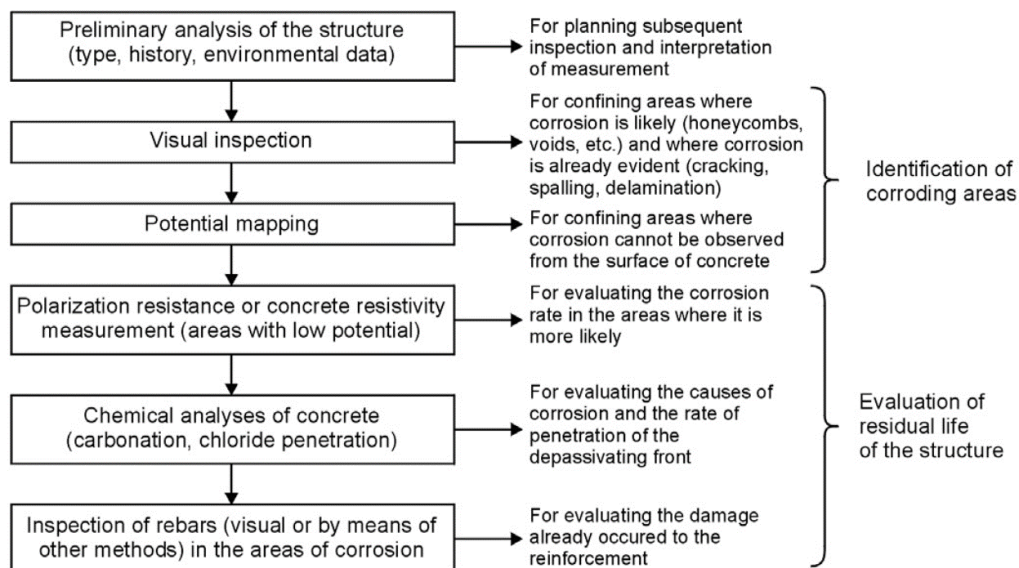


Figure 5.2: Example of integrated methodology of inspection for assessing corrosion in reinforcement (Bertolini, Elsener, Pedferri, Redaelli, & Polder, 2004)

Extensive literature can be found on durability performance surveys on reinforced concrete structures, involving a wide variety of tests for assessing the condition of

deteriorated concrete (i.e., chemical analysis, physical analysis, destructive testing, and nondestructive testing) (Coppola & Buoso, 2015; Dodge Woodson, 2009; Soutsos, 2010; Concrete Society, 2004; Concrete Bridge Development Group, 2002). Tests such as ground-penetrating radar, infrared thermography, impact echo, radiography, and ultrasonic pulse velocity are used to locate flaws, cracks and delaminations in concrete. There is also a far wider range of tests that will inform the engineer about concrete properties which impact its ability to resist ingress of aggressive agents. These include permeability and surface absorption.

Nondestructive testing (*NDT*) is used to determine various relative properties of concrete, such as strength, modulus of elasticity, homogeneity, and integrity. With regard to corrosion, a wide family of nondestructive techniques, namely *electrochemical inspection techniques*, can be employed to assess the corrosion rate and the corrosion state of steel reinforcement in concrete. Although a discussion of electrochemical inspection techniques falls outside the scope of this thesis, the methodology of conducting and interpreting such surveys are discussed more fully in the literature (ASTM, 2009; Concrete Society, 2004; Broomfield, 2006; Bertolini, Elsener, Pedferri, Redaelli, & Polder, 2004)

5.2.3 *Diagnosis: Identification of the Causes of Damage and Decay*

The most important step of repairing damaged or deteriorated concrete is to correctly determine the cause of the damage. If an incorrect determination is made, whatever damaged the original concrete will likely also damage the repaired concrete. Since a full understanding of the structural behavior and material characteristics is essential for the design of any restoration intervention, the diagnosis is the direct result of both historical information, visual inspection and detailed survey.

A review of the most common causes of damage can be found in Chapter 4; it seems clear that the majority of them are of a continuing and recurring nature. Moreover, it is not rare to find multiple causes of damage. Once the causes of damage have been evaluated, the present level of structural safety can be assessed.

5.3 Therapy: Methods for Maintenance and Repair

With respect to the selection of the repair technique, the interaction between the requirement for a long enough residual life after the restoration work and the necessity of reducing the impact of the repair work on the structure should be considered.

In the recent years, some recommendations and standards have been developed by different organizations, to help designers in the choice of the repair strategy (RILEM Technical Committee 124-SRC, 1994; Fib, 2010; UNI, EN 1504-1, 2005; UNI, EN 1504-9, 2008). However, in case of cultural heritage, strict requirements related to preservation of the original materials and texture must be met (Bertolini, Carsana, Gastaldi, Lollini, & Redaelli, 2011); thus, repair methods should reduce the amount of material to be replaced (e.g., to replace the carbonated concrete). As a consequence, the conventional repair technique, involving the replacement of carbonated concrete cover with a cementitious mortar, is usually not available.

The recent Model Code of the International Federation for Structural Concrete (*fib*) proposes and defines maintenance procedures to be included both within proactive and reactive approaches (Fib, 2010):

- *Proactive approach*. “is based on preventive (or protective) measures and interventions aimed at avoiding and minimizing future deterioration or loss by applying some form of treatment or taking action prior to damage becoming visible”. This approach should be applied to the structures (or to parts of a structure) where it is necessary to keep the performance above a specified minimum requirement.
- *Reactive approach*. “is based on remedial (or corrective) measures and interventions, aimed at arresting currently active processes which are causing deterioration or damage.

The reasons to adopt a proactive approach might include considerations about esthetic, technical, functional or economic issues. However, if existing structures are considered, reactive approach is often the only possibility since these structures were not subjected to a specific durability design at the time of construction (see Section 1.4) and the damage has already started and become apparent (typically involving visual indications, such as cracking or spalling of concrete).

Furthermore, according to the Model Code two different conservation objectives can be identified:

- Conservation activities to achieve the intended service life of a structure, as envisaged at the time of design;
- Conservation activities to achieve an extended service life of a structure or to enable it to meet revised performance requirements (e.g., revised loading or functionality needs).

For structures that are subjected to carbonation-induced or chloride-induced corrosion, the approach proposed by the RILEM 124-SRC recommendation can be followed (RILEM Technical Committee 124-SRC, 1994).

Repair methods should differ according to the part of the structure which is under consideration. For example, a distinction should be made according to the evolution of carbonation of the cover or the corrosion of the reinforcement. In order to define a proper repair option, the future evolution of the damage should also be estimated.

If corrosion is considered, the intervention can aim at either, replacing the damaged components, stopping corrosion, or reducing the corrosion rate (RILEM Technical Committee 124-SRC, 1994). Moreover, RILEM 124-SRC defines the principles of repair to stop corrosion of reinforcement (Figure 5.3).

A discussion on all the methods for maintenance and repair is beyond the scope of this thesis; however, a review of surface treatments and coatings available for concrete will be made in Chapter 10.

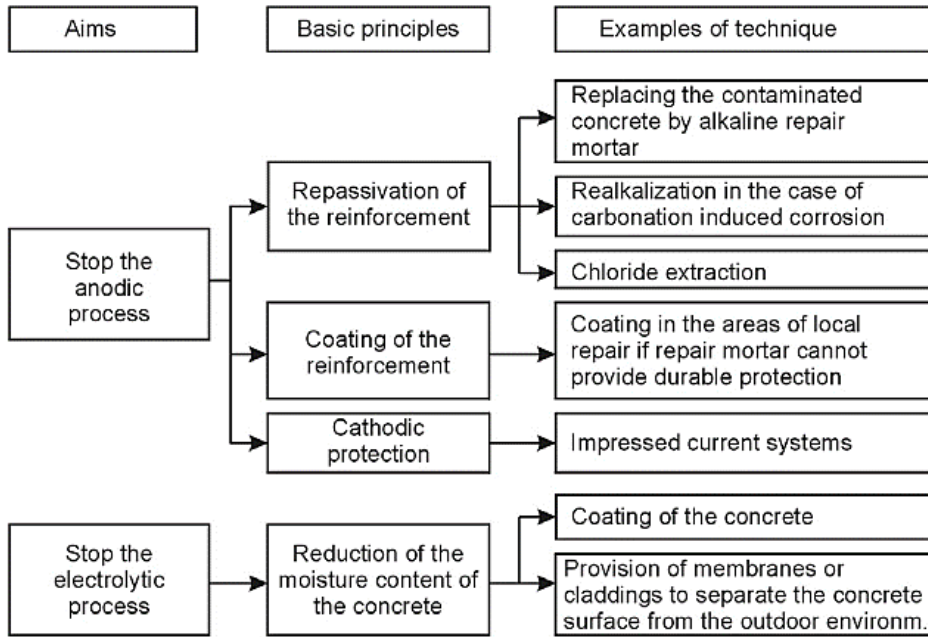


Figure 5.3: Principles of repair to stop corrosion of reinforcement (RILEM Technical Committee 124-SRC, 1994)

CHAPTER 6

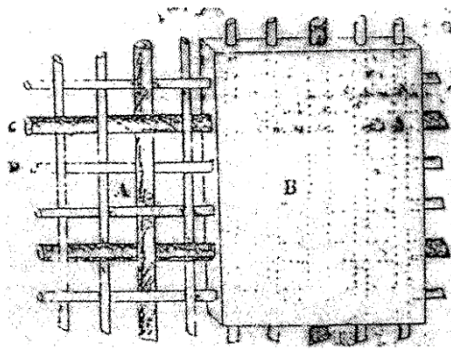
INTRODUCTION TO FERROCEMENT

6.1 History of Ferrocement

The concept of embedding reinforcement into wet concrete to form what is now recognized as reinforced concrete was almost simultaneously born from three people. Joseph Monier (1823-1906), a French gardener, incorporated a mesh of iron rods into large planting pots in 1849. An Englishman, Wilkinson, made reinforced concrete beams for buildings by putting old mining ropes in the tension side of beams (Gordon, 1968). And ultimately, a Frenchman, Joseph Louis Lambot, who made a concrete rowing boat in which the reinforcement was in the form of a network of wires and interlaced thin rods (Cassie, 1967; Morgan, 1968). The year was 1848; Lambot called his material *fer-ciment* (which translates into *iron-cement*); however, the commonly used English term is *ferrocement*. Lambot described his patent with the following words:

My invention shows a new product which helps to replace timber where it is endangered by wetness, as in wood flooring, water containers, plant pots etc... The new substance consists of a metal net of wire or sticks which are connected or formed like a flexible woven mat. I give this net a form which looks in the best possible way, similar to the articles I want to create. Then I put in hydraulic cement or similar bitumen tar or mix, to fill up the joints.

Lambot built two rowboats in 1848 and 1849, in length respectively about 3.6 m and 3 m (12 and 9 foot) and 38 mm (1.5 in.) thick and disclosed his patent at the Paris exhibition in 1855 (Figure 6.1). Detailed description of Lambot's original boat, depicted in Figure 6.2, has been given by Morgan and Morgan in the Proceedings of Ferrocement 6, the Sixth International Symposium on Ferrocement (Naaman, 1998), dedicated to Lambot.



French Patent Summary: (22120. 30 mars 1855.) *Combinaison de fer et de ciment, destinee a remplacer le bois dit fer-ciment succedant du bois de construction. Reseau metallique ou carcasse d 'un bateau, d'une caisse a eau ou a orangers.*

Figure 6.1: Lambot's patent on "fer-ciment"



Figure 6.2: Original 1848 Lambot's boat preserved in Brignoles Museum

Ferrocement is referred as the first invention of reinforced concrete, but subsequent developments differed from Lambot's concept. In fact, the technology of the period could not accommodate the time and effort needed to make mesh of thousands of wires. At that time, large rods were being used and the idea of ferrocement quickly led to conventional reinforced concrete of thicker form. Inevitably, reinforced concrete became the material of choice and the concept of ferrocement was almost forgotten for 100 years. An excellent review of the history of ferrocement is given by Morgan and Morgan in the Proceedings of Ferrocement 6 (Naaman, 1998).

Only in the early 1940s Pier Luigi Nervi recognized the many advantages of ferrocement not only for boat building, but also for terrestrial applications. Carrying out a series of engineering experiments, he observed that reinforcing concrete with layers of

wire mesh produced a material possessing the mechanical characteristics of an approximately homogeneous material and capable of resisting impact (Nervi, Structures, 1956). At first, Nervi proposed that ferrocement be utilized to build fishing boats and by showing its exceptional properties he received acceptance by the Italian Navy. Shortly after the Second World War, Nervi demonstrated the potential of ferrocement by building a 165-ton motor-sailor called *Irene* using a ferrocement hull 35 mm thick. After *Irene*, Nervi continued his work by using ferrocement in some architectural applications. He built a small storage warehouse in Rome in 1947. Later he covered the swimming pool at the Italian Naval Academy with a 15 m diameter dome, the Turin Exhibition Hall B with a roof system spanning 91 m (1948), the Turin Exhibition Hall C (1950). A more detailed description of these structures can be found in Chapter 7.

Despite the evidence that ferrocement was an adequate and economical building material, it gained wide acceptance only in the early 1960s (Eyers, 1972; Paramasivam, Ong, & Lee, 1991; Eyers, 1972). For an overview on the applications of ferrocement, the reader is referred to ACI 549R-97 (ACI Committee 549, 1997).

There has been widespread use of ferrocement throughout the world in several countries including Canada, United States, Australia, New Zealand, United Kingdom, Mexico, Brazil, the former USSR, Eastern European countries, China, Thailand, India, Indonesia, and other developing countries. Unfortunately, emphasis on ferrocement as a boat-building material during the 1960s has practically obscured Nervi's applications to buildings. Even though the use of ferrocement did not expand much beyond its application to boat construction, a new revival in the use of ferrocement can be witnessed during the last decades. This is especially true in applications where the desirable properties of ferrocement cannot be matched by other materials, such as strength, toughness, watertightness, lightness, durability and environmental stability. In addition to that, the universal availability of the basic ingredients of ferrocement created the interest in the potential application of this material in developing countries for water and food storage structures and housing.

In developed countries, the application of advanced technology of building systems and prefabrication makes it attractive for housing and other structural applications. However, the mesh construction phase may be excessively labor-intensive, and this may be a shortcoming for developed countries (ACI Committee 549, 1997). Thus, to alleviate the

acute shortage and high cost of skilled labor, more so in developed countries, mechanized methods must be used to expedite the speed of construction.

During the late 1960s and early 1970s, ferrocement began to be considered as a fertile field of study. ACI Committee 549, Ferrocement and Other Thin Reinforced Products, was organized in 1974 aiming to study and report information on thin reinforced cementitious products and ferrocement, and to develop guidelines for ferrocement constructions. A list of events and associations that were born at that time can be found in ACI 549R-97 (ACI Committee 549, 1997; ACI Committee 549, 1993) and in (Naaman, 2000). Among these, it is worth considering the International Ferrocement Society (IFS), which was officially established in the Fourth International Symposium on Ferrocement in Cuba in 1991. The IFS was founded to coordinate and to cater to the needs of practitioners, engineers and researchers on applications and development of ferrocement. IFS Committee 10 gave an important contribute by report the Ferrocement Model Code (IFS Committee 10, 2001).

6.2 Definition of Ferrocement

The term ferrocement implies the combination of a ferrous reinforcement embedded in a cementitious matrix. Although ferrocement implies the use of cement and, at first, steel reinforcement, other reinforcements have been used or implied in thin cement products. In its state-of-the-art report on ferrocement the American Concrete Institute defines ferrocement as follows (ACI Committee 549, 1982):

Ferrocement is a type of thin wall reinforced concrete commonly constructed of hydraulic cement mortar reinforced with closely spaced layers of continuous and relatively small size wire mesh. The mesh may be made of metallic or other suitable materials.

This rather general definition is surprisingly close to the initial definition of ferrocement described by Lambot. Furthermore, the last sentence opens the field to the use of polymeric reinforcements such as high-performance carbon, glass, or aramid fibers, and also encompasses some modern applications such as *textile reinforced concrete*. It is worth mentioning that the use of non-metallic mesh is being explored at several

universities. Such meshes include woven alkali resistant glass, organic woven fabrics such as polypropylene, and organic natural fabrics made with jute, burlap, or bamboo fibers.

Naaman suggested to extend this definition by adding the two following sentences (Naaman, 2012):

The fineness of the mortar matrix and its composition should be compatible with the mesh and armature systems it is meant to encapsulate. The matrix may contain continuous fibers.

By adding these two sentences it is possible to ensure the compatibility of the matrix with the reinforcement and to accommodate the use of discontinuous fibers or micro-fibers being able to obtain hybrid composites.

CHAPTER 7

PIER LUIGI NERVI

Pier Luigi Nervi (1891-1979) was one of the greatest and most inventive structural engineers of the 20th century. He contributed to create a glorious period for structural architecture. Nervi shared the culture of architects and engineers, operating at the very intersection between the art and the science and technology of building (Chiorino C. , 2010; Olmo & Chiorino, 2011; Abram, 2011). Although hundreds of references can be found addressing Nervi's biography and his major projects, only a select number of papers and books are cited in this thesis and should be considered a starting point to be conscious of the career and works of the great Italian artist (Abel, Arun, & Chiorino, 2013; Bologna & Giargiani, 2016; Chiorino M. , 2012; Carpanelli, 1955; Nervi, 1945)

7.1 The Nervi System

Nervi's works were closely related to the cultural and social conditions both domestically and worldwide (Iori & Poretti, 2013). From World War One through Fascist era to the enthusiastic second post-war reconstruction period, and on the booming years of economic euphoria up to the financial crisis of the Seventies. For this reason, three segments of Nervi's life can be identified. In the first life he was a modern architect, in the second an ingenious creator of a new building method, and in the last an international architect. Between the end of the Thirties and the end of the Sixties, in his second life, Nervi developed the so-called *Nervi System*, a completely new way of designing and constructing reinforced concrete structures. During the autarchic regime established by Mussolini, steel became one of the most rationed materials imported from abroad and for this reason had to be reserved exclusively for the war effort. As a result, reinforced concrete, obviously requiring steel for the reinforcement, suddenly became an anti-national construction material. Due to the restrictions applied, designers and constructors began to experiment with alternative solutions (Iori, 2001), primarily to save on steel.

Nervi's system was focused on two objectives: to save on steel and to reduce the amount of wooden formwork used for onsite casting. Great savings on steel can be obtained by reducing the amount of concrete, limiting the thicknesses of the load bearing elements. This concept drove Nervi to experiment with ferrocement. Moreover, Nervi made crucial changes to the building system to reduce or even eliminate the use of wooden formwork: he experimented a prefabrication technique he called *structural prefabrication* (Nervi, 1945), which was patented in November 1939 (Figure 7.1). In this technique, the structure had to be broken down and each element had to be prepared on the ground. Every element had to be small enough and light enough to be lifted and easily assembled. Each piece had to have a shape that would allow it to have enough strength and stiffness during the assembly. The building yard could therefore be divided into two autonomous sectors, where laborers could operate in parallel: on the one hand the actual building site, on the other hand, the prefabrication yard, used to prepare the pieces used to assembly the structure (Iori & Poretti, 2013). The first opportunity to test the structural prefabrication system arose with the "second series" of airplane hangars for the Italian Air-Force, between 1939 and 1942 (Figure 7.2).

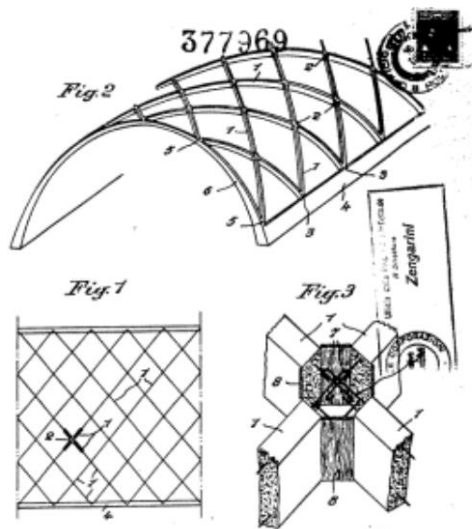


Figure 7.1: Italian patent n. 377969, "Structural prefabrication technique", 1939

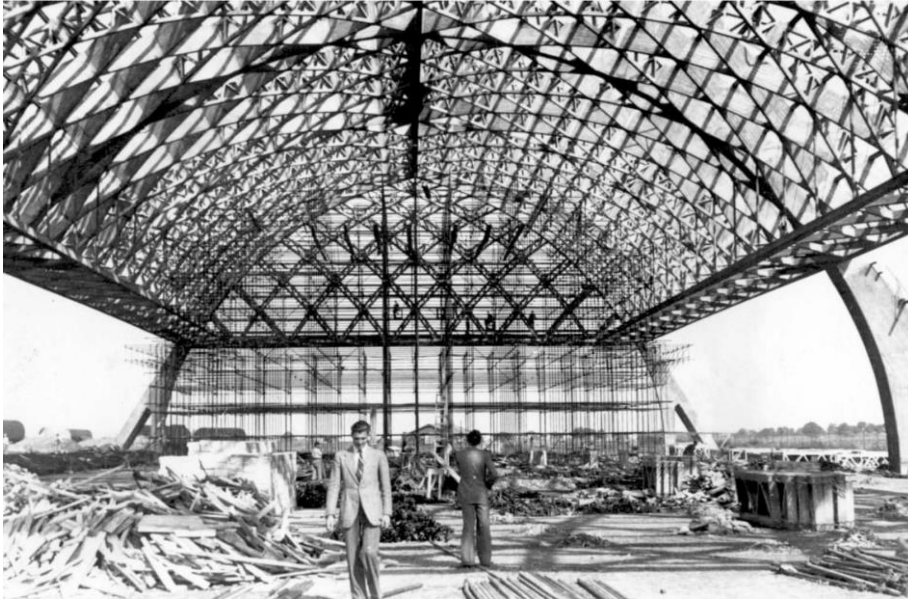


Figure 7.2: Aircraft Hangar, Orbetello. Pier Luigin Nervi & Bartoli, 1939-1941

7.2 Nervi's Ferro-Cementitious Felt

In the same years, Nervi began to experiment with thin steel-reinforced concrete slabs. The armistice of September 1943 came at a turning point for Nervi's research into cement materials. It was during that year that Nervi improved the technical and physical properties of ferrocement, as it was used during the 20th century.

The patent filed by Nervi in April 1943 was entitled "Perfecting the Construction of Slabs, Plates and Other Reinforced Cement Structures" and contained the definition of "ferro-cementitious felt" (Figure 7.3), which was obtained by superimposing multiple layers of mesh and cement mortar, compressed together by means of a trowel or a float. By pressing the mortar on one side of the mesh the cement came out on the other side after having filled the entire reinforcement. By choosing a proper water content of the compound, wooden formwork to shape the mortar until it hardened was no longer needed: at that point, any wooden formwork had been permanently removed from Nervi's manufacturing process. The term "felt" reflect the analogy between Nervi's material and the production of felt, which is not a conventional fabric, but a material obtained by pressing together wool fibers and possibly animal hair.

From the first experiments, the steel mesh used by Nervi was composed of wires with diameter $0.5 \div 1.5$ mm, square openings of 1 cm^2 , and had a weight variable between 0.6 kg/m^2 and 1.5 kg/m^2 . The mortar was obtained using high-quality sand with a cement

dosage oscillating between 800 kg and 1000 kg per cubic meter of sand (Carpanelli, 1955). To increase the thickness of the ferro-cementitious felt without exceeding 10 ÷ 12 layers of wire mesh, Nervi incorporated one or more layers of iron rods of diameter 6 ÷ 10 mm, which were placed in the center of the member. This allowed him to obtain elements with a thickness up to 6 ÷ 10 cm. In any case, the thickness of the whole ferro-cementitious felt was only slightly higher than that of the wire mesh layers, leading to a net cover of a few mm.

In his patent, Nervi emphasized the novelty of his ferro-cementitious felt compared to similar techniques of ferrocement in which the reinforcement consisted in only one or two meshes and the “cement part was predominant”. His ferro-cementitious felt was distinguished due to the greater quantity of iron, the form of the various superimposed layers of metal mesh, the reduced thickness, and the role of the cement, which is relegated to a simple waterproof and protective sealing material. Ferrocement was homogeneous, isotropic, elastic, and ductile.

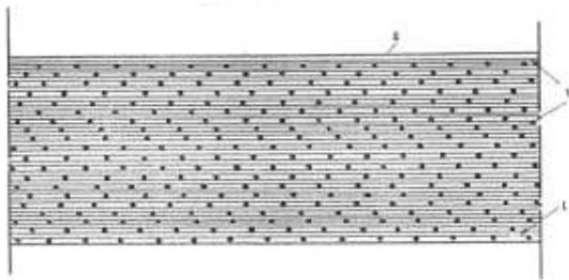


Figure 7.3: Italian patent n. 406296, “ferro-cementitious felt”, 1943

After the collapse of the Fascist regime, Italy was subjected to the post-armistice invasion of the Nazi forces during which Nervi decided to shut down his company. In June 1944 Rome was liberated and in September Nervi had already improved his own patent (Figure 7.4).

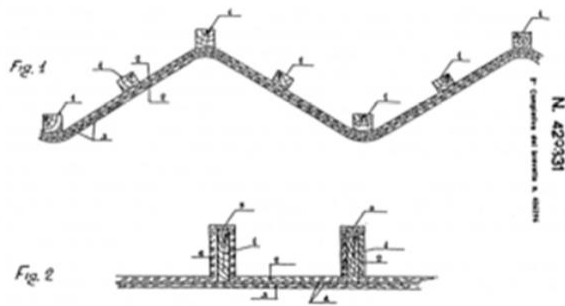


Figure 7.4: Italian patent n. 429331, 2nd supplement to patent n. 406296, 1944

At the beginning, Nervi experimented the use ferro-cementitious felt in the construction of hulls, developing a technique for replacing the timber planking of naval hulls with his ferro-cementitious felt. The construction of a hull for a 130-tonnes motor sailer provided him with an opportunity for testing his renewed kind of ferrocement. Nervi described the planking of that motor sailer as a “planking slab” (Nervi, 1945), a definition that was already in itself significant with regard to the potential application of the product to the building industry.

The first application of the new material to building construction was a 21.88 x 11.38 m warehouse at the Magliana Nervi & Bartoli place, in Rome (Figure 7.5). It was entirely made of ferro-cementitious felt, including the roof. The shell was 3 cm thick and variously folded with wide undulations and pleats to stiffen it and turn it into a building structure. The presence of waves allowed Nervi to get the most out of the inherent shape-resistant solution (Greco, 2008). The shed in Via della Magliana is important not only because it is the first use of ferro-cementitious felt for walls and roofs, but also because recent restorations, conducted by Tullia Iori and Sergio Poretti and sponsored by Italcementi Group, allowed to reveal some secrets of Nervi’s new material.

The presence of doors and windows made it necessary to break own the shell into three modules. One in the form of a simple rectangular panel to be inserted in the position of the windows, and two configured as vertical structures. The most elaborate of the last two modules is a soft V-shaped folded at the ends into truncated scrolls to prevent overturning (Figure 7.6). This module was defined as a “moving wave” and was 1.77 m wide and 3.9 m high.

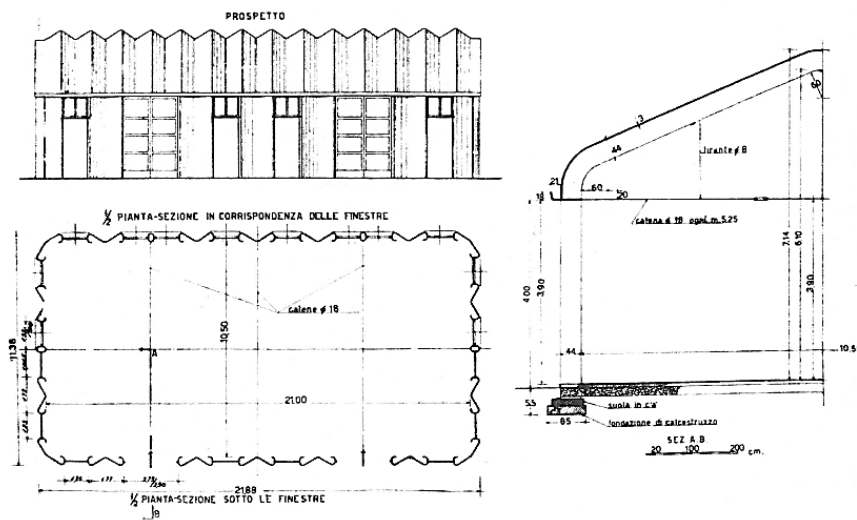
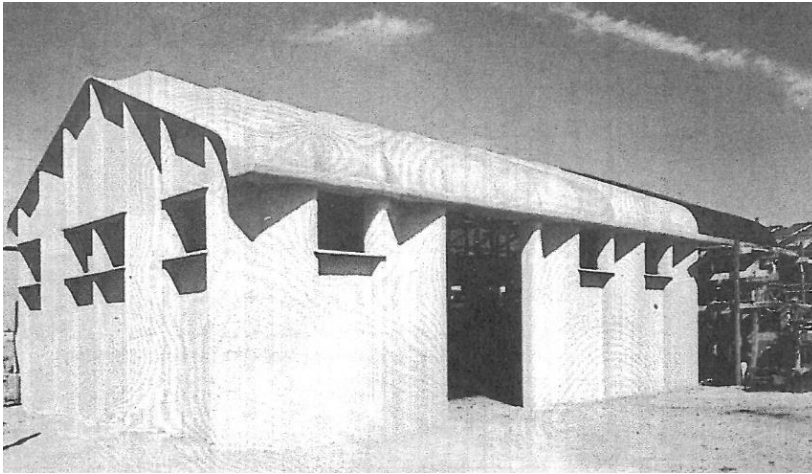


Figure 7.5: Shed in Via della Magliana, namely Magliana Warehouse (1945)

The shell of the roof was corrugated in a regular pleated pattern that concluded, in the two heads, in a flat surface, while the pleating was braced by three slender beams.

In this very first use of ferro-cementitious felt as a construction material, Nervi used a frame that was different from those he had experimented with planking slabs. The multiple layers of steel mesh were discarded and a considerable number of wooden slats and boards for permanent formwork remained buried in the shell. In the curly slabs, the steel inner weave was prepared with few 8 mm diameter vertical bars and couples of 6 mm diameter shaped horizontal bars (20 cm spaced) (Iori & Poretti, 2013). Within these re-bars, multiple wooden squared strips were used to support only two layers of mesh, one for each side. Once the reinforcement had been put into place, the workers covered it with cement mortar, made out of fine sand with a low water content, applied under pressure

with a laying trowel and then smoothed with plaster's trowel to obtain a constant thickness of 3 cm and a polished finish.

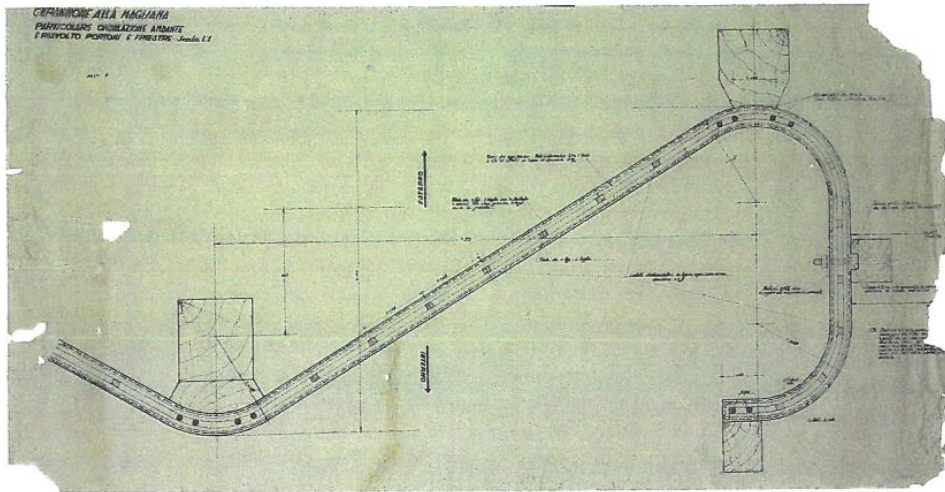


Figure 7.6: Shed in Via della Magliana, detail of a V-shaped module

Starting from the first patent, Nervi continued to refine his material and the construction technique. He tested his invention on various minor works in the years spanning from the reconstruction to the economic boom. In the end, three evolutionary steps can be identified in the changes in terminology adopted by Nervi for his product, from its advent as a material for hulls (ferro-cementitious felt), to its application to waved shells manufactured on-site (ferro-cementate), to its radical transformation into a crucial material for structural prefabrication that came about in 1948 when Nervi & Bartoli won the commission to carry out all the extension work on the Turin Exhibition Center (*Palazzo di Torino Esposizioni*). In that occasion the term became “ferrocement”, which represents the final stage in the evolution of this material.

7.3 Turin Exhibition Center

The Turin Exhibition Center is the most important of the projects linking Pier Luigi Nervi and his firm to Turin's mainly industrial patronage, a world that revolved around FIAT and its Construction and Plant Service (Olmo & Chiorino, 2011). The project was presented to the city in 1947 as a reconstruction and enlargement of an existing building Palazzo della Moda, designed by Ettore Sottsass in 1936 and prime example of rationalist architecture in Turin. Palazzo della Moda, inaugurated in 1938, had been seriously

damaged by bomb attacks in 1943 and had remained vacant (Garuzzo, 2002). The 1947 architectural project, which would be built by the firm Nervi e Bartoli, with Pier Luigi Nervi as site engineer, assisted by FIAT engineer Vittorio Bonadé Bottino, preserved Sottsass’s overall plan for the building: the indoor-outdoor theatre with areas for two orchestras; the principal façade on Corso Massimo d’Azeglio with its circular restaurant; a “giant foyer” made of reinforced concrete and glass blocks; and the buffer zone between the old and new exhibition halls and the street, a space already occupied by a “dance garden” (Olmo & Chiorino, 2011).

7.3.1 Hall B for Turin Exhibition Center

Turin Exhibition Center is composed of main Hall B (inaugurated on 15 September 1948) and additional Hall C (1950). Hall B, shown in Figure 7.7, represented the first chance for Nervi to apply structural prefabrication in a single large scale vaulted structure, combining it with the use of the ferrocement technique.

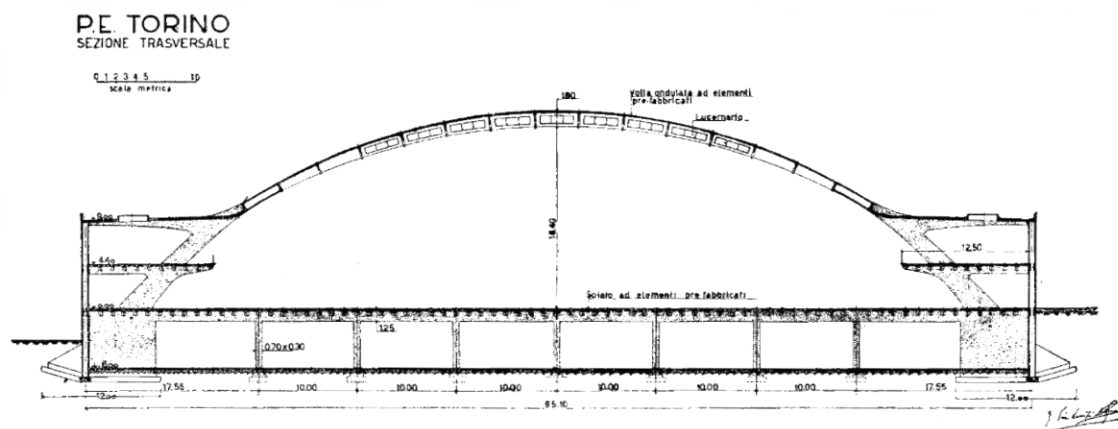


Figure 7.7: Cross section of Hall B

Hall B, conceived as a cathedral, is rectangular and covers an area of 94.3 m x 110.0 m. It consists of a wide nave covered by a cylindrical barrel vault with a span of 81 m, which he called “waved vault”, and an apse covered by a hemispherical dome. The arches of the vault were composed of wave-like prefabricated ferrocement elements, which Nervi significantly referred to as “wave ashlar”. The wave ashlar were patented in August 1948 (Figure 7.8), just before the inauguration of Hall B. The idea was to shape the prefabricated elements using a geometry that would guarantee a high moment of inertia

with a minimum amount of material. The advantages of using ferrocement for the construction of these elements is unquestionable, it was just a matter of bending wire meshes around a brick mold and then filling the mesh with mortar. The result was a lightweight element, only a few centimeters thick, and safely transportable due to its high moment of inertia (Figure 7.9).

Every arch is composed of 13 ferrocement elements, with a span of 2.5 m, a length of 4.5 m, a variable height, roughly 1.5 m, and a thickness of 38 mm. Each wave ashlar was closed at either end by non-deformable headers. The wave ashlars were installed in a metallic tubular scaffolding and joined by site-cast reinforced concrete ribs in the valleys and ridges of the waves. The amount of reinforcing steel used in the ferrocement elements totaled 18 kg/m^2 (Carpanelli, 1955). 9 out of the 13 ferrocement elements that compose each arch are perforated to serve as light sources, with windows inserted on the sloping sides of the undulating surfaces.

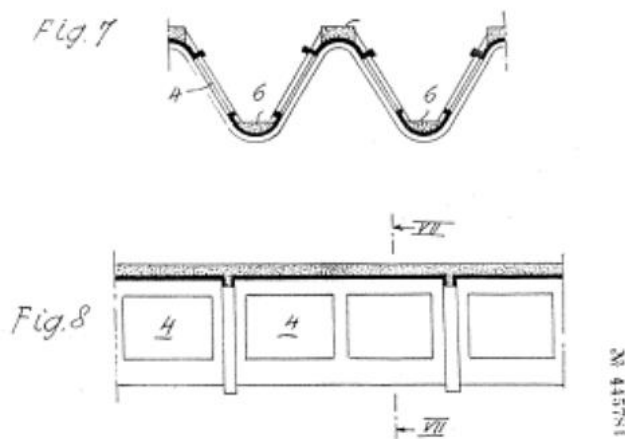


Figure 7.8: Italian patent n. 445781, Ferrocement wave, 1948

The static scheme that was adopted for a stripe of vault is that of a fully restrained arch with a variable section. It is rather complicated to find much information about the Nervi's original design and calculations; though, what is known is that a variable load of 150 kg/m^2 and a thermal variation of $\pm 20 \text{ }^\circ\text{C}$ were considered (Carpanelli, 1955).

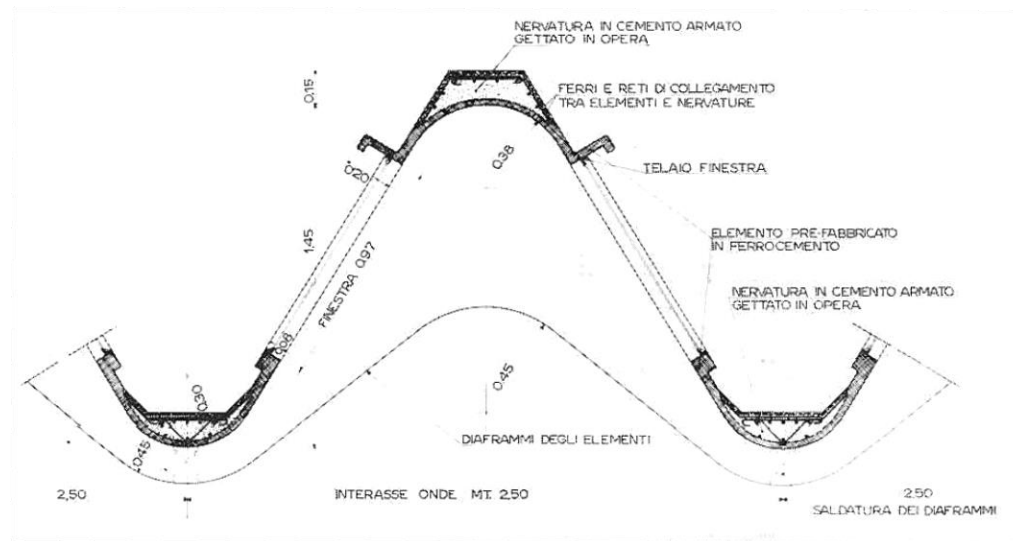


Figure 7.9: Hall B, cross section through a waved vault element

The arches were grouped together in threes and connected through fan-shaped units to in situ reinforced concrete spurs (with a spacing of 7.5 m) (Figure 7.10). The same reinforced concrete spurs support the balconies of the lateral galleries on two levels and rest on shaped plinths. The fan-shaped units are not at all an expression of a formal continuity between parts of the structure, but actual essential organs of the prefabricated sector stiffening device, made out of channels that direct the reinforcement bars towards the waves. Moreover, Nervi built a big triangular connection slab between the pairs of fans, with formwork consisting of wooden boards adjacent to the ferrocement permanent formwork of the fans in which the reinforced concrete could be cast in place. Certain about the properties of impermeability and crack-resistance of ferrocement (for which the material had been invented and used for hulls, floats, and tanks), instead of using a water-repellent material, Nervi employed a layer of ferrocement to protect against the elements the cast-in-place reinforced concrete ribs above the undulations. Nervi trusted the high impermeability of his material so much that he refused to protect the extrados of the vault with a water-repellent material. However, the extrados of the vault is nowadays covered by means of a bituminous waterproofing system.

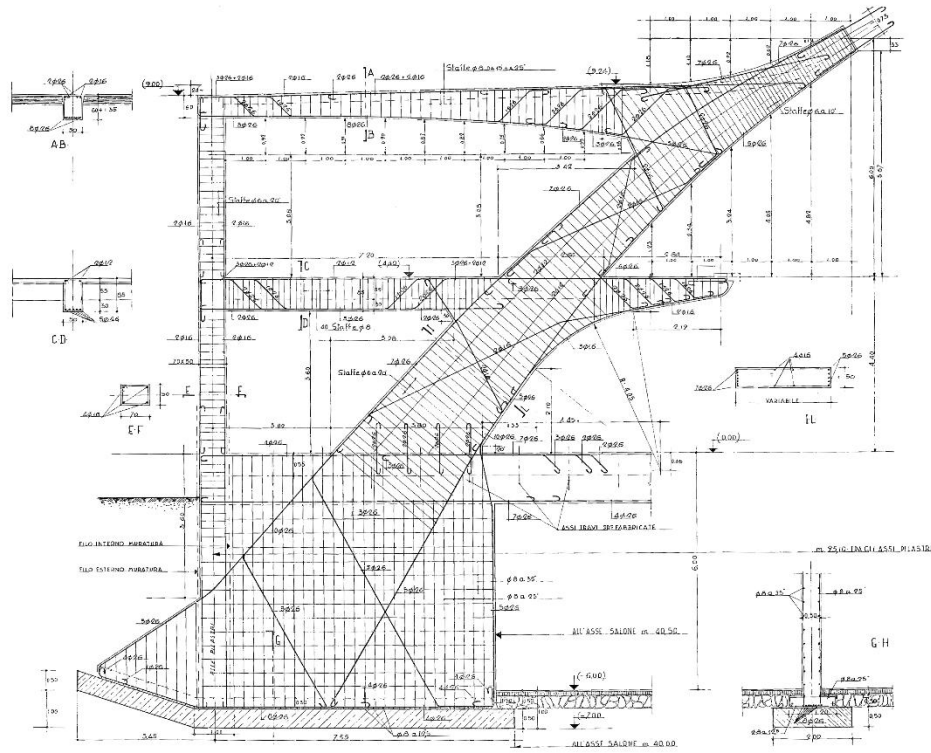


Figure 7.10: Hall B, reinforcement of spurs (Nervi, 1957)

The 40 m half-dome is Nervi’s first dome at a significant scale that featured interior ribs (Segal & Adriaenssens, 2013); it was constructed with precast diamond-shaped ferrocement tiles 2 cm thick, namely “Tavelloni”. The idea was inspired by the need to solve the problem regarding the construction of a thin curved surface stiffened by ribs. Tavelloni, patented in May 1950 (Figure 7.11), were used as permanent “sacrificial” formwork and connected by site-cast reinforced concrete on their tops and the lateral ribs, obtaining a total thickness of 6 cm. These elements were not removed when the building was finished but became an integral part of the completed structure. The ribbing distributed the thrust by transmitting it entirely on the beams on the edges and a flat annular perimetral slab having a span of 10 m (Figure 7.12).

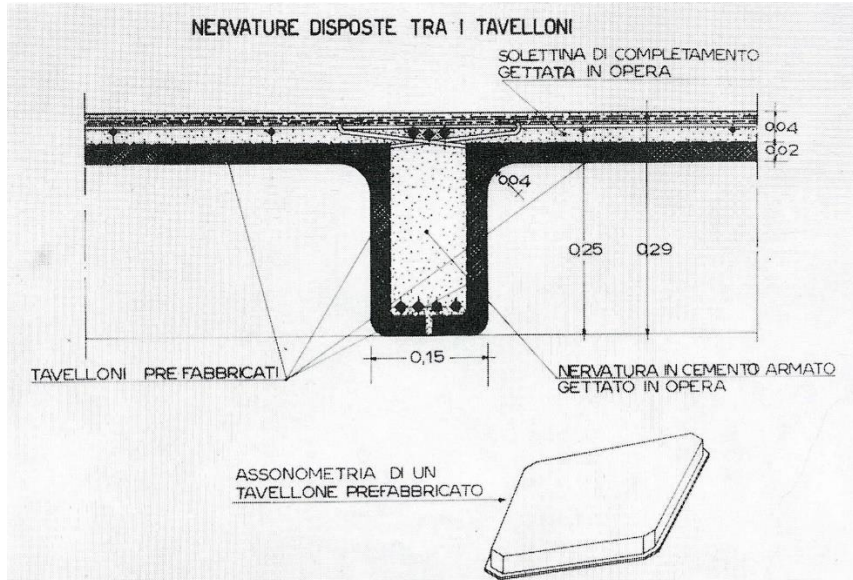


Figure 7.11: Hall B, Ferrocement elements “Tavellone” connected by site-cast reinforced concrete

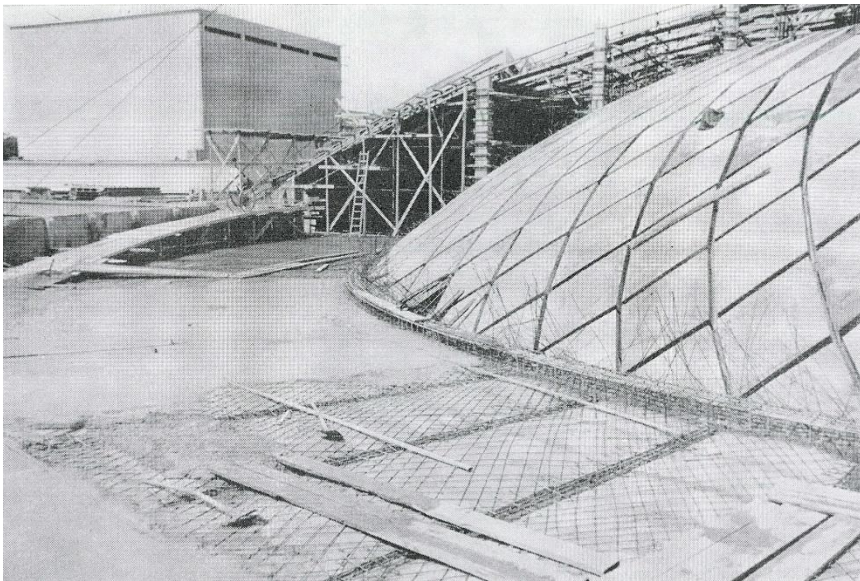


Figure 7.12: Hall B, the half-dome during construction

7.3.2 Hall C for Turin Exhibition Center

Hall C, adjacent to Hall B, was designed in November 1949, then revised and finalized the following year with the engineer Aldo Arcangeli from Nervi & Bartoli. Like Hall B, Hall C is rectangular and covers an area of 65.0 m x 50.0 m (Figure 7.13).

Nervi focused on a structure set on corner support points from which the vault configuration arose. The main reinforced concrete structure of Hall C was made up of four

inclined arches (buttresses), which sustain the ribbed vault. Hall C was Nervi's first use of buttresses (Segal & Adriaenssens, 2013), which were built using cast-in-place reinforced concrete in timber formwork. To build the vault, the same system of ferrocement tiles, i.e., Tavelloni, of the apse of Hall B was used.

The sources of natural lighting constituted a central concern in the design of the elements. Although the ashlar could be easily perforated at the side, radical modifications had to be applied to the design of Tavelloni in order to obtain an opening so that light could pass through. Thus, Nervi invented a special type of precast ferrocement Tavelloni to accommodate his plans for the natural lightning strips (Figure 7.14). Nervi broke down his Tavellone into two parts, the four sides and the lid, each always manufactured using the same ferrocement procedure. Installation of the sides created a grid of cavities in which the reinforced concrete ribs were cast in place.

Perimetral galleries run behind the arches, whose floors (bordering the roof of the Hall) are made with undulating prefabricated ferrocement elements having a length of 10 m and a width of 0.94 m. These elements absorb any accidental overload and provide rigidity along the perimeter of the roof.

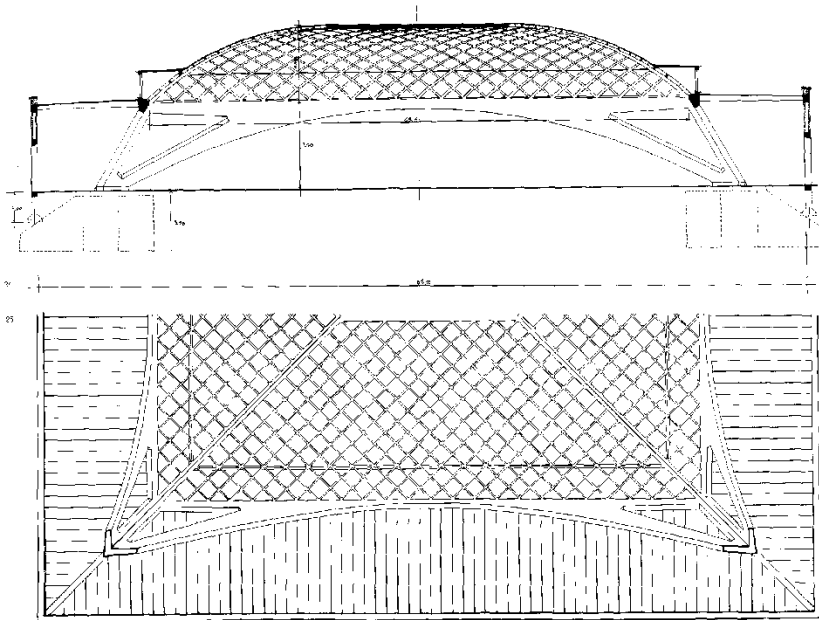


Figure 7.13: Map of Hall C

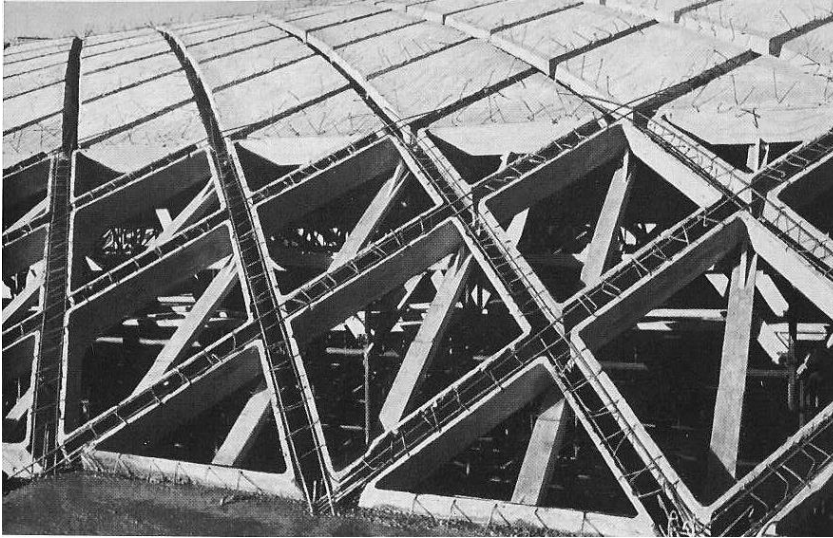


Figure 7.14: Assembling the vault, 1950

Regarding the cement-based mortar, Nervi used the same composition for each ferrocement element employed in the construction, that is 800 kg of high strength cement per cubic meter of sand (Carpanelli, 1955).

7.3.3 Visual Inspection and Durability Assessment of Hall B

The municipality of Turin is currently involved in a restoration plan for Turin Exhibition Center, including the surrounding buildings. The prospective application for Nervi's structures is that of city library and a feasibility study has almost been completed. However, detailed surveys must be carried out with focus on ferrocement elements, since their durability condition is still unclear.

A visual inspection was conducted on Hall B by Sintecna s.r.l. and METEC Engineering in 2003, in view of the 2006 Winter Olympics and the construction of emergency stairs. The authors argued that Hall B appears well preserved, even though visible cracks, are visible at the intrados of the balconies and, even more so, at the ground level slab.

What is interesting is the fact that colorimetric tests (1% phenolphthalein pH-indicator) performed on the intrados of some of the wave ashlar in the ribbed vault did not unveil any presence of deep carbonated layers (Figure 7.15). Considering the structure's age, the authors justified this impressive result by addressing the exceptional compactness of Nervi's material and the favorable environmental conditions.

Moreover, Nervi's halls were prepared for a temporary use during the 2006 Winter Olympics; in this occasion, paints of the brand "Sikkens" were used for aesthetic reasons. It is worth noticing that such paints do not offer any protection from the environment, though they can potentially hinder the effectiveness of prospective surface treatments whose function is to protect concrete surface and prolong service life of the structure. Thus, if protective measures are to be employed, removal of the current paint is recommended (for example, by means of sand blasting).



Figure 7.15: Wave ashlars, assessment of the carbonation depth (P.Q.R.S. s.r.l., Laboratorio Prove Materiali)

To properly evaluate the state of conservation and design restoration measures for Nervi's structures, a detailed survey shall be carried out in addition to the visual inspection. Since Turin Exhibition Center is considered a heritage structure, principles listed in Chapter 5 must be carefully followed. Furthermore; there is still a need for comprehensive

experimental studies on ferrocement durability, since little attention has been given to this aspect so far.

CHAPTER 8

CONSTITUENTS OF FERROCEMENT, COMPOSITION, AND REINFORCING PARAMETERS

In the 1960s and the 1970s ferrocement was made of a cement-based matrix and steel wire meshes of different forms, such as woven or welded square mesh, hexagonal (chicken wire mesh), and diamond shape (expanded metal or expanded lath as used in Stucco applications). Other potential reinforcements were also available including meshes made of natural fibers (jute or sisal) and polymeric meshes (or textiles or fabrics) of various forms. A broader definition for ferrocement should consider the possible presence of a skeletal steel and a cementitious matrix with and without short discontinuous fibers in addition to the mesh system. Typical reinforcement systems for ferrocement are shown in Figure 8.1. A very useful overview of ferrocement composition, reinforcing parameters and properties is given in Table 8.1.

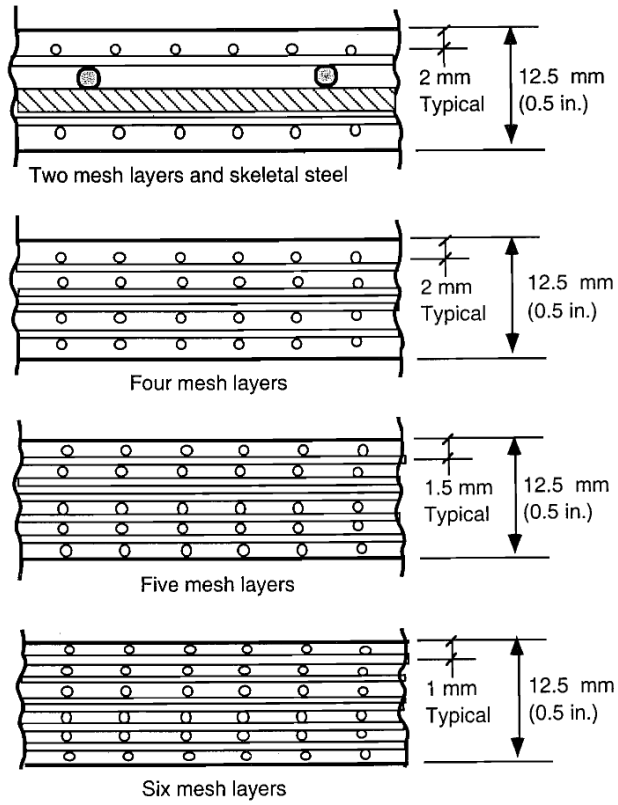


Figure 8.1: Typical sections of ferrocement (Naaman, 2000)

Table 8.1: Summary of ranges of composition, reinforcing parameters, and mechanical properties in ferrocement (Naaman, 2000)

| | | |
|---|---|--|
| WIRE-MESH REINFORCEMENT | <ul style="list-style-type: none"> • Wire Diameter: • Type of Mesh: • Size of Mesh Openings: • Number of Mesh Layers: • Volume Fraction of Reinforcement: • Specific Surface of Reinforcement: | <ul style="list-style-type: none"> • $0.5 \leq d_w \leq 1.5$ mm; ($0.020 \leq d_w \leq 0.062$ in.) • Square woven or welded galvanized wire mesh; aviary (chicken) wire mesh; or expanded metal mesh • $6 \leq D \leq 25$ mm ($1/4 \leq D \leq 1$ in.) • Up to 6 layers per cm of thickness (Up to 14 layers per in. of thickness) • Up to 8% in both directions corresponding to up to 630 kg/m³ (40 lb per ft³) of steel mesh reinforcement • Up to 4 cm²/cm³ in both directions (up to 10 in.²/in.³ in both directions) |
| INTERMEDIATE SKELETAL REINFORCEMENT | <ul style="list-style-type: none"> • Type: • Diameter: • Grid Size: <p>Skeletal reinforcement not always present.</p> | <ul style="list-style-type: none"> • Wires; wire fabric, rods; strands • $3 \leq d_b \leq 10$ mm; ($1/8$ to $3/8$ in.) • $5 \leq G \leq 15$ cm; ($2 \leq G \leq 6$ in.) |
| TYPICAL MORTAR COMPOSITION | <ul style="list-style-type: none"> • Portland Cement: • Sand-to-Cement Ratio: • Water-to-Cement Ratio: • Recommendations: | <ul style="list-style-type: none"> • Any type depending on application • $1 \leq S/C \leq 2.5$ by weight • $0.35 \leq W/C \leq 0.6$ by weight • Fine sand all passing U.S. sieve No. 16 (1.5 mm) and having 5% by weight passing No. 100 (0.25 mm), with a continuous grading curve in-between. • Additives: (Fly Ash / C) = 0.2 Air entraining agent; Corrosion inhibitor; Water reducing agent, or Superplasticizer, as needed. |
| COMPOSITE PROPERTIES | <ul style="list-style-type: none"> • Thickness: • Steel Cover: • Ultimate Tensile Strength: • Allowable Tensile Stress: • Modulus of Rupture: • Ratio Bending/Tension: • Compressive Strength: | <ul style="list-style-type: none"> • $6 \leq h \leq 50$ mm ; ($1/4 \leq h \leq 2$ in.) [mostly < 30 mm] • $1.5 \leq cover \leq 3$ mm; ($1/16 \leq cover \leq 1/8$ in.) • Up to 35 Mpa (5,000 psi) • Up to 14 MPa (2,000 psi) • Up to 70 MPa (10,000 psi) • From 2 to 2.5 • 21 to 96 MPa (3,000 to 12,000 psi) |

8.1 Mortar Matrix

The materials used in ferrocement should satisfy standards similar to those used for quality reinforced concrete construction. The mortar matrix has a great influence on the behavior of the final ferrocement element since it usually comprises more than 95 percent of ferrocement volume. It primarily consists in Portland cement (sometimes blended with

a pozzolan) and inert filler material such as a well-graded sand capable of passing a 2.36 mm (No. 8 ASTM) sieve. However, a sand passing a 1.16 mm (No. 16 ASTM) sieve has been reported to give satisfactory results in improving workability of mortar mix (ACI Committee 549, 1997). Small-size coarse aggregate may be added to the sand if permitted by the size of the mesh openings and the distance between layers of mesh. ACI 549.1R-93 (ACI Committee 549, 1993) provides a series of requisites that cement, aggregates, water and chemical admixtures should verify to be used in ferrocement construction. Sand is the most common aggregate used in ferrocement, it should comply with ASTM C 33 requirements or an equivalent standard. Regarding the grading of the sand, ASTM C 33 provides the guidelines for showed in Table 8.2.

Table 8.2: Grading requirements for sand, provided by ASTM C 33

| Sieve size, U.S. standard square mesh | Percent passing by weight |
|--|----------------------------------|
| No. 8 (2.36 mm) | 80-100 |
| No. 16 (1.18 mm) | 50-85 |
| No. 30 (0.60 mm) | 25-60 |
| No. 50 (0.30 mm) | 10-30 |
| No. 100 (0.15 mm) | 2-10 |

Both in ferrocement and in reinforced concrete the mixing water should be fresh, clean, potable, and relatively free from organic matter. It should have a pH greater than 7 to minimize the reduction in the pH of the mortar slurry.

The mix proportion ranges of the mortar for ferrocement are (ACI Committee 549, 1997):

- sand-cement ratio by weight, 1.4 to 2.5;
- water-cement ratio by weight, 0.3 to 0.5.

The amount of water used should be the minimum consistent with compactibility. A proper workability should allow the mix to completely penetrate and surround the mesh reinforcement and will have acceptable amount of shrinkage and porosity. The mix should be as stiff as possible (except when closed molds are used), provided it does not prevent

full penetration of the mesh. Normally the slump of fresh mortar should not exceed 50 mm.

Additives such as fly ash, silica fume, air-entraining agents, superplasticizers, viscous agents, and the like, are used in ferrocement for one of the following purposes: 1) water reduction to increase strength and reduce permeability; 2) improvement of impermeability; and 3) air entrainment to increase resistance to freezing and thawing. In addition to the numerous admixture commercially available and commonly used in the production of both ferrocement and reinforced concrete, ferrocement may require chemical additives to reduce the reaction between the mortar matrix and reinforcement when a galvanized steel mesh is used. In this regard, multiple studies reported successful results by adding chromium trioxide to the mix water (Haynes & Guthrie, 1974; Disenbacher & Brauer, 1984). A generally recommended solution concentration is approximately 300 parts per million of chromium trioxide by weight of mortar, however the precise solution concentration depends on the w/c ratio used. If a nongalvanized steel is used, no special precautions need to be taken.

8.2 Skeletal Steel

In the traditional method of ferrocement construction, the mesh layers are tied by hand to a skeletal steel, and mortar is forced through this armature and finished on both sides by conventional plastering techniques. Alternatively, mortar may be shot through a spray gun device (shotcreting). A proprietary technique, called the *lay-up technique* (or laminating process) was developed by Martin Iorns. It involves placing the mesh in the mortar rather than the mortar in the mesh and has shown to provide excellent mesh encapsulation.

In ferrocement construction, skeletal steel is often used in the form of welded wire fabric, or simply a grid of steel wires, rods, or strands. The purpose of skeletal steel is to create the shape of the structure that is being built. However, the use of skeletal steel can be very cost effective for the following reasons: first, it acts as a spacer, allowing to save in mesh layers, it also adds significantly to the tensile and punching shear resistance of ferrocement. Ultimately, considering that skeletal steel is generally placed in the middle of the section, it can mildly contribute to increase the bending resistance of ferrocement.

The properties of the skeletal reinforcement are typically those of standard reinforcing bars or prestressing strands used in reinforced or prestressed concrete structures.

Construction methods that imply the use of skeletal steel can be highly labor-intensive and prone to leave voids in the shadows of the mesh and rods. Also, U.S. Navy research on high performance ferrocement hulls showed that rods are an inefficient use of reinforcing because they are not loaded to take advantage of their strength, their spacing allows regions of unreinforced mortar that contribute to weight but not to strength, and they act as stress concentrator (Disenbacher & Brauer, 1984).

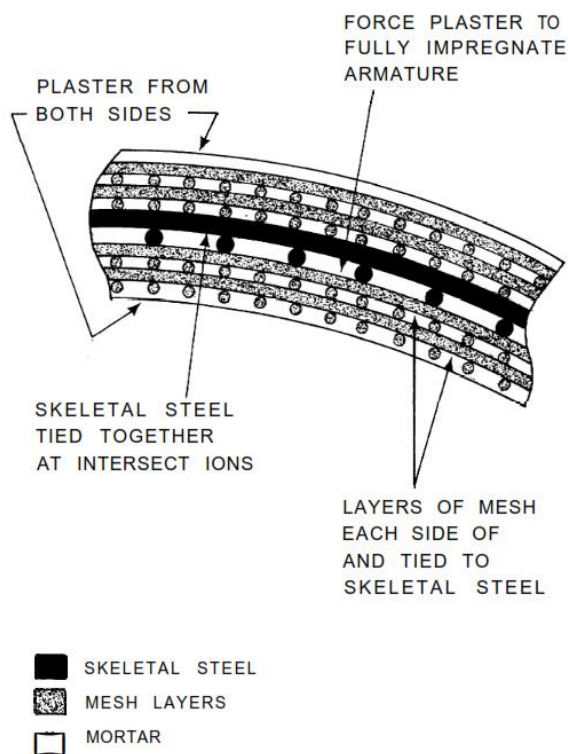


Figure 8.2: Armature system (ACI Committee 549, 1993)

The need of rods can be eliminated by changing the construction technique. In fact, it is possible to apply mortar to layers of mesh supported by molds made of wood strips, plywood, fiberglass, rigid foam, ferrocement, concrete and even compacted earth. Detailed information on construction techniques are given by ACI Committee 549 (ACI Committee 549, 1993; ACI Committee 549, 1997) and can be found in (Naaman, 2000)

8.3 Mesh Reinforcement

So far, wire mesh with closely spaced wires is the most common used reinforcement in ferrocement. Common wire meshes have hexagonal (also referred as chicken wire mesh or aviary mesh) or square openings. Hexagonal meshes are easy to install for doubly curved elements, but they are not as efficient as meshes with square openings, in which the wires are generally oriented in the directions of the principal stresses. Meshes with square openings are available in welded or woven form. Welded wire mesh is made from straight wires in both the longitudinal and transverse directions, while woven mesh is made of longitudinal wires woven around straight transverse wires.

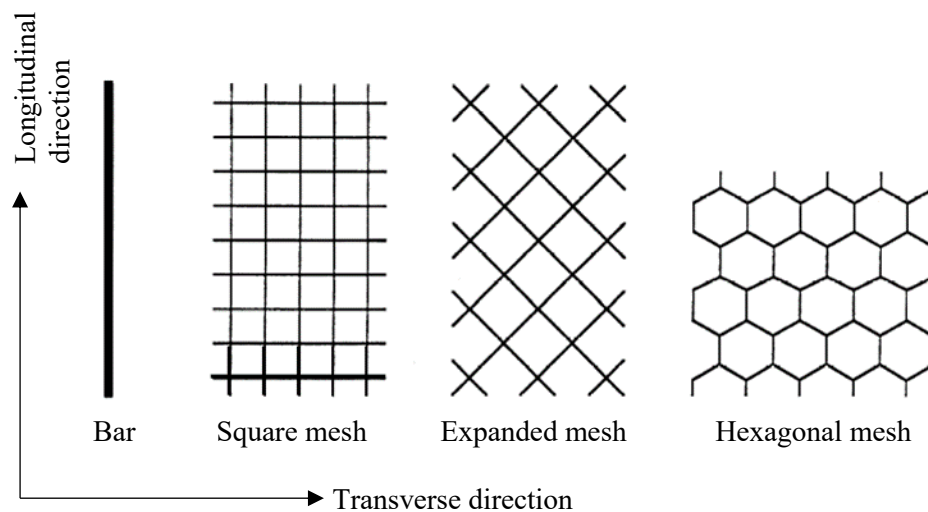


Figure 8.3: Assumed longitudinal and transverse directions of reinforcement (ACI Committee 549, 1993)

The properties of welded wire mesh are closest to the steel reinforcing bars used in reinforced concrete. Due to the weaving effect of the wire, which under tension tends to straighten up leading to a decrease in modulus, woven meshes have a lower apparent elastic modulus than welded wire meshes, and they lead to higher crack widths in the initial portion of the load-deformation curve (ACI Committee 549, 1993). On the other end, it has been showed that welding reduces the tensile strength of the wire (Cohen, 1960). Wire meshes are also available in galvanized form; however, galvanizing, like welding, reduces the tensile strength. Minimum values of yield strength and effective elastic moduli recommended for design are reported in Table 8.4.

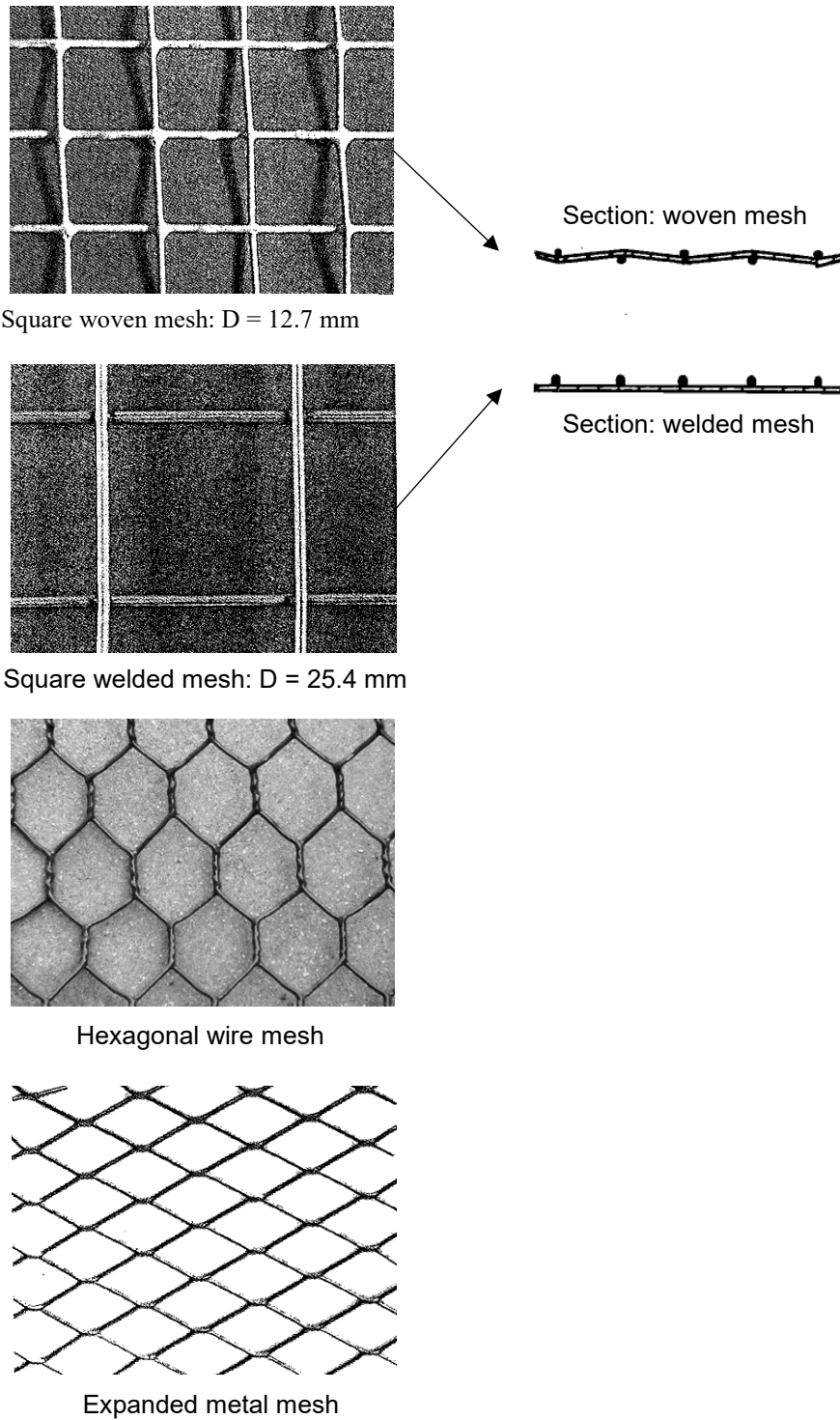


Figure 8.4: Typical steel meshes used in ferrocement applications

Other than traditional wire mesh, expanded metal, welded wire fabric, wires or rods, prestressing tendons and discontinuous fibers are also being used in special applications. In addition, research has been done on fiber reinforced polymeric or plastic meshes.

Table 8.3: Common types and sizes of steel meshes used in ferrocement (ACI Committee 549, 1993)

| Type | Shape | Fabrication | Designation, gage* | Wide spacing, mm | Wire diameter, mm |
|-------------|---------------------|-----------------|---|------------------------|-------------------|
| Wire mesh | Square | Woven or welded | $\frac{3}{4} \times \frac{3}{4}$ No. 16 | 19.0 | 1.60 |
| | | | 2 × 2 No. 19 | 13.0 | 1.00 |
| | | | 3 × 3 No. 22 | 8.5 | 0.72 |
| | | | 4 × 4 No. 23 | 6.4 | 0.64 |
| | | Welded | 1 × 1 No. 14 | 25.0 | 2.00 |
| | Rectangular | Welded | 2 × 1 No. 14 | 50 × 25 | 2.00 |
| | Hexagonal | Twisted | 1 No. 18 | 25.0 | 1.20 |
| | | | 1 No. 20 | 25.0 | 0.88 |
| | | | $\frac{1}{2}$ No. 22 | 13.0 | 0.72 |
| | Expanded metal mesh | Diamond | Slit and drawn | 3.4 lb/yd ² | |
| Gage No. 18 | | | | 1.00 | |
| Gage No. 20 | | | | 0.76 | |

* American wide gage

Table 8.4: Common types and sizes of steel meshes used in ferrocement (ACI Committee 549, 1993)

| | | Woven square mesh | Welded square mesh | Hexago- nal mesh | Expanded metal mesh | Longitudi- nal bars |
|------------------------------|--|----------------------------------|-----------------------------------|-----------------------------|------------------------------------|--------------------------------|
| Yield strength | f_y , MPa | 450 | 450 | 310 | 310 | 414 |
| Effective modulus | Longitudi- nal direc- tion $(E_r)_{long}$, 10^3 MPa | 138 | 200 | 104 | 138 | 200 |
| | Transverse direction $(E_r)_{trans}$, 10^3 MPa | 165 | 200 | 69 | 69 | – |

8.4 Similarities and Differences Between Ferrocement and Reinforced Concrete

Some similarities may be identified between ferrocement and traditional reinforced concrete. Both ferrocement and reinforced concrete use similar matrix and reinforcement materials; in addition to that, they obey to the same principles of mechanics and can be modelled according to the same theories. Moreover, they can be designed and analyzed with the same techniques and in both ferrocement and reinforced concrete the limit state design philosophy can be adopted.

Several differences between ferrocement and reinforced concrete do exist, leading ferrocement to behave differently from conventional reinforced concrete in strength, deformation, and potential application.

First, compared to reinforced concrete, ferrocement has a matrix made of fine mortar (the maximum size of the particles in ferrocement is controlled by the average

openings of the stack of mesh system to be encapsulated); it is a thinner material with a reinforcement that is distributed throughout its whole thickness. More importantly, ferrocement differs from conventional reinforced or prestressed concrete by the way the reinforcing elements are dispersed and arranged. In the words of Pier Luigi Nervi (Nervi, 1956), the most notable characteristic of ferrocement is:

greater elasticity and resistance to cracking given to the cement mortar by the extreme subdivision and distribution of the reinforcement.

Many of the properties unique to ferrocement derive from the fact that its reinforcement is placed in the two directions (generally the directions of the principal stresses). All these differences in physical characteristics translate into important dissimilarities in mechanical properties. In fact, ferrocement has been showed to have homogeneous-isotropic properties in two directions, high tensile strength and high modulus of rupture. Its tensile strength can be on the same order as its compressive strength. Because of its two-dimensional reinforcement, ferrocement has a better impact and punching shear resistance than reinforced concrete. Ferrocement has a high reinforcement ratio in both tension and compression (recommended to be between 2 and 8 percent), however it is not significantly higher than reinforced concrete. Since the wire diameter of a mesh layer is much smaller than rebars in reinforced concrete (recommended values between 0.5 and 1.5 mm), high values of specific surface of reinforcement can be reached (up to $4 \text{ cm}^2/\text{cm}^3$ in both directions). In fact, specific surface of reinforcement is one to two orders of magnitude that of reinforced concrete. Primarily due to the high specific surface of reinforcement and of the presence of transverse reinforcement, the cracking behavior of ferrocement under tension differs from reinforced concrete. More specifically, the average crack width and spacing are more than an order of magnitude smaller. In addition to that, ferrocement has showed great extensibility (i.e., the elongation to failure in tension, or the deflection to maximum load), which increases with an increase in the number of mesh layers used. This is equivalent to say that the ductility of ferrocement increases with an increase in the volume fraction and specific surface of reinforcement. This is in contrast with what observed in reinforced concrete, where ductility control is also achieved by limiting the reinforcement ratio.

8.5 Geometrical Properties of Reinforcement

To fully understand many of the mechanical properties of ferrocement, it is necessary to introduce the geometrical properties that define the subdivision and distribution of reinforcement. Furthermore, such geometrical parameters must be carefully structured for ferrocement to show its outstanding mechanical properties, making sure it does not behave like conventional reinforced concrete.

8.5.1 Cover

The net cover to the first layer of reinforcement should be selected regarding the thickness of the reinforcement element, the wire diameter of the mesh used, and the environmental exposure of the structure. For ferrocement elements between 10 and 25 mm in thickness the recommended average net cover is about 2 mm, while for very thin composite such as $h = 5 \text{ mm}$, a one mm cover should be appropriate. Overall, the following criteria should be preferably satisfied (ACI Committee 549, 1997; Naaman, 2000):

$$\text{net cover} \begin{cases} \leq 2 \text{ mm} \\ \leq h/5 \\ \leq 2 d_w \end{cases} \quad (8-1)$$

where d_w is the diameter of the mesh wire and h is the thickness of the ferrocement member. Lesser values can be used provided the reinforcement is galvanized, the surface protected by an appropriate coating, and the crack width limited to 0.05 mm (ACI Committee 549, 1997).

8.5.2 Volume Fraction of Reinforcement

The volume fraction of reinforcement is defined as the ratio of volume of reinforcement to the volume of composite:

$$V_r = \frac{V_{\text{reinforcement}}}{V_{\text{composite}}} \quad (8-2)$$

$V_{\text{reinforcement}}$ includes the skeletal steel, which has a relevant contribution in evaluating the resistance of tensile members. However, if the skeletal steel is placed in the

center of the ferrocement member and if bending is considered, its influence may be ignored.

The volume fraction of reinforcement can be divided into longitudinal (V_{rL}) and transverse (V_{rT}) parts:

$$V_r = V_{rL} + V_{rT} \quad (8-3)$$

that is:

$$V_{rL} = V_r \eta_L \quad (8-4)$$

$$V_{rT} = V_r \eta_T \quad (8-5)$$

where η_L and η_T are the efficiency factor in the longitudinal and transverse direction, respectively. Their recommended design values are listed in Table 8.5.

Table 8.5: Recommended design values of the global efficiency factor of mesh reinforcement η_0 for uniaxial tension or bending (ACI Committee 549, 1993)

| | | Woven square wire mesh | Welded square wire mesh | Hexagonal wire mesh * | Expanded metal lath | Longitudinal bars |
|------------------------------------|--|------------------------|-------------------------|-----------------------|---------------------|-------------------|
| Global efficiency factor: η_0 | Longitudinal direction: η_L | 0.50 | 0.50 | 0.45 | 0.65 | 1 |
| | Transverse direction: η_T | 0.50 | 0.50 | 0.30 | 0.20 | 0.00 |
| | At $\theta = 45^\circ$: η_θ | 0.35 | 0.35 | 0.30 | 0.30 | 0.70 |

* chicken wire mesh or aviary mesh

For square or rectangular meshes the volume fraction of reinforcement can be calculated from

$$V_r = \frac{N \pi d_w^2}{4 h} \left(\frac{1}{D_L} + \frac{1}{D_T} \right) \quad (8-6)$$

where N is the number of layers of mesh, d_w is the diameter of mesh wire, D_L and D_T are the distance to center between longitudinal wires and transvers wires, respectively (Figure 8.5), h is the thickness of reinforcement element.

Hence:

$$V_{rL} = V_r \eta_L = \frac{N \pi d_w^2}{4 h} \left(\frac{1}{D_L} \right) \quad (8-7)$$

$$V_{rT} = V_r \eta_T = \frac{N \pi d_w^2}{4 h} \left(\frac{1}{D_T} \right) \quad (8-8)$$

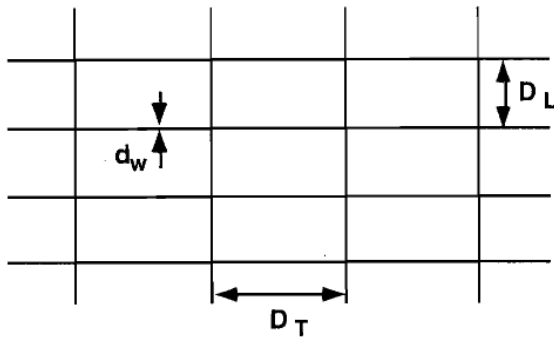


Figure 8.5: Rectangular mesh

8.5.3 Specific Surface of Reinforcement

The specific surface of reinforcement (S_r) is the total lateral surface area of reinforcement (assumed bonded) divided by the volume of composite. The following expression for the specific surface of reinforcement can be easily derived:

$$S_r = \frac{4 V_r}{d_w} \quad (8-9)$$

If a ferrocement member and a reinforced concrete one having the same volume fraction of reinforcement are considered, the specific surface of reinforcement in ferrocement will be one to two orders of magnitude higher than that of reinforced concrete, thanks to the quite small diameter of wires in ferrocement (between 0.5 and 1.5 mm).

Limiting values of both volume fraction and specific surface of reinforcement are often found in the technical literature. For non-prestressed, non-water-retaining ferrocement structures, the total volume fraction of steel mesh reinforcement should not be less

than about 1.8 percent and the total specific surface of reinforcement should not be less than $0.8 \text{ cm}^2/\text{cm}^3$. For water-retaining ferrocement structures the set limits are higher, that is, 3.5 percent and $1.6 \text{ cm}^2/\text{cm}^3$ respectively.

8.6 Mechanical Properties of Ferrocement

Under various loading conditions, ferrocement exhibits a distinctive mechanical behavior when compared to traditional reinforced concrete. A good review of the mechanical properties of ferrocement can be found in (ACI Committee 549, 1982). Some current limits of common mechanical properties are listed in Table 8.6.

Table 8.6: Mechanical properties of ferrocement reinforced with conventional steel meshes and cement mortar matrices (Naaman, 2000)

| Property | Highest Values |
|---------------------------|---|
| Ultimate Tensile Strength | Up to 35 MPa |
| Modulus of Rupture | Up to 70 MPa (equivalent elastic bending strength) |
| Compressive Strength | 80 to 100 percent of mortar matrix strength |
| Ultimate Tensile Strain | Up to the tensile strain of the reinforcement |
| Crack widths | Up to 100 times smaller than in reinforced concrete for same composite tensile stress. As low as $10 \mu\text{m}$ were observed at working stresses |

Ferrocement can be described as a wonder material that has a variety of marvelous properties. It can be indeed considered a small-scale model of a super reinforced concrete: it does crack, but cracking under service loads can be so fine that it is not visible to the naked eye.

8.6.1 Tensile behavior

The typical behavior of a reinforced concrete tensile prism is schematized in Figure 8.6, where the tensile stress-strain response of the reinforcing steel is assumed to be elastic perfectly plastic. Stage I (segment OA) corresponds to the ascending linear elastic portion of the curve; this stage ends with the beginning of the formation of cracks along the specimen (Stage II, segment AB). In concrete, most cracks are formed within a relatively small increment of load beyond first structural cracking. The number of cracks stabilizes, that is, cracks stop forming, in point B with the beginning of Stage III (segment BC), where cracks are almost equidistant and crack widths increase with an increase in applied load. The load-elongation response is almost linear in Stage III, and the slope of the curve is smaller than that of the initial portion because of cracking, being governed by the elastic modulus of steel in tension. Stage III ends with the yielding of the reinforcing steel. Stage III ends with the of the reinforcing steel.

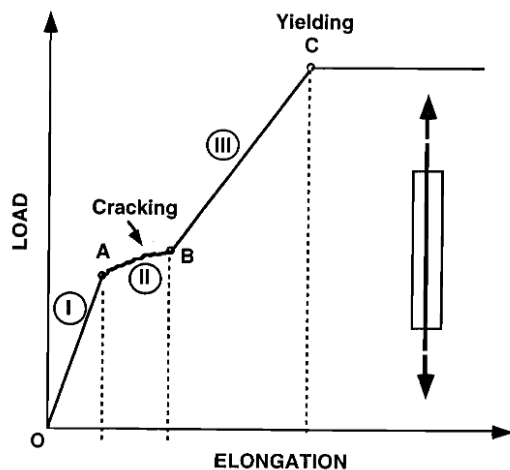


Figure 8.6: Schematic load-elongation curve of reinforced concrete in tension (Naaman, 2000)

If a ferrocement tensile prism is considered (Figure 8.7) its excellent cracking behavior can be emphasized. Compared to reinforced concrete, the main difference is in Stage II, which can be so extensive that it completely takes over Stage III. During Stage II, cracking develops gradually with increasing load to a point where the spacing of the cracks corresponds to the spacing of the transverse wire in the mesh (Mattar, 1971). If the reinforcing parameters are appropriate, multiple cracking can be extensive (i.e., ductile behavior is exhibited) and the end of multiple cracking can be close to the yielding point of the reinforcing steel.

The fact that cracks keep forming reducing the length of Stage III means that crack width does not increase proportionally to the applied load. As a result, crack widths in ferrocement can be one to two orders of magnitude smaller than in reinforced concrete.

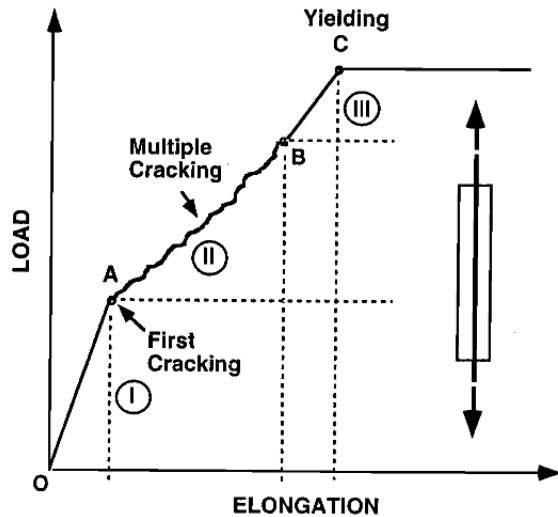


Figure 8.7: Schematic load-elongation curve of ferrocement in tension (Naaman, 2000)

8.6.2 First Crack

The term First-crack strength appears frequently in literature, when the behavior of ferrocement under tension and flexure is studied. However, this term can carry different meanings. It can be shown (Walkus, 1975) that cement matrices develop microcracks as soon as they are subjected to tensile loading. The *percolation theory* can be usefully addressed to distinguish between an isolated microcrack from a real structural crack. In such theory it is assumed that many microcracks can form randomly in the cement matrix to the point where such microcracks merge together to form a three-dimensional surface separating the specimen into two totally unconnected parts: a true structural crack is formed. However, other definitions for first crack can be found in literature (Walkus, 1975; Balaguru, Naaman, & Shah, 1977; Austriaco, Lee, & Pama, 1975; Logan & Shah, 1973; Rao & Gowdar, 1971) and sometimes it is simply defined as the first visible crack (Johnston & Mattar, 1976; Johnston & Mowat, 1974; Greenius, 1975).

Despite the disagree on the definition, there is a general agreement (Naaman & Shah, 1971; Mattar, 1971) that, at least in direct tension, resistance to cracking is directly related to the specific surface of reinforcement, with the trend depicted in Figure 8.8.

Furthermore, the specific surface of reinforcement influences other crack-related properties of ferrocement (Figure 8.9).

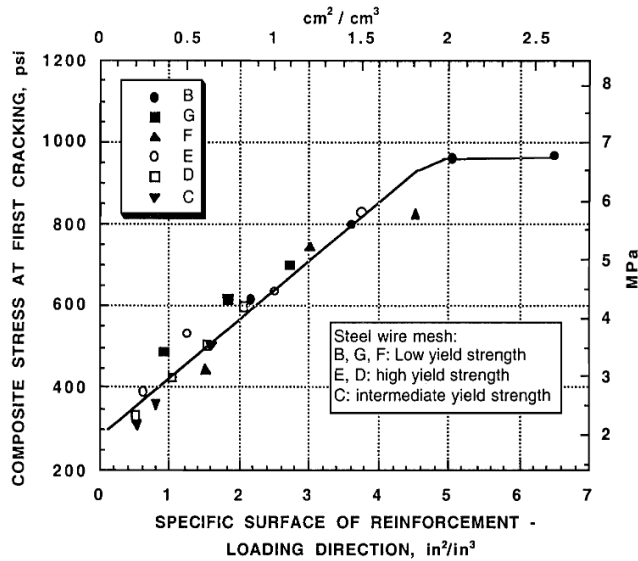


Figure 8.8: Influence of specific surface of reinforcement on stress at first cracking (Naaman, 2000)

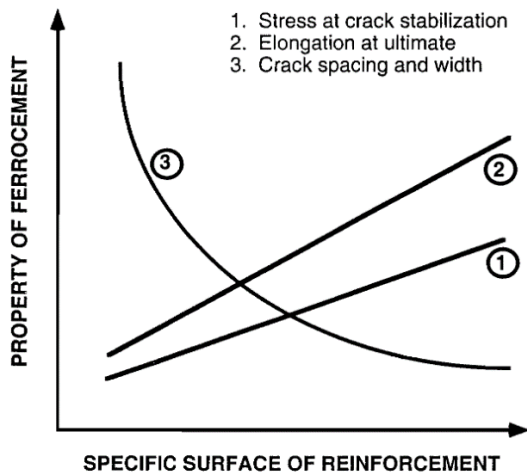


Figure 8.9: Typical quantitative influence of specific surface of reinforcement on properties of ferrocement (Naaman, 2000)

In flexure, relationships linking cracking with specific surface are less well defined. In this case, the specific surface of reinforcement is generally defined as the surface area of total reinforcement per unit volume of reinforcement located in the tension zone only. The available experimental results show that cracking resistance increases from a lower bound value corresponding to the strength of the mortar matrix to higher values that are

proportional to the specific surface. Hence, other variables come into play (Logan & Shah, 1973; Mansur & Paramasivam, 1986; Austriaco, Lee, & Pama, 1975; Walkus, 1975; Mowat, 1970). The bending behavior of ferrocement plates will be described and tested in Chapter 10.

CHAPTER 9

DURABILITY OF FERROCEMENT

Ferrocement can be truly considered a highly versatile form of reinforced concrete, and it has been successfully used as a structural material. However, like in reinforced concrete, ferrocement structures may be hindered by severe exposure conditions. The aim of this chapter is to outline the main reasons why durability of ferrocement deserves dedicated comprehensive studies. In other words, one cannot just refer to the vast literature available on durability of reinforced concrete, since deterioration mechanisms, such as reinforcement corrosion, may be substantially different in ferrocement.

9.1 Deterioration Associated with the Mortar Matrix

When chemicals react with the cement paste, deterioration arises on the matrix side. Furthermore, physical deterioration mechanisms like freezing or surface wear due to abrasion can be considered. The main strategies to minimize the deterioration associated with the matrix consist in limiting the water-to-cement ratio and employing supplementary cementing materials such as fly ash, ground granulated slag, and silica fume. Attack by chemicals that react with cement paste is minimized by ensuring low permeability in limiting the water-to-cement ratio to a maximum of 0.5 (ACI Committee 549, 1997). A water-to-cement ratio of 0.5 can be considered a threshold beyond which the permeability increases vertiginously (Powers, Copeland, Hayes, & Mann, 1954; Ruettgers, Vidal, & Wing, 1935). In case of exposure to sea water or ground water, which is generally rich in sulfates, the water-to-cement ratio should be further reduced to 0.45 or less (ACI Committee 211, 1991). Just like happens for concrete, freeze-thaw deterioration is most effectively prevented by proper air entrainment, with a dosage of about 10 to 13 percent of the mortar volume (Klieger, 1956). Maintenance of low water-to-cement ratio, less than 0.45, is also recommended for freeze-thaw exposure (ACI Committee 211, 1991); however, unlike concrete, the freeze-thaw resistance of ferrocement has received little

study. By limiting the water-to-cement ratio a higher resistance to abrasion can be achieved, since it is governed by the compressive strength of the matrix (Lane, 1978).

9.2 Deterioration Associated with Reinforcement

If a galvanized reinforcement is used, the zinc coating can be attacked by the alkalis in the fresh cement paste, leading to the formation of calcium zincate and hydrogen. To inhibit the formation of hydrogen, 100 to 300 ppm of chromium trioxide may be added to the mixing water (Hansen, 1971; Disenbacher & Brauer, 1984).

Another deterioration mechanism which is associated with the reinforcement and is typical of ferrocement is the galvanic corrosion caused when the galvanized mesh and the skeletal bars (generally made of ordinary steel) are in contact via the electrolytic solution present in the mortar matrix. The formation of zincate leads to an increase in solid volume which may cause blistering, reduce bond, and weaken the ferrocement structurally.

Corrosion of reinforcement is a major concern both in reinforced concrete and in ferrocement. when the matrix becomes cracked, the width of cracks and their continuity may affect corrosion resistance. It is recommended that the maximum predicted value of crack width be less than 0.10 mm for noncorrosive environment and 0.05 mm for corrosive environments or water-retaining structures (ACI Committee 549, 1997).

9.3 Considerations on Durability of Ferrocement

As a matter of fact, the same measures required to ensure durability in conventional reinforced concrete also apply to ferrocement. Such measures are, for example, provided by ACI 201.2R (ACI Committee 201, 2016). However, experimental works pointed out that durability of ferrocement is influenced by the following two factors (ACI Committee 549, 1997): 1) small cover makes easier for aggressive substances to reach the reinforcement; and 2) high surface area of the reinforcement leads to a high area of contact over which corrosion can take place; thus, the resulting corrosion rate can potentially be very high. Despite these two factors, the fact that there is no report in the literature of serious corrosion of steel in ferrocement (other than that associated with poor plastering or poor matrix compaction) suggests that other considerations have to be done with respect to ferrocement durability.

9.3.1 *Cracking Behavior*

Despite the small cover, ferrocement exhibits excellent cracking behavior, which leads to very small crack widths under service load. With respect to serviceability limit state, maximum crack widths in ferrocement are much lower than that of traditional reinforced concrete. In fact, the maximum crack width should not exceed 0.05 mm for corrosive environments and/or water retaining structures, and 0.1 mm for other structures. Analytical expressions can be used to predict the crack widths for tensile and bending members (IFS Committee 10, 2001; Naaman, Ferrocement & laminated cementitious composites, 2000).

Because of its very small crack widths under service load and its great extensibility, ferrocement provides excellent leakage characteristics; it therefore finds application in water tanks. The fact that ferrocement is characterized by small crack widths is often used to explain why ferrocement has shown good durability under various environmental exposures. However, ferrocement has only a thin mortar cover over the outermost layers of reinforcement; this feature should draw attention to corrosion mechanisms of the steel mesh.

To increase the durability of ferrocement, galvanized steel mesh is often used nowadays. Nonetheless, important ferrocement structures, such as Nervi's Turin Exhibition Hall, were built in the past century using plain steel meshes. As a result, the question arises of how to preserve these historical structures and prolong their service life.

9.3.2 *Corrosion*

The reinforcement mesh is distributed throughout the thickness, is characterized by very high specific surface and is composed of small diameter wires. Due to the initially small diameter of the wires, cross section loss of the wire mesh is of great importance in ferrocement. Moreover, in case of corrosion, the expansive corrosion products will induce internal tensile stresses that are expected to be smaller than that of rebars in traditional reinforced concrete.

Kosa et al. investigated the deterioration of steel fiber reinforced concrete and mortar due to fiber corrosion accelerated by intermittent drying and wetting conditions in a 3.5 percent standard sodium chloride solution and in laboratory air (Kosa, Naaman, &

Hansen, 1991; Kosa & Naaman, 1990). Steel fibers, 0.5 mm in diameter and 30 mm long, were used in these studies. The authors pointed out that although all specimens suffered severe corrosion, ranging from 5.4 to 70 percent reduction in the minimum fiber diameter, no corrosion-induced cracks were detected on the surface of the specimens.

Despite the fact that both steel fibers and steel mesh have relatively small diameters and have little or no cover, important differences between those two reinforcements should be taken into consideration:

- fibers have random orientation inside the volume of the composite; hence, assuming a fiber is corroded and expanding, there will likely be other fibers crossing the volume around the corroded fiber and consequently providing confinement;
- in ferrocement, it is likely that the corrosion reaches multiple layers of mesh within a short space of time thus creating a much more severe effect than that in fiber reinforced concrete.

Therefore, corrosion of fibers in concrete is a different phenomenon than that of ferrocement, which deserves new comprehensive experimental studies.

On top of that, the range of mix proportions recommended for common ferrocement applications are sand-cement ratio by weight, 1.5 to 2.5, and water-cement ratio by weight, 0.35 to 0.5. The absence of coarse aggregate leads to a high cement dosage which results in a high alkalinity of the pore solution. High alkalinity is proven to improved durability with regards to chloride-induced and carbonation-induced reinforcement corrosion.

9.3.3 *Alkali-Silica Reaction*

Alkali-silica reactions must be taken into account when the cementitious matrix contains critical amounts of a reactive form of silica (present as a mineral constituent in the aggregate particles) and high concentration of alkali hydroxide (sodium and potassium). Even though there is some evidence that alkalis may be derived in part from external sources, they are usually derived from the Portland cement used.

The effect of aggregate size and amount has been previously studied, mostly in mortars, and both parameters have been reported to either increase or decrease the

expansion. Poyet et al. studied the effect of different reactive size fractions, they found that very fine fractions do not cause expansion (Poyet, et al., 2007). French found that the most deleterious fraction in terms of expansion is the 4-10 mm fraction (French, 1995). Furthermore, French's results have been confirmed by Zhang et al., who studied the influence of the large aggregate content in a concrete mix where all the aggregates were reactive (Zhang, Wang, Tang, Wu, & Zhang, 1999). These researchers argued that depending on the reactivity of the aggregate the overall effect of larger aggregates could be either a reduction or an increase of the measured expansion.

Since in ferrocement the mortar matrix is made of cement and fine sand, little or no expansion can be witnessed during the service life of the structure.

9.4 Techniques to Improve Durability of Ferrocement

Reinforced concrete and ferrocement structures often undergo physical and chemical attacks due to environmental exposures. According to Drochytka and Petranek, the following protective measures can be adopted to increase service life of concrete structures: 1) improving physical properties of concrete and repair materials; 2) altering the electrochemical behavior of steel; and 3) applying surface treatments (Drochytka & Petranek, 2002).

To ensure adequate durability, a fully compacted matrix is necessary. The use of pozzolanic materials (e.g., Class F fly ash and ground granulated blast furnace slag) in ferrocement can improve resistance to sulfate and seawater attack in a similar manner as in conventional concrete (ACI Committee 549, 1997). A protective coating may be desirable in case of particularly aggressive environment or for restoration purposes on existing ferrocement structures. ACI Committee 515 addresses the effect of various substances on untreated concrete and provides recommendations for protective treatments (ACI Committee 515, 2013). In theory, the same kinds of treatments can be applied to ferrocement, even though there is a paucity of literature on this problem.

If a heritage structure is under consideration for a restoration project, "traditional" techniques involving removal and replacement of the old and carbonated mortar with a new layer should be avoided due to the possible alterations in appearance and the

objective difficulty of removing mortar layers around the fine mesh¹. Therefore, the employment of "traditional" techniques should be limited to those cases of extreme degradation and may not involve large quantities of materials.

Electrochemical techniques, such as cathodic protection, corrosion inhibitors, and re-alkalization, can be of great help in stopping ongoing destruction of the existing structure due to corrosion. However, these techniques are not the primary goal of this thesis.

¹ Often, the old mortar to be removed extends beyond the reinforcement.

CHAPTER 10

EXPERIMENTAL STUDY ON IMPROVEMENT OF FERROCEMENT DURABILITY BY NANOMATERIALS

10.1 Introduction

Research work carried out so far reveals that ferrocement possesses advantages such as ease of construction, improved tensile properties, high resilience, ability to take large deflections before collapse, high static ductility, high compressive strength, high resistance to cracking, improved toughness, fatigue resistance, light weight, and economy when compared to reinforced concrete (ACI Committee 549, 1997). Even though a great deal of research has already been conducted on ferrocement, there is still a need for further studies on ferrocement durability.

Cement-based composite materials such as reinforced concrete and ferrocement often undergo physical and chemical attacks due to environmental exposures, which lead to physical and chemical deterioration processes such as sulfate attack, reinforcement corrosion due to chloride penetration, carbonation and freezing-thawing (Moon, Shin, & Choi, 2007). In the recent decades, the deterioration of cement-based composite structures has become a major concern and the cost of repair is sometimes even higher than the original investment (Ibrahim, Al-Gahtani, Maslehuddin, & Almusallam, 1997). Under aggressive environmental exposures, reinforced concrete and ferrocement structures require particular attention to the factors influencing durability.

As most of the aggressive agents gradually penetrate through the composite from the surface to the inner structure, it is accepted that an improvement of the durability can be obtained by blocking ingress of gaseous or aqueous substances through the pore structure of the matrix. As the pores provide the primary transport routes of substances in and

out of cement-based materials, the volume and the structural features of pores will affect the mechanical properties (Kumar & Bhattacharjee, 2003), the diffusion characteristics (Haga, Sutou, & Hironaga, 2005; Sercombe, Vidal, & Gallé, 2007; Gallé, 2011), and the durability (Hou, Cheng, Qian, Cao, & Shah, 2015). Based on this assumption, the application of protective surface treatments can improve the performance of ferrocement and extend its service life (ACI Committee 549, 1993). Many surface treatments are currently available on the market and are used for protection of new and existing concrete and ferrocement structures.

While extensive literature exists on the effectiveness of organic surface treatments on concrete, little attention has been given to those newly developed nanomaterials, such as ethyl silicate, which can be used as penetrating agents to protect the material from aggressive environments. Moreover, the use of surface treatments to improve durability of ferrocement is rarely sighted in the literature. The objective of this study is to investigate the use of ethyl silicate and other penetrative protective agents for the surface treatment of ferrocement. Three kinds of protective treatments were applied (i.e., ethyl silicate, sodium silicate, and isobutyl-triethoxy-silane sealer) to both mortar and ferrocement samples and comparative studies on performances and mechanisms were conducted. Since cracking is a major issue in both concrete and ferrocement structures, ferrocement specimens were prepared with a view to assessing the effectiveness of protective treatments on cracked members.

10.1.1 Classification of Surface Treatments

The surface protection treatments for cement-based materials are classified into three groups by EN 1504-2:2004 (UNI, EN 1504-2, 2004): *hydrophobic impregnation*, *impregnation*, and *coatings*. Hydrophobic impregnation produces a water-repellent surface with no pore filling effect. It is usually performed through silane- or siloxane-based water repellent products, which penetrate into concrete pores and react with hydrated cement particles, forming a reaction product that acts as a hydrophobic lining on the pore walls (Dai, Akira, Wittmann, Yokota, & Zhang, 2010). Impregnation and coatings are often achieved by means of organic polymers, which create a physical barrier that prevents the environmental aggressive agents from penetrating into concrete (Pigino, Leemann, Franzoni, & Lura, 2012). The difference between impregnation and coating is

that the former reduces the surface porosity with partial or total pores filling effect, while the latter produces a continuous protective film on the material surface.

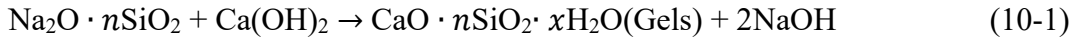
Organic treatment agents, including silane/siloxane, epoxy resin, acrylic resin, etc., are the most widely used on account of their availability and easy application. These surface-treatment methods are effective in ceasing the migration of substances in and out of the surface of hardened cement-based materials to some extent, but they have drawbacks in the long run. For example, alkali-silicate reaction risk increases when the alkali sealing agents are used; organic coatings are prone to aging because of (UV) weathering, which will gradually deteriorate the concrete protection (Almusallam, Khan, Dulaijan, & Al-Amoudi, 2003; Zafeiropoulou, Rakanta, & Batis, 2011; Moradllo, Shekarchi, & Hoseini, 2012; Li, Lei, & Yang, 2013; Kozak, 2015; Basheer, Basheer, Cleland, & Long, 1997; Li, Guo, Gao, Ji, & Geng, 2016).

Considering the characteristics of the superficial part of hardened cement-based materials and the environment they face, (Hou, Cheng, Qian, Cao, & Shah, 2015) identified the following desirable features of the treatment materials. First, an inorganic protection layer should be formed near the surface of the cement-based material to ensure weather-resistivity, mainly with respect to UV radiation. Secondly, the treatment agent should easily penetrate inside the pores with size ranging from nanometer to millimeter. And finally, a strong bond between the old concrete and the new treatment material should be achieved.

10.1.2 Inorganic Surface Treatments

Due to the unsatisfactory long-term performance of many organic products and the subsequent need for frequent re-application, growing interest has been recently addressed toward inorganic materials. These products are mainly aqueous solution of sodium silicate, also known as *waterglass*, and, to a much lower extent, potassium silicates and fluosilicates (LaRosa Thompson, Silsbee, Gill, & Scheetz, 1997). These silicates are usually considered as pore-blockers, that is, they can block the capillary pores in the material's surface. Sodium silicate is supposed to react with Portlandite to form C-S-H gel and NaOH as shown in Eq. (10-1) (Jiang, et al., 2015; Pan, Shi, Jia, Zhang, & Wu, 2016), hence increasing the performance of the impregnated layer, in terms of hardness and impermeability. However, experimental evidences of the performance of sodium silicate for

protection of hardened cement-based materials are limited (Dai, Akira, Wittmann, Yokota, & Zhang, 2010), and its mechanism inside of the pore structure is still unclear (LaRosa Thompson, Silsbee, Gill, & Scheetz, 1997). Moreover, the possible increase in the risk of alkali-silica reaction due to the formation of NaOH as a by-product from the reaction with Portlandite should be taken into account (Pigino, Leemann, Franzoni, & Lura, 2012).



Some studies have demonstrated that sodium silicate treatment can improve the durability of concrete, especially after post-treatment of cationic surfactant (alkyl quaternary ammonium salts) (Li, Yi, & Xie, 2012; Moon, Shin, & Choi, 2007; Kupwade-Patil, Cardenas, Gordon, & Lee, 2012). On the other hand, Ibrahim and Dai (Dai, Akira, Wittmann, Yokota, & Zhang, 2010; Ibrahim, Al-Gahtani, Maslehuddin, & Dakhil, 1999) showed that sodium silicate treatment cannot significantly improve resistance to penetration of water and chloride ions. Furthermore, having sodium silicate a pore-blocking effect, the possible presence of water trapped behind the consolidated layer (e.g. from infiltration) might lead to its detachment, especially in case of freeze-thaw cycles (Pigino, Leemann, Franzoni, & Lura, 2012).

This discrepancy between studies is most likely due to the fact that sodium silicate-based sealers are essentially surface hydrophilic agents, that is, they form C-S-H which is hydrophobic, yet they can increase the water impermeability and the compactness of the material because the produced C-S-H partially fills the micro-pores, micro-voids and micro-cracks in the cementitious matrix (Song, et al., 2016).

It has been recognized that the pozzolanic reaction is highly correlated to the calcium ion concentration, the alkalinity of the solution, and the reactivity of the pozzolans (Shi, Krivenko, & Roy, 2006). However, in the case of surface-treatment of hardened cement-based materials with pozzolans, a limited amount of Portlandite and a low concentration of the calcium ion in the pore solution are the features that may prevent the pozzolanic reaction (Taylor, 1997). As a result, a valuable option for surface treatment of hardened cement-based materials should have high pozzolanic reactivity and be able to penetrate into the fine pores (Hou, Cheng, Qian, & Shah, 2014). During the last decades, some researchers have attempted to use nanoparticles for surface treatment of hardened

cement-based materials. The prerequisite of effectiveness of nano-materials treatment is its penetration into the hardened matrix, and the pozzolanic reaction with calcium hydroxide. Encouraging results on surface-treatments have been recently obtained with colloidal nano-SiO₂ and its precursor ethyl silicate. Hou et al. (Hou, Cheng, Qian, Cao, & Shah, 2015; Hou, Cheng, Qian, & Shah, 2014; Cai, et al., 2016) found that nano-SiO₂ treatment can increase the impermeability of hardened cement pastes, because it can reduce the volume of pores larger than 50 nm. It was reported that pores with size of about 10 μm are easy to observe in the untreated sample, while such pores become rare in both samples treated with nano-SiO₂ and ethyl silicate, as shown in Figure 10.1.

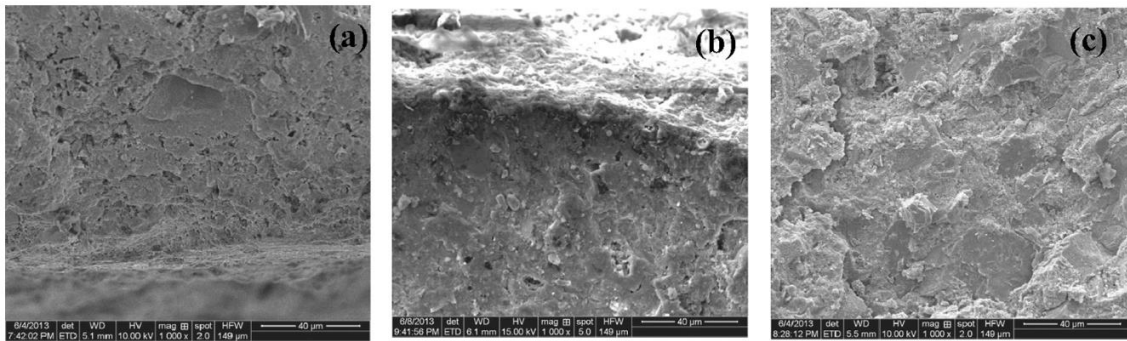


Figure 10.1: SEM images of nano-SiO₂/ethyl silicate-treated mortar: (a) control, (b) nano-SiO₂, (c) TEOS (Hou, Cheng, Qian, & Shah, 2014)

10.1.3 Hydrophobic impregnation

Hydrophobic impregnation operates through penetrating concrete pores, enlarging the contact angle. The surface becomes hydrophobic when the contact angle is larger than 90°. Thus, hydrophobic impregnation can inhibit penetration of water and water-born ions but allow water vapor to enter or exit. Surface-treatments by means of water repellents can thus reduce chloride ingress and stop heavy rain from penetrating through the surface layer. Unlike conventional coatings, such as epoxy or acrylic paints, hydrophobic impregnation is open to diffusion and the risk for frost damages caused by entrapment of water is, therefore, eliminated or decreased.

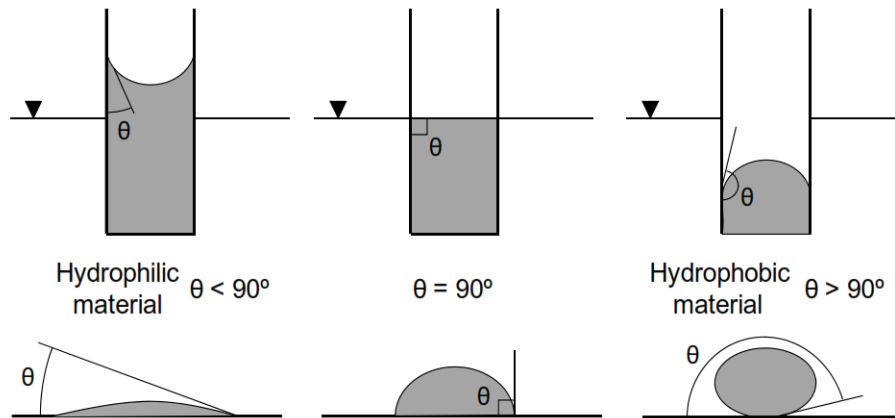


Figure 10.2: Illustration of the difference between a hydrophilic and a hydrophobic material by the means of a contact angle: on top capillary pores and underneath a water droplet (Johansson, 2005)

Silane, siloxane and a mixture of these two components are the commonly used hydrophobic impregnation. Their small molecular structures allow them to penetrate effectively into a highly dense substrate.

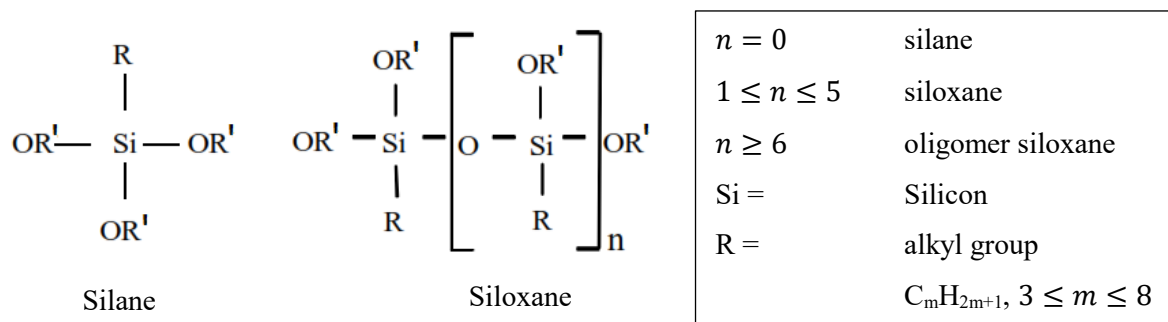


Figure 10.3: Molecular structure of silane and of siloxane (Salander, 2010)

Both silane and siloxane contain an alkyl group and several alkoxy groups (Batis, Pantazopoulou, & Routoulas, 2003; Johnson, Schultz, French, & Reneson, 2009). While the structure of the alkoxy group is related to how silane/siloxane bonds to the surface of the cement-based material (McGettigan, 1995), the alkyl group has the effect to reduce the surface tension of the matrix substrate depending on the molecular weight. In fact, the alkyl group with higher molecular weight (e.g. iso-butyl and n-octyl) provides a higher degree of hydrophobicity than the lower molecular weight alkyl group (e.g. methyl and

ethyl). On the other hand, the characteristics of the alkoxy groups influence the penetration depth of the protective agent.

The chemical reaction between silane and cementitious substrate is shown in Figure 10.4. The stages in the reaction will be the same for both silane and siloxane. In the first step, silane hydrolysis reacts with water or water vapor in capillary pores, and the alkoxy group will undergo hydrolysis and form silanol groups. Then, the unstable silanol molecules will lose water and condensate into silicone resin. Consequently, the silanol groups in silicon resin react with hydroxyl groups on the cementitious substrate through hydrogen bonds. Finally, the silicon resin bonds to substrate during drying, and provides a water-repellent effect. The alkalinity of pore solution acts as a catalyst in this reaction (Woo, Zhu, Chow, Leung, & Kim, 2008). Once the penetrative protective film has fully formed, it can offer protection for more than 20 years (Christodoulou, Goodier, & Austin, 2012).

Several studies (Basheer & Long, 1997; Basheer & Cleland, 1998; Polder, Borsje, & Vries, 2000; Polder, Borsje, & Vries, 2001) have pointed out the effectiveness of hydrophobic impregnation by means of silane and siloxane in preventing the absorption and penetration of external liquid water and dissolved substances. This feature protects concrete from chloride ingress and freeze-thaw damage (Liu & Hansen, 2016).

On the other hand, the influence of the silane-based penetrative protective agent on carbonation resistance is still greatly controversial (Qiang, et al., 2016). In fact, some scholars think that hydrophobic impregnation hardly prevents the CO₂ from penetrating into the pore structure (Vries, Polder, & Borsje, 1998). Moreover, other studies (Attanayaka, Ng, & Aktan, 2002; Schueremans, Van Gemert, & Giessler, 2007) showed that water repellent agent could improve the diffusion of CO₂, hence accelerating carbonation, since the entrance of water is prevented by means of the hydrophobic agent. On the other hand, Qiang et al. (Qiang, et al., 2016) showed that silane-based surface treatments can improve carbonation resistance of hardened cement-based materials. However, they pointed out that the matrix compactness plays an important role in the effectiveness of the surface treatment, that is, penetrative protective agent will improve the carbonation resistance only if the matrix has higher compactness. Furthermore, corrosion rate in carbonated concrete may be reduced by hydrophobic treatment (Sergi, Lattey, & Page, 1990) due to the lower moisture content of treated materials.

10.1.4 Ethyl Silicate for Surface Treatment of Cement-Based Materials

Ethyl silicate (often referred to as TEOS, i.e., tetraethylorthosilicate) is a silicon-based consolidant of the alkoxy silanes group and is mainly known as a consolidant material for weathered stones in architectural restoration (Wheeler, 2005). Ethyl silicate cannot be included in the category of hydrophobic impregnation, since it exhibits a hydrophobic effect (as an alkoxy silane) but also changes the microstructure in the matrix cover.

Commercially available ethyl silicate (ethyl ester of silicic acid – $\text{Si}(\text{OC}_2\text{H}_5)_4$ or $\text{Si}(\text{OEt})_4$ – often referred to as TEOS – tetraethylorthosilicate) normally consists of $\text{Si}(\text{OC}_2\text{H}_5)_4$ and the solvent like ethanol. The former will not hydrolyze without water or catalyst. When present in catalytic environment, i.e., the pore solution of a cement-based material, ethyl silicate will undergo a two-stage curing process (Mosquera, De Los Santos, Montes, & Valdez-Castro, 2008) divided into hydrolysis and condensation.

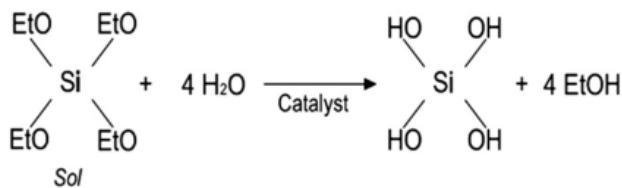


Figure 10.5: Hydrolysis reaction scheme for ethyl silicate ($\text{Et} = \text{C}_2\text{H}_5$), with silanol and ethanol formation (Sandrolini, Franzoni, & Pigino, 2012)

During hydrolysis process, $\text{Si}(\text{OEt})_4$ reacts with water (Zárraga, Cervantes, Salazar-Hernandez, & Wheeler, 2010) forming silanol (with $\text{Si} - \text{OH}$ groups) and ethanol, which evaporates without any damaging residues in the material. During the consolidation process, amorphous silica gel precipitates inside the material's porous structure (Amoroso & Fassina, 1983). (Dei & Salvadori, 2006; Scherer & Wheeler, 2009) showed that in carbonate stones (e.g. marble) silica gel precipitates inside the pores, resulting in a filling of pores and a limited re-adhesion and consolidation effects. On the other hand, in stones containing silicate phases (e.g. sandstones), silica gel also reacts with the hydroxyl groups present onto the pore surface resulting in a partial restoration of the natural binder which had been lost during the weathering processes. Hence, a consolidating effect and an

appreciable increase in the material mechanical strength can be witnessed (Zárraga, Cervantes, Salazar-Hernandez, & Wheeler, 2010).

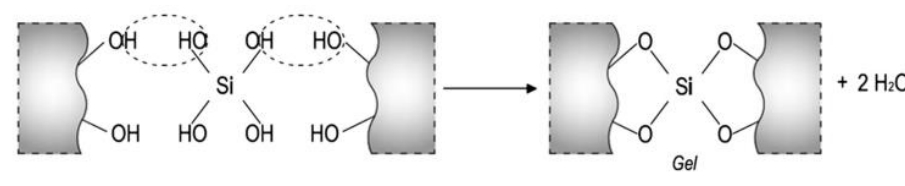


Figure 10.6: Simplified condensation reaction scheme in presence of -OH groups in the stone (Sandrolini, Franzoni, & Pigino, 2012)

Sandrolini et al. (Sandrolini, Franzoni, & Pigino, 2012) identified four reasons to explain the widespread use of ethyl silicate for stone consolidation. First, its small monomer size and low viscosity lead to deep penetration into the stone; secondly, its hardening by-products (ethanol and water) are volatile and do not damage the stone. Moreover, the final reaction products of TEOS is silica gel, which exhibits good compatibility with stone and good durability, unlike many polymeric consolidants (Lazzarini & Laurenzi Tabasso, 2010). However, the authors described three drawbacks: 1) slow reactive rate (Amoroso & Fassina, 1983); 2) easy to crack during shrinkage and drying (Maravelaki-Kalaitzaki, Kallithrakas-Kontos, Agioutantis, Maurigiannakis, & Korakaki, 2008); and 3) limited effectiveness in carbonate stones. These drawbacks may be improved by the addition of a catalyst, nanoparticles, and additives, but these additions require further investigation (Miliani, Velo-Simpson, & Scherer, 2007; Kim, Won, Do, Kim, & Kang, 2009; Maravelaki-Kalaitzaki, Kallithrakas-Kontos, Agioutantis, Maurigiannakis, & Korakaki, 2008).

The application of TEOS to hardened cement-based materials is expected to take advantage of the same features exploited for stone consolidation. TEOS itself does not have binding ability, but it can form a silica gel and fill the pore network through the hydrolyzing process. As an alkoxy silane, it exhibits a hydrophobic effect that can last for more than 6 months (Scherer & Wheeler, 2009). Moreover, Pigino et al. (Pigino, Leemann, Franzoni, & Lura, 2012) showed that TEOS displays pozzolanic behavior thanks to the formation of amorphous silica, which is pozzolanic reactive. Amorphous silica reacts with calcium hydroxide, forming calcium silicate hydrate as shown in Figure

10.7. The formation of C-S-H is expected to improve the compatibility of the treatment with concrete and its final performance.

Hou et al. (Hou, Zhang, Cai, Cheng, & Shah, 2016) pointed out that TEOS treatment results in a gradient distribution of calcium hydroxide on the surface to a depth of several millimeters. The study pointed out that Ca-leaching and sulfate attack resistivity of hardened cement-based material can be improved due to the reduction of calcium hydroxide content and the polymerization of the C-S-H introduced by the in-situ reaction of TEOS. Figure 10.8 exhibits the effects of surface-treatment of hardened cement paste with TEOS on the mineral compositions; results show that calcium hydroxide has been effectively consumed by TEOS.

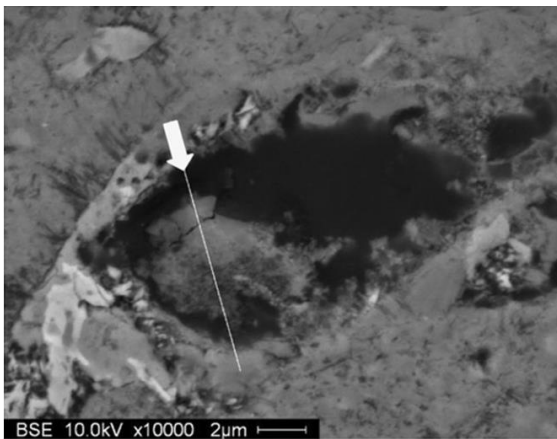


Figure 10.7: Pore partially filled with calcium silicate gel, due to the reaction between penetrated ethyl silicate and Portlandite (Pigino, Leemann, Franzoni, & Lura, 2012)

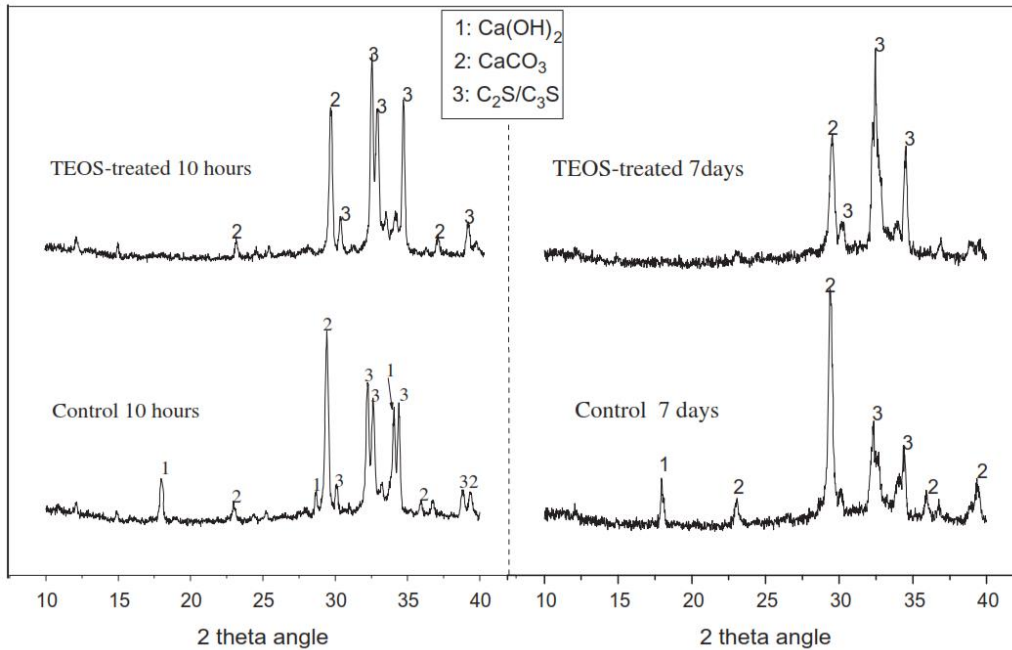


Figure 10.8: Superficial XRD patterns of TEOS-treated cement pastes at 10 h and 7 days old (Hou, Cheng, Qian, & Shah, 2014)

10.2 Materials Used in This Study

10.2.1 Cement and Mortar Mixtures

Ordinary Portland cement, Type I complying ASTM C 150 “Standard Specification for Portland Cement”, was used in this work and its physiochemical properties are listed in Table 10.1. Mortar and ferrocement samples with water-to-cement (w/c) ratio of 0.4 and 0.6 were prepared; all mortars used in this study had the same sand-to-cement ratio of 2. The high w/c ratio (0.6) was chosen to simulate the scarce properties and performance of deteriorated and/or low-quality materials as did in (Franzoni, Pigino, & Pistolesi, 2013).

A sieve analysis (ASTM C 136 “Standard Test Method for Sieve Analysis of Fine and Coarse Aggregates”) was conducted on a 350-gram samples of sand used in this work, the results are listed in Table 10.2. The sand is well-graded and capable of passing a 2.36 mm (No. 8 ASTM) sieve, in accordance with (ACI Committee 549, 1993).

Table 10.1: Physiochemical properties of cement

| SiO ₂ | Al ₂ O ₃ | Fe ₂ O ₃ | SO ₃ | CaO | MgO | Density, g/cm ³ | Fineness, m ² /kg | 28-day compressive strength, MPa |
|------------------|--------------------------------|--------------------------------|-----------------|------|-----|-------------------------------|---------------------------------|-------------------------------------|
| 21.1 | 3.9 | 3.2 | 3.5 | 65.7 | 0.9 | 3.2 | 423 | 43.6 |

Table 10.2: Particle size distribution of sand

| Sieve Size, U.S. Standard Square Mesh | Percent Passing by Weight |
|---------------------------------------|---------------------------|
| No. 8 (2.36 mm) | 100,0 |
| 16 (1.18 mm) | 93,9 |
| 30 (0.60 mm) | 78,2 |
| 50 (0.30 mm) | 45,7 |
| 100 (0.15 mm) | 2,8 |

A superplasticizer dosage of 0.9 wt.% was added to the mortar mixtures having w/c of 0.4 to achieve a comparable workability to the mixtures with w/c of 0.6. Raw materials were mechanically mixed in compliance with ASTM C 305 “Standard Methods of Test for Mechanical Mixing of Hydraulic Cement Pastes and Mortars of Plastic Consistency”.

To obtain the proper dosage of superplasticizer, the flow of hydraulic cement mortars was determined in compliance with ASTM C 1437 “Standard Test Method for Flow of Hydraulic Cement mortar”; a *Flow Mold* and a *Flow Table* with a circular rigid table top 10 in. in diameter were used (Figure 10.9), in compliance with ASTM C 230 “Flow Table for Use in Tests of Hydraulic Cement”. The dosage of superplasticizer in the mixtures with w/c of 0.4 was gradually adjusted to the point that the flow was comparable to that of the mixtures having w/c of 0.6.



Figure 10.9: Flow Table and Flow Mold

10.2.2 Sample Preparation and Curing

Four different groups of tests were performed in this work: 1) bending behavior of mortar and ferrocement samples; 2) water absorption rate on mortar and pre-cracked ferrocement samples; 3) accelerated carbonation tests on ferrocement samples; and 4) microstructure characterization by means of ESEM-EDS to identify the mortar composition before and after surface treatments. A summary of the samples utilized in this study can be found in Table 10.3. Three replicate specimens were prepared and tested for each parameter set, with the only exception of MOR-ESEM, for which only one sample for each parameter set was prepared.

The following curing procedure was used for the cast of each sample. After mixing, mortar mixtures were cast in rectangular molds, covered with plastic sheet, and cured for 1 day at ambient environment (about 20 ± 1 °C/50%RH) before being demolded and stored for 28 days in curing chamber at 20 ± 1 °C and RH 99%.

Table 10.3: List of the samples utilized in the study

| Group of Tests | Sample's Name | Description | Surface Treatment ² | N. of Samples |
|-----------------------|----------------------|---------------------------------------|---------------------------------------|----------------------|
| Bending behavior | MOR-FL | Mortar samples (40x40x160 mm) | None | 6 |
| | FERRO-FL | Ferrocement samples (240x70x16 mm) | None | 6 |
| Water absorption | MOR-S1 | Mortar samples (40x40x10 mm) | TEOS | 24 |
| | MOR-S2 | Mortar samples (40x40x10 mm) | TEOS, SS, ISOB | 24 |
| | FERRO-S | Ferrocement samples (240x70x16 mm) | TEOS, SS, ISOB | 24 |
| Carbonation Depth | FERRO-CARB | Ferrocement samples (40x40x16 mm) | TEOS, SS, ISOB | 96 |
| Microstructure | MOR-ESEM | Mortar samples (40x40x10 mm) | TEOS, SS, ISOB | 3 |

10.2.3 Mortar Samples

Rectangular molds of size 40x40x160 mm were used to cast mortar samples. The 28-days old samples were then divided in two groups: 1) samples used for water absorption tests, ESEM-EDS analysis were cut into slices with dimensions of 40x40x10 mm to obtain MOR-S1, MOR-S2, and MOR-ESEM respectively; 2) samples used for bending tests, namely MOR-FL, were notched and tested right after curing.

10.2.4 Ferrocement Samples

Two groups of ferrocement samples were manufactured in this study: 1) ferrocement plates of size 240x70x16 mm were cast and subjected to flexure test or water

² TEOS = ethyl silicate, SS = sodium silicate, ISOB = isobutyl-triethoxy-silane, see Section 10.2.5

sorptivity test, that is, FERRO-FL and FERRO-S respectively; 2) ferrocement samples of size 40x40x15 mm, namely FERRO-CARB, were exposed to accelerated carbonation conditions. Five layers of steel welded wire mesh with square opening were used to reinforce specimens FERRO-FL and FERRO-S, while only two layers were used for specimens FERRO-CARB. In both cases, the same mesh was used having wire diameter and wire spacing of 1.04 mm and 11.66 mm respectively. Details of the ferrocement samples manufactured in this study can be found in Table 10.4, Figure 10.10, Figure 10.11, and Figure 10.12.

Table 10.4: Details of the ferrocement samples

| | Samples | |
|--|-------------------|------------|
| | FERRO-FL, FERRO-S | FERRO-CARB |
| Cover, mm | 2 | 3 |
| N. of layers | 5 | 2 |
| V_r, % | 4,57 | 1.83 |
| S_r, cm²/cm³ | 1.75 | 0.70 |



Figure 10.10: Reinforcement for samples FERRO-CARB

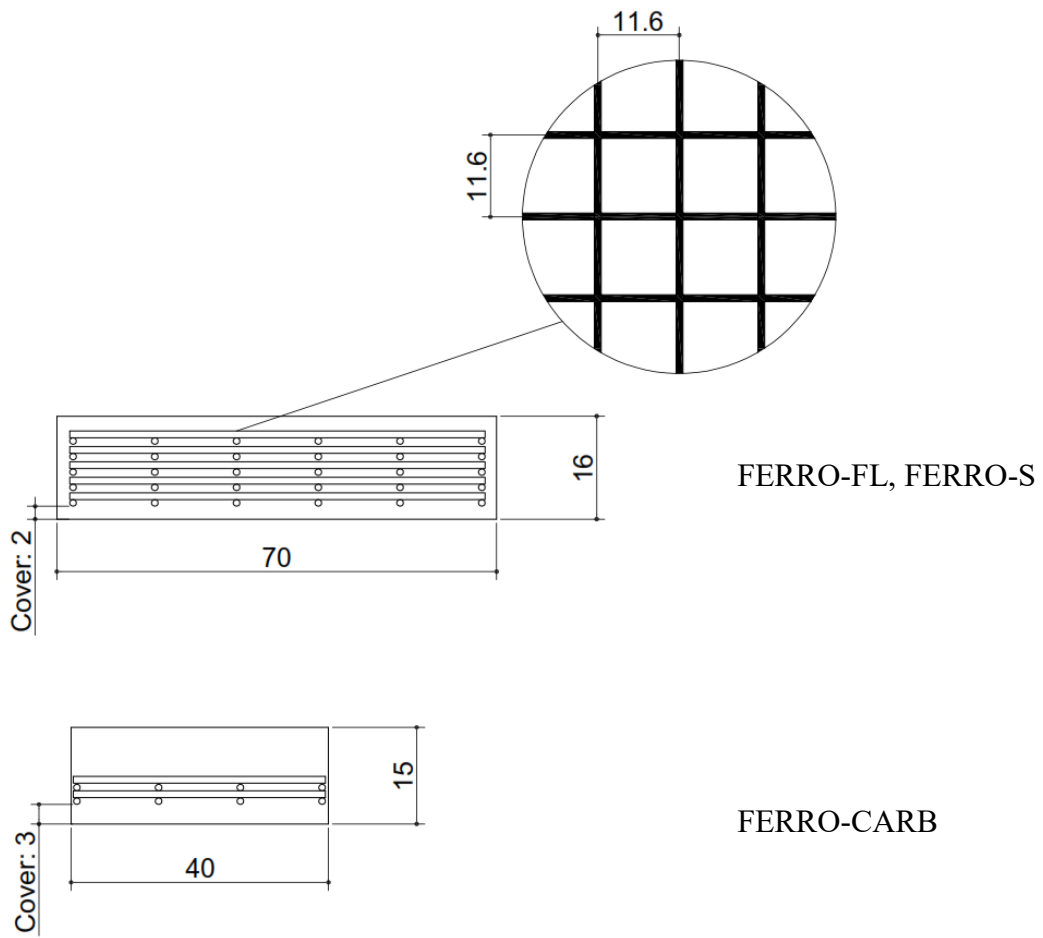


Figure 10.11: Cross section of samples, dimensions in mm



Figure 10.12: Mold and steel mesh reinforcement used for both specimens FERRO-FL and FERRO-S (left); FERRO-FL samples after curing (right)

10.2.5 Surface Treatments

For the protection of mortar and ferrocement samples, the following protective treatments were considered: an alcoholic ethyl silicate solution (**TEOS**) obtained by mixing 75 wt.% of TEOS and 25 wt.% of ethanol; sodium silicate-based concrete sealer (**SS**), composed by 12 wt.% of sodium silicate and 88 wt.% of deionized water; Isobutyl-triethoxy-silane sealer (**ISOB**) composed by 95 wt.% of Isobutyl-triethoxy-silane and 5 wt.% of ethanol.

As specified in Section 10.2.3, mortar samples were cut into small pieces with dimensions of 40x40x10 mm. After the cut, these samples were submerged in water and cleaned by means of a Branson 5510 Ultrasonic Cleaner for 5 minutes (Figure 10.13).



Figure 10.13: Ultrasonic cleaner Branson 5510

Before applying surface treatments (and after the ultrasonic cleaning, in case of mortar samples) the samples were oven-dried at 60 °C for 1 day. Then one face of each sample was left uncovered while the other five faces were sealed with two-component epoxy as did in (Hou, Cheng, Qian, Cao, & Shah, 2015; Dang, Xie, & Kessel, 2014).

Two different techniques were used to surface-treat the samples. Being TEOS a material of very recent application to cement-based materials, it was necessary to evaluate the influence of the application process on its effectiveness in limiting the ingress of aqueous substances through the pore structure of the matrix. Therefore, samples MOR-S1 were used to evaluate the effectiveness of ethyl silicate for surface treatments of mortar and to investigate the influence of the number of TEOS applications on water absorption

rate. Brushing technique was used for these samples, a saturated wet condition was achieved after each brushing.

Samples MOR-S2, MOR-ESEM, FERRO-S, and FERRO-CARB were used to compare the performance (water absorption, carbonation resistance and microstructure) between the surface treatments considered in this study. Those samples were dipped in the sealing agent two times for 40 seconds each and at a time-interval of 20 minutes.

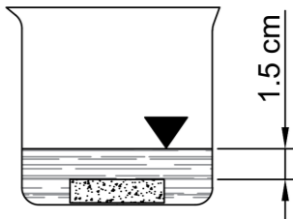


Figure 10.14: Surface treatment of mortar sample by dipping it into the treatment agent

Table 10.5: Application techniques

| Sample | Surface Treatments | Application |
|--|--------------------|---|
| MOR-S1 | TEOS | Brushing technique A) Brushing application repeated 3 times in a day at a time-interval of 20 min.: total of 3 times B) Brushing application repeated 6 times in a day at a time-interval of 20 min.: total of 6 times C) Brushing application repeated 3 times in a day at a time-interval of 20 min. for 2 subsequent days: total of 6 times |
| MOR-S2, FERRO-S, FERRO-CARB, MOR-ESEM | TEOS, SS, ISOB | Dipping Samples are dipped two times in the sealing agent for 40 seconds at a time-interval of 20 min. |

At the end of the treatment, the specimens treated with ethyl silicate were left under a ventilated hood for 1 day, in order to enhance the first evaporation of the solvent. Then

the samples were cured for 6 days in a climatic chamber at 20 ± 1 °C and RH 75%. Control samples and samples treated with SS and ISOB were directly cured in the climatic chamber at 20 ± 1 °C and RH 75% for 7 days.

10.2.6 Climatic Chamber

The climatic chamber that has been used for the curing of the samples is shown in Figure 10.15. The temperature inside the chamber can be assumed to be constant and equal to the temperature in the laboratory, i.e., 20 ± 1 °C. An especially useful method of humidity control in a closed space involves the use of binary saturated aqueous solutions (primarily of single salts), that is, a given saturated salt solution provides only one relative humidity at any desired temperature. By selecting the appropriate salt and temperature, it is possible to obtain the desired relative humidity (Greenspan, 1977). To achieve 75% RH at 20 °C, the climatic chamber was partially filled with a saturated sodium chloride solution (Greenspan, 1977; British Standard Institution, 1967; Hickman, 1970). A sensor was added to the apparatus for measuring the relative humidity and the temperature in the system.

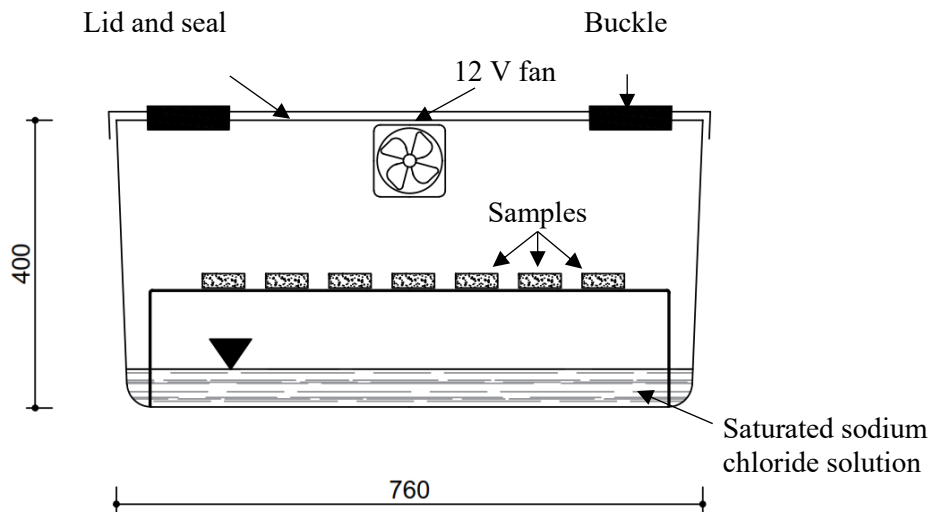


Figure 10.15: Climatic chamber for curing of surface treatments (dimensions in mm)

10.3 Test Methods

10.3.1 Flexure Test on Mortar and Ferrocement

In this work, mortar samples were subjected to a three point closed loop bending test (as depicted in Figure 10.16), using the crack mouth opening displacement, C.M.O.D., as the feedback signal. The experimental determination of the modulus of elasticity and the flexural strength is based on the load versus C.M.O.D. curve for a loading-unloading cycle of the specimen. The modulus of elasticity, E , is calculated by:

$$E = \frac{6 S a_0 g_2(\alpha_0)}{C_i b^2 t} \quad (10-2)$$

where: C_i is the compliance of the loading part of the load versus C.M.O.D. curve, defined as the value of the crack tip opening displacement per unit load, a_0 is the crack length, S is the span length, b is the specimen depth, t is the specimen thickness, $\alpha_0 = a_0/b$, and $g_2(\alpha_0)$ is a geometric function defined by:

$$g_2(\alpha_0) = 0.76 - 2.28 \alpha_0 + 3.87 \alpha_0^2 - 2.04 \alpha_0^3 + \frac{0.66}{(1 - \alpha_0)^2} \quad (10-3)$$

The flexural strength, $\sigma_{f,R}$ was calculated according to the theory of elasticity, by using the following equation:

$$\sigma_{f,R} = \frac{3 P_c S}{2 t (b - a_0)^2} \quad (10-4)$$

where P_c is the peak load.

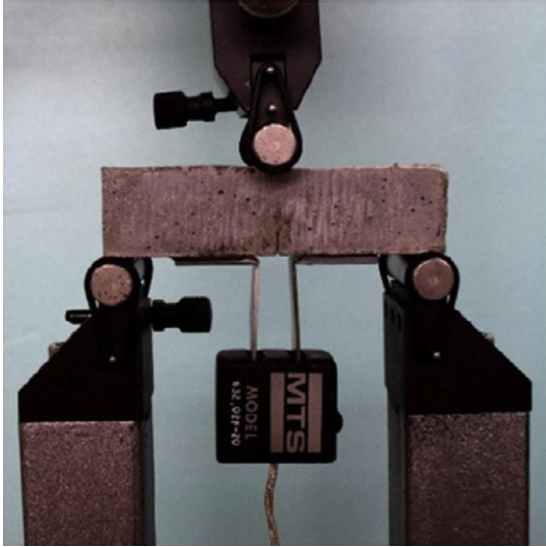


Figure 10.16: Experimental setup

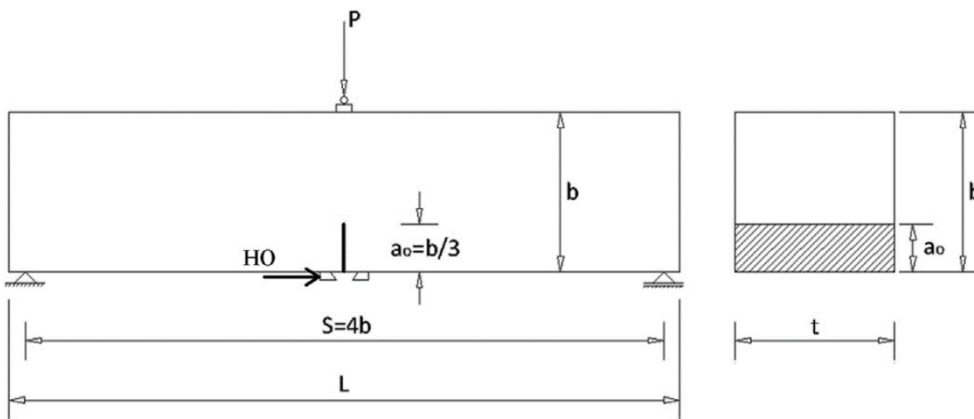


Figure 10.17: Schematic representation of the experimental setup

Tests were conducted to observe the flexural behavior of ferrocement specimens FERRO-FL having two different w/c ratios. The specimens were tested under center point bending with a constant span. A computer was used to record the load signal from the load cell and the deflection at mid span from an LVDT. The first crack load, ultimate load, and the corresponding deflection were observed; the flexure tests were carried out to the specimen's failure.

To evaluate the effectiveness of surface treatments on the water absorption of ferrocement specimens, ferrocement plates FERRO-S were loaded and pre-cracked before being subjected to the water absorption test. The aim was to achieve the formation of visible cracks, thus having a width of at least $100 \mu\text{m}$, to ensure that the ferrocement

specimens were subjected to severe conditions. At first, it was decided to apply 60% of average ultimate loads for all pre-cracked specimens; however, the crack width would substantially decrease during the unloading phase, eventually becoming invisible to the naked eye (ferrocement exhibits exceptional elasticity and resistance to cracking, as pointed out in Section 8.4). Thus, it was decided to load each specimen up to failure.

10.3.2 ESEM-EDS Analysis

SEM/ESEM is a very useful tool to show the morphology and microstructure in the mortar matrix of ferrocement. Environmental Scanning Electron Microscopy, ESEM, in combination with Energy Dispersive X-ray Spectroscopy, EDS, (Hitachi S-3400N-II, Figure 10.18) was used to study the effect of the surface treatments on the microstructures of mortar samples.

In backscattered images, brightness is proportional to the average atomic number of a phase, that is, the higher the average atomic number of a phase, the brighter its image. For the major phases present in Portland cement, the phases from brightest to darkest are tetracalcium aluminoferrite (C_4AF), tricalcium silicate (C_3S), tricalcium aluminate (C_3A) and dicalcium silicate (C_2S), gypsum, and voids (Bentz & Stutzman, 1994). Based on this concept, a phase identification can be attempted by segmenting the backscattered images based on analysis of the greylevel histogram (a histogram of the number of pixels in the image assigned to each greylevel). Unfortunately, phases such as C_3A and C_2S have similar intensities but very different chemical composition; thus, an accurate separation cannot be based solely on the backscattered images. X-ray spectrum (a plot of signal intensity vs energy level) and maps for chemical elements, such as calcium and silicon, can be obtained by means of EDS technique. In fact, EDS allows one to identify chemical elements and their relative proportions (Atomic percentage or weight percentage).

EDS analysis involves the generation of X-ray spectra from the entire scan area of the SEM/ESEM or from designated areas. The Y-axis of an X-ray spectrum shows the counts (number of X-ray received and processed by the detector), while the X-axis shows the energy level of those counts.



Figure 10.18: Hitachi S-3400N-II SEM

Proper sample preparation is critical to the successful imaging of cement-based materials. Sample preparation was conducted according to the procedure described in Section 10.2.3 and 10.2.5. After curing of the surface treatments, treated and non-treated samples MOR-ESEM were cut as shown in Figure 10.19. The slices were then encapsulated in hot mounting resin of thermosetting type and the cross section was left exposed and carefully polished by means of a Buehler EcoMet 250 Polisher (Figure 10.20). After being polished, samples MOR-ESEM were ready for the observation (Figure 10.21).

For this study, an accelerating voltage of 20 kV and probe current of 70 nA was used in the low vacuum mode for collecting backscattered electrons images and for X-ray imaging. X-ray spectra of different areas of the samples were collected and compared; “Aztec” Software (Oxford Instruments) was used to perform data analysis and associate these energy level of the X-rays with the elements and shell levels that generated them. Moreover, a quantitative analysis was conducted to measure the Ca/Si ratio in the outer and inner layer of each sample.

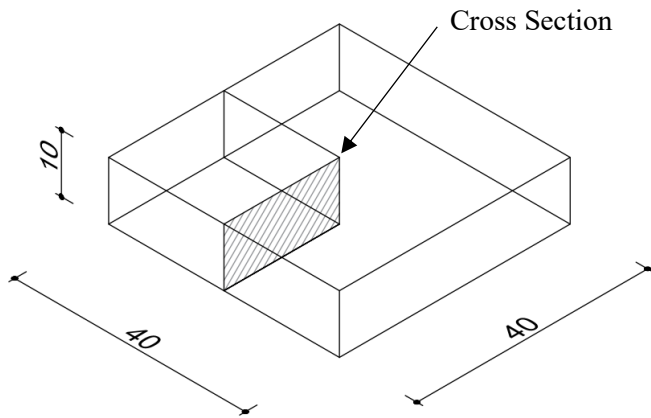


Figure 10.19: Sample MOR-ESEM cut to expose the cross section (dimensions in mm)



Figure 10.20: Buehler EcoMet 250 Polisher



Figure 10.21: Samples MOR-ESEM after polishing

10.3.3 Carbonation Depth

Carbonation properties of cement-based materials can be obtained in natural environment where the samples are exposed to real natural conditions over a long term. However, this method is very time consuming, normally taking a few years. Various accelerated carbonation test methods, using high CO₂ concentration, have been developed and allow to obtain carbonated samples in a short time. If a cement-based material is exposed to high CO₂ concentrations, the resulting carbonated material can be different when compared to that formed under the natural environment. However, accelerated carbonation tests can be served as the basis for predicting the carbonation behavior of cement-based materials under real atmospheric environments.

(Cui, Tang, Liu, Dong, & Xing, 2015) investigated the relationship between the depth of concrete carbonation and CO₂ concentration. The researchers argued that 20% concentration of CO₂ is a dividing point for defining the influence of CO₂ concentration on the carbonation depth of concrete. That is, for CO₂ concentration less than 20% the increase of CO₂ concentration can lead to an increase of carbonation depth remarkably, while increasing CO₂ concentration by more than 20% has practically no influence on the carbonation depth. Furthermore, the researchers pointed out that different diffusion mechanisms take place between high and low CO₂ concentration, thus, employing an accelerated carbonation test with CO₂ concentration higher than 20% may not represent the natural process of carbonation.

As stated in Chapter 4, carbonation rate is significantly influenced by the moisture content of the cement-based material. It was concluded that rates of carbonation are highest in the range 50 to 75 percent relative humidity. In this study, the accelerated carbonation test was performed by placing treated and untreated ferrocement samples FERRO-CARB (Figure 10.22) in a controlled atmosphere having CO₂ concentration 20%, temperature 20 ± 1 °C, and RH 81% (Figure 10.23). The value of relative humidity considered in this study is very close to the peak in the carbonation rate versus relative humidity curve, as illustrated in Figure 4.4.

To achieve such controlled atmosphere, a saturated potassium bromide solution has been used following the approach described in Section 0. In fact, according to (Greenspan, 1977) a relative humidity of 81.67% can be obtained in a sealed chamber partially filled with a saturated potassium bromide solution. To ensure the proper CO₂

concentration, a CO₂ sensor (Measurement Range: 0-100% CO₂, Accuracy: ± 70 ppm \pm 5% of reading) was inserted into the chamber and connected via USB to a computer running GasLab Software.

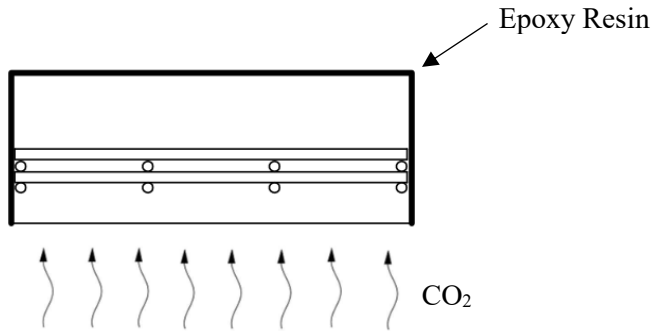


Figure 10.22: sample FERRO-CARB during the accelerated carbonation test

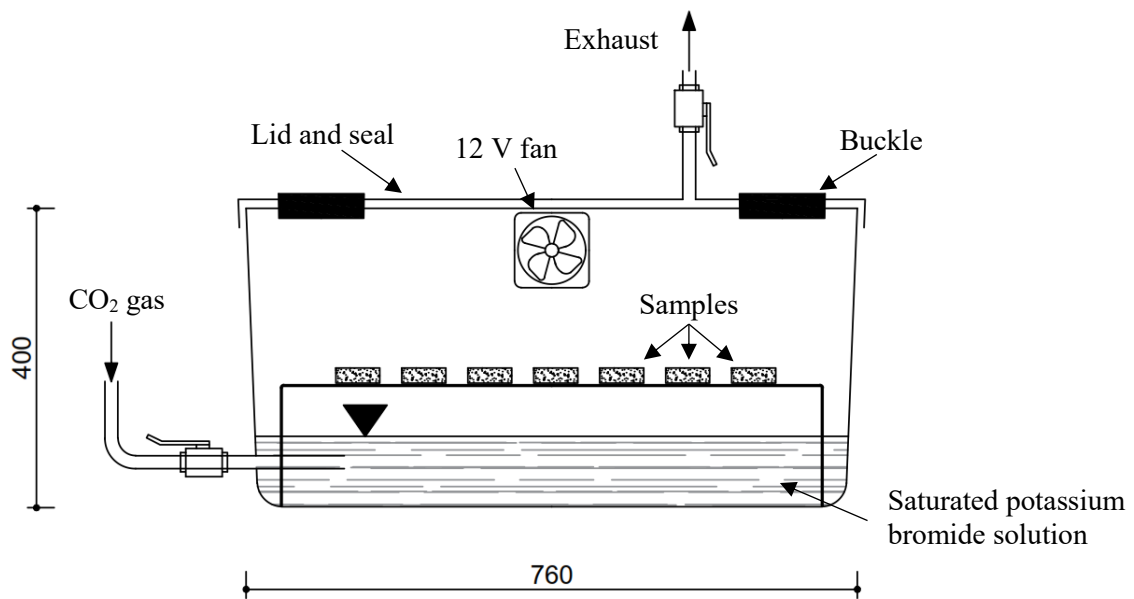


Figure 10.23: Accelerated carbonation test chamber (dimensions in mm)

The usual, simple method to monitor the carbonation in cement-based materials is a calorimetric method based on phenolphthalein spraying. It assesses a carbonation depth corresponding to a pH value roughly equal to 9 and is applied either on cores of real structures or on specimens carbonated in laboratory conditions. In this study, after 5, 10, 18 and 28 days of permanence in the carbonation chamber, the samples were halved, and carbonation depth was measured by spraying on the inner surface a 1% phenolphthalein pH-indicator, in compliance with UNI EN 13295:2005. A digital caliper gauge (0.01 mm

resolution) and a magnifying desk lamp were used to measure the penetration depth right after spraying the phenolphthalein solution.

10.3.4 Water absorption

A similar process to the ASTM C 1585 “Standard Test Method for Measurement of Rate of Absorption of Water by Hydraulic-cement concretes” was used to evaluate the water absorption rate. In this process, the uncovered face of the samples was immersed into water for a certain time and sample mass after various soaking times was recorded in the saturated-dry condition by using a precise scale with a resolution of 0.1 g (Figure 10.24). The mass increase is ascribed to the water-intake by the capillary pore effect. The water absorption rate was obtained by dividing the mass increase (mg) by the surface area (cm²) of the sample. For each test, the water absorption rates of three replicates at 4, 10, 30 minutes and 1, 2, 3, 6, 24 hours of water-soaking time were tested and average was taken as the representative value.

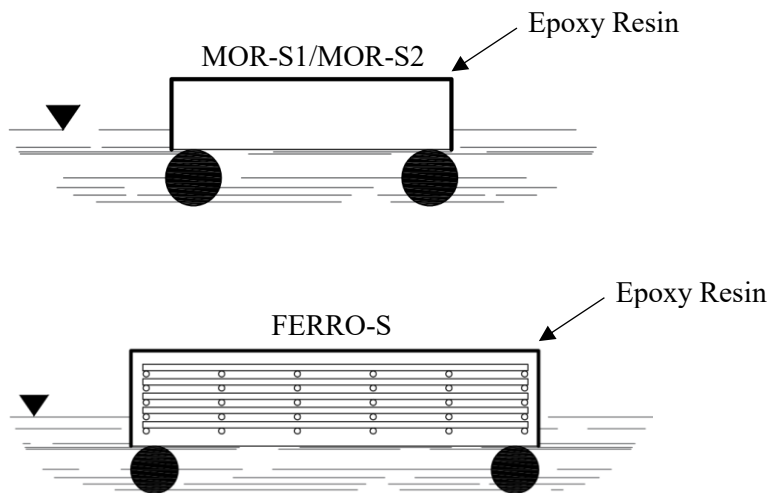


Figure 10.24: Samples MOR-S1/MOR-S2 and FERRO-S during the water absorption test

10.4 Results

10.4.1 Flexure Test on Mortar and Ferrocement

Load versus C.M.O.D. curves from mortar samples are shown in Figure 10.25, consisting of a linear elastic stage before crack initiation, non-linear stage of stable crack propagation and unstable extension stage after the peak load (i.e., fracture load).

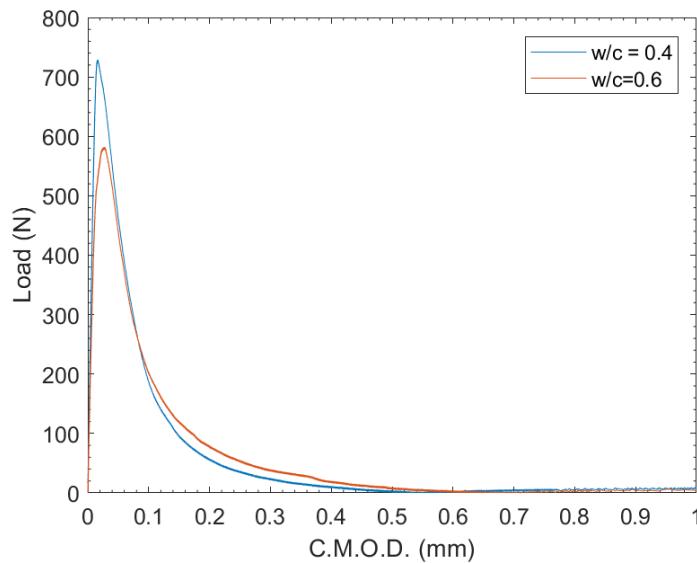


Figure 10.25: Load-C.M.O.D. curves for 28 days old mortar specimens MOR-FL

Three specimens were tested for each w/c ratio and mechanical parameters were calculated following the approach described in Section 10.3.1. The mean values for the mechanical parameters are listed in Table 10.6.

Table 10.6: Mean values for mortar specimens MOR-FL

| Sample | w/c | Fracture load, N | Flexural strength, MPa | Modulus of Elasticity, MPa |
|--------|-----|---------------------|---------------------------|-------------------------------|
| MOR-FL | 0.4 | 729 | 5.37 | 13882 |
| MOR-FL | 0.6 | 560 | 4.70 | 10485 |

The load versus deflection behavior of the ferrocement plates is shown in Figure 10.26. Mechanical parameters of ferrocement specimens FERRO-FL are listed in Table 10.7 and Table 10.8.

Table 10.7: Comparison of strengths and deflections of ferrocement specimens FERRO-FL

| Sample | w/c | Load at first crack, N | Deflection at first crack, mm | Failure load, N | Deflection at failure load, mm |
|--------------|-----|------------------------|-------------------------------|-----------------|--------------------------------|
| FERRO-FL (1) | 0.4 | 400 | 0.49 | 1668 | 6.84 |
| FERRO-FL (2) | 0.4 | 500 | 0.54 | 2041 | 4.57 |
| FERRO-FL (3) | 0.4 | 400 | 0.29 | 1828 | 4.99 |
| FERRO-FL (4) | 0.6 | 270 | 0.29 | 823 | 7.37 |
| FERRO-FL (5) | 0.6 | 300 | 0.42 | 1178 | 5.49 |
| FERRO-FL (6) | 0.6 | 215 | 0.24 | 741 | 7.75 |

Table 10.8: Mean values for ferrocement specimens FERRO-FL

| Sample | w/c | Load at first crack, N | Deflection at first crack, mm | Failure load, N | Deflection at failure load, mm |
|----------|-----|------------------------|-------------------------------|-----------------|--------------------------------|
| FERRO-FL | 0.4 | 433 | 0.44 | 1846 | 5.47 |
| FERRO-FL | 0.4 | 262 | 0.32 | 914 | 6.87 |

The load versus deflection behavior of some of the ferrocement specimens FERRO-S, that is, pre-cracked specimens in preparation for the water absorption test, is shown in

Figure 10.27. The surface of pre-cracked specimens was observed and maximum crack widths (w_{max}) were measured by means of optical microscopy; moreover, the presence of a second substantial crack, if any, was noted and its width measured. Table 10.9 provides the values of crack widths obtained at the end of the flexure test, that is, after the unloading phase.

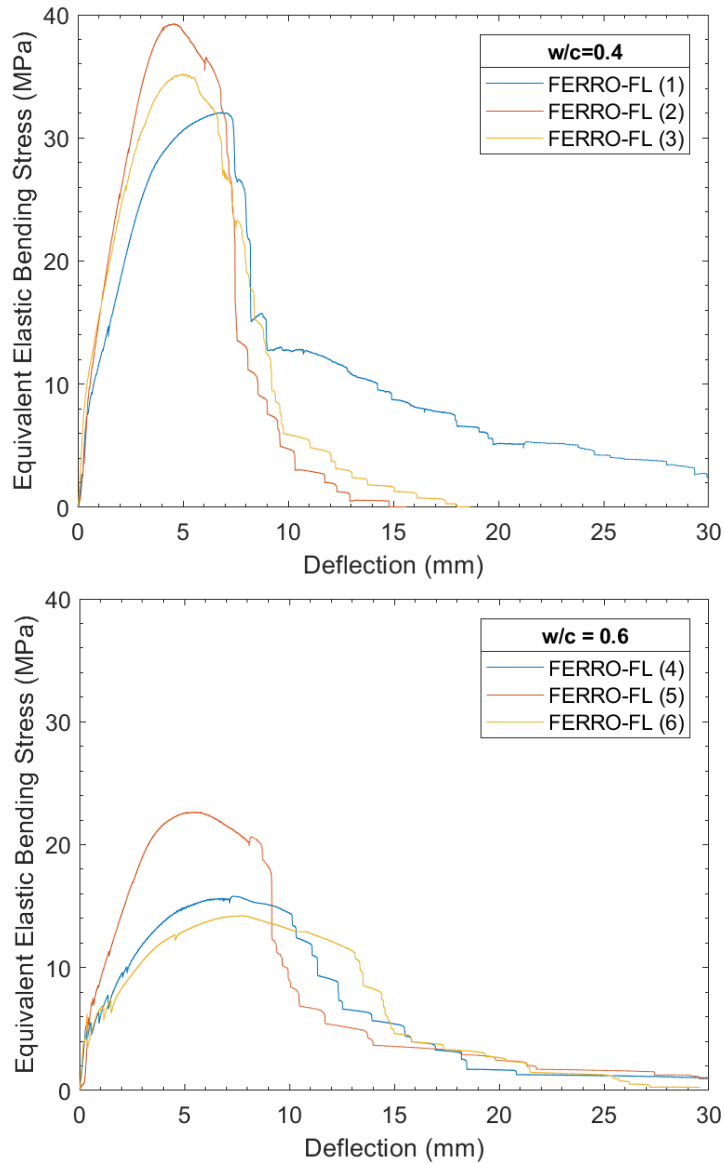


Figure 10.26: Bending response of ferrocement specimens FERRO-FL

Prior to perform the water absorption test, specimens FERRO-S were grouped as shown in Table 10.10. The grouping was done so that the average values of w_{max} would be comparable between one group and the other. Each group was then subjected to a different surface treatment.

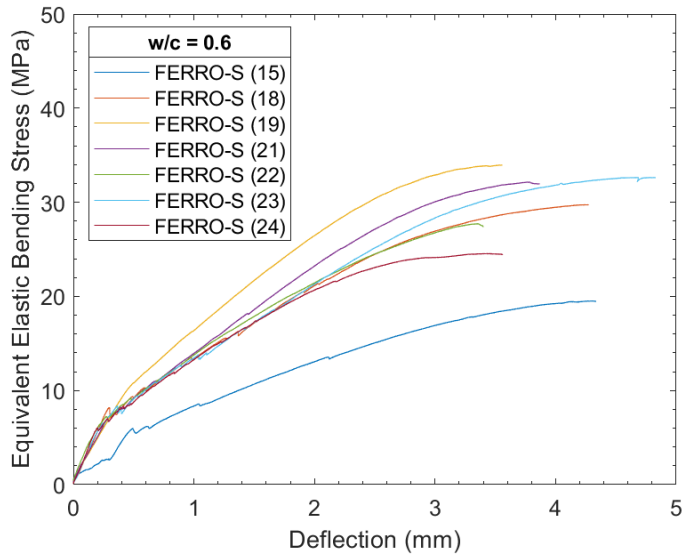
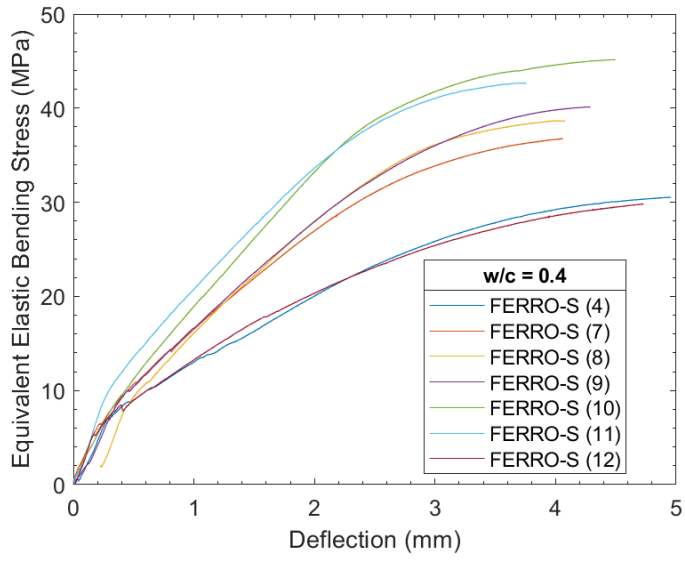


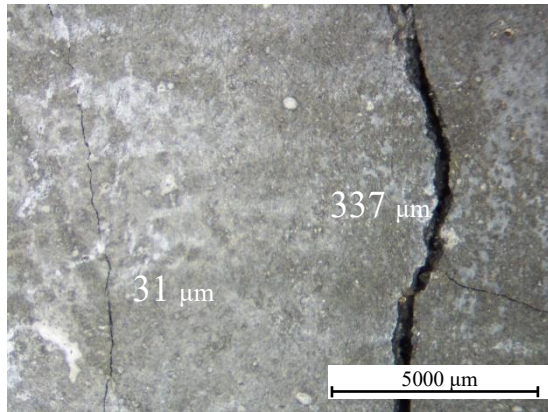
Figure 10.27: Bending response of ferrocement specimens FERRO-S

Table 10.9: Details of crack width for different pre-cracked specimens FERRO-S

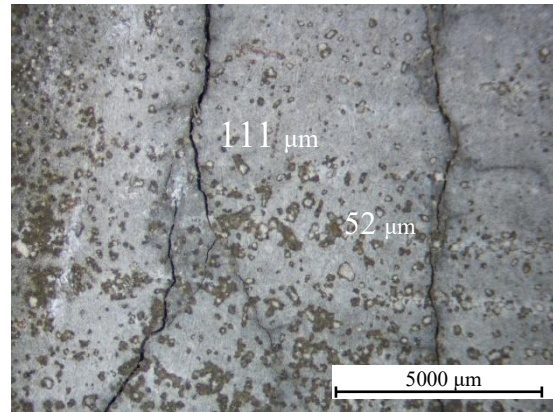
| Sample | w/c | Maximum Crack Width (w_{max}), μm | Secondary Crack Width, μm |
|---------------------|------------|---|---|
| FERRO-S (1) | 0.4 | 337 | 31 |
| FERRO-S (2) | 0.4 | 111 | 52 |
| FERRO-S (3) * | 0.4 | n.a. | n.a. |
| FERRO-S (4) | 0.4 | 346 | - |
| FERRO-S (5) | 0.4 | 118 | 15 |
| FERRO-S (6) | 0.4 | 89 | 65 |
| FERRO-S (7) | 0.4 | 179 | 57 |
| FERRO-S (8) | 0.4 | 249 | 29 |
| FERRO-S (9) | 0.4 | 133 | 40 |
| FERRO-S (10) | 0.4 | 213 | - |
| FERRO-S (11) | 0.4 | 115 | 44 |
| FERRO-S (12) | 0.4 | 331 | - |
| FERRO-S (13) | 0.6 | 114 | 101 |
| FERRO-S (14) | 0.6 | 124 | - |
| FERRO-S (15) | 0.6 | 102 | 41 |
| FERRO-S (16) | 0.6 | 142 | - |
| FERRO-S (17) | 0.6 | 161 | 17 |
| FERRO-S (18) | 0.6 | 81 | - |
| FERRO-S (19) | 0.6 | 106 | - |
| FERRO-S (20) | 0.6 | 95 | - |
| FERRO-S (21) | 0.6 | 69 | 54 |
| FERRO-S (22) | 0.6 | 121 | 38 |
| FERRO-S (23) | 0.6 | 134 | - |
| FERRO-S (24) | 0.6 | 214 | - |

* sample FERRO-S (3) was irretrievably damaged during the test

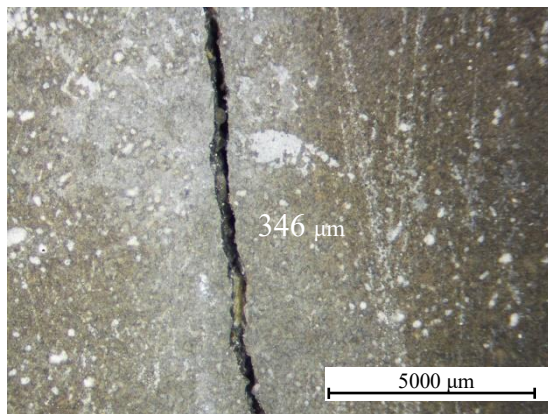
FERRO-S (1)



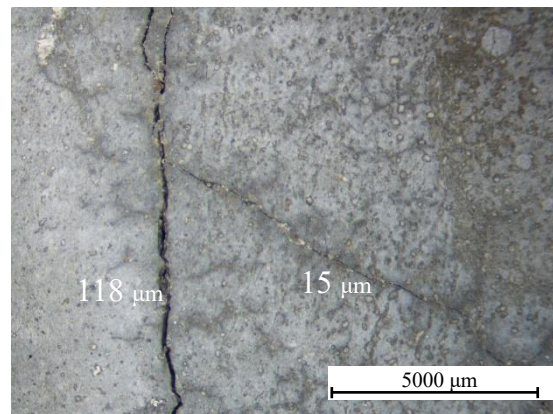
FERRO-S (2)



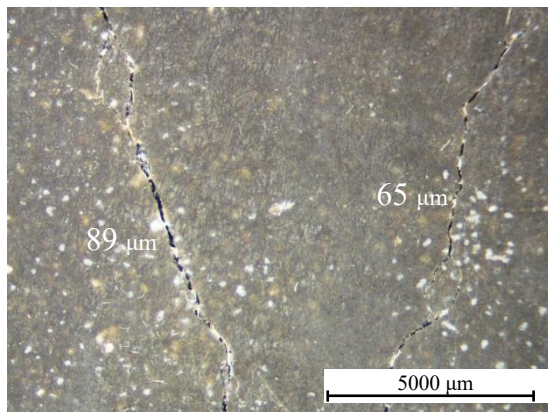
FERRO-S (4)



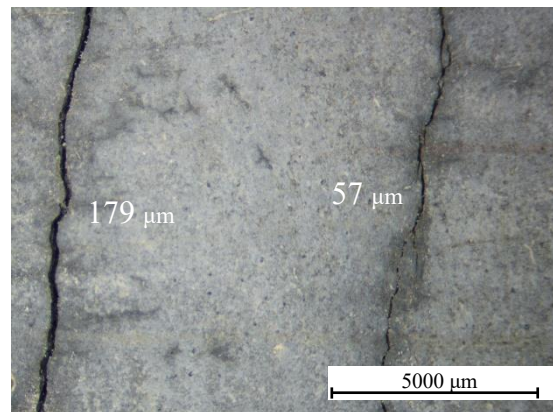
FERRO-S (5)



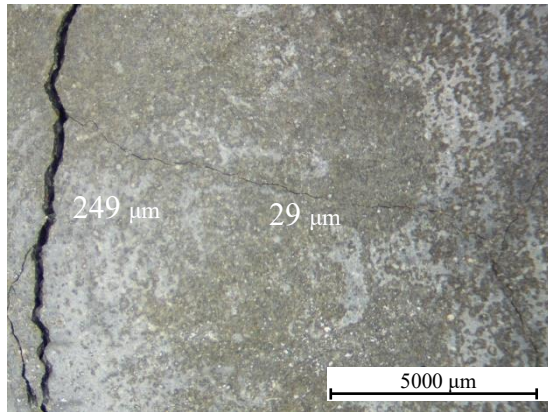
FERRO-S (6)



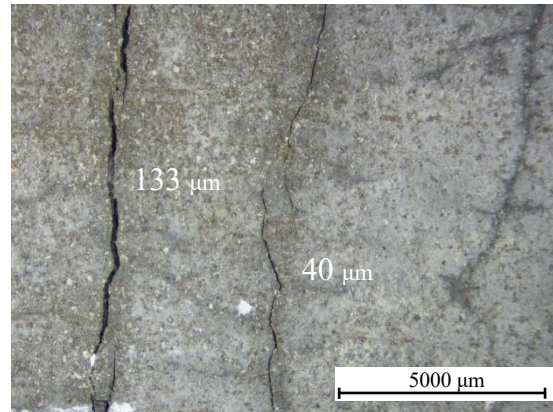
FERRO-S (7)



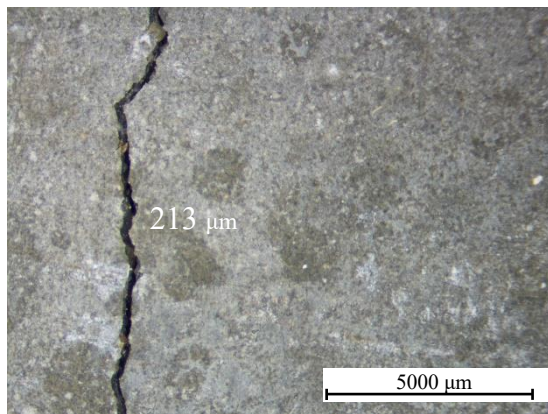
FERRO-S (8)



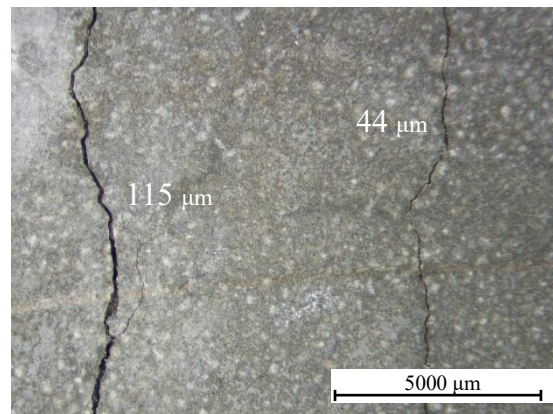
FERRO-S (9)



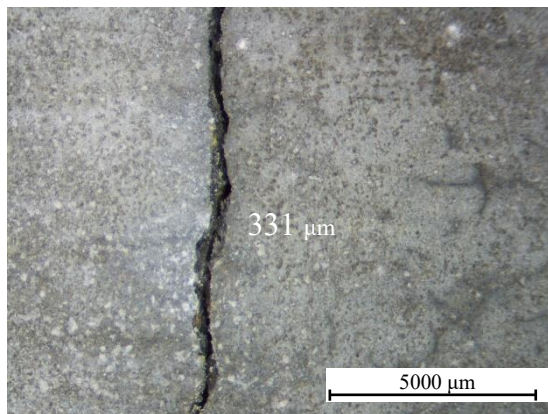
FERRO-S (10)



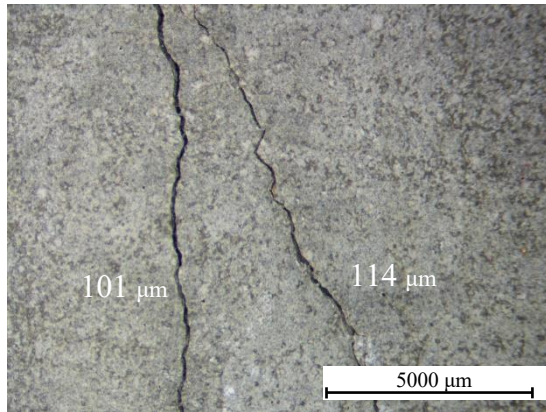
FERRO-S (11)



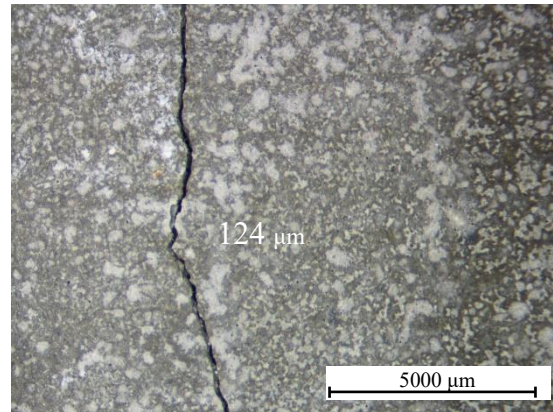
FERRO-S (12)



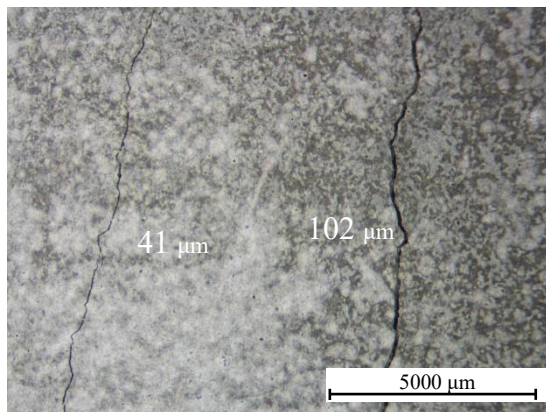
FERRO-S (13)



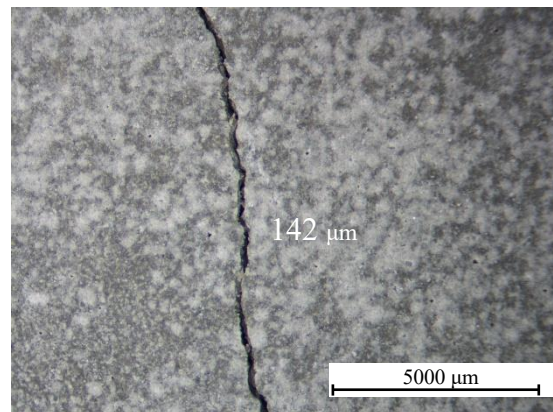
FERRO-S (14)



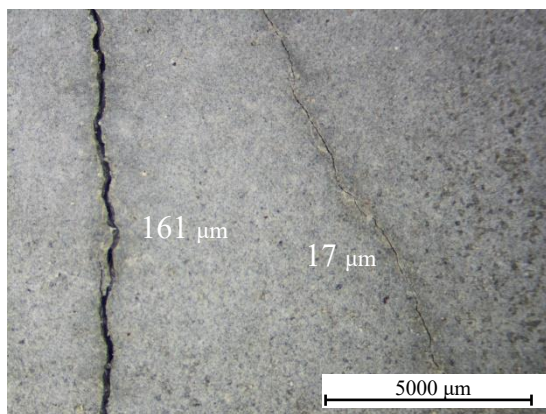
FERRO-S (15)



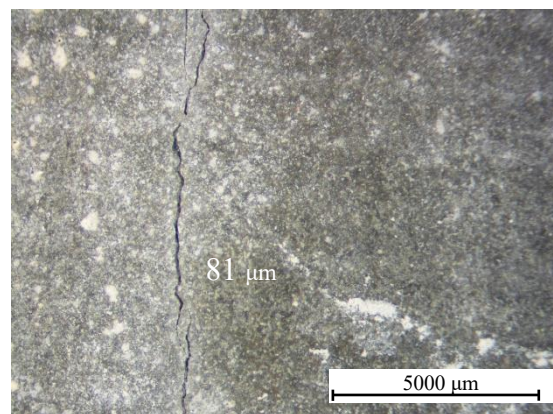
FERRO-S (16)



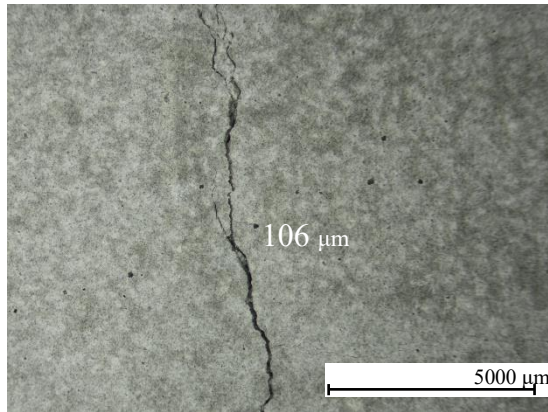
FERRO-S (17)



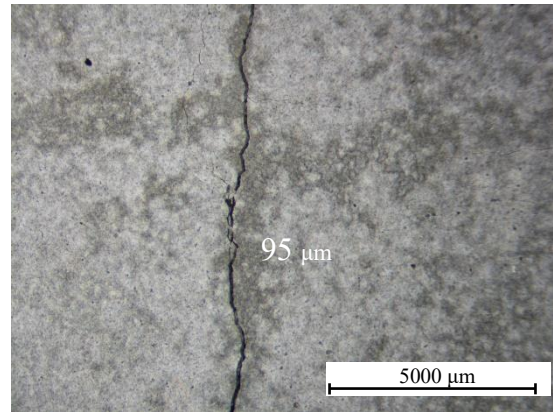
FERRO-S (18)



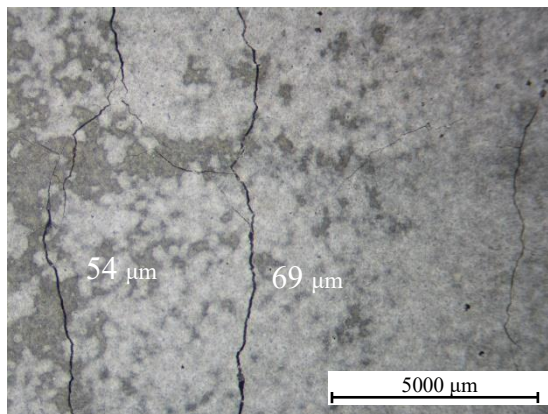
FERRO-S (19)



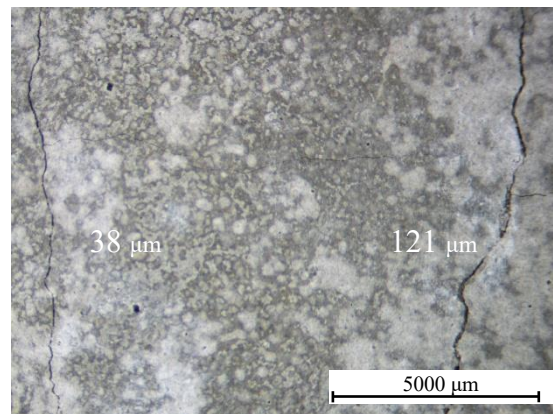
FERRO-S (20)



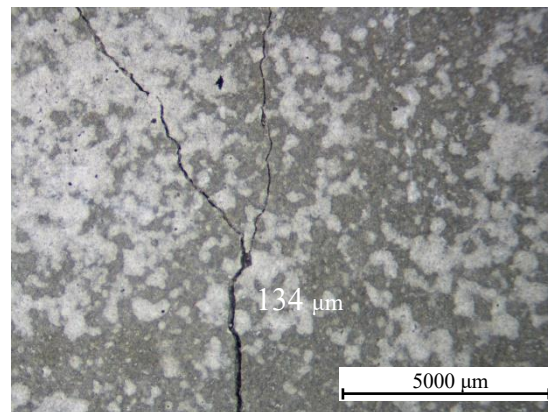
FERRO-S (21)



FERRO-S (22)



FERRO-S (23)



FERRO-S (24)

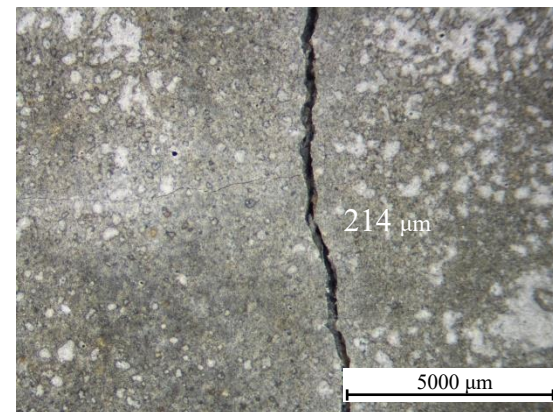


Figure 10.28: Surface of pre-cracked specimens observed by means of optical microscopy

Table 10.10: Samples FERRO-S grouped for surface treatments, prior to water absorption test

| Surface Treatment | Sample | w/c | w_{max} , μm | Average value of w_{max} , μm |
|-------------------|--------------|-----|---------------------------|--|
| TEOS | FERRO-S (7) | 0.4 | 179 | 211 |
| | FERRO-S (5) | 0.4 | 118 | |
| | FERRO-S (1) | 0.4 | 337 | |
| ISOB | FERRO-S (9) | 0.4 | 133 | 197 |
| | FERRO-S (2) | 0.4 | 111 | |
| | FERRO-S (4) | 0.4 | 346 | |
| SS | FERRO-S (10) | 0.4 | 213 | 220 |
| | FERRO-S (11) | 0.4 | 115 | |
| | FERRO-S (12) | 0.4 | 331 | |
| Control | FERRO-S (6) | 0.4 | 89 | 169 |
| | FERRO-S (8) | 0.4 | 249 | |
| TEOS | FERRO-S (13) | 0.6 | 114 | 99 |
| | FERRO-S (18) | 0.6 | 81 | |
| | FERRO-S (15) | 0.6 | 102 | |
| ISOB | FERRO-S (16) | 0.6 | 142 | 142 |
| | FERRO-S (17) | 0.6 | 161 | |
| | FERRO-S (14) | 0.6 | 124 | |
| SS | FERRO-S (23) | 0.6 | 134 | 123 |
| | FERRO-S (21) | 0.6 | 69 | |
| | FERRO-S (19) | 0.6 | 106 | |
| Control | FERRO-S (20) | 0.6 | 95 | 143 |
| | FERRO-S (24) | 0.6 | 214 | |
| | FERRO-S (22) | 0.6 | 121 | |

10.4.2 ESEM-EDS Analysis

ESEM images of cross sections of samples MOR-ESEM are shown in Figure 10.30, Figure 10.31, Figure 10.32, and Figure 10.33 at magnifications $60\times$ (top) and $350\times$ (bottom). The observed area is highlighted in Figure 10.29 and the external surface of each sample is located on the left side of the image. In fact, the brighter portion slightly visible on the left side of the images (especially at the lowest magnification) represents the hot mounting resin used to encapsulate the samples.

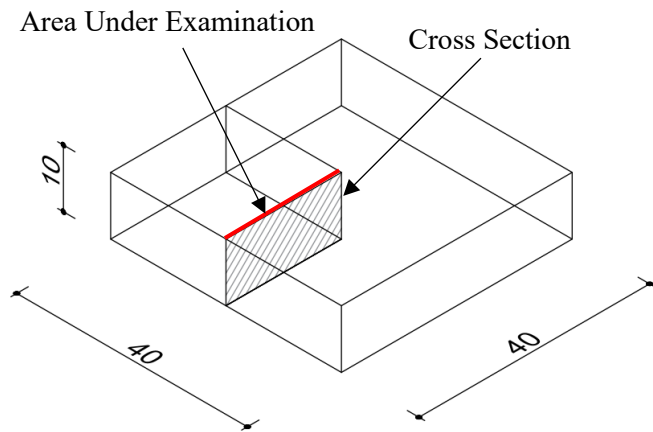


Figure 10.29: Sample MOR-ESEM, area under examination (dimensions in mm)

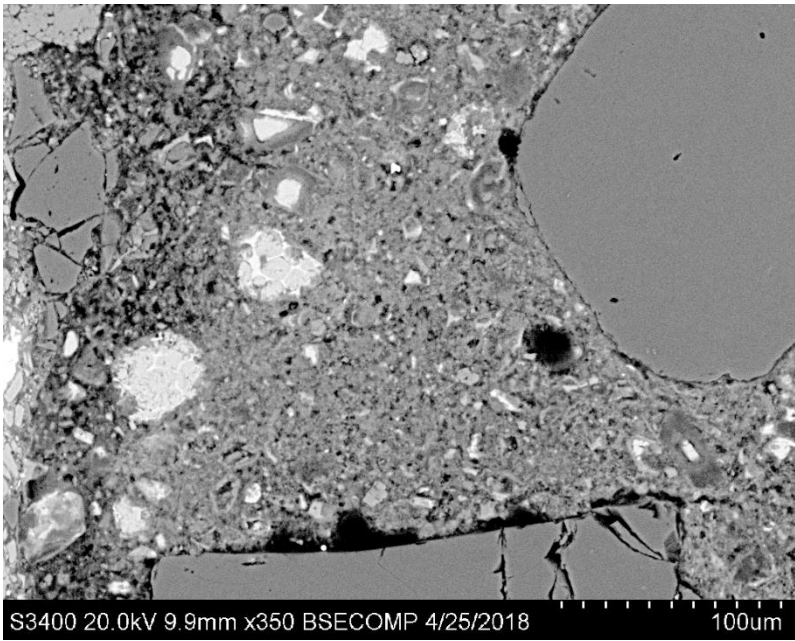
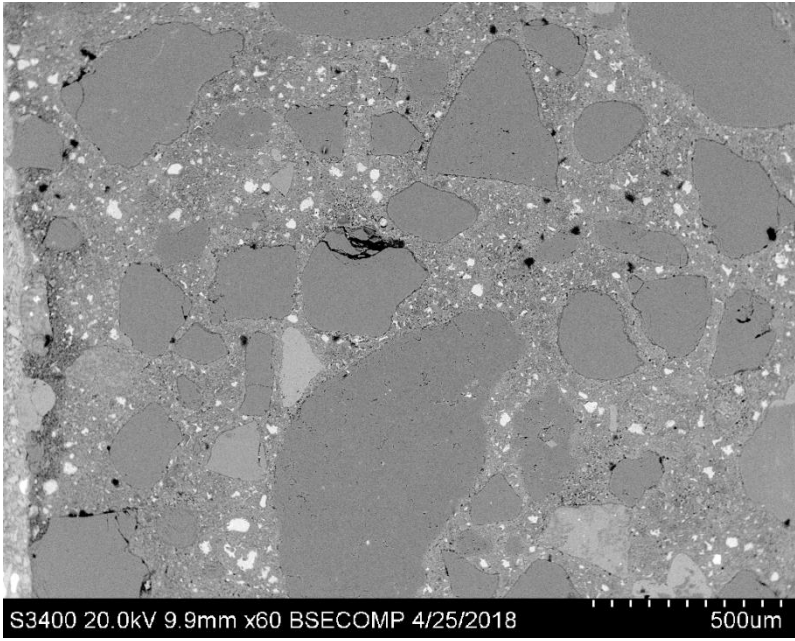


Figure 10.30: ESEM images of MOR-ESEM, Control

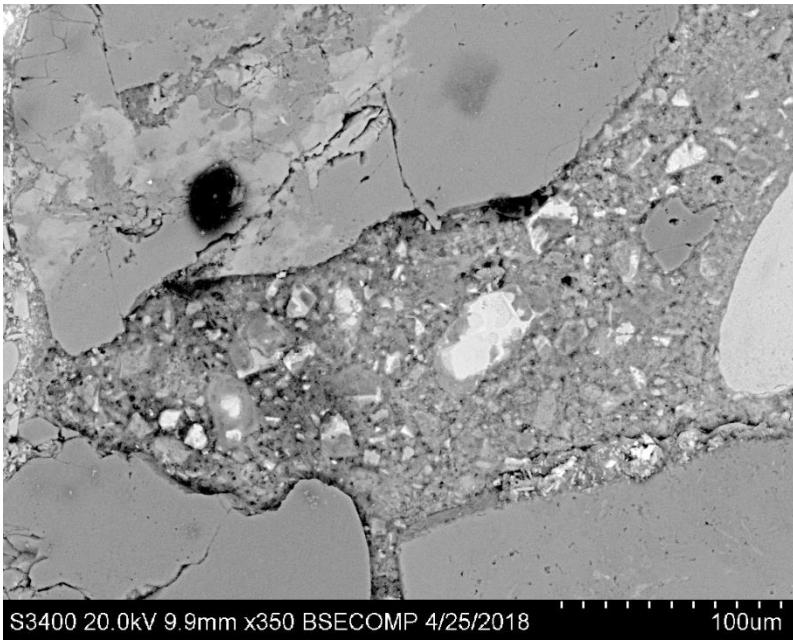
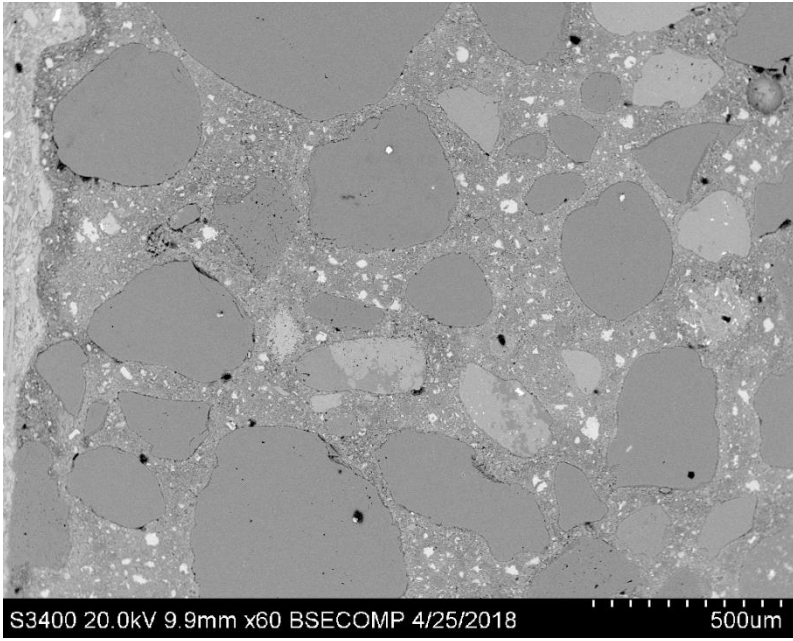


Figure 10.31: ESEM images of MOR-ESEM, TEOS

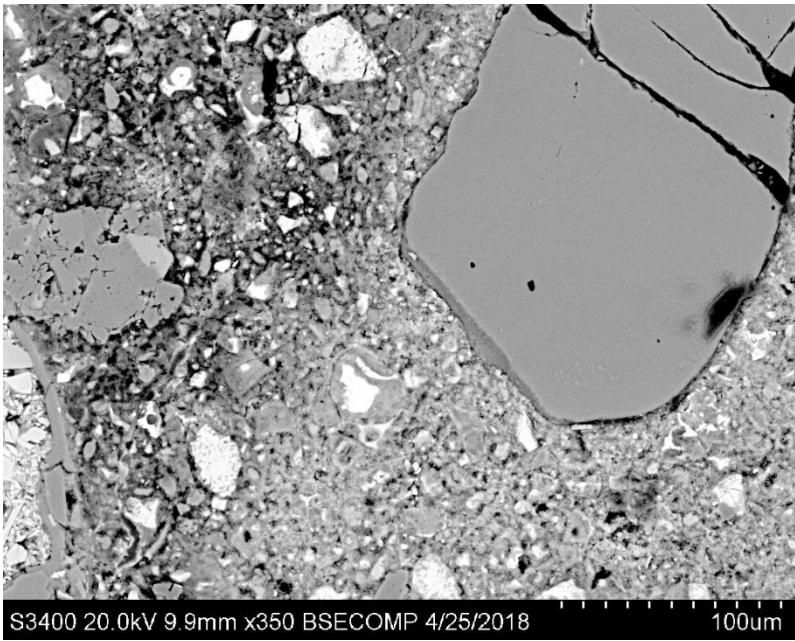
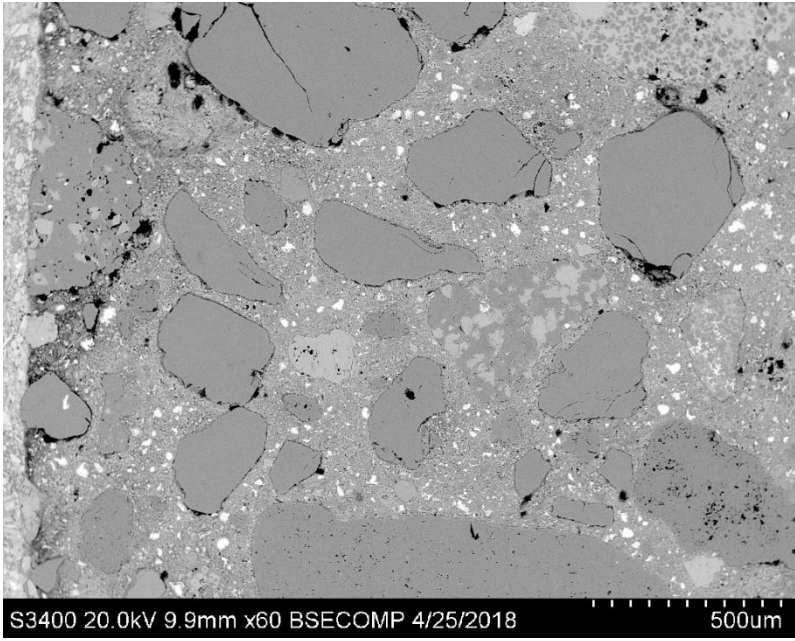


Figure 10.32: ESEM images of MOR-ESEM, SS

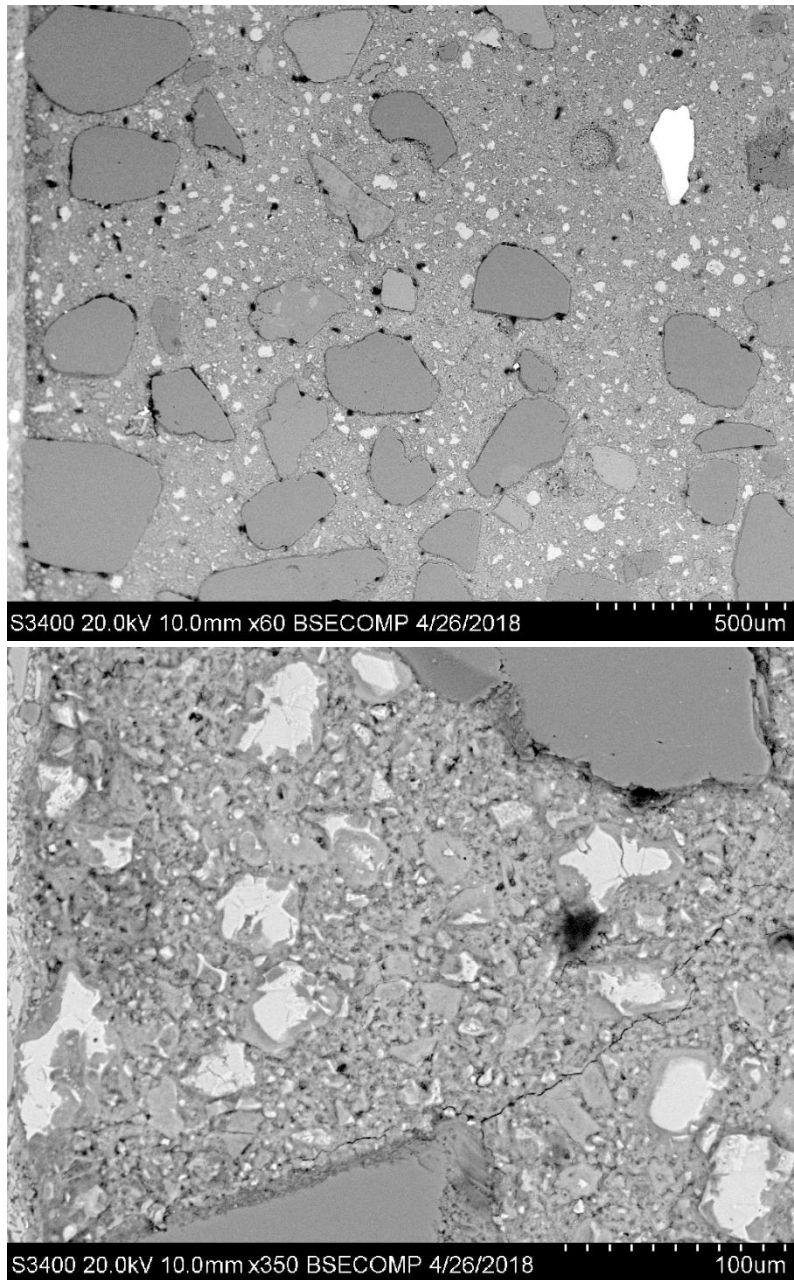


Figure 10.33: ESEM images of MOR-ESEM, ISOB

From ESEM images, the presence of two main areas with two different levels of brightness can be noticed. To investigate the differences between those two areas, EDS analysis was conducted on both darker (A) and brighter (B) areas. The results are illustrated in Figure 10.34, Figure 10.35, Figure 10.36, and Figure 10.37. For each plot, the spectra are normalized over a selected region (yellow band visible on the right side of the plot), that is, they are scaled along the Y-axis to the average value in the selected region.

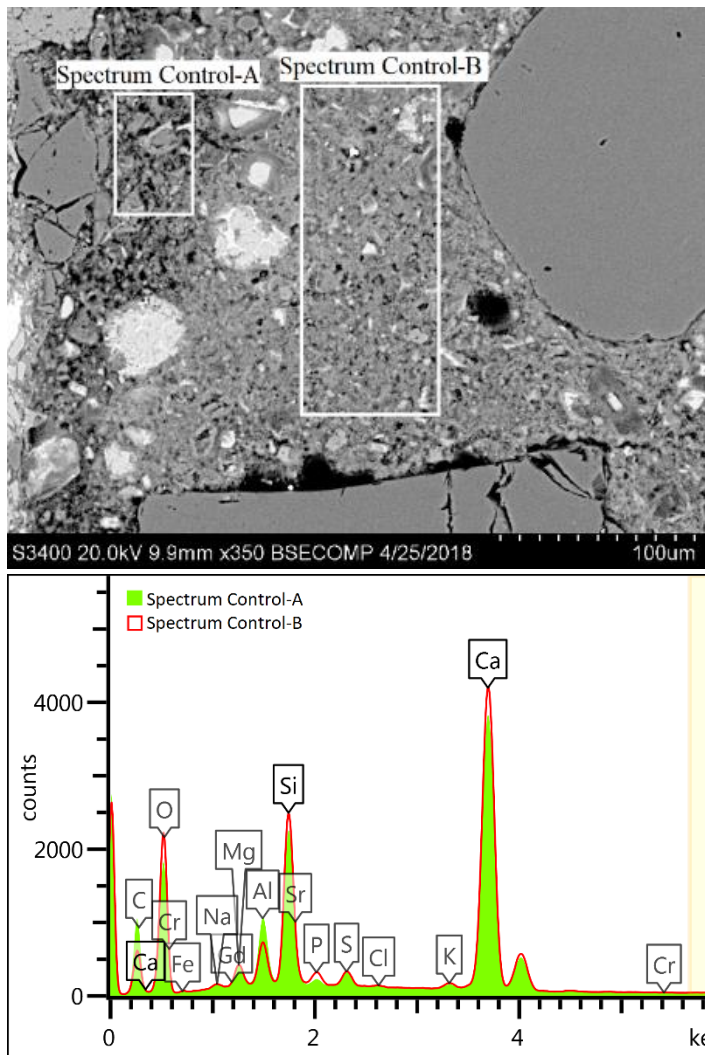


Figure 10.34: ESEM image (top) and X-ray spectra (bottom) for areas A and B of sample MOR-ESEM Control

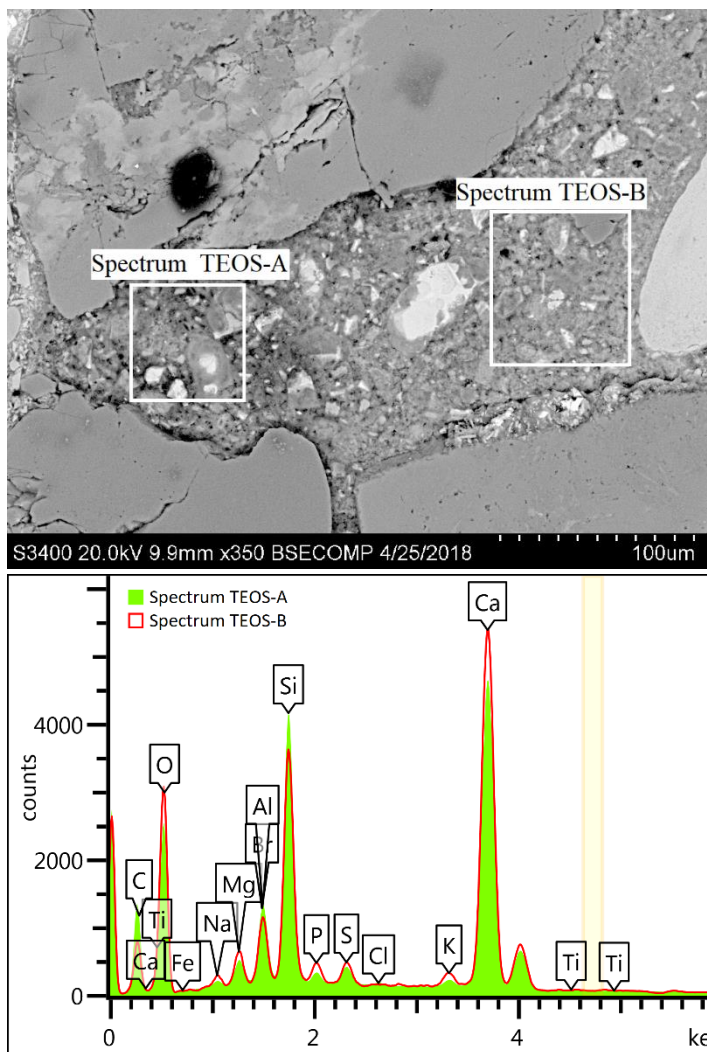


Figure 10.35: ESEM image (top) and X-ray spectra (bottom) for areas A and B of sample MOR-ESEM, TEOS-treated

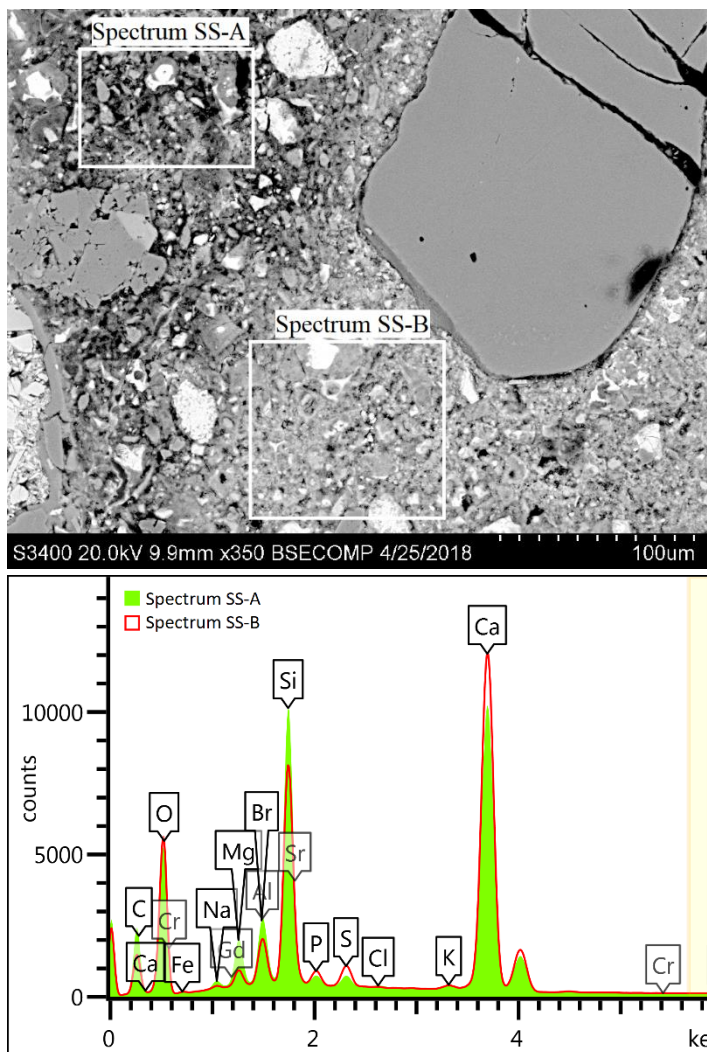


Figure 10.36: ESEM image (top) and X-ray spectra (bottom) for areas A and B of sample MOR-ESEM, SS-treated

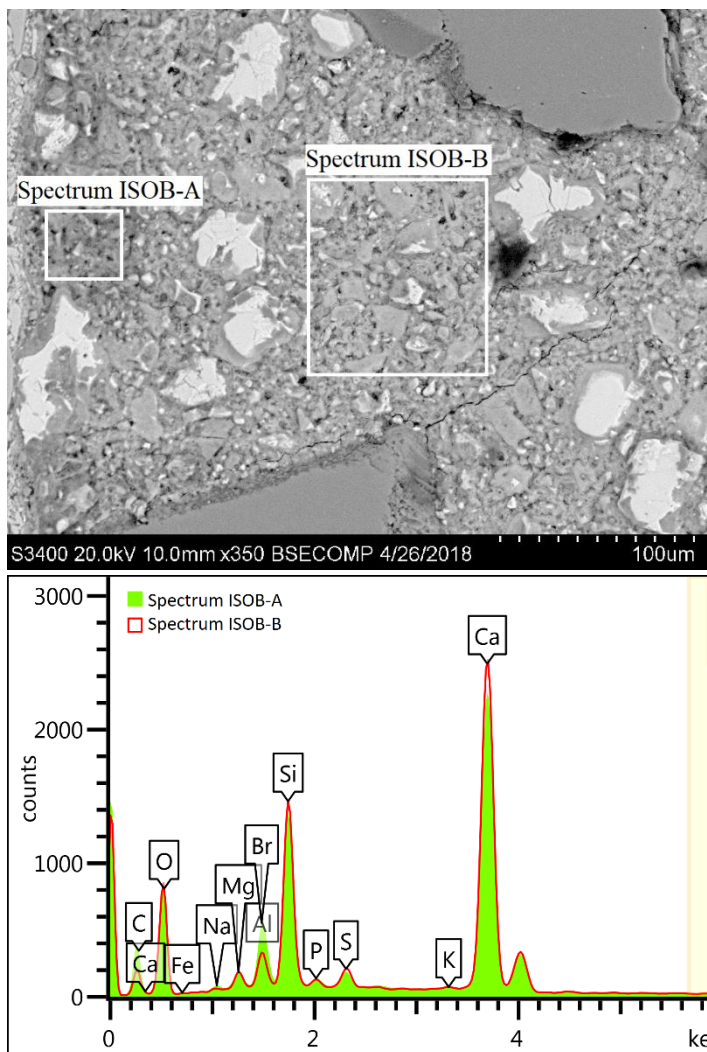


Figure 10.37: ESEM image (top) and X-ray spectra (bottom) for areas A and B of sample MOR-ESEM, ISOB-treated

Spectra obtained from the outer and inner layer of each sample were compared and the results are shown in Figure 10.38. Finally, results from the quantitative analysis are shown in Figure 10.39.

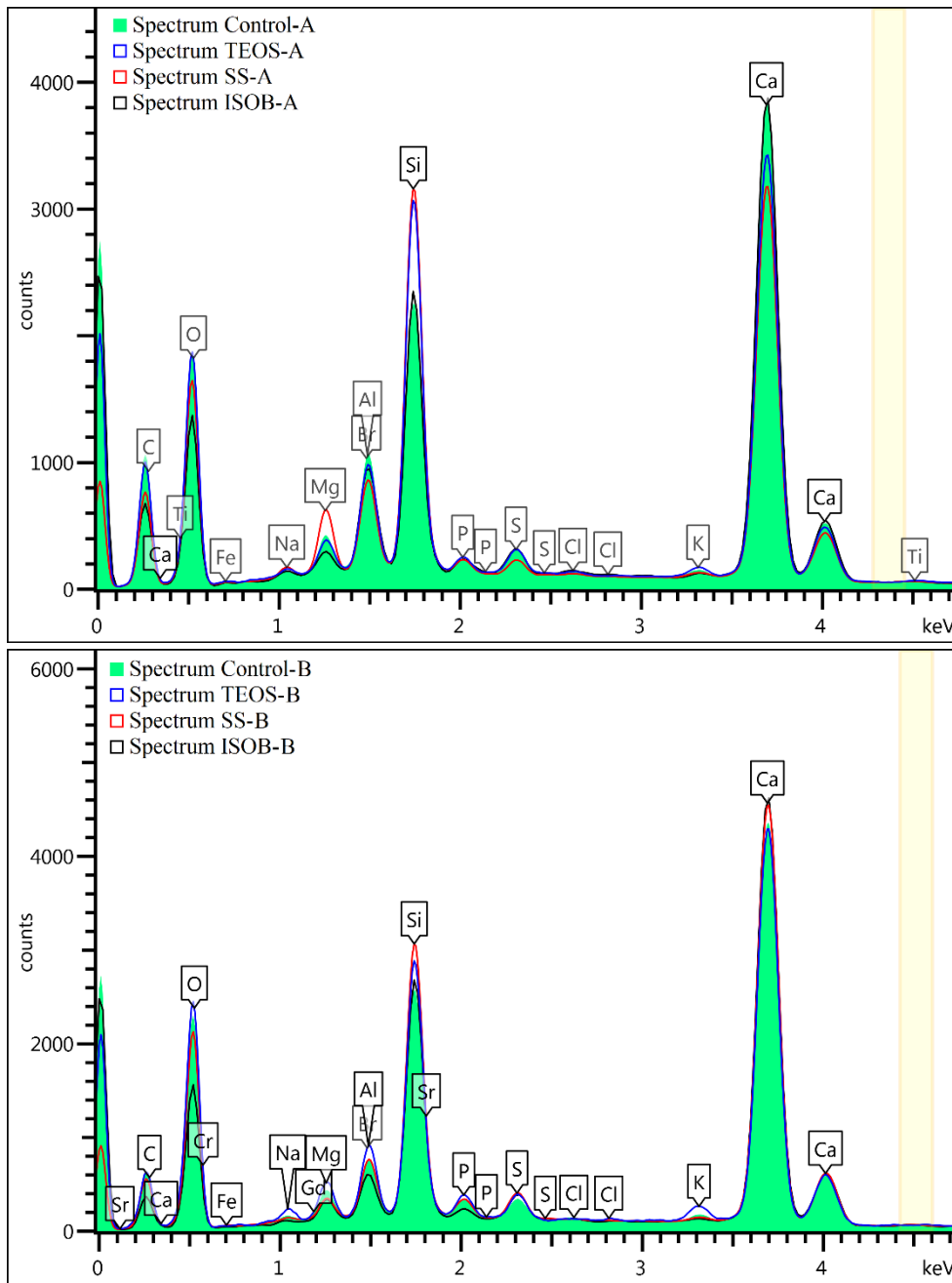


Figure 10.38: Comparison between X-ray spectra obtained from the outer (top) and inner (bottom) layer of each sample

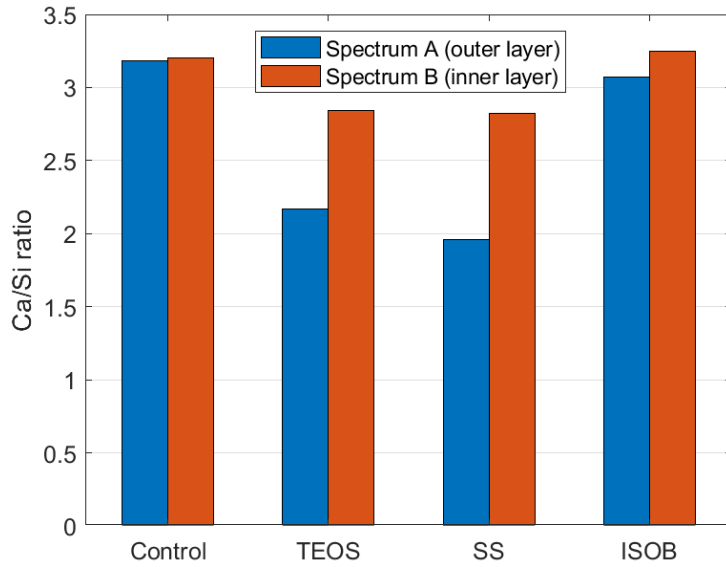


Figure 10.39: Ca/Si ratios obtained from the quantitative analysis associated with the obtained spectra

10.4.3 Carbonation Depth

The results of the colorimetric test performed on treated and untreated ferrocement samples after 5, 10, 18, and 28 days of accelerated carbonation are reported in Figure 10.40. The percentage increase in carbonation resistance compared to non-treated samples were calculated at 28 days (Table 10.11).

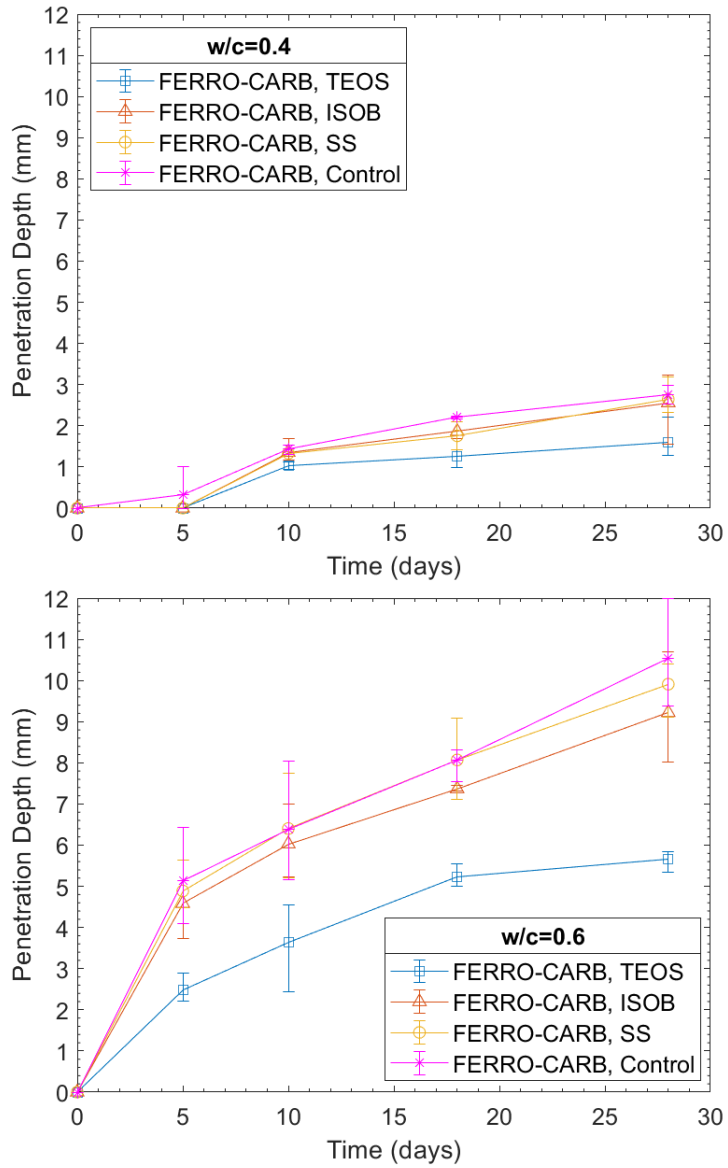


Figure 10.40: Penetration depth of untreated and treated ferrocement samples FERRO-CARB

Table 10.11: Samples FERRO-CARB, increase of carbonation resistance compared to non-treated samples

| Sample | w/c | Increase of carbonation resistance compared to non-treated samples at 28 d, % |
|------------------|------------|--|
| FERRO-CARB, TEOS | 0.4 | 41.9 |
| FERRO-CARB, ISOB | 0.4 | 6.9 |
| FERRO-CARB, SS | 0.4 | 3.9 |
| FERRO-CARB, TEOS | 0.6 | 46.2 |
| FERRO-CARB, ISOB | 0.6 | 12.5 |
| FERRO-CARB, SS | 0.6 | 5.9 |

10.4.4 Water Absorption Test

The influence of number of TEOS applications (by brushing technique using the same ethyl silicate solution described in Section 10.2.5) on the water absorption of cement mortar is shown in Figure 10.41; moreover, the percentage decreases in permeability compared to non-treated samples were calculated at 24 hours (Table 10.12).

The influence of different treatment agents on the water absorption characteristics of mortar and pre-cracked ferrocement samples (MOR-S2 and FERRO-S, respectively) is shown in Figure 10.42 and Figure 10.43; the percentage decreases in permeability compared to non-treated samples at 24 hours are listed in Table 10.13 and Table 10.14.

Table 10.12: Samples MOR-S1, decrease in permeability compared to non-treated samples

| Sample | w/c | Decrease in permeability compared to non-treated samples at 24 h (%) |
|-------------|-----|--|
| MOR-S1 (A) | 0.4 | 35.3 |
| MOR- S1 (B) | 0.4 | 43.5 |
| MOR-S1 (C) | 0.4 | 45.6 |
| MOR-S1 (A) | 0.6 | 22.5 |
| MOR- S1 (B) | 0.6 | 28.4 |
| MOR-S1 (C) | 0.6 | 32.9 |

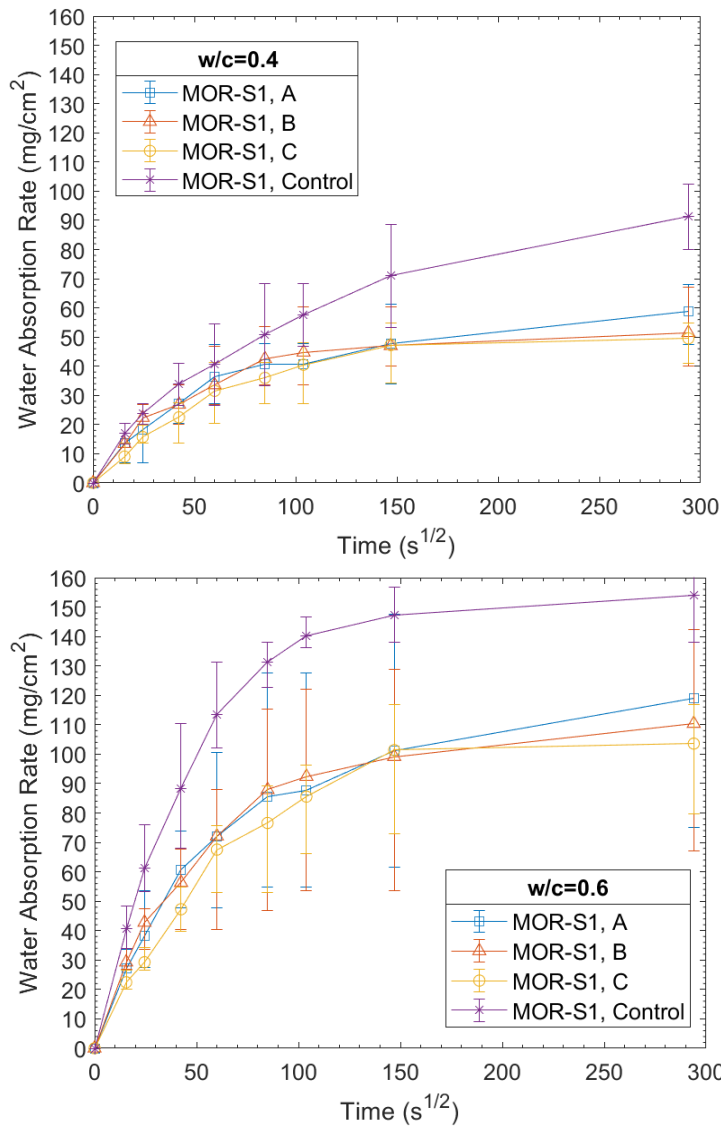


Figure 10.41: Water absorption test on treated and untreated mortar samples MOR-S1

Table 10.13: Samples MOR-S2, decrease in permeability compared to non-treated samples

| Sample | w/c | Decrease in permeability compared to non-treated samples at 24 h (%) |
|--------------|-----|--|
| MOR-S2, TEOS | 0.4 | 30.0 |
| MOR-S2, ISOB | 0.4 | 84.3 |
| MOR-S2, SS | 0.4 | 65.7 |
| MOR-S2, TEOS | 0.6 | 17.4 |
| MOR-S2, ISOB | 0.6 | 95.4 |
| MOR-S2, SS | 0.6 | 41.3 |

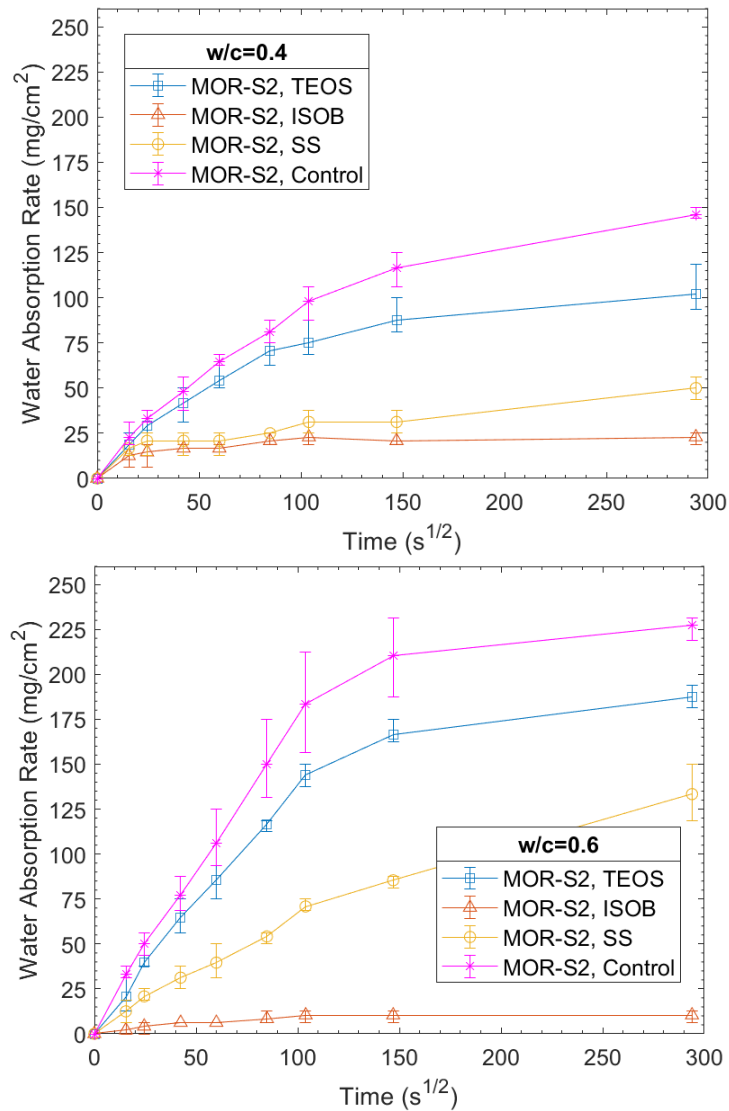


Figure 10.42: Water absorption test on treated and untreated mortar samples MOR-S2

Table 10.14: Samples FERRO-S, decrease in permeability compared to non-treated samples

| Sample | w/c | Decrease in permeability compared to non-treated samples at 24 h (%) |
|---------------|-----|--|
| FERRO-S, TEOS | 0.4 | 15.0 |
| FERRO-S, ISOB | 0.4 | 93.6 |
| FERRO-S, SS | 0.4 | 57.9 |
| FERRO-S, TEOS | 0.6 | 20.7 |
| FERRO-S, ISOB | 0.6 | 94.9 |
| FERRO-S, SS | 0.6 | 32.1 |

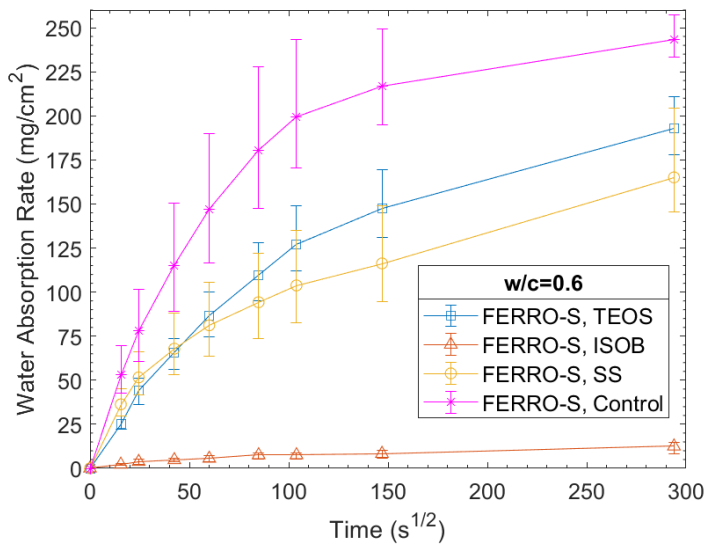
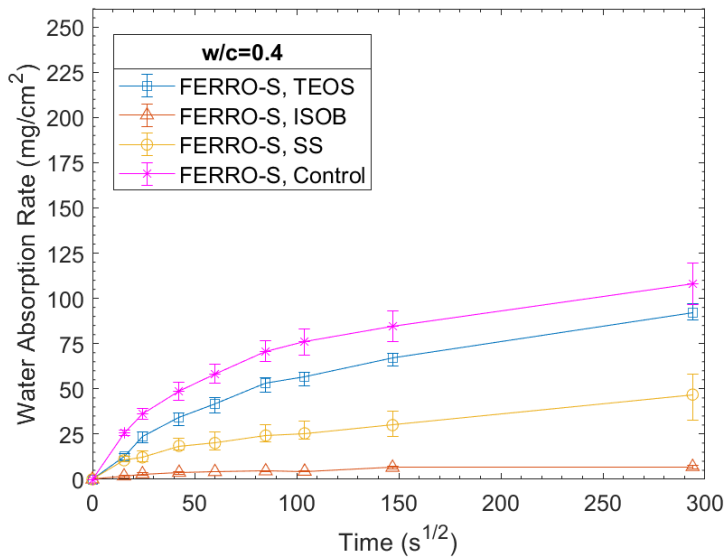


Figure 10.43: Water absorption test on treated and untreated ferrocement samples FERRO-S

10.5 Discussion

10.5.1 Flexure Test on Mortar and Ferrocement

Since flexure tests on mortar have been conducted under C.M.O.D. control (Figure 10.25), the derived values for flexural strength and modulus of elasticity (listed in Table 10.6) are much more reliable than those which would have been obtained if the tests had been conducted under displacement control. Fracture mechanics characterization can be effectively performed by means of three-point bending notched specimens and C.M.O.D. control. However, the determination of fracture parameters was beyond the scope of this study, since the primary focus was to evaluate the effectiveness of surface treatment on durability. Thus, effect of surface treatment on mechanical parameters was not attempted in this study.

The main purpose of flexure test on ferrocement plates FERRO-FL was to evaluate if the bending behavior described by Naaman (Naaman, 2000) can be ascribable to the specimens obtained in this study. In fact, one of the main concerns was to obtain specimens characterized by a cracking behavior that is typical for ferrocement, in preparation for the water sorptivity test on cracked ferrocement samples. Naaman argued that the typical bending response of ferrocement can be divided into 5 stages, as shown in Figure 10.44: 1) an initial portion where structural cracking does not occur; 2) a multiple cracking region where cracks develop and their width increases with increasing load; 3) a region where gradual yielding of the steel reinforcement occurs (gradual yielding always occurs because several layers of mesh, placed at different depths of the section, undergo yielding at different loading levels); 4) a post-yielding plastic or strain-hardening region during which the maximum or ultimate load is attained; and 5) a post-peak portion where failure occurs either due to mortar failure in compression or due to failure of the extreme layer of mesh.

As can be seen in Figure 10.26, the bending behavior of ferrocement plates built in this study is similar to that reported in the literature (Naaman, 2000; Shah & Balaguru, 1984). Moreover, it is worth noting that ferrocement specimens featured great deformability, attaining high deflections at failure load (up to about 7 mm for w/c 0.6 specimens).

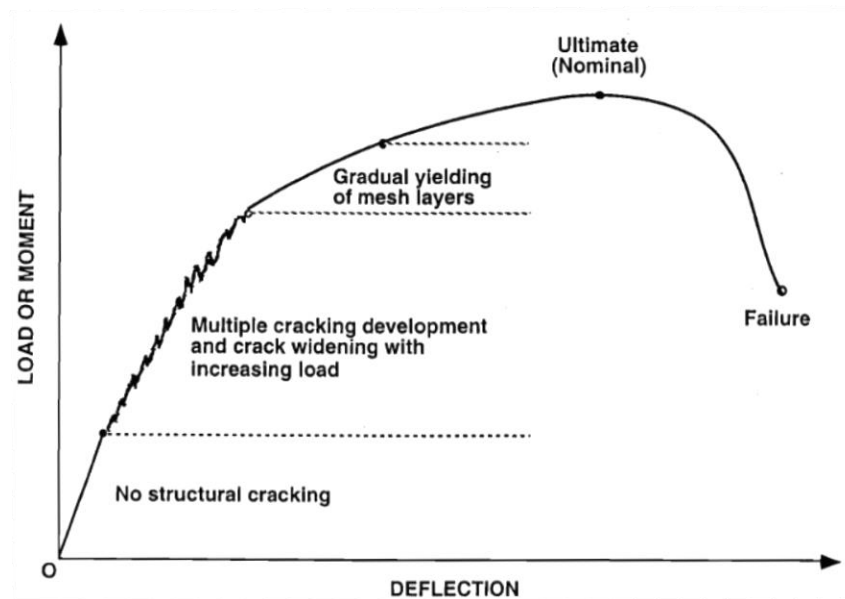


Figure 10.44: Typical load-deflection response of ferrocement illustrating various stages of behavior (Naaman, 2000)

Samples FERRO-S exhibited high variability with respect to the load versus deflection behavior and, thus, crack widths after unloading phase. A reasonable explanation for this variability may be the impossibility to obtain a perfectly flat mesh at the moment of the casting, since the steel mesh is sold in rolls.

With respect to the high variability, it is interesting to note that specimens FERRO-S (1), FERRO-S (4), and FERRO-S (12) have unusually high values of crack width. At first it was thought to exclude these samples from the study, however, after water absorption test, the author found out that water absorption rates of these three samples were very similar to those of the samples characterized by smaller crack width (see error bars in Figure 10.43).

10.5.2 ESEM-EDS Analysis

The ESEM-EDS analysis of the cross section of untreated samples, TEOS- treated samples, and SS-treated samples (Figure 10.30, Figure 10.31, Figure 10.32) revealed the existence of a darker and superficial area no wider than 200 μm . This darker external layer was called “A”, while the brighter internal layer was called “B”. Since this darker region is found in both treated and non-treated samples, it is reasonable to assume that

this less dense area is caused by to the sample preparation process rather than the treatment agents.

Further EDS analysis allowed to compare the X-ray spectra obtained from those regions. Since TEOS and SS are both expected to display pozzolanic activity, EDS analysis only focused on calcium and silicon peaks; the basic assumption is that the protective agent is able to consume calcium hydroxide to form calcium silicate hydrate, thus refining the pore structure and reducing the calcium content in the cement matrix.

As can be seen in Figure 10.34 and Figure 10.39, the untreated sample featured very similar spectra and Ca/Si ratios between regions A and B. The only difference is represented by a higher porosity in the darker external layer, which caused the Ca and Si peaks in spectrum “Control-A” to be lower than those in spectrum “Control-B”. A similar conclusion can be drawn for the sample treated with ISOB (Figure 10.37), that is, the surface treatment did not display pozzolanic behavior as no significant difference in Ca/Si ratio can be detected between "ISOB-A" and "ISOB-B". Furthermore, the ISOB-treated sample has almost the same Ca/Si ratio than that of the untreated sample.

Different results were obtained for mortar specimens treated with TEOS and SS (Figure 10.35 and Figure 10.36). The protective agent was indeed able to decrease the Ca/Si ratios at least in the external layer “A” (Figure 10.39). Moreover, peak intensity for calcium in the EDS plots of treated specimens decreased greatly relative to the EDS plots of the untreated specimen. This observation indicates that calcium hydroxide reacts with TEOS and SS to form more C-S-H, as depicted in the final comparison between spectra “Control-A”, “TEOS-A”, and “SS-A” (Figure 10.38).

Even though both TEOS and SS led to a decrease in Ca/Si ratio, such decrease was found to be maximum for SS-treated sample. It can thus be suggested that sodium silicate exhibits higher pozzolanic reactivity, resulting in a higher CH consumption than that of TEOS.

10.5.3 Water Absorption on TEOS-Treated Samples MOR-S1

The rate and extent of water suction of cementitious materials have been widely used to reflect their surface quality (ASTM, 2000). If samples MOR-S1 are considered (Figure 10.41), the only difference between samples A, B, and C is the number of

applications of the protective agent (See Table 10.5). The water absorption is much lower in w/c 0.4 samples, as expected due to the finer pore structure. A decisive decrease in water permeability was noted for every treated sample, showing that TEOS can be effective in reducing the ingress of aqueous substances for both high and low water-to-cement ratios, with a considerable advantage in terms of expected durability. Moreover, TEOS exhibited better performance when applied to samples with lower w/c ratio, as showed in Table 10.12. After 24 hours, samples with w/c ratio 0.4 featured a decrease of up to 45.6% compared to the control samples, while samples with w/c ratio 0.6 decreased their permeability up to 32.9%. This is not trivial, since the w/c 0.6 samples should feature a higher TEOS absorption than that of w/c 0.4 samples, due to their higher porosity.

The most remarkable result to emerge from the data is that given the same w/c ratio, it is true that a higher number of ethyl silicate applications lead to a higher decrease in permeability; however, the differences in water absorption rate between samples A, B, and C are not so conspicuous. Therefore, the number of ethyl silicate applications is not an essential parameter with regard to water absorption of mortar samples treated with TEOS.

10.5.4 Carbonation Depth

The results obtained from the accelerated carbonation test (Figure 10.40 and Table 10.11) establish that TEOS is able to greatly limit the penetration of CO₂ in ferrocement specimens with both high and low water-to-cement ratios, leading to a percentage decrease in carbonation depth of up to 46.2% compared to the control samples. In contrast, SS and ISOB did not provide any significant reduction in the carbonation depth.

As stated in Section 10.1.3, there is still much considerable controversy surrounding the effectiveness of hydrophobic treatments (such as ISOB) in preventing the ingress of CO₂ into cement-based materials. Results obtained from the accelerated carbonation test are in complete agreement with several other studies which proved that the carbonation depth after a long period of exposure is the same for hydrophobized as for nontreated concrete (Yang, Li, & Zhao, 2012; Attanayaka, Ng, & Aktan, 2002; Polder, Borsje, & Vries, 2000; Polder, Borsje, & Vries, 2001). This happens because hydrophobic treatment agents can only control the moisture content of the concrete substrate, without reducing

the air permeability, and thus the diffusivity of CO₂ (Basheer, Basheer, Cleland, & Long, 1997; Zhu, Kou, Poon, Dai, & Li, 2013).

What is surprising is the fact that samples treated with SS featured such a low carbonation resistance, especially in comparison with that exhibited by TEOS-treated samples. To justify this, two considerations can be taken into account. First, as confirmed by ESEM-EDS results, SS treatment results in a greater CH consumption leading to a low alkaline reserve; this has a detrimental effect with respect to carbonation resistance. Secondly, the hydrophobic effect of TEOS contributes to decrease the moisture content of mortar (Raupach & Wolff, 2005). Given the particular relative humidity conditions inside the carbonation chamber (RH 81%, very close to the peak in the carbonation rate versus relative humidity curve, as depicted in Figure 4.4), a reasonable drop in moisture content in the pores can be expected to reduce the carbonation rate in TEOS-treated samples.

10.5.5 Water Absorption on Samples MOR-S2 and FERRO-S

TEOS was the most effective treatment with respect to carbonation resistance; however, if the influence of different treatment agents on the water absorption is considered, the other protective agents employed in this study were more effective in blocking the ingress of water into the cementitious matrix.

As can be seen in Figure 10.42 and Table 10.13. All the treatment agents selected in this study were able to effectively enhance the water absorption properties of mortar samples (MOR-S2). Surprisingly, the decrease in water absorption is minimum for TEOS (up to 30%, better performance was obtained again for samples with lower w/c ratio). Samples treated with ISOB showed the highest reduction in permeability (up to 95%), exhibiting outstanding performance as a matter of water absorption rate. Furthermore, a significant improvement in terms of water absorption was achieved by means of SS (up to 65.7%).

Further tests carried out with pre-cracked ferrocement specimens (FERRO-S) confirmed the initial findings, as illustrated in Figure 10.43. This time, TEOS was more effective when applied to samples with higher w/c ratio (w/c 0.6 samples showed a decrease of up to 20.7% compared to the control samples, while 15.0% of percentage decrease was observed for w/c 0.4 samples), due to the fact that the protective agent was able to achieve a higher penetration depth thanks to the presence of cracks.

Application of hydrophobic treatment to cement-based materials aims at reducing the capillary absorption of water and dissolved aggressive substances. Thus, the reason why ISOB exhibits better performance with respect to water absorption is clear; it forms a hydrophobic layer of molecular thickness on the pore walls with no pore blocking effect.

TEOS and SS are both expected to display strong pozzolanic activity, since they react with calcium hydroxide forming calcium silicate hydrate and resulting in a block of the capillary pores. However, while SS owes its effectiveness solely to the pore blocking effect, TEOS can be defined as a *multifunctional* surface treatment. In fact, as an alkoxy silane, a long-lasting hydrophobic effect is obtained in addition to the pozzolanic activity.

In contrast with earlier findings, water absorption tests revealed that SS is more successful than TEOS in reducing the capillary absorption of water. Franzoni et al. investigated the performance and effectiveness of SS and TEOS in terms of morphology and microstructure, water absorption, water contact angle, chloride resistance, carbonation resistance and abrasion resistance (Franzoni, Pigino, & Pistolesi, 2013). The authors pointed out that TEOS exhibits better performance than SS with respect to both water absorption and carbonation resistance.

The reason for this contradictory result is still not completely clear; however, the following considerations can be done. Sodium silicate-based penetrating sealers should have low enough viscosity to achieve satisfactory penetration (Litvan, 1996) because a thin liquid is more quickly attracted than a viscous liquid substance (Vries I. , 1997). The viscosity of a sodium silicate-based sealer is controlled by the content of sodium silicate, additives and water (Jiang, et al., 2015). Given the lower viscosity of TEOS (Sandrolini, Franzoni, & Pigino, 2012), it is likely that by dipping the samples in the penetrating sealers for longer TEOS will achieve a higher penetration depth while SS will not. Moreover, Franzoni et al. employed a sodium silicate-based sealer with a higher concentration of sodium silicate (25%) (Franzoni, Pigino, & Pistolesi, 2013), this could have resulted in a lower penetration of the protective agent into the pore structure. Finally, Amoroso et al. pointed out that the slow reactive rate of TEOS can be significantly improved by means of catalysis addition (Amoroso & Fassina, 1983).

Cai et al. investigated the effects and mechanisms of TEOS with a comparison study of sodium silicate-based sealer and the water repellent methyltriethoxysilane (MT-silane)

(Cai, et al., 2016). The authors used an alcoholic ethyl silicate solution containing 35 wt.% of SiO₂ and declared that the viscosity of all the treatment agents were comparable (about 1 mPa s). For mortar samples surface-treated at 90 days, the water absorption was comparable between TEOS-treated samples and SS-treated samples.

Given the discrepancy between experimental results, further studies would be needed to determine how exactly the different parameters (such as viscosity, application method and concentration of the reactants) influence the efficacy of TEOS and SS.

CHAPTER 11

SUMMARY AND CONCLUSIONS

This thesis has called into question the sensitive issue of maintenance, repair and conservation of ferrocement architectural heritage. Although durability of concrete has already been the focus of research for many decades and many deterioration phenomena are well explained, there is still a paucity of literature on durability of ferrocement structures.

The main focus of this thesis is the exploration of different surface treatments to extend the durability of ferrocement in the context of a multidecade re-use of Nervi's masterwork Turin Exhibition Center; however, other related topics such as transport mechanisms in cement-based materials, geometrical and mechanical properties of ferrocement and its wire mesh reinforcement, and principles for maintenance and repair of heritage structures are explored too.

Due to the homogeneity and the excellent cracking behavior of ferrocement (its average crack width and spacing are more than an order of magnitude smaller than those of traditional reinforced concrete), surface treatments are expected to be quite effective in ceasing the migration of substances in and out of the mortar matrix. In this work, investigations of the effectiveness of ethyl silicate, sodium silicate and Isobutyl-triethoxy-silane sealers were made with respect to pozzolanic behavior, carbonation resistance, and water sorptivity. All the penetrating sealers investigated in this study were effective in decreasing the mortar permeability with respect to water absorption; however, only ethyl silicate was shown to properly increase the carbonation resistance.

The comparison of the effects of these surface treatments led the author to the conclusion that ethyl silicate is a promising surface treatment for ferrocement protection when carbonation-induced corrosion is a concern, while Isobutyl-triethoxy-silane hydrophobic sealer gave the best performance for water capillary absorption. Thus, the latter can be of great help in preventing chloride-induced corrosion.

Sodium silicate-based sealer was able to improve the waterproofing performance of mortar and ferrocement specimens, despite its poor efficiency in decreasing the carbonation rate. This particular aspect of sodium silicate remains unclear; however, the high CH consumption resulting from sodium silicate pozzolanic activity may be the answer. Moreover, ethyl silicate and isobutyl-triethoxy-silane are easier to apply than sodium silicate because sodium silicate features a high viscosity which is greatly influenced by the concentration of active ingredient and can undermine the penetration of protective agent (this is the reason why a sodium silicate concentration of only 12 wt.% was used in this study).

Because of the limited research on the durability of ferrocement, it is very difficult to predict the residual service life of a ferrocement structure after surface treatment. This is especially true if newly developed surface treatments (such as ethyl silicate) are considered. It is recommended that further research should be undertaken in the following areas:

- 1) the influence of parameters such as concentration and viscosity of the protective agents, which will surely influence the penetration depth of the penetrating agent and the extent of pozzolanic reactions in the pore structure;
- 2) time dependence of carbonation resistance of ferrocement with surface treatments. In fact, as a surface treatment ages, its carbonation resistance may decrease;
- 3) carbonation and corrosion behavior of cracked ferrocement specimens before and after surface treatment. In fact, this experimental study only focused on uncracked ferrocement specimens under accelerated carbonation conditions;
- 4) corrosion mechanism of the mesh reinforcement in ferrocement members. So far, no prior study is sufficient to fully understand corrosion in ferrocement; in fact, corrosion mechanism and structural behavior with corrosion are certainly different from that of common reinforced concrete, mainly due to the geometric properties of mesh reinforcement.

With respect to Turin Exhibition Center, chlorides are not a matter of concern since there is no marine environment, and no de-icing salts will ever be applied to the ribbed vault. Most likely, the biggest threat to the ferrocement elements (i.e., wave ashlar and tavelloni) is the carbonation-induced corrosion. Thus, the results obtained in this thesis

suggest that, amongst the considered surface treatments, TEOS is the most appropriate to be employed to improve the durability of the ferrocement elements in Turin Exhibition Center. However, given that these findings are based on young mortar and ferrocement specimens, further research would be needed to determine whether TEOS is effective in increasing carbonation resistance in both young and old ferrocement elements.

BIBLIOGRAPHY

- Abel, J., Arun, G., & Chiorino, M. (2013). Pier Luigi Nervi: Art and Technology in Building: Preface. *Journal of the International Association for Shell and Spatial Structures*, 54(2 & 3), 79-86.
- Abram, J. (2011). Pier Luigi Nervi: Strength Through Form, Form as Structure. In *Pier Luigi Nervi: Architecture as Challenge* (p. 41-57). Silvana Editoriale.
- ACI Committee 116. (2000). *116R-00: Cement and Concrete Terminology (Reapproved 2005)*. American Concrete Institute.
- ACI Committee 201. (2008). *ACI 201.1R-08: Guide for Conducting a Visual Inspection of Concrete in Ser-vice*. American Concrete Institute.
- ACI Committee 201. (2016). *ACI 201.2R-16 Guide to durable concrete*. American Concrete Institute.
- ACI Committee 211. (1991). *ACI 211.1-91: Standard Practice for Selecting Proportions for Normal, Heavyweight, and Mass Concrete (Reapproved 2009)*. American Concrete Institute.
- ACI Committee 224. (2001). *ACI 224R-01, Control of Cracking in Concrete Structures*. American Concrete Institute.
- ACI Committee 228. (2013). *ACI 228.2R-13: Report on Nondestructive Test Methods for Evaluation of Concrete in Structures*. American Concrete Institute.
- ACI Committee 515. (2013). *ACI 515.2R-13: Guide to Selecting Protective Treatments for Concrete*. American Concrete Institute.
- ACI Committee 546. (2014). *ACI 546.3R-14: Guide to Materials Selection for Concrete Repair*. American Concrete Institute.

- ACI Committee 546. (2014). *ACI 546R-14: Guide to Concrete Repairs*. American Concrete Institute.
- ACI Committee 549. (1982). *State-of-the-art report on ferrocement*. Farmington Hills: American Concrete Institute.
- ACI Committee 549. (1993). *ACI 549.1R-93: Guide for the design, construction, and repair of ferrocement (Reapproved 2009)*. American Concrete Institute.
- ACI Committee 549. (1997). *ACI 549R-97: Report on ferrocement*. American Concrete Institute.
- ACI Committee 562. (2016). *ACI 562-16: Code for Assessment, Repair, and Rehabilitation of Existing Concrete Structures*. American Concrete Institute.
- Ackermann, G., Jugelt, W., Möbius, H.-H., Suschke, H., & Werner, G. (1974). *Elektrolytgleichgewichte und Elektrochemie*. Weinheim: Verlag Chemie.
- Al-Ahmad, S., Toumi, A., Verdier, J., & Francois, R. (2009). Effect of Crack Opening on Carbonation Dioxide Penetration in Cracked Mortar Samples. *Materials and Structures*, 42, 559-566.
- Aligizaki, K. (2006). *Pore structure of cement-based materials: testing, interpretation and requirements*. London: Taylor & Francis.
- Allen, R., & Forrester, J. (1983). The Investigation and Repair of Damaged Reinforced Concrete Structures. In A. Crane (A cura di), *Corrosion of Reinforcement in Concrete Construction* (p. 193-222). London: Society of Chemical Industry.
- Almusallam, A., Khan, F., Dulaijan, S., & Al-Amoudi, O. (2003). Effectiveness of Surface Coatings in Improving Concrete Durability. *Cement and Concrete Composites*, 25(4-5), 473-481.
- Alonso, C., & Andrade, C. (1994). Life Time of Rebars in Carbonated Concrete. In J. Costa, & A. Mercer (A cura di), *Progress in Understanding and Prevention of Corrosion* (p. 624). London: Institute of Materials.

- Alonso, C., Andrade, C., & Gonzales, J. (1988). Relation Between Resistivity and Corrosion Rate of Reinforcement in Carbonated Mortar Made with Several Cement Types. *Cement and Concrete Research*, 18(5), 687-698.
- American Concrete Institute. (2008). *ACI 201.2R-08 Guide to durable concrete*.
- Amoroso, G., & Fassina, V. (1983). *Stone Decay and Conservation: Atmospheric Pollution, Cleaning, Consolidation and Protection*. Amsterdam: Elsevier.
- Andrade, C., & Alonso, C. (1996). Corrosion Rate Monitoring in the Laboratory and on Site. *Construction and Building Materials*, 10(5), 315-328.
- Andrade, C., Alonso, C., Gulikers, J., Polder, R., Cigna, R., Vennesland, Ø., . . . Elsener, B. (2004). Recommendations on Test Methods for On-Site Corrosion Rate Measurement of Steel Reinforcement in Concrete by Means of the Polarization Resistance Method. *Materials and Structures*, 37(9), 623-643.
- Arup, H. (1983). The Mechanisms of the Protection of Steel by Concrete. In *Corrosion of Reinforcement in Concrete Construction* (p. 151-157). Chichester: Hellis Horwood Ltd.
- Arya, C., & Darko, F. (1996). Influence of Crack Frequency on Reinforcement of Corrosion in Concrete. *Cement and Concrete Research*, 26(3), 345-353.
- Arya, C., & Wood, L. (1995). The Relevance of Cracking in Concrete to Corrosion of Reinforcement. Camberly, Surrey: Technical Report No. 44.
- ASTM. (2000). *ASTM E96-00: Standard Test Methods for Water Vapor Transmission of Materials*. Washington: American Society of Testing and Materials.
- ASTM. (2009). *ASTM C876: Standard Test Method for Half-Cell potentials of Uncoated Reinforcing Steel in Concrete*. West Conshohocken, PA: American Society of Testing and Materials.

- ASTM. (2016). *ASTM C125: Standard Terminology Relating to Concrete and Concrete Aggregates*. West Conshohocken, PA: American Society of Testing and Materials.
- Attanayaka, U., Ng, S., & Aktan, H. (2002). *Criteria and Benefits of Penetrating Sealants for Concrete Bridge Decks*. Michigan: Michigan Department of Transportation.
- Austriaco, N., Lee, S., & Pama, R. (1975). Inelastic Behaviour of Ferrocement Slabs in Bending. *Magazine of Concrete Research (London)*, 27(93), 193-209.
- Bakker, R. (1994). Prediction of Service Life of Reinforcement in Concrete Under Different Climatic Conditions at Given Cover. Int Conf. on Corrosion and Corrosion Protection of Steel in Concrete. Sheffield.
- Balaguru, P., Naaman, A., & Shah, S. (1977). Analysis and Behaviour of Ferrocement in Flexure. In *Proceedings, V.103, ST10* (p. 1973-1951). ASCE.
- Basheer, L., & Cleland, D. (1998). Protection Provided by Surface Treatment Against Chloride Induced Corrosion. *Materials and Structures*, 31, 459-464.
- Basheer, P., & Long, A. (1997). Protective Qualities of Surface Treatments for Concrete. *Proceedings of the Institution of Civil Engineers, Structures and Building*, 122, 339-346.
- Basheer, P., Basheer, L., Cleland, D., & Long, A. (1997). Surface Treatments for Concrete: Assessment Methods and Reported Performance. *Constr Build Mater*, 11(7-8), 413-429.
- Batis, G., Pantazopoulou, P., & Routoulas, A. (2003). Corrosion Protection Investigation of Reinforcement by Inorganic Coating in the Presence of Alkanolamine-Based Inhibitor. *Cement and Concrete Composites*, 25(3), 371-377.
- Beeby, A. (1983). Cracking, Cover and Corrosion of Reinforcement. *Concrete International*, 5(2), 35-40.

- Bentur, A., Diamond, S., & Berke, N. (1997). *Steel Corrosion in Concrete, Fundamentals and Civil Engineering Practice*. London: E & FN Spon.
- Bentz, D., & Stutzman, P. (1994). SEM Analysis and Computer Modelling of Hydration of Portland Cement Particles. In S. DeHayes, & D. Stark (A cura di), *ASTM STP 1215, Petrography of Cementitious Materials* (p. 60-73). Philadelphia: American Society for Testing and Materials.
- Benvenuto, E. (1981). *La scienza delle costruzioni e il suo sviluppo storico (Structural mechanics and their historical development; in Italian)*. Firenze: Sansoni.
- Berkowski, P., & Dmochowski, G. (2014). Examples of Concrete Structural Elements in Early 20th Century Buildings in Wrocław (Poland) - Case studies. In M. Grantham, P. Muhammed Basheer, B. Magee, & M. Soutsos (A cura di), *Concrete Solutions: Proceedings of Concrete Solutions, 5th International Conference on Concrete Repair, Belfast, Northern Ireland, 1–3 September 2014* (p. 699-706). Boca Raton: CRC Press.
- Bertolini, L. (2006). *Materiali da costruzione, Vol. 2, degrado, prevenzione, diagnosi, restauro*. Milano: Città Studi.
- Bertolini, L. (2006). *Materiali da costruzione: Vol. 1, struttura, proprietà e tecnologie di produzione*. Milano: Città Studi.
- Bertolini, L., Carsana, M., Gastaldi, M., Lollini, F., & Redaelli, E. (2011). Corrosion Assessment and Restoration Strategies of Reinforced Concrete Building of the Culturale Heritage. *Materials and Corrosion*, 62(2), 146-154.
- Bertolini, L., Elsener, B., Pedferri, P., Redaelli, E., & Polder, R. (2004). *Corrosion of steel in concrete: prevention, diagnosis, repair*. Wiley-VCH.
- Bijen, J. (2003). *Durability of Engineering Structures: Design, Repair and Maintenance*. Cambridge, UK: Woodhead Publishing.

- Bologna, A., & Giargiani, R. (2016). *The Rhetoric of Pier Luigi Nervi : Concrete and Ferrocement Forms*. Lausanne: EPFL Press.
- British Standard Institution. (1967). *Relative Humidity of Air Over Saturated Solutions of Salts, British Standard 3718;1964, Specification for Laboratory Humidity Ovens (Non-Injection Type)*.
- British Standards Institution. (1983). *BS 1881 part 122, Testing concrete - method for determination of water absorption*.
- Brocklebank, I. (2005). Concrete, Carbonation, and Corrosion. *Journal of the Building Limes Forum*, 12, 34-45.
- Broomfield, J. (2006). *Corrosion of Steel in Concrete, Understanding, Investigation, and Repair*. London: Taylor and Francis.
- Brunauer, S. (1962). *American Scientist*, 50(1), 210-229.
- Bürchler, D., Elsener, B., & Böhni, H. (1996). Electrical resistivity and dielectrical properties of hardened cement paste and mortar. *Electrically based microstructural characterization*, 411, 407.
- Cai, Y., Hou, P., Duan, C., Zhang, R., Zhou, Z., Cheng, X., & Shah, S. (2016). The Use of Tetraethyl Orthosilicate Silane (TEOS) for Surface-Treatment of Hardened Cement-Based Materials: A Comparison Study with Normal Treatment Agents. *Construction and Building Materials*, 117, 144-151.
- Carnot, A., Frateur, I., Marcus, P., & Tribollet, B. (2002). Corrosion Mechanisms of Steel Concrete Moulds in the Presence of a Demoulding Agent. *Journal of Applied Electrochemistry*, 32, 865-869.
- Carpanelli, F. (1955). *Come si Costruisce Oggi nel Mondo*. Milano: U. Hoepli.
- Cassie, W. (1967). Lambot's Boats: A Personal Discovery. *Concrete (London)*, 1(11), 380-382.

- CEB. (1992). Durable concrete structures. *Bulletin d'information*, 183.
- CEN - European Committee for standardization. (2000). *EN 197-1*.
- Chefdeville, J. (1953). Application of the Method toward Estimating the Quality of Concrete. *RILEM bulletin*(15, Special Issue - Vibrating Testing of Concrete, 2nd part).
- Chiorino, C. (2010). Eminent Structural Engineer: Pier Luigi Nervi (1891-1979), Art and Science of Building. *Structural Engineering International*, 20(1), 107-109.
- Chiorino, M. (2012). Art and Science of Building in Concrete: The Work of Pier Luigi Nervi. *Concrete International*, 34(3), 32-40.
- Chiorino, M. (2016). The role of structural engineering and geotechnics in the conservation of historical monuments - the case study of the Sanctuary of Vicoforte with its large elliptical dome. *Cornell Engineering, Gergely Seminar Series - CEE Infrastructure Group*.
- Chrisp, T., McCarter, W., Starrs, G., Basheer, P., & Blewett, J. (2002). Depth-related variations in conductivity to study cover-zone concrete during wetting and drying. *Cement and Concrete Composites*, 24, 415-426.
- Christodoulou, C., Goodier, C., & Austin, S. (2012). Assessing the Long-Term Durability of Silanes on Reinforced Concrete Structures, Proceedings of ICDC 2012. Trondheim, Norway.
- Clear, C. (1985). The Effects of Autogenous Healing Upon the Leakage of Water Through Cracks in Concrete. UK: Cement and Concrete Association, Report No. 559.
- Cohen, L. (1960). Some experiments in design and construction with ferro-cement. *Transactions*, 86, 40.

- Concrete Bridge Development Group. (2002). *Technical Guide 2: Guide to Testing and Monitoring the Durability of Concrete Structures*. Camberly, Surrey, UK: Concrete Society.
- Concrete Society. (2004). *Electrochemical Tests for Reinforcement Corrosion* (Technical Report 60 ed.). Camberly, Surrey, UK: Concrete Society.
- Concrete Society;. (1988). *Permeability Testing of Site Concrete: A Review of Methods and Experience: Report of a Concrete Society Working Group*. London: Concrete Society.
- Coppola, L., & Buoso, A. (2015). *Il restauro dell'architettura moderna in cemento armato*. Hoepli.
- Cui, H., Tang, W., Liu, W., Dong, Z., & Xing, F. (2015). Experimental Study on Effect of CO₂ Concentrations on Concrete Carbonation and Diffusion Mechanisms. *Construction and Building Materials*, 93, 522-527.
- Dai, J.-G., Akira, Y., Wittmann, F., Yokota, H., & Zhang, P. (2010). Water Repellent Surface Impregnation for Extension of Service Life of Reinforced Concrete Structures in Marine Environments: the Role of Cracks. *Cem Concr Comp*, 32, 101-109.
- Dang, V., Francois, R., & Hostis, V. (2013). Effects of Pre-Cracks on Both Initiation and Propagation of Rebar Corrosion in Pure Carbon Dioxide. *EPJ Web of Conferences*, 56(06006), 1-11.
- Dang, Y., Xie, N., & Kessel, A. (2014). Accelerated Laboratory Evolution of Surface Treatments for Protecting Concrete Bridge Decks from Salt Scaling. *Constr Build Mater*, 55, 128-135.
- D'Ayala, D., & Forsyth, M. (2007). What is Conservation Engineering? In M. Forsyth (A cura di), *Structures & Construction in Historic Building Conservation* (p. 248). Oxford: Wiley-Blackwell.

- Dei, L., & Salvadori, B. (2006). Nanotechnology in Cultural Heritage Conservation: Nanometric Saked Lime Saves Architectonic and Artistic Surfaces from Decay. *J Cult Heritage*, 7, 110-115.
- Disenbacher, A., & Brauer, F. (1984). Material Development Design, Construction and Evaluation of Ferrocement Planning Boat. *Marine Technology & S.*, 11(3), 277-296.
- Dodge Woodson, R. (2009). *Concrete Structures - Protection, Repair and Rehabilitation*. Butterworth-Heinemann.
- Drochytka, R., & Petranek, V. (2002). Atmospheric Concrete Deterioration. In *Proc. of the First FIB Conference in Concrete Structures in the 21st Century* (p. 10-19). Osaka, Japan.
- Elsener, B. (1990). Ionenmigration und elektrische Leitfähigkeit im Beton. *SIA Doc. D065 Schweiz. Ingenieur- und Architektenverein*, 51-59.
- Elsener, B., Flückiger, D., & Böhni, H. (2000). A percolation model for water sorption in porous cementitious materials. In *Materials for buildings and structures* (p. 163-169). Weinheim: Wiley-VCH Verlag GmbH.
- Elsener, B., Müller, S., Suter, M., & Böhni, H. (1990). Corrosion Monitoring of Steel in Concrete - Theory and Practice. In C. Page, K. Treadaway, & P. Bamforth (A cura di), *Corrosion of Reinforcement in Concrete* (p. 348). London: Elsevier Applied Science.
- EN 1015-18. (2002). *Methods of test for mortar for masonry. Determination of water absorption coefficient due to capillary action of hardened mortar*.
- EN 13057. (2002). *Products and systems for the protection and repair of concrete structures. Test Methods. Determination of resistance of capillary absorption*, European Committee for Standardization.

- EN 480-5. (2005). *Admixtures for concrete, mortar and grout. Test methods. Determination of capillary absorption.*
- Eyers, J. (1972). Survey of ferrocement fishing boats built in New Zealand. *FAO seminar on the design and construction of ferrocement fishing vessels*, 30.
- Feldman, R., & Sereda, P. (1968). A Model for Hydrated Portland Cement Paste as deduced from Sorption - Length Change and Mechanical Properties. *RILEM Bulletin*, 1(6), 509-520.
- Fib. (2010). *Model Code 2010 - Chapter 9 "Conservation"*. Berlin: Wilhelm Ernst & Sohn.
- Franzoni, E., Pigino, B., & Pistolesi, C. (2013). Ethyl Silicate for Surface Protection of Concrete: Performance in Comparison with other Inorganic Surface Treatments. *Cement & Concrete Composites*, 44, 69-76.
- French, W. (1995). Avoiding concrete aggregate problems. In *Improving Civil Engineerings - Old and New* (p. 69-95). Essex, UK: W.J. French.
- Gallé, C. (2011). Effect of Drying on Cement-Based Materials Pore Structure as Identified by Mercury Intrusion Porosimetry. A Comparative Study Between Oven-, Vacuum-, and Freeze-Drying. *Cem Constr Res*, 31, 1467-1477.
- Garuzzo, V. (2002). Il Palazzo Torinese della Moda al Valentino. In *Studi Piemontesi*, Vol. 31, fasc. 1 (p. 63-64).
- Gordon, J. (1968). *The new science of strong materials*. Baltimore: Penguin Books.
- Greco, C. (2008). *Pier Luigi Nervi. Dai Primi Brevetti al Palazzo delle Esposizioni di Torino 1917-1948*. Luzern: Quart.
- Greenius, A. (1975). *Ferrocement for Canadian Fishing Vessels: A Summary and Interpretation of Test Results 1969-1974*. Ottawa: Industrial Development Branch, Fisheries and Marine Service, Environmental Canada.

- Greenspan, L. (1977). Humidity Fixed Points of Binary Saturated Aqueous Solutions. *Journal of Research of the National Bureau of Standards Section A: Physics and Chemistry*, 81A(1), 89-96.
- Haga, K., Sutou, S., & Hironaga, M. (2005). Effect of Porosity on Leaching of Ca From Hardened Ordinary Portland Cement Paste. *Cem Concr Res*, 35, 1764-1775.
- Hall, C. (1989). Water sorptivity of mortars and concretes: a review. *Mag. Concr. Res.*, 41(147).
- Hansen, F. (1971). Investigation of the Effect of Distribution and Amount of Reinforcement on the Physical Properties of Ferrocement. In *Research Report No. 2* (p. 25). Bangkok: Applied Scientific Research Corporation of Thailand.
- Hansson, C., Poursaee, A., & Jaffer, S. (2017). Corrosion of Reinforcing Bars in Concrete, PCA R&D Serial No. 3013. *Portland Cement Association (PCA)*.
- Haynes, H., & Guthrie, G. (1974). *Ferrocement construction Panels, Technical Note No. 1341*. Civil Engineering Laboratory. Port Hueneme: Naval Construction Battalion Center.
- Hickman, M. (1970). Measurement of Humidity. *National Physical Laboratory Notes on Applied Science*, 4(31).
- Hou, P., Cheng, X., Qian, J., & Shah, S. (2014). Effect and Mechanisms of Surface Treatment of Hardened Cement-Based Materials with Colloidal NanoSiO₂ and its Precursor. *Construction and Building Materials*, 53, 66-73.
- Hou, P., Cheng, X., Qian, J., Cao, W., & Shah, S. (2015). Characteristics of Surface-Treatment of Nano-SiO₂ on the Transport Properties of Hardened Cement Pastes with Different Water-to-Cement Ratios. *Cement and Concrete Composites*, 55, 26-33.
- Hou, P., Zhang, R., Cai, Y., Cheng, X., & Shah, S. (2016). In situ Ca(OH)₂ Consumption of TEOS on the Surface of Hardened Cement-Based Materials and its Improving

Effects on the Ca-Leaching and Sulfate-Attack Resistivity. *Construction and Building Materials*, 113, 890-896.

Ibrahim, M., Al-Gahtani, A., Maslehuddin, M., & Almusallam, A. (1997). Effectiveness of Concrete Surface Treatment Materials in Reducing Chloride-Induced Reinforcement Corrosion. *Constr Build Mater*, 11(7-8), 443-451.

Ibrahim, M., Al-Gahtani, A., Maslehuddin, M., & Dakhil, F. (1999). Use of Surface Treatment Materials to Improve Concrete Durability. *Journal of Materials in Civil Engineering*, 11(1), 36-40.

IFS Committee 10. (2001). *IFS 10-01: Ferrocement model code, building code recommendations for ferrocement*. International Ferrocement Society.

International Council on Monuments and Sites. (2003). *ICOMOS Charter – Principles for the Analysis, Conservation and Structural Restoration of Architectural Heritage*. Paris.

Iori, T. (2001). *Il Cemento Armato in Italia dalle Origini alla Seconda Guerra Mondiale*. Rome: Edilstampa.

Iori, T., & Poretti, S. (2013). Pier Luigi Nervi: His Construction System for Shell and Spatial Structures. *Journal of the International Association for Shell and Spatial Structures*, 54(2-3), 117-126.

Jiang, L., Xue, X., Zhang, W., Yang, J., Zhang, H., Li, Y., . . . Qin, J. (2015). The Investigation of Factors Affecting the Water Impermeability of Inorganic Sodium Silicate-Based Concrete Sealers. *Construction and Building Materials*, 93, 729-736.

Johansson, A. (2005). Impregnate Concrete with a System Open to Diffusion (Impregnera betong med diffusionsöppet system). *The Journal Husbyggaren*, 4, 18-20.

Johnson, K., Schultz, A., French, C., & Reneson, J. (2009). *Crack and Concrete Deck Sealant Performance*.

- Johnston, C., & Mattar, S. (1976). Ferrocement in Tension and Compression. In *Proceedings, ASCE, V.102, ST5* (p. 857-899).
- Johnston, C., & Mowat, D. (1974). Ferrocement: Material Behavior in Flexure. In *Proceedings, ASCE, V. 100, ST10* (p. 2053-2069).
- Karagiannis, N., Karoglou, M., Bakolas, A., & Moropoulou, A. (2016). Building materials capillary rise coefficient: concepts, determination and parameters involved. In *New approaches to building pathology and durability* (p. 27-44). Springer.
- Khatib, J., & Mangat, P. (2002). Influence of high-temperature and Low-umidity curing in chloride penetration in blended cement concrete. *Cement and Concrete Research, 4*(2), 110-114.
- Kim, E., Won, J., Do, J., Kim, S., & Kang, Y. (2009). Effects of Silica Nanoparticle and GPTMS Addition on TEOS-Based Stone Consolidants. *Journal of Cultural Heritage, 10*(2), 214-221.
- Klieger, P. (1956). Effect of Entrained Air on Strenght and Durability of Concrete with Various Sizes of Aggregate. In *Bulletin No. 128* (p. 1-19). Washington D.C.: Highway Research Board.
- Klieger, P., & Lamond, J. (1994). *significance of tests and properties of concrete and concrete-making materials*. Philadelphia, PA: ASTM.
- Kosa, K., & Naaman, A. (1990). Corrosion of Steel Fiber Reinforced Concrete. *ACI Materials Journal, 87*(1), 27-37.
- Kosa, K., Naaman, A., & Hansen, W. (1991). Durability of Fiber Reinforced Mortar. *ACI Materials Journal, 88*(3), 310-319.
- Kozak, A. (2015). Multi-criteria Assessment of an Acrylic Coating Exposed to Natural and Artificial Weathering. *Procedia Engineering, 108*, 664-672.

- Kumar, R., & Bhattacharjee, B. (2003). Porosity, Pore Size Distribution and in Situ Strength of Concrete. *Cem Concr Res*, 33, 155-164.
- Kupwade-Patil, K., Cardenas, H., Gordon, K., & Lee, L. (2012). Corrosion Mitigation in Reinforced Concrete Beams via Nanoparticle Treatment. *ACI Mater J*, 109(6), 617-626.
- Kurdowski, & Wieslaw. (2014). *Cement and Concrete Chemistry*. Netherlands: Springer.
- Kurtz, H., & Long, B. (1943). Effect of Curing Methods Upon the Durability of Concrete as Measured in the Dynamic Modulus of Elasticity. *Proc. ASTM*, 43:1051.
- Lane, R. (1978). Abrasion Resistance. In *STP169B - Significance of Tests and Properties of Concrete and Concrete-Making Materials* (p. 332-350). Philadelphia: ASTM.
- LaRosa Thompson, J., Silsbee, M., Gill, P., & Scheetz, B. (1997). Characterization of Silicate Sealers on Concrete. *Cem Concr Res*, 27, 1561-1567.
- Lazzarini, L., & Laurenzi Tabasso, M. (2010). *Il Restauro della Pietra*. Torino: Utet Scienze Tecniche.
- Li, G., Guo, C., Gao, X., Ji, Y., & Geng, O. (2016). Time Dependence of Carbonation Resistance of Concrete with Organic Film Coatings. *Construction and Building Materials*, 114, 269-275.
- Li, G., Lei, M., & Yang, P. (2013). Influence of Deterioration on the Carbonation Resistance Capability of Concrete with Coatings. *J. Xuzhou Inst. Technol. (Nat. Sci.)*, 2, 62-66.
- Li, J., Yi, Z., & Xie, Y. (2012). Progress of Silane Impregnating Surface Treatment Technology of Concrete Structure. *Mater. Rev.*, 26(3), 120-125.
- Litvan, G. (1996). Waterproofing of parking garage structures with sealers and membranes: the Canadian experience. *Construction and Building Materials*, 10(1), 95-100.

- Liu, Z., & Hansen, W. (2016). Effect of Hydrophobic Surface Treatment on Freeze-Thaw Durability of Concrete. *Cement and Concrete Composites*, 69, 49-60.
- Logan, D., & Shah, S. (1973). Moment Capacity and Cracking Behavior of Ferrocement in Flexure. *ACI Journal*, 70(12), 799-804.
- Mansur, M., & Paramasivam, P. (1986). Cracking Behaviour and Ultimate Strength of Ferrocement in Flexure. *Journal of Ferrocement (Bangkok)*, 16(4), 405-4015.
- Maravelaki-Kalaitzaki, P., Kallithrakas-Kontos, N., Agioutantis, Z., Maurigiannakis, S., & Korakaki, D. (2008). A Comparative Study of Porous Limestones Treated with Silicon-Based Strengthening Agents. *Prog Org Coat*, 62, 49-60.
- Mattar, S. (1971). "*Ferrocement in Tension and Compression*", master's thesis. Calgary: University of Calgary.
- McCarter, W., Emerson, M., & Ezirim, H. (1995). Properties of concrete in the cover zone: developments in monitoring techniques. *Magazine of Concrete Research*, 47, 243-251.
- McGettigan, E. (1995). Factors Affecting the Selection of Water-Repellent Treatments. *APT Bulletin: The Journal of Preservation Technology*, 26(4), 22-26.
- Mehta, P., & Gerwick, B. (1982). *Concr. Int.*, 4, 45-51.
- Mehta, P., & Monteiro, P. (2006). *Concrete: microstructure, properties and materials* . New York: McGraw-Hill.
- Mercer, L. (1945). Permeability of concrete - 1, theoretical consierations, laboratory tests methods, details of experimental work with new apparatus. *The Commonwealth Engineering*, 349-357.
- Miliani, C., Velo-Simpson, M., & Scherer, G. (2007). Particle-Modified Consolidants: A Study on the Effect of Particles on Sol–Gel Properties and Consolidation Effectiveness. *Journal of Cultural Heritage*, 8(1), 1-6.

- Millard, S., Harrison, J., & Edwards, A. (1989). Measurements of the Electrical Resistivity of Reinforced Concrete Structures for the Assessment of Corrosion Risk. *Journal of Non-destructive Testing*, 31, 11.
- Mohammed, T., Otsuki, N., & Hamada, H. (2001). Oxygen Permeability in Cracked Concrete Reinforced with Plain and Deformed Bars. *Journal of Cement and Concrete Research*, 31(5), 829-834.
- Molhotra, V., & Carino, N. (1991). *Handbook of Nondestructive Testing of Concrete*. Boca Raton, Florida: CRC Press.
- Montemor, M., Simoes, A., & Ferreira, M. (1998). Analytical Characterization of the Passive Film Formed on Steel in Solutions Simulating the Concrete Interstitial Electrolyte. *Corrosion*, 54(5), 347-353.
- Montes, P., Bremner, T., & Lister, D. (2004). Influence of Calcium Nitrite Inhibitor and Crack Width on Corrosion of Steel in High Performance Concrete Subjected to a Simulated Marine Environment. *Cement and Concrete Composites*, 26, 243-253.
- Moon, H., Shin, D., & Choi, D. (2007). Evaluation of the Durability of Mortar and Concrete Applied with Inorganic Coatings Material and Surface Treatment System. *Constr Build Mater*, 21(2), 362-369.
- Moore, W. (1972). *Physical chemistry* (4th ed.). London: Longman.
- Mor, A., & Mehta, P. (1984). Effect of Superplasticising Admixtures on Cement Hydration. *Cement and Concrete Research*, 14(5), 754-756.
- Moradillo, M., Shekarchi, M., & Hoseini, M. (2012). Time-Dependent Performance of Concrete Surface Coatings in Tidal Zone of Marine Environment. *Construction and Building Materials*, 30, 198-205.
- Morgan, R. (1968). Lambot's Boats. *Concrete (London)*, 2(3), 128.
- Mosquera, M., De Los Santos, D., Montes, A., & Valdez-Castro, L. (2008). New Nanomaterials for Consolidating Stone. *Langmuir*, 24, 2772-2778.

- Moss, G. (1998). *Advancing a comprehensive understanding of concrete durability*. Dissertation Abstracts International.
- Mowat, D. (1970). *"Flexural Testing of Ferrocement Planks"*, master's thesis. Calgary: University of Calgary.
- Naaman, A. (A cura di). (1998). *Ferrocement 6 Lambot symposium: Proceedings of the Sixth International Symposium on Ferrocement*. University of Michigan, Ann Harbor, Michigan USA.
- Naaman, A. (2000). *Ferrocement & laminated cementitious composites*. Ann Arbor: Techno Press 3000.
- Naaman, A. (2012). Evolution in ferrocement and thin reinforced cementitious composites. *Arabian Journal for Science and Engineering*, 37(2), 421-441.
- Naaman, A., & Shah, S. (1971). Tensile Tests of Ferrocement. *ACI Journal, Proceedings*, 68(9), 693-698.
- Nanukuttan, S. (2007). *Development of a new test protocol for the PERMIT ion migration test*. PhD thesis. Queen's University Belfast.
- National Research Council Committee on Concrete. (1988). *Concrete durability: a multibillion-dollar opportunity*.
- Nervi, P. (1945). *Scienza o Arte del Costruire? Caratteristiche e Possibilità del Cemento Armato*. Roma: Bussola.
- Nervi, P. (1956). Ferrocement: its characteristics and potentialities. *Cement and Concrete Association*, 60, 17.
- Nervi, P. (1956). *Structures*. New York: F.W. Dodge Corp.
- Nervi, P. (1957). *The Works of Pier Luigi Nervi*. London: Architectural Press.
- Neville, A. (1995). *Properties of concrete*. Harlow, UK: Longman Group Limited.

- Neville, A. (2002). Autogenous Healing - A Concrete Miracle? *Concrete International*, 24(11), 76-82.
- Olmo, C., & Chiorino, C. (2011). *Pier Luigi Nervi: Architecture as Challenge*. Milano: Silvana Editoriale.
- Otieno, M., Alexander, M., & Beushausen, H. (2010). Corrosion in Cracked and Uncracked Concrete - Influence of Crack Width, Concrete Quality and Crack Opening. *Magazine of Concrete Research*, 62(6), 393-404.
- Pan, X., Shi, C., Jia, L., Zhang, L., & Wu, L. (2016). Effect of Inorganic Surface Treatment on Air Permeability of Cement-Based Materials. *Journal of Materials in Civil Engineering*, 28(3).
- Paramasivam, P., Ong, K., & Lee, S. (1991). Ferrocement: R & D applications. *U.S.-Korea-Japan Trilateral Seminar on Frontier R & D for Constructed Facilities* (p. 413-421). Honolulu: Proceedings, U.S.-Korea-Japan Trilateral Seminar on Frontier R & D for Constructed Facilities.
- Parrott, L. (1992). Carbonation, Moisture and Empty Pores. *Advances in Cement Research*, 4(15), 111-118.
- Parrott, L. (1994). Design for Avoiding Damage Due to Carbonation-Induced Corrosion. Proc. of Canmet/ACI Int. Conf. Durability of Concrete. Nice.
- Pedefferri, P., & Bertolini, L. (2000). *La Durabilità del Calcestruzzo armato (in english: Durability of Reinforced Concrete)*. Milan: McGrawHill Italia.
- Pettersson, K., & Jorgensen, O. (1996). The Effect of Cracks on Reinforcement Corrosion in High-Performance Concrete in a Marine Environment. *Proceedings of the 3rd ACI/CANMET International Conference on the Performance of Concrete in the Marine Environment, St. Andrews-by-the-Sea, Canada, 163*, 185-200.

- Pigino, B., Leemann, A., Franzoni, E., & Lura, P. (2012). Ethyl Silicate for Surface Treatment of Concrete - Part II: Characteristics and Performance. *Cem Concr Comp*, 34(3), 313-321.
- Polder, R. (1996). Durability of New Types of Concrete for Marine Environments. Gouda: CUR report 96-3.
- Polder, R. (1996). The Influence of Blast Furnace Slag, Fly Ash and Silica Fume on Corrosion of Reinforced Concrete in Marine Environment. *Heron*, 41(4), 287-300.
- Polder, R., Andrade, C., Elsener, B., Vennesland, Ø., Gulikers, J., Weydert, R., & Raupach, M. (2000). Test Methods for on Site Measurement of Resistivity of Concrete. *Materials and Structures*, 33(10), 603-611.
- Polder, R., Borsje, H., & Vries, J. (2000). Corrosion Protection of Reinforcement by Hydrophobic Treatment of Concrete. In J. Mietz, R. Polder, & B. Elsener (A cura di), *Corrosion of Reinforcement in Concrete. Corrosion Mechanisms and Corrosion Protection* (p. 73-84). London: The Institute of Materials.
- Polder, R., Borsje, H., & Vries, J. (2001). Prevention of Reinforcement Corrosion by hydrophobic treatment of concrete. *Heron*, 46(4), 227-238.
- Polder, R., Peelen, W., Bertolini, L., & Guerrieri, M. (2002). Corrosion Rate of Rebars from Linear Polarization Resistance and Destructive Analysis in Blended Cement Concrete After Chloride Loading. Granada: ICC 15th International Corrosion Congress.
- Pourbaix, M. (1973). *Lectures on Electrochemical Corrosion*. New York: Plenum Press.
- Poursaei, A. (2016). Corrosion of steel in concrete structures. In *Corrosion of steel in concrete structures*. Woodhead Publishing.
- Powers, T. (1958). *Journal of the American Ceramic Society*, 61(1), 1-5.

- Powers, T. (1958). Structure and Physical properties of Hydrated Portland Cement Paste. *Journal of the American Ceramic Society*, 41(1).
- Powers, T., Copeland, L., Hayes, J., & Mann, H. (1954). Permeability of portland cement paste. *ACI J.*, 51(3), 285-298.
- Poyet, S., Sellier, A., Capra, B., Foray, G., Torrenti, J.-M., Cognon, H., & Bourdarot, E. (2007). Chemical Modelling of Alkali Silica Reaction: Influence of the Reactive Aggregate Size Distribution. *Materials and Structures*, 40(2), 229-239.
- Qiang, X., Shulin, Z., Bingzheng, X., Hui, Y., Xiaoqian, Q., & Xiaofu, D. (2016). Effect of isobutyl-triethoxy-silane penetrative protective agent on the carbonation resistance of concrete. *Journal of Wuhan University of Technology-Mater. Sci. Ed.*, 31(1), 139-145.
- Quero, V., Garcia, P., & Bremner, T. (2010). Influence of Concrete Cracking on the Corrosion of Steel Reinforcement. In P. Castro-Borges, E. Moreno, K. Sakai, O. Gjorv, & N. Banthia, *Concrete Under Severe Conditions: Environment and Loading* (p. 383-389). Boca Raton, FL: CRC Press.
- Rao, A., & Gowdar, C. (1971). A Study of the Behavior of Ferrocement in Flexure. *Indian Concrete Journal (Bombay)*, 45(4), 178-183.
- Raupach, M., & Wolff, L. (2005). Long-Term Durability of Hydrophobic Treatment on Concrete. *Surface Coatings International Part B: Coatings Transactions*, 88(2), 127-133.
- Richardson, M. (2002). *Fundamentals of Durable Reinforced Concrete*. London: CRC Press.
- RILEM Technical Committee 124-SRC. (1994). Draft Recommendations for Repair Strategies for Concrete Structures Damaged by Reinforcement Corrosion. *Materials and Structures*, 27, 415-436.

- Rose, D. (1965). Water movement in unsaturated porous materials. *RILEM bulletin*(29), 119-124.
- Ruettgers, A., Vidal, E., & Wing, S. (1935). An Investigation of the Permeability of Mass Concrete with Particular Reference to Boulder Dam. *ACI Journal, Proceedings*, 31(4), 382-416.
- Sahmaran, M., & Yaman, I. (2008). Influence of Transverse Crack Width on Reinforcement Corrosion Initiation and Propagation in Mortar Beams. *Canadian Journal of Civil Engineering*, 35, 236-245.
- Salander, A. (2010). *Hydrophobic Impregnation of Concrete Structures: Effects on Concrete Properties, Doctoral Thesis*. Stockholm: KTH.
- Sandrolini, F., Franzoni, E., & Pigino, B. (2012). Ethyl Silicate for Surface Treatment of Concrete - Part I: Pozzolanic Effect of Ethyl Silicate. *Cement & Concrete Composites*, 34, 306-312.
- Scherer, G., & Wheeler, G. (2009). Silicate Consolidants for Stone. *Key Eng Mater*, 39, 1-25.
- Schiebl, P., & Raupach, M. (1997). Laboratory Studies and Calculations on the Influence of Crack Width on Chloride Induced Corrosion of Steel in Concrete. *ACI Materials Journal*, 94(1), 56-61.
- Schueremans, L., Van Gemert, D., & Giessler, S. (2007). Chloride Penetration in RC-Structures in Marine Environment—Long Term Assessment of A Preventive Hydrophobic Treatment. *Construction and Building Materials*, 21(6), 1238-1249.
- Scott, A., & Alexander, M. (2007). The Influence of Binder Type, Cracking and Cover on Corrosion Rates of Steel in Chloride Contaminated Concrete. *Magazine of Concrete Research*, 59(7), 495-505.

- Segal, E., & Adriaenssens, S. (2013). Norfolk Scope Arena: A US Dome With a Unique Configuration of Interior Ribs and Buttresses. *Journal of the International Association for Shell and Spatial Structures*, 54(2 & 3), 189-198.
- Sercombe, J., Vidal, R., & Gallé, C. (2007). Experimental Study of Gas Diffusion in Cement Paste. *Cem Concr Res*, 37, 579-588.
- Sergi, G., Lattey, S., & Page, C. (1990). Influence of Surface Treatments on Corrosion Rates of Steel in Carbonated Concrete. In C. Page, K. Treadaway, & P. Bamforth (A cura di), *Corrosion of Reinforcement in Concrete* (p. 409-419). Elsevier.
- Shah, S., & Balaguru, P. (1984). Ferrocement. In R. Swamy (A cura di), *New Reinforced Concrete 2* (p. 5-24). Glasgow: Blackie and Sons Limited.
- Shaikh, F. (2018). Effect of Cracking on Corrosion of Steel in Concrete. *International Journal of Concrete Structures and Materials*, 12(1), 1-12.
- Shi, C., Krivenko, P., & Roy, D. (2006). *Alkali-Activated Cement and Concrete*. New York: Taylor & Francis Press.
- Sistonen, E., Kari, O., Tukiainen, P., & Huovinen, S. (2007). The Influence of the Crack Width on the Durability of Different Reinforcement Bar Materials. In F. Toutlemonde (A cura di), *Concrete Under Severe Conditions: Environment and Loading* (p. 419-428). Tours, France: CONSEC07.
- Song, Z., Xue, X., Li, Y., Yang, J., He, Z., Shen, S., . . . Zhang, N. (2016). Experimental Exploration of the Waterproofing Mechanism of Inorganic Sodium Silicate-Based Concrete Sealers. *Construction and Building Materials*, 104, 276-283.
- Soroka, J. (1979). *Portland cement paste and concrete*. London: Macmillan.
- Soutsos, M. (2010). *Concrete durability, A practical guide to design of durable concrete structures*. Thomas Telford Limited.
- Suzuki, K., Ohno, Y., Praparntanatorn, S., & Tamura, H. (1990). Mechanism of Steel Corrosion in Cracked Concrete. In C. Page, K. Treadaway, & P. Bramforth (A

- cura di), *Corrosion of Reinforcement in Concrete* (p. 19-28). London: Society of Chemical Industry.
- Taylor, H. (1997). *Cement Chemistry* (2nd ed.). New York: Thomas Telford.
- Transportation Research Board. (1991). *Highway deicing – comparing salt and calcium magnesium acetate. Special report 235*. Washington, DC: National Academy of Sciences.
- Tuutti, K. (1982). *Corrosion of Steel in Concrete*. Stockholm: Foundation for Concrete Research.
- UNI, EN 1504-1. (2005). Products and Systems for the Protection and Repair of Concrete Structures. Definitions, Requirements, Quality Control and Evaluation of Conformity - Part 1: Definitions, Requirements, Quality Control and Evaluation of Conformity.
- UNI, EN 1504-2. (2004). *Products and Systems for the Protection and Repair of Concrete Structures. Definitions, Requirements, Quality Control and Evaluation of Conformity - Part 2: Surface Protection Systems for Concrete*.
- UNI, EN 1504-9. (2008). Products and Systems for the Protection and Repair of Concrete Structures. Definitions, Requirements, Quality Control and Evaluation of Conformity - Part 9: General Principles for the Use of Products and Systems.
- Vries, D., Polder, R., & Borsje, H. (1998). Durability of Hydrophobic Treatment of Concrete. *Proc of the Second International Conference on Concrete under Severe Conditions*, 98, 1341-1350.
- Vries, I. (1997). Hydrophobic Treatment of Concrete. *Construction and Building Materials*, 11(4), 259-265.
- Walkus, B. (1975). The Behavior of Ferrocement in Bending. *Journal of Structural Engineering*, 3(3), 113-125.

- Wallbank, E. (1983). *The Performance of Concrete in Bridges. A Survey of 200 Highway Bridges*. London: HMSO.
- Wheeler, G. (2005). *Alkoxysilanes and the consolidation of stone*. Los Angeles: Getti Conservation Institute.
- Wierig, H. (1994). Long-Time Studies on the Carbonation of Concrete Under Normal Outdoor Exposure, RILEM Seminar on Durability of Concrete Structures Under Normal Outdoor Exposure. Hannover.
- Woo, R., Zhu, H., Chow, M., Leung, C., & Kim, J. (2008). Barrier Performance of Silane–Clay Nanocomposite Coatings on Concrete Structure. *Composites Science and Technology*, 68(14), 2828-2836.
- Yang, P., Li, W., & Zhao, T. (2012). Protective Effect of Surface Coatings on Concrete. *Journal of The Chinese Ceramic Society*, 40(11), 1613-1617.
- Yu, S., Sergi, G., & Page, C. (1993). Ionic diffusion across an interface between chloride-free and chloride-containing cementitious materials. *Magazine of Concrete Research*, 45(165), 257-261.
- Zafeiropoulou, T., Rakanta, E., & Batis, G. (2011). Performance Evaluation of Organic Coatings Against Corrosion in Reinforced Cement Mortars. *Progress in Organic Coatings*, 72(1-2), 175-180.
- Zakroczymski, T., Fan, C., & Szklarska-Smialowska, Z. (1985). Kinetics and Mechanism of Passive Film Formation on Iron in 0.05M NaOH. *Journal of Electrochemical Society*, 132(12), 2862-2867.
- Zárraga, R., Cervantes, J., Salazar-Hernandez, C., & Wheeler, G. (2010). Effect of Addition of Hydroxyl-Terminated Polydimethylsiloxane to TEOS-Based Stone Consolidants. *J Cult Heritage*, 11, 138-144.

Zhang, C., Wang, A., Tang, M., Wu, B., & Zhang, N. (1999). Influence of Aggregate Size and Aggregate Size Grading on ASR Expansion. *Cement and Concrete Research*, 29(9), 1393-1396.

Zhu, Y., Kou, S., Poon, C., Dai, J., & Li, Q. (2013). Influence of Silane-Based Water Repellent on the Durability Properties of Recycled Aggregate Concrete. *Cement and Concrete Composites*, 35(1), 32-38.